UNIVERSITY OF CALGARY

Algorithmic Quantum Channel Simulation

by

Dongsheng Wang

A THESIS

SUBMITTED TO THE FACULTY OF GRADUATE STUDIES

IN PARTIAL FULFILLMENT OF THE REQUIREMENTS FOR THE

DEGREE OF DOCTOR OF PHILOSOPHY

DEPARTMENT OF PHYSICS AND ASTRONOMY

CALGARY, ALBERTA

SEPTEMBER, 2015

Abstract

Quantum simulation, which is generically the task to employ quantum computers to simulate quantum physical models, has been one of the most significant motivations and applications of quantum computing. Quantum dynamics, unitary or nonunitary Markovian dynamics driven by local interactions, has been proved to be efficiently simulatable on quantum computers. Extending the underlying models in quantum computation and quantum simulation from unitary to general nonunitary evolution, and from continuous-time to discrete-time evolution is essential not only for quantum simulation of more general processes, e.g., dissipative processes with evident non-Markovian effects, but also for developing alternative quantum computing models and algorithms. In this thesis, we explore quantum simulation problems mainly from the following three themes.

First, we extend quantum simulation framework of Hamiltonian-driven evolution to quantum simulation of quantum channels, combined with the scheme of algorithmic simulation that accepts a promised simulation accuracy, hence *algorithmic quantum channel simulation*. Our simulation scheme contains a classical preprocessing part, i.e. a classical algorithm for quantum-circuit design, and a quantum part that is the execution of a quantum circuit for the quantum channel simulator. The classical algorithm accepts the description of an arbitrary quantum channel and a simulation error tolerance as input, and delivers the description of the implementation of a quantum circuit and an actual error as output. The quantum simulator circuit then generates final state within the actual error, which should be smaller than the tolerance in the worst case, which guarantees the accurate simulation of further observable effects on the simulator. Our quantum channel simulation framework is distinct from non-algorithmic simulation scheme, and also some dedicated simulation for particular instead of arbitrary quantum processes.

Second, we employ nonstandard yet beneficial quantum simulation algorithms for arbi-

trary quantum channels beyond the dilation method. We explore the method of quantum channel decomposition in terms of convex combination of smaller channels, known as generalized extreme channels, for which the channel decomposition is known as a nontrivial open problem. To attack the channel decomposition problem, we develop an optimization algorithm for approximate decomposition into a convex sum of generalized extreme channels from our construction. We provide an ansatz for generalized extreme channels that proves to be able to yield arbitrary generalized extreme channels and allows a precise quantum circuit description. Furthermore, our numerical simulation has demonstrated the validity of our optimization algorithm for low-dimensional quantum channels.

Third, we also attempt to provide general definitions of quantum simulation problems by exploring the freedom of the notion of simulation. By considering quantum simulation problems beyond the rough distinction between digital and analog simulations, and beyond the quantum-state generation problem, we can define various quantum simulation problems, namely, uniform, strong, and weak quantum simulations from the point view of operator topology. Our quantum channel simulation developed above is a strong simulation, which simulates the effects of a channel on arbitrary input states. For the other two possible simulation methods, we define a general weak quantum simulation problem, which actually simulates observable effects instead of the effects on state generation. Also we study the channel simulation problem in the quantum query model, and provide the query complexity by employing uniform quantum simulation method.

Acknowledgements

I want to express my great acknowledgement to my PhD supervisor Dr. Barry C. Sanders, who initially provided me the opportunity to Canada, and has gradually changed my view towards mathematics, computer science, and research on quantum foundation. Particularly, I want to thank him for the training of scientific work writing, and his patience of endless writings and discussions. Also I want to thank him for providing financial support and many chances for conference, collaboration and summer school. Last but not least, I also want to thank him for choosing such a significant research topics.

I want to thank Dr. Peter Høyer and Dr. David Feder for serving as my PhD committee member, and for their occasional discussions and help, which have certainly triggered many ideas, and some of them have contributed to this thesis. I also would like to thank Dr. Gilad Gour for accepting me to join his group meeting.

I want to thank Dr. Dominic Berry from Macquarie university and Dr. Marcos C. de Oliveira from Universidade Estadual de Campinas for their collaborations. Particularly, I want to thank Dominic for his mathematical insights, and Marcos for his inspirations and kindness especially during my first year in Canada.

I want to thank the group of Prof. Jian-Wei Pan in Shanghai, China for the collaboration on the experimental realization of our qubit channel simulator. I want to thank my collaborators there, particularly, Dr. Yu-Ao Chen, He Lu, and Chang Liu.

I want to thank Ms. Lucia Wang and Ms. Nancy Lu for their selfless help, especially when I have trouble in my personal life in Calgary or the department. I want to thank the group members, former or current, and other candidates sitting in the same office with me, and also other classmates and friends, particularly, I want to mention Yunjiang Wang, Jianming Wen, Ran Hee Choi, Mohammad Khazali, Ehsan Zahedinejad, Khulud Almutairi, and Farokh Mivehvar for bringing joy in my research career and personal life. Particularly, I

want to thank Varun Narasimhachar and Pantita Palittapongarnpim for reading my thesis and providing comments.

Finally, I want to thank my family for their understandings of my decision to go abroad, to study physics, and to continue my career.

Table of Contents

List of Tables

List of Figures and Illustrations

List of Symbols, Abbreviations and Nomenclature

Symbol	Definition
$\mathbb{R}$, $\mathbb{Z}$	The set of real numbers, integers
$\mathbb{R}^+$, $\mathbb{Z}^+$	The set of positive real numbers, positive integers
$\mathbb{Z}_d$	The set of integer numbers $0, 1, 2, \ldots, d-1$
$\mathbb{C}$	The set of complex numbers
$\mathscr{H}$	A finite dimensional Hilbert space
ρ	Density operator
$\mathscr{L}(\mathscr{H})$	The set of bounded linear operators on $\mathscr{H}$
$\mathscr{D}(\mathscr{H})$ or $\mathscr{D}$	The set of density operators
$L^2(\mathbb{R})$	The space of square-integrable functions
$\mathcal{M}_{n,m}$, $\mathcal{M}_n$	The set of $n \times m$, $n \times n$ complex matrices
$\|\boldsymbol{v}\|$	Euclidean norm of a vector $\boldsymbol{v}$
$\|\cdot\|_p$	Schatten p-norm
$\|\cdot\|_\diamond$	Diamond norm
$\mathcal{E}$	Quantum channel
$\mathcal{N}$	Completely positive mapping
$\mathcal{P}$	Positive mapping
$\mathcal{C}$	Choi state
$A \geq 0$	Positive semidefinite matrix A
$A \leq 1$	Contraction matrix A such that $\|A\| \leq 1$
A^{T}	The transpose of matrix A
span$\{e_i\}$	The linear span of the set $\{e_i\}$
aff$\{f_i\}$	The affine span of the set $\{f_i\}$
conv$\mathscr{S}$	The convex hull of the set $\mathscr{S}$

$\mathbf{\Delta}$	Simplex
CPTP	Completely positive and trace preserving
POVM	Positive operator-valued measure
P	Polynomial time
BPP	Bounded-error probabilistic polynomial time
BQP	Bounded-error quantum polynomial time
NP	Non-deterministic polynomial-time
QMA	Quantum Merlin Arthur
MPS	Matrix product states
H	Hadamard gate
T	$Z^{1/4}$ gate
CNOT	Quantum controlled-NOT gate
AQCS	Algorithmic quantum channel simulation
U of C	University of Calgary

Chapter 1

Introduction

Quantum simulation is an emerging field during the recent years. In the introduction part of this thesis, we provide necessary background and motivations for our study on quantum simulation of quantum channels and also open-system dynamics. We first explain why physicists are interested in building quantum computers in §1.1, and then in §1.2 we attempt to convince you the importance of algorithmic quantum channel simulation (AQCS), which is the main theme of this thesis. We gradually narrow down the topics to AQCS, as shown in Fig. 1.2. Finally, we present the summary of results and significance in §1.3 and layout the structure of the thesis in §1.4.

1.1 Quantum simulation of quantum physics

Solving quantum physical problems is one of the earliest motivations of quantum computing. We first explain in §1.1.1 why quantum physicists want quantum computers, and then we focus on quantum simulation by pointing out the basic differences between quantum computation and quantum simulation in §1.1.2, and then the differences between digital and analog quantum simulations in §1.1.3. Afterwards, two different ways to propose quantum simulation problems, algorithmic and non-algorithmic, are explained in §1.1.4, and furthermore, in §1.1.5 we point out that there could be various kinds of more general quantum simulation tasks.

1.1.1 Solving quantum physical problems

It is widely accepted that Feynman launched the campaign of simulating quantum physics with quantum computers. In his seminal 1982 paper [56], Feynman heuristically discussed

the simulation of quantum dynamics using a particular well controlled quantum system, namely, a *universal quantum simulator* or so-called quantum computer. In the concluding remark, he said:

> *And I'm not happy with all the analyses that go with just the classical theory, because nature isn't classical, dammit, and if you want to make a simulation of nature, you'd better make it quantum mechanical, and by golly it's a wonderful problem, because it doesn't look so easy.*

Following Feynman's great physics intuition, nowadays quantum computation has become a significant research field in modern physics and science, and quantum simulation is recognized as one of its most important motivations and applications [123].

Physicists encounter lots of difficulties when studying quantum dynamics. Problems such as finding the ground state, correlation functions, spectrum, and partition function are of central interest in condensed matter physics, particle physics, as well as quantum chemistry, while these problems are extremely difficult. Some examples would help to get a sense how hard they are. Finding the ground state, which is cleverly represented as a matrix product state [129], for gapped one-dimensional Hamiltonian is NP-complete [144]. Here, NP stands for 'nondeterministic polynomial time', which, roughly, can be understood as the set of problems that cannot be solved on classical computers in efficient time (while an answer can be efficiently verified once the answer is provided). The two and higher dimensional many-body systems are even harder to deal with [145]. In practice, many algorithms can be effective for particular cases while in general still inefficient. The density-matrix renormalization group algorithm [174] can effectively converge to approximate ground state of one-dimensional Hamiltonians and small two-dimensional Hamiltonians, while it can get trapped for some instances [54]. Many other numerical methods are also available, such as the quantum Monte Carlo, which relies on a sampling method, yet there is a notorious

"sign problem" for fermions [159].

Although there are promising advances for solving quantum physical problems on classical computers, as briefly mentioned above, it is believed that not all quantum physical problems can be efficiently solved on classical computers. In other words, a quantum computer can surpass a classical computer. In computer science terminology, the class of decision problems efficiently solvable by a quantum computer, known as BQP (bounded error quantum polynomial time), is no smaller than the class of decision problems efficiently solvable by a classical computer, known as P (polynomial time), and also the class BPP (bounded error probabilistic polynomial time). The general relation is

$$\mathrm{P} \subseteq \mathrm{BPP} \subseteq \mathrm{BQP},$$

although there is no proof for both the strict inclusion relations [123]. For solving quantum physical problems, unfortunately, it turns out some important problems cannot be efficiently solved by quantum computers. The Local Hamiltonian problem, which, roughly speaking, asks for the ground state of a given local Hamiltonian, is QMA-complete [92]. Here, QMA stands for quantum Merlin Arthur (MA), which is the quantum analog of the class NP or its probabilistic version MA [92]. QMA-hard problems are believed not to be efficiently solvable on quantum computers. However, the limitation on quantum computers does not deny Feynman's expectation. Instead, it proves that quantum computation, as an alternative of classical computation, is a rigorous subject and researchers should instead explore and focus on the quantum advantages over classical computation. For instance, Grover [67] discovered a quantum algorithm that demonstrates a quadratic speedup, although not efficient, for searching problems compared to classical algorithms.

It turns out, compared with studying static properties such as finding the ground state, simulating dynamics could be much easier on quantum computers. A heuristic understanding of the differences between simulation of dynamics and finding ground states is as follows. For a local Hamiltonian $\hat{H}$, the evolution $e^{-\beta\hat{H}}$ would drive the system to its ground state when β

goes to infinity (or exponential with system size), which is the basic method employed by simulated annealing [73]. As one can see, even the dynamics $e^{-\beta\hat{H}}$ can be efficiently simulated on a quantum computer for a given value of β, finding ground states basically requires β to be infinity (or exponential with system size), which in turn requires infinite (or exponential) number of steps in the simulation.

The problem of simulating quantum dynamics, in the form $e^{-it\hat{H}}$ with a local Hamiltonian operator $\hat{H}$, is systematically analyzed by Lloyd in 1996 [108]. Lloyd refined Feynman's study as the conjecture that *quantum computers could provide efficient simulations not of arbitrary quantum systems but of systems that evolve according to local interactions.* Lloyd confirmed that, the quantum simulation takes resources of quantum computer time and memory space directly proportional to the time and space taken up by the system to be simulated. Also the problem of simulating quantum dynamics specified by local Hamiltonian is in BQP and probably outside P. This can be understood as follows. In terms of matrix, the simulation of dynamics is to multiply a sequence of matrices. Matrix multiplication can be naturally executed on quantum computers since composition of quantum gates is a matrix multiplication operation. While on classical computers matrix multiplication is carried out by addition and multiplication for the matrix elements, which is ploynomial of the size of the matrix [103], i.e. the Hilbert space dimension, thus exponential of the number of quantum particles.

The quantum simulation of local Hamiltonian dynamics has been extended to sparse Hamiltonian without a tensor-product structure [3, 13], and non-sparse Hamiltonian yet with some other well-defined properties [40]. In general, if a Hamiltonian is specified by an efficient number of parameters, then the dynamics can be efficiently simulated on a quantum computer. At the same time, if a unitary operator U [1] is provided without a Hamiltonian, then the quantum circuit for simulating U is efficient if U contains an efficient number of

[1] In this thesis by 'unitary' operator we always mean 'special unitary' operator, i.e., we ignore the global overall phase factor.

parameters [123], while in general the simulation of U is inefficient [9, 123].

1.1.2 Quantum computation vs. quantum simulation

At this stage, let us explain the notion of simulation in a general sense before our further study on the quantum case. Simulation has quite a long history in computer science, such as in the field of computer simulation [8, 113, 150], since it is a very useful methodology for many studies, e.g., when the simulated objects are not accessible [150]. In general terms, simulation is a task to use a system to reproduce the properties of another system, e.g., the dynamics over time [150]. Put differently, simulation is a correspondence between the simulator and the simulated system, and there exists a 'mapping', which may not be exact, between the two systems. If the system being used for the simulation is a computer, or a network of computers, the simulation is known as computer simulation. Note that the task of simulation varies in practice, e.g., ranging from being a scientific method of inquiry involving experiments with a model rather than with the portion of reality that the model represents, to a methodology for extracting information from a model by observing the behavior of the model as it is executed [150]. Various simulations based on different methods have been developed for different purposes, such as the process simulation [136], categorical simulation [46], stochastic simulation [61], and deterministic simulation [132].

The field of quantum simulation [33, 60] has been developed rather independently of the simulation in computer science and other fields, and it has been seldom investigated whether those different kinds of simulations mentioned above, such as the process simulation, can be properly generalized to quantum simulation. The comparison between the quantum and classical cases would be interesting, which, yet, is beyond the scope of this thesis. However, the basic notion of simulation carries over straightforwardly to the quantum case. The task of quantum simulation is to use quantum computers, universal or not, to reproduce the properties of other systems, and in particular, we are interested in the quantum simulation of models of quantum systems, which is also the basic motivation of Feynman [56]. As in

the classical case, there could be various kinds of quantum simulations depending on different simulation methods and purposes. Quantum computer can be viewed as a *universal quantum simulator*, as hinted by Feynman [56] and also Lloyd [108], which can in principle execute any quantum simulation algorithms. While quantum simulator only accepts particular objects to be simulated, or in other words, quantum simulator is a *nonuniversal quantum computer*. From the perspective of algorithm, quantum simulation algorithm is a special type of quantum algorithms that can be executed on quantum computers.

We find that it is helpful to recall the basic criteria for quantum computation, known as DiVincenzo criteria [50], which mainly contain five criteria. (1) Stability. Physical qubit needs to be stable for logical qubit. (2) Coherence. The dynamics needs to be coherent and can be coherently controlled. (3) Initialization. The input needs to be prepared with high fidelity. (4) Universality. There needs to be a universal set of gates. (5) Measurement. The output needs to be read out with high fidelity. In addition, if qubits are encoded with different physical carriers, such as electrons and photons, the ability of reliable transition between flying qubits (i.e. photons) and other qubits is also required. These criteria are also improved by including the requirement on quantum memory [128].

By comparison, the study of the ability of quantum simulators are also under way and criteria for building them have been proposed [33, 44, 74, 60]. In particular, here we review the five criteria of Ref. [44]. (1) Quantum system. There need to be stable systems and coherent dynamics. (2) Initialization. The state of a quantum system needs to be well initialized. (3) Hamiltonian engineering. This means the dynamics needs to be coherent and can be coherently controlled. (4) Detection. The simulation result can be obtained by measurement. (5) Verification. This means the output is trustable. We can notice that there is no criterion on universality, which is stronger than verification, and the absence of universality indicates that fault-tolerant protection of quantum gates may not be necessary. The task of building quantum simulators is also viewed as a short-term goal [44], since a

general-purpose quantum computer requires many components such as quantum memory.

1.1.3 Digital vs. analog quantum simulations

Now we can focus on quantum simulators, and we first discuss the basic classification of quantum simulations, which has already been touched upon by Feynman and also Lloyd. Feynman [56] observed that many-body systems in condensed matter physics can imitate quantum field systems. For instance, the spin wave in a spin lattice can imitate bosons in the field theory. Feynman did not intend to make a distinction between simulation and imitation, also digital and analog simulation, though. Lloyd [108] discussed analog simulation, particularly, when considering dissipation effects he stated that the effect of the environment on a system can be mimicked by the effect of the computer's environment on the computer.

For a better understanding of the difference between digital and analog simulations, first we recall the two notions in the classical case. There are both analog and digital classical simulators. For instance, an electrical simulator that uses electrical circuits can be employed to model the dynamics of a mechanical system based on the similarity between linear mechanical components such as springs and electrical components such as capacitors, inductors, and resistors [81]. As an analog simulator contains continuous parameters in $\mathbb{R}$ instead of just $\mathbb{Z}_2$, there would be analog noise on these continuous parameters, and the simulation cannot be reliably repeated with exact equivalence. In contrast, digital simulator encodes quantities as strings of bits and performs gate-array computation. Instead of analog noise, there are discrete noises on the digital bits and gates.

In the quantum case, we would like to point out that the notions of analog and digital for quantum simulators are similar, while not exactly the same with those for classical simulators. For quantum simulation, a digital quantum simulator usually employs simulation based on qubits and a sequence of discrete-time elementary quantum gates, while a simulation with a sequence of gates generated by Hamiltonians is also treated to be digital [102]. Analog quantum simulation is to use a quantum simulator to mimic the dynamics of another well-

defined dynamics, without encoding all the information of the problem as strings of qubits. For instance, a superconducting circuit can be modeled as a quantum harmonic oscillator. As a result, a superconductor quantum simulator can be employed to simulate the dynamics of quantum harmonic oscillators [126]. Atomic simulators that use atoms in optical lattice or trapped ions can be employed to simulate many-body dynamics including the quantum Ising chain, the Heisenberg model, and the Hubbard model [27, 104, 105, 172].

However, the reliability of analog quantum simulators is limited [74]. Also analog quantum simulators do not allow general error correction for quantum computing, which is in principle designed for digital information processing. Therefore, we focus on digital quantum simulation. However, analog quantum simulation is still a valuable task for quantum computing especially for experimentalists to build near-term nonuniversal quantum computers.

1.1.4 Algorithmic vs. non-algorithmic quantum simulations

Now we can focus on digital quantum simulation, which basically is a task to construct quantum simulation algorithms to be executed on quantum computers. For digital quantum simulation, there could also be different simulation tasks. Here we clarify as algorithmic and non-algorithmic quantum simulations.

Non-algorithmic quantum simulation does not require the representation of a simulated system as input of a classical algorithm for the design of a quantum circuit. Instead, it often aims to design a quantum circuit to construct some quantum dynamics. An example would be helpful here. For instance, one wants to simulate the amplitude-damping channel non-algorithmically. As the mathematical formula for amplitude-damping channel is known [123], we then design and implement a quantum circuit for this channel with some chosen parameters. By tuning the parameters, one can sample different amplitude-damping channels. The exact process realized by the simulator circuit can be obtained by process tomography. For non-algorithmic simulation, there is actually no promised simulated object. Instead, the simulator "simulates itself" and the simulated process can only be known after

the execution of the simulation.

Algorithmic quantum simulation is to simulate a system with the representation of the simulated system as the input of a classical circuit-design algorithm. The simulation accuracy can be obtained and well controlled. Algorithmic quantum simulation contain three stages. First, a classical preprocessing stage, which is a classical algorithm for the design of quantum circuit. Second, a quantum stage, which is to perform the quantum circuit. Third, a postprocessing stage, which can be quantum or classical depending on different problems; e.g., it can be measurement, state (or process) tomography, or an algorithm to analyze the output of the circuit or measurement. Compared with the non-algorithmic case, we can see that the simulated system is given as input before the execution of the simulation, instead of as output of the simulation.

In light of solving or simulating quantum physics, algorithmic quantum simulation is promising, at least for the following two reasons. First, a quantum simulator could provide some computational ability by taking a simulated object and the simulation accuracy as input, and it may yield output that contains some unknown information before the simulation. Second, due to its potential computational ability, quantum simulators can solve some problems faster than classical computers, such as local Hamiltonian evolution simulation [108].

In order to emphasize the essence of algorithmic quantum simulation, next we make a connection of algorithmic quantum simulation with the problem of local Hamiltonian evolution simulation, which was the primary problem considered by Feynman [56] and Lloyd [108]. The basic technique employed by Lloyd is the Trotter formula [158], which can be improved with Suzuki's higher-order expansion formula [153].

Consider this problem: construct an efficient classical algorithm which designs efficient quantum circuit to approximate a given k-local Hamiltonian evolution $e^{-it\hat{H}}$ on an n-qudit system within accuracy ϵ. The Hamiltonian $\hat{H}$ is specified by a set of local terms $\{\hat{H}_i\}$ as $\hat{H} = \sum_{i=1}^{m} \hat{H}_i$, each $\hat{H}_i$ acting on at most $k \in O(\log n)$ qudits, and $m \in O(n^k)$. The classical

algorithm takes the description of $\hat{H}$, t, n, d, k, and ϵ as input, and then use the Trotter-Suzuki formula to decompose $U := e^{-it\hat{H}}$ as a product sequence $U_r := \prod_i e^{-it_i\hat{H}_i}$ such that the distance between U and U_r, quantified by the spectral norm or trace distance, is bounded by ϵ [13, 135]. Each exponent $e^{-it_i\hat{H}_i}$ can be further decomposed into product sequence of single-qubit rotations and controlled-NOT (CNOT) gates based on matrix decomposition techniques [123]. Finally single-qubit rotations can be further decomposed into product sequences of gates from a universal set, such as the set $\{\mathrm{T}, \mathrm{H}\}$ of the Hadamard gate H and $\mathrm{T} := Z^{1/4}$ gate, according to the Solovay-Kitaev theorem and algorithm [49, 92, 123]. Then the quantum circuit that is composed by gates from the set $\{\mathrm{CNOT}, \mathrm{T}, \mathrm{H}\}$ is executed so that the output states are good enough to approximate the true final states.

Efficient simulation here means that the simulation uses resources such as space and time that do not scale exponentially with the problem size. The efficiency of the classical algorithm means that the procedure using the Trotter-Suzuki formula is efficient, and the efficiency of the quantum circuit means that the size of the circuit, e.g. number of gates, scales polynomially with respect to any of the input. However, the scaling with respect to $\log \frac{1}{\epsilon}$ is exponential, i.e. polynomial with $\frac{1}{\epsilon}$, which is a main drawback of the algorithm based on the Trotter-Suzuki formula. An exponential improvement has been achieved recently using the Taylor expansion [15].

1.1.5 Classification of quantum simulations

Actually, to classify quantum simulation as digital and analog types is too rough, since some protocols cannot easily fit into this framework, such as simulations protocols based on other universal quantum computing models [17]. The simulation for fermionic systems based on Jordan-Wigner transformation [84, 151], which builds a duality equivalence relation between qubits systems and fermionic systems, is analog due to such a duality, while can also be digital if a digital method is employed to perform the qubit-based quantum circuits. The simulation for observable effects can be analog if some duality relations are employed. For

Figure 1.1: The three stages in standard quantum computation: preparation, evolution, and measurement.

instance, an open-system quantum simulator can be used to calculate observable effects for a dual many-body system based on matrix-product state framework [10], while the open-system quantum simulator can also be designed to be a digital simulator.

In this thesis, we do not intend to provide a systematic classification of various quantum simulations, which is not an easy task. However, we find that indeed there could be a type of classification regarding different simulation objects corresponding to different quantum computing processes, explained below.

Quantum computing process in general includes three stages: preparation, evolution, and measurement, depicted in Fig. 1.1. As a result, quantum simulation problems can be considered by involving different stages of a quantum computing process. For instance, the implementation of measurement, described by positive operator-valued measure (POVM) [123], can be formalized as a quantum simulation problem, and methods have been proposed such as the one using a convex sum of projectors [147]. Also quantum state generations, corresponding to the preparation stage or treated as the output of the computation after measurement, can also be considered as quantum simulation problems [5, 30, 55, 173]. It is clear that the local Hamiltonian evolution simulation problem [13, 108] corresponds to the second stage of a quantum computing process.

We find that different quantum simulations can be defined by considering the simulations involving different stages of a quantum computing process. It turns out, mathematically, this corresponds to defining quantum simulation based on different operator topologies on

a Hilbert space [18]. There exist three types of commonly used operator topologies: the uniform (or norm), strong, and weak operator topologies. Accordingly, we construct three different kinds of quantum simulations, namely, uniform, strong, and weak quantum simulations.

Generally, given an operator $\hat{T}$, the uniform simulation of it is to approximate the operator $\hat{T}$ itself, and the strong simulation is to approximate the effects of $\hat{T}$ on something else, while the weak simulation is to approximate the observable effects of $\hat{T}$. For instance, given a unitary operator U, the uniform simulation is to approximately generate or prepare U, and the strong simulation is to approximate the effects of U on quantum states, while the weak simulation is to approximate the measurement effects on the final states generated by U. It is quite straightforward to see that there exists an "order" on the simulation abilities of them: the uniform simulation is stronger than the strong simulation, which is in turn stronger than the weak simulation. For instance, once the evolution U can be accurately simulated, we can safely infer that the observable effects on final states can also be simulated, although no direct simulation of observable effects are performed.

Considering different simulations can provide us more alternatives for constructing quantum simulation schemes. For instance, the weak quantum simulation is more suitable in the setting of physics, since usually one mainly cares about observable effects of a certain underlying quantum process. As a result, one can simulate observable effects without the simulation of the dynamics directly. In this sense, the simulation methods discussed above based on duality, including the one by Jordan-Wigner transformation [84, 151] and the one by matrix-product state [10], are weak simulation since the simulator would only yield approximate observable effects, rather than simulating the desired process itself.

The uniform simulation has a close connection with tomography. Quantum tomography [123], such as state tomography and process tomography, aims to determine the formula of the state or process. The uniform simulation considers the approximation of one object

(state, process, or observable) itself, instead of simulating its effects on something else. As uniform simulation is the strongest one, it may help to study the ability and limitation of quantum computers or simulators, as will be studied in Chapter 8.

1.2 Algorithmic quantum simulation of quantum channels

We now turn to explain algorithmic quantum simulation of quantum channels. Firstly, we explain how quantum channel characterizes quantum processes in §1.2.1, and then we motivate nonunitary quantum simulation in §1.2.2. For our problem, in §1.2.3 we highlight the main challenges we have encountered, and finally we address some promising applications of quantum channel simulators in §1.2.4.

1.2.1 Quantum processes characterized by quantum channels

In this thesis, we consider finite-dimensional quantum system and the quantum simulation of the most general dynamics of quantum system. A finite-dimensional pure quantum state is usually denoted as $|\psi\rangle \in \mathscr{H}$ for a Hilbert space $\mathscr{H}$. Given a Hamiltonian $\hat{H}$, assumed to be time independent, the Schrödinger equation for the evolution is

$$i|\dot{\psi}\rangle = \hat{H}|\psi\rangle. \tag{1.1}$$

Define the unitary evolution operator $U = e^{-it\hat{H}}$, and then $|\psi_t\rangle = U|\psi_0\rangle$ with initial state $|\psi_0\rangle$ at time $t = 0$ and final state $|\psi_t\rangle$ at time t. Note there is the 'hat' symbol on the Hamiltonian, which is a generator, while no hat on evolution operator. We also follow this convention across this thesis, that we do not put hat on evolution operator and also quantum state. Also we let Planck constant $\hbar \equiv 1$.

A more general quantum state is represented by density operator ρ, which is a positive semidefinite trace class operator acting on $\mathscr{H}$. That is, $\rho \geq 0$, and $\mathrm{tr}\rho = 1$. Denote the set of density operators as $\mathscr{D}(\mathscr{H})$, sometimes $\mathscr{D}$ for simplicity, which is a proper subset of the

set of all bounded linear operators acting on $\mathscr{H}$, denoted as $\mathscr{L}(\mathscr{H})$. The quantum evolution is specified by the Liouville-von Neumann equation

$$i\dot{\rho} = [\hat{H}, \rho], \tag{1.2}$$

where the brackets denote a commutator and $[\hat{H}, \rho] = \hat{H}\rho - \rho\hat{H}$. Analog to the pure state case, let the so called Liouvillian superoperator be defined as $\mathcal{L}\bullet := -i[\hat{H}, \bullet]$, which can also be generalized to nonunitary case, then the Liouville-von Neumann equation becomes

$$\dot{\rho} = \mathcal{L}\rho. \tag{1.3}$$

The solution can be obtained as $\rho_t = e^{t\mathcal{L}}\rho_0 = U\rho_0 U^\dagger$ for $U = e^{-it\hat{H}}$ and initial state ρ_0 at time $t = 0$ and final state ρ_t at time t.

The merit of the Liouvillian superoperator form is that it is straightforward to generalize to the nonunitary case. From the conditions of completely positive, trace preserving mappings, and one-parameter semigroup, Lindblad [107], and also Gorini, Kossakowski, Sudarshan (GKS) [65], derived the most general type of Markovian and time-homogeneous quantum master equation as

$$\dot{\rho} = \mathcal{L}\rho = -i[\hat{H}, \rho] + \sum_{i,j=1}^{d^2-1} G_{ij}\left(F_i\rho F_j^\dagger - \frac{1}{2}\left\{F_j^\dagger F_i, \rho\right\}\right) \tag{1.4}$$

for $d := \dim\mathscr{H}$, $\{F_i\}$ as an operator basis for $\mathscr{L}(\mathscr{H})$, and G_{ij} form a positive semidefinite matrix G, known as the GKS matrix. Furthermore, G can be diagonalized as $VGV^\dagger = \mathrm{diag}(\gamma_1, \gamma_2, \ldots, \gamma_{d^2-1})$ for a basis transformation V. Then we arrive at the diagonal form of quantum master equation

$$\dot{\rho} = \mathcal{L}\rho = -i[\hat{H}, \rho] + \sum_{k=1}^{d^2-1} \gamma_k\left(L_k\rho L_k^\dagger - \frac{1}{2}\left\{L_k^\dagger L_k, \rho\right\}\right), \tag{1.5}$$

with Lindblad operators L_k and $F_i = \sum_{k=1}^{d^2-1} V_{ki}L_k$. The solution can still be expressed as $\rho_t = e^{t\mathcal{L}}\rho_0$, while more algebra are required to actually compute this expression.

There are also quantum processes that do not contain the time variable t explicitly. As in the classical case, there are bother discrete-time and continuous-time Markovian processes in

probability theory. Discrete-time processes, called discrete processes for short, are common in quantum computation. A quantum circuit comprises a sequence of quantum gates, and the execution of gates represents time evolution. Usually, it is assumed that there is no time evolution between any two sequential gates, and each gate occupies a certain time interval. Also quantum measurement described by POVM is usually treated as a discrete process. In general, a discrete quantum process is characterized by a completely positive, trace preserving (CPTP) mapping, known as quantum channel $\mathcal{E}$

$$\mathcal{E}(\rho) = \sum_{i=0}^{r-1} K_i \rho K_i^\dagger \tag{1.6}$$

for all qudit states $\rho \in \mathscr{D}(\mathscr{H})$ with a set of Kraus operators [98] K_i such that

$$\sum_{i=0}^{r-1} K_i^\dagger K_i = \mathbb{1}. \tag{1.7}$$

When the set $\{K_i\}$ is linearly independent, the form (1.6) is canonical [42] and $r \leq d^2$ is called the Kraus rank of the channel $\mathcal{E}$.

It is widely accepted that so far quantum channel provides the most general characterization of (nonrelativistic) quantum processes, which could be unitary or not. Quantum channels include the unitary evolution, Markovian dynamics and also quantum measurement as special cases. A channel is unitary when there is only one Kraus operator that is unitary. The Markovian dynamics specified by the quantum master equation (1.4) can be derived from the formula (1.6) with the one-parameter semigroup property [26]. For any POVM $\{M_i\}$ with $\sum_i M_i = \mathbb{1}$ and $M_i \geq 0$, a set of Kraus operators K_i can be found, although not unique, such that $M_i = K_i^\dagger K_i$. Then the POVM can be performed by the realization of a channel defined by the set $\{K_i\}$.

It turns out a nonunitary quantum channel can be converted into a unitary evolution acting on an extended space, following from Stinespring's seminal result [152]. Given a system S, a quantum channel $\mathcal{E}$ acting on it can be realized by the interaction, specified by

a unitary evolution U, with one ancillary system A prepared in state σ such that

$$\mathcal{E} : \mathscr{D}(\mathscr{H}) \to \mathscr{D}(\mathscr{H}) : \rho \mapsto \mathcal{E}(\rho) = \mathrm{tr}_{\mathrm{A}} U(\rho \otimes \sigma)U^{\dagger}. \tag{1.8}$$

Usually, the ancilla state σ is chosen as the ground state $|0\rangle\langle 0|$, and then the Kraus operators take the form $K_i = \langle i|U|0\rangle$. The dimension of the ancilla is maximally d^2, which is the upper bound on the rank of $\mathcal{E}$.

Nonunitary processes characterized by CPTP mappings play important roles in quantum physics. For instance, the spontaneous emission of an atom is a dissipative nonunitary process, and can be described by the quantum master equation [37]. In quantum thermodynamics [59], usually we consider a quantum system weakly interacting with a large heat bath, and the quantum thermal processes are nonunitary and can be described by quantum channels. In many-body physics, dissipation can also play a crucial role such as in quantum phase transitions [134].

In addition, situations for infinite-dimensional quantum systems, such as a quantum harmonic oscillator, are not considered in this thesis, while those dynamics can be converted to finite-dimensional versions by the truncation of Hilbert space. For instance, the Schrödinger evolution for a harmonic oscillator

$$i\dot{\psi}(x) = \hat{H}(x)\psi(x) \tag{1.9}$$

with Hamiltonian $\hat{H}(x) = -\frac{1}{2m}\frac{d^2}{dx^2} + \frac{1}{2}m\omega^2 x^2$ and wave function $\psi(x) \in L^2(\mathbb{R})$ can be discretized with alternative methods [175, 176, 181], whereas the Hilbert space $L^2(\mathbb{R})$ is replaced by an n-qubit Hilbert space for some integer n, and $\psi(x)$ and $\hat{H}(x)$ are approximately encoded by an n-qubit state and Hamiltonian, respectively. This discretization and truncation procedure is also an ingredient for the quantum simulation of dynamics characterized by quantum field theory [85].

1.2.2 From unitary to nonunitary quantum simulation

The Hamiltonian evolution simulation has been the main focus for quantum simulation problems, since a quantum physical system is usually represented by a Hamiltonian. When dissipations are present in practice, the resulting nonunitary processes are often described by the quantum master equation (1.4). The Hamiltonian evolution simulation algorithm based on the Trotter-Suzuki decomposition [13, 135] has been generalized to the Markovian dynamics simulation using a superoperator version of the Trotter-Suzuki decomposition [93] or breaking the dynamics into the Hamiltonian evolution part and the Lindblad jump operators [172]. Although quantum master equation (1.4) is important, it cannot describe non-Markovian processes, wherein memory effects are particularly important [26, 41, 116].

In light of quantum channel simulation, we do not necessarily need to confine to the Hamiltonian evolution simulation. Indeed, quantum computation and also general quantum physics is more suitable to be formalized in an operational framework [36, 98]. A classical system or statistical system is usually characterized by its Hamiltonian. The dynamics of a classical particle in phase space is completely determined by the Hamiltonian. Also the properties of a thermodynamical system can be obtained once the Hamiltonian is known; e.g., the partition function is $Z = \mathrm{tr} e^{-\beta H}$ with β as the reciprocal of the thermodynamic temperature, and all other quantities can be obtained. However, it is drastically different for the quantum case, in which it is the quantum state that provides the complete description. A Hamiltonian can represent the energy, and also the evolution only for the unitary case. Instead, the formalism with density operator and quantum channel, which can be obtained by tomography [123], provides the complete description of quantum system and its dynamics, without any mention of Hamiltonian of the system.

Due to the importance of quantum channels in quantum physics, it is necessary to develop quantum simulation algorithms for quantum channels, and quantum channel simulation would be an important part in quantum simulation and quantum computation. Indeed,

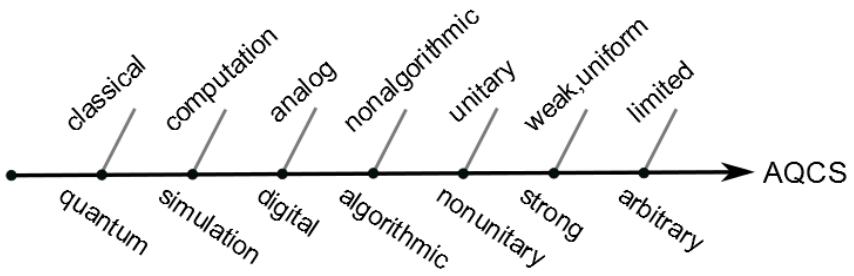

Figure 1.2: The diagram to show the "binary-tree" for determining the topics of this thesis. AQCS represents algorithmic quantum channel simulation.

quantum computation based on channels and mixed states has been formalized [2], which is shown to be equivalent in computational ability to standard unitary quantum circuits. Furthermore, a model called *dissipative quantum computing* [165] is proposed, which showed that a quantum Markovian dynamics can be designed to simulate a given arbitrary unitary quantum circuit with a ploynomial overhead. Also in the framework of quantum circuit model, quantum channel simulation is more natural than Hamiltonian evolution simulation, since a quantum channel is a discrete process, while a Hamiltonian evolution contains time.

Those discussions above serve as a reasoning for why and how we choose the subject of this thesis, which is the algorithmic quantum simulation of quantum channels, or shortly, *algorithmic quantum channel simulation* (AQCS), and this logic flow is shown in Fig. 1.2.

1.2.3 Challenges and our basic methods

For our main problem of algorithmic quantum channel simulation, we are interested in developing a classical algorithm that designs quantum circuit for the channel simulator. This framework is depicted in Fig. 1.3. The input to the classical algorithm $\mathcal{A}$ include the dimension of the system d, the description of a channel $\mathcal{E}$, and the simulation error tolerance ϵ. The output of the classical algorithm is the description of the quantum circuit that specifies the simulator $\tilde{\mathcal{E}}$. For this general purpose, there are several challenging problems and we describe them as well as our strategies as follows.

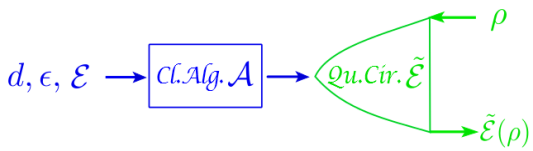

Figure 1.3: The quantum channel simulation problem. The classical algorithm $\mathcal{A}$ (blue color) takes the dimension d, error tolerance ϵ, and the description of a channel $\mathcal{E}$ as input, and yields a quantum circuit to realize $\tilde{\mathcal{E}}$ (green color) as an approximation of $\mathcal{E}$. The quantum circuit takes arbitrary input state ρ and then yields $\tilde{\mathcal{E}}(\rho)$ as output. The arrows represent input and output.

The classical algorithm should be efficient with respect to the problem size, e.g., the inverse error tolerance $1/\epsilon$ and the dimension d. The quantum circuit for the simulator accepts arbitrary system state ρ and outputs the final state $\tilde{\mathcal{E}}(\rho)$, which is within the error tolerance ϵ to the ideal final state $\mathcal{E}(\rho)$. The quantum circuit should also be efficient with respect to the problem size. Furthermore, usually there are tighter restrictions on the simulation efficiency. The scaling with respect to ϵ should be a polynomial of $\log(1/\epsilon)$ instead of just a polynomial of $1/\epsilon$. There is an exponential difference between these two cases. The reason is that, if let $\epsilon = c10^{-a}$, a polynomial of $\log(1/\epsilon)$ becomes a polynomial of a, which basically represents the exponent of ϵ, while a polynomial of $1/\epsilon$ is exponential with a. At the same time, the scaling with respect to d should be a polynomial of $\log d$ instead of just a polynomial of d, since $\log d$ corresponds to the number of subsystems, which is commonly treated as the physical size in practice. We find that for the simulation of a general quantum channel, it is possible to have a quantum circuit efficient with respect to $\log(1/\epsilon)$, while it is only possible to be efficient with respect to d instead of $\log d$.

We are also interested in the quantum channel simulation using as few resources as possible. For the simulation of a general unitary channel, the quantum circuit cost, which is the number of CNOT and qubit gates, scales as $O(d^2)$ [9]. We ask the question of whether it is possible to achieve this scaling for circuit cost pertaining to the quantum channel

simulation. Standard dilation method [123, 152] would lead to a unitary operator acting on a larger Hilbert space, thus rendering the cost $O(d^2)$ not achievable. There are also other methods, which are discussed in Chapter 4, while they all have some drawbacks and bottlenecks. We find that the method of channel decomposition in terms of convex sum of (generalized) extreme channels is appealing and promising, which simulates a channel by classical mixing of several smaller channels.

One major problem is to develop channel decomposition based on extreme channel theory. The set of quantum channels is convex, while there are uncountably infinite number of extreme points. Convex set property ensures that there always exists a convex sum decomposition in terms of extreme channels for a given channel, yet we actually do not know how many extreme channels are needed in general. It is conjectured that, in terms of generalized extreme channels, a qudit quantum channel can be written as a convex sum of up to d generalized extreme channels [139]. The conjecture is true for the qubit case [140], while it is still an open problem for the general cases. For the quantum channel simulation purpose, we develop a classical optimization algorithm and rely on the conjecture to design quantum channel simulators. We have performed numerical simulation for low dimensional cases, including qubit, qutrit, and two-qubit, and the simulation confirms our method and also provides support for the channel decomposition conjecture.

Our knowledge of extreme channels are quite limited, for instance, there is no concise characterization of them suitable for quantum simulation purpose. Our primary strategy is that we construct a Kraus operator-sum representation as well as a quantum circuit representation for arbitrary extreme channels. Our construction may not be the unique construction, while it does not matter whether it is unique or not since in general the decomposition of a unitary matrix is not unique [64]. The quantum circuit representation for extreme channels are used in the classical optimization algorithm for the design of the simulator.

1.2.4 Applications of quantum channel simulators

We now turn to the final aspect, which is also the eventual concern of our study, the application of quantum simulators, and particularly, quantum channel simulators.

Quantum simulators are useful for both quantitative and qualitative studies. A well-controlled simulator whose simulation accuracy can be assessed can be used for quantitative studies for particular kind of processes, such as single-qubit channels. A simulator of arbitrary single-qubit channels can be used as a quantum noise generator, which can be further employed for the test of robustness and other properties of various protocols [112, 155]. The Hamiltonian evolution simulators can be used to generate quantum states, simulate Markovian dynamics [172], and also for mathematical problems such as solving linear equations [71].

Analog quantum simulators whose simulation accuracy cannot be well controlled can be used for qualitative studies [6, 19, 44, 74]. For instance, by engineering a system such as trapped ions to behave similarly to a target system such as the Hubbard model or quantum field theories [27, 38, 39, 63, 99], one can obtain some heuristic understandings of the unknown properties of those models.

It is not easy to imagine the possible applications of quantum channel simulators in the future, since for now our understandings of quantum channels and simulators are still not good enough. But, some applications are straightforwardly forseeable. Quantum channel simulators could have broader applications than Hamiltonian evolution simulators. Examples that are within the ability of channel simulators while probably outside the range of Hamiltonian evolution simulators are discussed below.

First, quantum channel simulators can serve as specific quantum state generators. For instance, in dissipative quantum computing [165] it is shown that a dissipative quantum computer can be used to efficiently generate the ground states for some local Hamiltonian. Also quantum channel simulators can prepare quantum states represented by matrix-product

states. It is shown that [143] any matrix-product state can be treated as the output of a quantum circuit acting on the system and an ancilla, which contains a sequence of two-body unitary operators, and each of them is actually the dilation of a quantum channel acting on the ancilla. Second, quantum channel simulators can serve as quantum noise generator to test properties of quantum protocols, such as the robustness against decoherence [112, 155]. Third, quantum channel simulators can be employed for the study of dissipative quantum dynamics, such as non-Markovian effects, quantum thermodynamics and dissipative quantum phase transition.

1.3 Summary of results and significance

In this thesis, for the purpose of algorithmic quantum channel simulation, we have obtained the following results.

First, we have improved the Solovay-Kitaev algorithm [49, 92, 123], which is one of the most important and primary algorithms for single-qubit unitary gate compiling as a product of gates from a universal gate library. Particularly, we have built up a lookup database that can be used for the initial step of Solovay-Kitaev algorithm, and also a geometric search method to address a specific data point in the database. This result is discussed in Chapter 3.

Second, we have developed a single-qubit quantum channel simulator. Particularly, we designed a classical algorithm that takes an arbitrary qubit channel to be simulated and the simulation accuracy as input, and employs a channel decomposition in terms of convex sum of two (generalized) extreme qubit channels, and then delivers the quantum circuit for the simulator. Our simulator is deterministic in that it does not require post-selection, and universal in that it can be used to simulate arbitrary qubit channels instead of particular types. Our simulator is also, as far as we know, the most economic one, if not optimal, that it only consumes one CNOT gate, one ancillary qubit, and several qubit rotations, together with one classical bit and classical feedback. This result is discussed in Chapter 5. A photonic

realization of our simulator has also been achieved, which is presented in Chapter 6.

Third, we have developed a general algorithm for the algorithmic simulation of arbitrary qudit channels. This result is a generalization of the qubit channel simulation. In order to employ the convex sum decomposition of qudit channels, we have developed the Kraus operator-sum, quantum circuit, and also Choi state representations of arbitrary generalized extreme channels. Our classical algorithm for the channel decomposition is formalized as an optimization problem, which, however, should scale at least quadratically with the dimension d. The quantum circuit for realizing an extreme channel contains in general $O(d^2)$ primary quantum gates. Similar with the qubit case, our qudit channel simulator also consumes classical bits and requires classical feedback to save the cost of quantum resources. These results are discussed in Chapter 4 and also Chapter 7.

Forth, regarding the concepts of quantum simulations, we have proposed three different notions, namely, uniform, strong, and weak quantum simulations according to operator topologies on a Hilbert space. Particularly, we have proposed a general weak quantum simulation problem and then an algorithm for it. Also we have proposed the quantum channel simulation problem in the uniform quantum simulation framework, and algorithms to solve this problem. These results are discussed in Chapter 8.

Our results have the following significance. First, we have developed the general framework for algorithmic quantum channel simulation, which is a different simulation framework from the Hamiltonian evolution simulation, and could have broader applications than the latter. Also the simulation method is algorithmic (accept accuracy as input), universal (accept arbitrary channel as input), deterministic (no post-selection), and economic (reducing simulation cost as better as one can).

Second, we have developed the quantum channel decomposition method in terms of convex sum of generalized extreme channels. It is conjectured that [139] a qudit channel can be decomposed into a convex sum of up to d generalized extreme channels, while an

analytical form for the channel decomposition is unknown, and whether the conjecture is true or false is still an open problem. Our decomposition algorithm for the low-dimensional cases support this conjecture, and our construction of (generalized) extreme channels may serve as a step towards the final solution of this problem, which has a fundamental implication to the understanding of quantum channels.

Third, our definitions of different quantum simulations provide a systematic way of understanding quantum simulation problems and also the design of quantum simulation algorithms. Different simulation methods can be chosen for different purposes in practice. Also it is known that different simulations of quantum computing processes by classical computers can manifest gaps on simulation efficiency [24, 161], it would be important to explore whether such gaps on simulation efficiency exist for the quantum simulation of quantum processes in different simulation frameworks.

1.4 Structure

This thesis contains the following parts. Chapter 2 contains the most relevant background knowledge for the purpose of this thesis. We present the definitions and basic properties for quantum states and quantum channels, and then discuss distance measures on operators. We then analyze the convex set property of quantum channels.

Chapter 3 presents our study of Solovay-Kitaev algorithm. We first review the definition of universality and the Solovay-Kitaev theorem, and then we present our work on lookup database (table), which can be used to initiate the Solovay-Kitaev algorithm. In the discussion part, we briefly discuss some possible improvements on our lookup table, and some alternative qubit gate compiling methods.

Chapter 4 systematically studies the problem of channel simulation. We first study the properties of extreme channels and also generalized extreme channels, and then we present the constructions for generalized extreme channels, including Kraus operator-sum, quantum

circuit, and Choi state representations. Next we present the framework for algorithmic quantum channel simulation, with a classical optimization for the channel decomposition and the analysis of complexity. We also perform a comparison with other available simulation methods, and highlight the merits and drawbacks for various methods.

Chapter 5 contains our results on single-qubit quantum channel simulation. We first review the theory developed by Ruskai, Szarek, and Werner [140] and highlight the differences from our approach. We then study the classical algorithm for the design of quantum simulator circuit and the properties of the qubit channel simulator.

Chapter 6 presents the construction of photonic qubit channel simulator. The simulations of some particularly well known qubit channels are performed. In particular, we simulate some interesting protocols, including the simulation of weak measurement process for superposition protection and the simulation of an approximated transpose operation.

Chapter 7 focuses on the simulation of qutrit and two-qubit quantum channels in terms of convex sum of generalized extreme channels. We study the qutrit case first and then the two-qubit case. For both cases, we present the details for the generalized extreme channels, and classifications of special generalized extreme channels. Numerical simulation results are also discussed.

Chapter 8 presents the studies on alternative concepts of quantum simulations. The definitions of uniform, strong, and weak quantum simulations are firstly presented. Next a channel simulation problem in the weak quantum simulation framework is proposed, and then a quantum algorithm to address the weak quantum simulation problem is constructed. Furthermore, a uniform channel simulation problem in the quantum query model is also presented.

Chapter 9 concludes this thesis. We present a brief review and discussion of the main results in this thesis, and then we focus on some possible improvement of our results, and also some valuable developments along the research line of this thesis.

Chapter 2

Background

In this chapter, we intend to present some primary results that would be used in later chapters. We review the definitions and basic properties for quantum states and quantum channels firstly in §2.1, and then discuss distance measures on operators and superoperators in §2.2. Also we present some inequalities that play crucial roles for quantum channel simulation problems. Furthermore, in §2.3 we analyze the convex set property of quantum channels by firstly drawing connections with some well known convex sets, and then focus on the convex set of quantum channels. We conclude in §2.4.

2.1 Quantum states and quantum channels

2.1.1 Quantum states and operator basis

A d-dimentional pure quantum state $|\psi\rangle \in \mathscr{H}$ can be expressed as

$$|\psi\rangle = \sum_{i=0}^{d-1} c_i |i\rangle, \tag{2.1}$$

for $\{|i\rangle\}$ a basis of the Hilbert space $\mathscr{H}$, $d \in \mathbb{Z}^+$, $d \geq 2$, and the normalization condition $\sum_{i=0}^{d-1} |c_i|^2 = 1$. A density operator ρ, also called mixed state, is a semidefinite positive trace class operator acting on a Hilbert space $\mathscr{H}$, and $\rho \geq 0$, $\mathrm{tr}\rho = 1$. Denote the set of linear operators acting on $\mathscr{H}$ as $\mathscr{L}(\mathscr{H})$, and the set of density operators acting on $\mathscr{H}$ as $\mathscr{D}(\mathscr{H})$, and clearly $\mathscr{D}(\mathscr{H}) \subset \mathscr{L}(\mathscr{H})$. Sometimes we use the shorthand $\mathscr{D}$ for $\mathscr{D}(\mathscr{H})$, also we use $\mathscr{D}_d$ to indicate that the underlying Hilbert space is of dimension d. The space $\mathscr{L}(\mathscr{H})$ is also a Hilbert space with respect to Hilbert-Schmidt inner product

$$\mathrm{tr}(A^\dagger B),\ \forall A, B \in \mathscr{L}(\mathscr{H}). \tag{2.2}$$

A basis for $\mathscr{L}(\mathscr{H})$ is a linearly independent spanning set, denoted as $\{M_\alpha\}_{\alpha=0}^{d^2-1}$, which is an operator basis instead of vector basis. An orthogonal basis is a basis with $\mathrm{tr}(M_\alpha^\dagger M_\beta) = 0$ for $\alpha \neq \beta$. Furthermore, every finite-dimensional inner product space has an orthonormal basis satisfying

$$\mathrm{tr}(M_\alpha^\dagger M_\beta) = d\delta_{\alpha\beta}. \tag{2.3}$$

Note our definition of an orthonormal basis involves the coefficient d, which may be absent following other conventions.

For a clean representation of density operator $\rho \in \mathscr{D}(\mathscr{H})$, there exists such a basis satisfying (i) $M_0 = \mathbb{1}$, (ii) $\mathrm{tr}M_\alpha = 0$ for $\alpha \neq 0$, (iii) $\mathrm{tr}(M_\alpha^\dagger M_\beta) = 0$ for $\alpha \neq \beta$, which is called a trace-free and trace-orthogonal basis [34], and, for simplicity, termed as *canonical* basis here. In a canonical basis, a density operator ρ can be written as

$$\rho = \frac{1}{d}\left(\mathbb{1} + \sum_{\alpha=1}^{d^2-1} \sqrt{\frac{d(d-1)}{\mathrm{tr}(M_\alpha^\dagger M_\alpha)}} p_\alpha M_\alpha\right). \tag{2.4}$$

The parameters p_α form the *polarization vector* $\boldsymbol{p} := (p_1, \ldots, p_{d^2-1})$ with $\|\boldsymbol{p}\| = 1$ for pure state and $\|\boldsymbol{p}\| < 1$ for mixed state. If each M_α is hermitian, $p_\alpha \in \mathbb{R}$. We can see that a canonical basis may be orthonormal or not. For the qubit system, an example of orthonormal as well as canonical basis is the Pauli basis, shown in Example 1.

Another type of basis, which is known as Kronecker basis, is formed by $|i\rangle\langle j|$, which is a matrix with a single entry 1 in ith row and jth column, and all others 0. The Kronecker basis $\{|i\rangle\langle j|\}$ is orthonormal yet not canonical. The merit of this basis is that it is related to the Choi-Jamiołkowski isomorphism [82, 42] $\mathcal{J} : \mathscr{D}(\mathscr{H}) \to \mathscr{H} \otimes \mathscr{H}$, from which $\mathcal{J} : |i\rangle\langle j| \mapsto |i, j\rangle$. The action of this isomorphism on matrices is the same with the reshaping operation [11], which is defined as

$$\mathrm{res}A := (a_{11}, \ldots, a_{1m}, \ldots, a_{m1}, \ldots, a_{mm})^{\mathrm{T}} \tag{2.5}$$

for an $m \times m$ matrix $A = [a_{ij}]$ with elements a_{ij}. With the inverse of reshaping operation, the matrix A can be obtained from the vector res$A$, i.e., $\mathrm{res}^{-1}(\mathrm{res}A) = A$. In addition, a

vectorization operation can be defined such that $\mathrm{vec}A = \mathrm{res}A^{\mathrm{T}}$.

Example 1 (Qubit)**.** *In Pauli basis* $\{\sigma_i\} = \{\mathbb{1}, X, Y, Z\}$ $(i = 0, 1, 2, 3)$ *with*

$$X = \begin{pmatrix} 0 & 1 \\ 1 & 0 \end{pmatrix}, Y = \begin{pmatrix} 0 & -i \\ i & 0 \end{pmatrix}, Z = \begin{pmatrix} 1 & 0 \\ 0 & -1 \end{pmatrix}, \tag{2.6}$$

a qubit state $\rho = \frac{1}{2}(\mathbb{1} + \boldsymbol{p}\cdot\boldsymbol{\sigma})$ *is represented by a real polarization vector* $\boldsymbol{p}$ *for* $\boldsymbol{\sigma} := (X, Y, Z)$.

In Kronecker basis $\{\tau_j\} = \{|0\rangle\langle 0|, |0\rangle\langle 1|, |1\rangle\langle 0|, |1\rangle\langle 1|\}$ $(j = 0, 1, 2, 3)$ *a qubit state* ρ *is represented as a vector*

$$\rho \mapsto \mathrm{res}\rho = (\rho_{00}, \rho_{01}, \rho_{10}, \rho_{11})^{\mathrm{T}}. \tag{2.7}$$

For higher-dimensional cases the Kronecker basis carries over easily, while there are different generalizations of Pauli basis. The Pauli basis is both hermitian and unitary, i.e. self-invertible. There are two well-known canonical bases, one is Gell-Mann basis, which is hermitian, and the other is Heisenberg-Weyl basis, which is unitary. We focus on Heisenberg-Weyl basis, while properties of Gell-Mann basis can be found elsewhere [29, 90, 142].

Definition 2. *The Heisenberg-Weyl basis* $\{M_{jk}\}$ *for a qudit system is specified by*

$$X_j = \sum_{i=0}^{d-1} |i\rangle\langle i + j|, \quad Z_k = \sum_{l=0}^{d-1} \omega^{lk}|l\rangle\langle l| \pmod d, \tag{2.8}$$

for $M_{jk} = X_j Z_k$*, and* $\omega = e^{i2\pi/d}$*,* $j, k \in \{0, \ldots, d-1\}$.

Example 3 (Qutrit)**.** *For qutrit, the Heisenberg-Weyl basis matrices are*

$$M_0 \equiv M_{00} = \mathbb{1}, M_1 \equiv M_{01} = \mathrm{diag}(1, \omega, \omega^2), M_2 \equiv M_{02} = \mathrm{diag}(1, \omega^2, \omega), \tag{2.9}$$

$$M_3 \equiv M_{10} = \begin{pmatrix} 0 & 1 & 0 \\ 0 & 0 & 1 \\ 1 & 0 & 0 \end{pmatrix}, M_4 \equiv M_{11} = \begin{pmatrix} 0 & \omega & 0 \\ 0 & 0 & \omega^2 \\ 1 & 0 & 0 \end{pmatrix}, M_5 \equiv M_{12} = \begin{pmatrix} 0 & \omega^2 & 0 \\ 0 & 0 & \omega \\ 1 & 0 & 0 \end{pmatrix},$$

$$M_6 \equiv M_{20} = \begin{pmatrix} 0 & 0 & 1 \\ 1 & 0 & 0 \\ 0 & 1 & 0 \end{pmatrix}, M_7 \equiv M_{21} = \begin{pmatrix} 0 & 0 & \omega^2 \\ 1 & 0 & 0 \\ 0 & \omega & 0 \end{pmatrix}, M_8 \equiv M_{22} = \begin{pmatrix} 0 & 0 & \omega \\ 1 & 0 & 0 \\ 0 & \omega^2 & 0 \end{pmatrix},$$

and $\omega := e^{i2\pi/3}$*. A qutrit state is represented as*

$$\rho = \frac{1}{3}\left(\mathbb{1} + \sqrt{2}\sum_{\alpha=1}^{8} p_\alpha M_\alpha\right). \tag{2.10}$$

In Kronecker basis, a qutrit state ρ *is just mapped to its reshaping version* resρ*.*

In particular, we will use the Heisenberg-Weyl basis for our study of quantum channel decomposition in Chapter 4, so here we review more properties of it. The following two operators

$$X_1 = \sum_{i=0}^{d-1} |i\rangle\langle i+1|,\ Z_1 = \sum_{l=0}^{d-1} \omega^l |l\rangle\langle l|, \tag{2.11}$$

are the generators for the so-called Heisenberg-Weyl group $\mathcal{G}_{\text{HW}}$ containing group element $\{\omega^{i-jk} M_{jk}\}$ with degree d and order d^3. The center of $\mathcal{G}_{\text{HW}}$ is $\{\omega^{i-jk}\mathbb{1}\}$. The two generators do not commute

$$X_1 Z_1 = \omega Z_1 X_1, \quad \omega = e^{i2\pi/d}. \tag{2.12}$$

The X_1 is sometimes called the "shift" operator, and Z_1 is called the "clock" operator. The order of X_1 and Z_1 is both d

$$X_1^d = \mathbb{1}, \quad Z_1^d = \mathbb{1}. \tag{2.13}$$

The two generators X_1 and Z_1 are related by a Hadamard operator W, understood as discrete Fourier transform

$$W := \frac{1}{\sqrt{d}} \begin{pmatrix} 1 & 1 & 1 & \cdots & 1 \\ 1 & \omega^{d-1} & \omega^{2(d-1)} & \cdots & \omega^{(d-1)^2} \\ 1 & \omega^{d-2} & \omega^{2(d-2)} & \cdots & \omega^{(d-1)(d-2)} \\ \vdots & \vdots & \vdots & \ddots & \vdots \\ 1 & \omega & \omega^2 & \cdots & \omega^{d-1} \end{pmatrix}, \tag{2.14}$$

and

$$X_1 = W Z_1 W^\dagger. \tag{2.15}$$

The eigenvectors of Z_1 are the standard computational basis $|l\rangle$ with eigenvalues ω^l such that $Z_1|l\rangle = \omega^l|l\rangle$. The eigenvectors of X_1 are $W|l\rangle$ with eigenvalues ω^l such that $X_1 W|l\rangle = \omega^l W|l\rangle$. As $|\langle l|W|l'\rangle| = 1/d$, their eigenbasis of X_1 and Z_1 are mutually unbiased.

The Heisenberg-Weyl basis $\{M_{jk}\}$ is orthonormal

$$\mathrm{tr}\left(M_{jk}^{\dagger} M_{j'k'}\right) = d\delta_{jj'}\delta_{kk'}. \tag{2.16}$$

The following commutation relations hold

$$X_j Z_k = Z_k X_j \omega^{jk}, \tag{2.17}$$

$$M_{jk} M_{j'k'} = M_{j'k'} M_{jk} \omega^{jk'-kj'}, \tag{2.18}$$

$$M_{jk} M_{j'k'} = M_{j+j',k+k'} \omega^{-kj'}. \tag{2.19}$$

A state is represented as

$$\rho = \frac{1}{d}\left(\mathbb{1} + \sqrt{d-1}\sum_{\alpha=1}^{d^2-1} p_\alpha M_\alpha\right), \tag{2.20}$$

with $M_\alpha \equiv M_{jk}$, $p_\alpha \equiv p_{jk}$. $p_{jk}^* = p_{-j-k}\omega^{-jk}$.

2.1.2 Representations of quantum channels

Next we present different representations of quantum channels, including the Stinespring dilation theorem, Kraus operator-sum representation, quantum channel-state duality, and the affine representation.

2.1.2.1 Stinespring dilation theorem and Kraus operator-sum representation

A C^*-algebra $\mathscr{A}$ is a Banach $*$-algebra with C^*-axiom $\|x^*x\| = \|x\|^2$ for all $x \in \mathscr{A}$ [16]. Here $*$ is an involution operation. Stinespring dilation theorem [152] characterizes any completely positive mapping on a C^*-algebra. The set of linear operator acting on Hilbert space forms a C^*-algebra with adjoint as involution.

Theorem 1 (Stinespring dilation theorem [16, 152]). *For a C^*-algebra $\mathscr{A}$ and a Hilbert space $\mathscr{H}$, a completely positive mapping $\varphi : \mathscr{A} \to \mathscr{L}(\mathscr{H})$ takes the form*

$$\varphi(x) = T^\dagger \pi(x) T, \ \forall x \in \mathscr{A}, \tag{2.21}$$

where there exists a Hilbert space $\mathcal{K}$ and a contraction T such that $T : \mathscr{H} \to \mathcal{K}$, and a unital $*$-representation $\pi : \mathscr{A} \to \mathscr{L}(\mathcal{K})$.

Choi [42] proved a form of completely positive mapping on complex matrices, which can be viewed as an application of Stinespring dilation theorem. Denote the set of $n \times n$ and $m \times n$ complex matrices as $\mathcal{M}_n$ and $\mathcal{M}_{m,n}$, respectively.

Theorem 2 (Choi [42]). *A linear mapping $\mathcal{N} : \mathcal{M}_n \to \mathcal{M}_m$ is completely positive iff it takes the form*

$$\mathcal{N}(A) = \sum_i K_i A K_i^\dagger, \tag{2.22}$$

for all $A \in \mathcal{M}_n$, $K_i \in \mathcal{M}_{m,n}$.

Both Stinespring's and Choi's theorems can be rephrased with respect to the set of density matrices $\mathscr{D}(\mathscr{H})$, which was also originally studied by Kraus [98]. The operators K_i are often known as Kraus operators, and the form (2.22) above is also called the Kraus operator-sum representation of completely positive mappings.

Regarding this theorem there are several important properties of channels. i) Given a linear mapping $\mathcal{N}$, there exists a *canonical* representation such that the set $\{K_i\}$ is linearly independent [42] and the cardinality of the set $\{K_i\}$ is called the Kraus rank of $\mathcal{N}$, or, simply, the rank of $\mathcal{N}$, denoted as $r_\mathcal{N}$, which is upper bounded by mn. ii) There exists a *unitary freedom* for the canonical representation [42, 123], which means there exists a unitary matrix U such that another set $\{M_j\}$ is also canonical with $M_j = \sum_i u_{ij} K_i$ for $U = [u_{ij}]$. iii) With a canonical representation, the Stinespring contraction is $T = [K_1^\dagger, \cdots, K_{r_\mathcal{N}}^\dagger]^{\mathrm{T}}$, and $\pi(A) = \oplus^{r_\mathcal{N}} A$. iv) A quantum channel $\mathcal{E}$ with its Kraus operators $\{K_i\}$ is completely positive and trace-preserving, i.e., $\sum_i K_i^\dagger K_i = \mathbb{1}$, which is called the trace-preserving or

normalization condition. For a qudit system, $m = n := d$, the rank of a qudit channel $r_{\mathcal{E}} \leq d^2$.

Regarding physical settings, the Kraus operator-sum representation can be characterized by a unitary operator acting on an extended space. For a qudit system S, a quantum channel $\mathcal{E} : \mathscr{D}(\mathscr{H}) \to \mathscr{D}(\mathscr{H})$ acting on it can be dilated to a unitary evolution U such that

$$\mathcal{E}(\rho) = \mathrm{tr}_{\mathrm{A}} U(\rho \otimes \sigma) U^\dagger, \tag{2.23}$$

with one ancillary system A prepared in state σ. Usually, the ancilla state σ is chosen as the ground state $|0\rangle\langle 0|$ such that $K_i = \langle i|U|0\rangle$, and the channel takes the form

$$\mathcal{E}(\rho) = \sum_{i=0}^{r_{\mathcal{E}}-1} K_i \rho K_i^\dagger, \tag{2.24}$$

with $r_{\mathcal{E}} \leq d^2$, and

$$\sum_{i=0}^{r_{\mathcal{E}}-1} K_i^\dagger K_i = \sum_{i=0}^{r_{\mathcal{E}}-1} \langle 0|U^\dagger|i\rangle\langle i|U|0\rangle = \mathbb{1}. \tag{2.25}$$

2.1.2.2 Quantum channel-state duality

Choi [42] as well as Jamiołkowski [82] proved the isomorphism, usually terms as Choi-Jamiołkowski isomorphism $\mathcal{J} : \mathscr{D}(\mathscr{H}) \to \mathscr{H} \otimes \mathscr{H}$ and also $\mathcal{J} : \mathscr{L}(\mathscr{D}(\mathscr{H})) \to \mathscr{L}(\mathscr{H} \otimes \mathscr{H})$, which maps an operator $\mathcal{E} \in \mathscr{L}(\mathscr{D}(\mathscr{H}))$ into a quantum state, called Choi state $\mathcal{C} \in \mathscr{L}(\mathscr{H} \otimes \mathscr{H})$. This isomorphism is also known as the quantum channel-state duality, and the Choi state is the dual of the channel $\mathcal{E}$. The Choi state takes the form

$$\mathcal{C} := \mathcal{E} \otimes \mathbb{1}(|\eta\rangle\langle\eta|), \tag{2.26}$$

with bipartite maximally entangled state

$$|\eta\rangle := \frac{1}{\sqrt{d}} \sum_{i=0}^{d-1} |i, i\rangle. \tag{2.27}$$

Here the Choi state is normalized, and the un-normalized version is also used in some cases. One celebrated property is that the condition of complete positivity is equivalent to the positive semidefiniteness of the Choi state, i.e., $\mathcal{C} \geq 0$.

The Kraus operator-sum representation is equivalent to the Choi state representation, in that the Kraus operators relate to the eigenvectors of Choi state by reshaping [11, 115]. For instance, for a unitary operator U, the Choi state is a pure state $|\psi_U\rangle = (U \otimes \mathbb{1})|\eta\rangle = \text{res}U/\sqrt{d}$. Given the state $|\psi_U\rangle$, the unitary operator can be recovered by $\sqrt{d}\text{res}^{-1}|\psi_U\rangle = U$. On the other hand, given the set of Kraus operators, the Choi state can be derived as

$$\begin{aligned}\mathcal{C} &= \frac{1}{d}\sum_i \text{res}K_i \ (\text{res}K_i)^\dagger \\ &= \sum_i (K_i \otimes \mathbb{1}) |\eta\rangle\langle\eta| \left(K_i^\dagger \otimes \mathbb{1}\right). \end{aligned} \tag{2.28}$$

In addition, the Choi state can also be equivalently defined as $\mathcal{C} = \mathbb{1} \otimes \mathcal{E}(|\eta\rangle\langle\eta|)$, and then the relation with Kraus operators becomes $\mathcal{C} = \frac{1}{d}\sum_i \text{vec}K_i(\text{vec}K_i)^\dagger$. In this thesis, we do not employ this version.

2.1.2.3 Affine representation

In a canonical and orthonormal basis, denoted as $\{\sigma_i\}$, a quantum state can be written as $\rho = \frac{1}{d}(\mathbb{1} + \sum_i p_i\sigma_i)$. As a result, the state ρ can be represented by the vector $\boldsymbol{p} := (p_i)$. Examples of canonical and orthonormal basis include the Pauli basis for qubit case and generalized Pauli bases for qudit case. While a quantum state can be represented as a vector, a quantum channel can be represented as a matrix, which specifies an affine map represented by $\mathcal{T}$

$$\mathcal{E} \mapsto \mathcal{T} = \begin{pmatrix} 1 & \boldsymbol{0} \\ \boldsymbol{t} & \boldsymbol{T} \end{pmatrix}, \ \mathcal{T}_{ij} = \frac{1}{d}\text{tr}\left[\sigma_i \mathcal{E}(\sigma_j)\right], \tag{2.29}$$

which contains the shift vector $\boldsymbol{t}$ and distortion matrix $\boldsymbol{T}$. The affine map is

$$\mathcal{T}\begin{pmatrix} 1 \\ \boldsymbol{p} \end{pmatrix} = \begin{pmatrix} 1 \\ \boldsymbol{T}\boldsymbol{p} + \boldsymbol{t} \end{pmatrix}, \tag{2.30}$$

or simply denoted as

$$\mathcal{T} : \boldsymbol{p} \mapsto \boldsymbol{T}\boldsymbol{p} + \boldsymbol{t}. \tag{2.31}$$

In this form, the quantum dynamics is described as the shrink and shift of $\boldsymbol{p}$. One crucial point is that the parameters in the affine map $\mathcal{T}$ are constrained by the complete positivity condition of a quantum channel. This means that quantum channels do not correspond to arbitrary affine maps.

It is necessary to consider the effects of prior $\mathcal{V}$ and posterior $\mathcal{W}$ unitary channels in the affine form. From $\mathcal{T}_{ij} = \frac{1}{d}\mathrm{tr}(\sigma_i \mathcal{W} \circ \mathcal{E} \circ \mathcal{V}(\sigma_j))$, we find $\mathcal{T}_{i0} = \frac{1}{d}\mathrm{tr}(\sigma_i \mathcal{W} \circ \mathcal{E} \circ \mathcal{V}(\mathbb{1}))$, and $\mathcal{T}_{0j} = \frac{1}{d}\mathrm{tr}(\mathcal{W} \circ \mathcal{E} \circ \mathcal{V}(\sigma_j))$, and then $\mathcal{T}_{i0} = \frac{1}{d}\mathrm{tr}(\sigma_i \mathcal{W} \circ \mathcal{E}(\mathbb{1}))$, and $\mathcal{T}_{0j} = \frac{1}{d}\mathrm{tr}(\mathcal{W} \circ \mathcal{E} \circ \mathcal{V}(\sigma_j)) = 0$. We find that the shift vector $\boldsymbol{t}$ is affected only by the posterior unitary channel. At the same time, the distortion matrix $\boldsymbol{T}$ is affected by both the unitary channels.

There are also other representations of quantum channels, summarized in Fig. 2.1, while we emphasize the following details. i) The Choi state (2.26) is actually a representation in the tensor-product Kronecker basis $\{|i\rangle\langle j| \otimes |i\rangle\langle j|\}$. The process state $\mathcal{S}$, which is usually denoted as χ [123], is a matrix equivalent to Choi state $\mathcal{C} = U\mathcal{S}U^\dagger$ by a basis transformation $U = [u_{\alpha\beta}]$ from generalized Pauli basis $\{\sigma_\beta\}$ to Kronecker basis $\{\tau_\alpha\}$

$$u_{\alpha\beta} = \mathrm{tr}(\tau_\alpha^\dagger \sigma_\beta). \tag{2.32}$$

This can be shown as follows. Given the Kraus operators $\{K_i\}$ for a channel and the generalized Pauli basis $\{\sigma_\beta\}$, each Kraus operator is a combination $K_i = \sum_\beta \mathrm{tr}(K_i^\dagger \sigma_\beta)\sigma_\beta$. Then $\mathcal{E}(\rho) = \sum_{\alpha\beta} S_{\alpha\beta}\sigma_\alpha(\rho)\sigma_\beta$, with $S_{\alpha\beta} = \sum_i \mathrm{tr}(K_i^\dagger \sigma_\alpha)\mathrm{tr}(K_i\sigma_\beta)^*$ [26]. In the generalized Pauli basis, the channel can be represented as $\mathcal{S} = [S_{\alpha\beta}]$. ii) In the affine representation the $\mathcal{T}$ operator is defined in an orthonormal and canonical basis, such as the generalized Pauli basis, while a so-called dynamical operator, denoted as $\mathcal{D}$, can be defined in the Kronecker basis $\{\tau_i\}$. Clearly, $\mathcal{D} = U\mathcal{T}U^\dagger$. Also the $\mathcal{D}$ operator takes the form $\mathcal{D} = \frac{1}{d}\sum_i K_i \otimes K_i^*$. It can be derived from $\mathcal{D}_{ij} = \frac{1}{d}\mathrm{tr}[\tau_i^\dagger \mathcal{E}(\tau_j)]$. It is equivalent to the Choi state by reshuffling $\langle ik|\mathcal{D}|jl\rangle = \langle ij|\mathcal{C}|kl\rangle$ [11]. In this form, a quantum state ρ is represented by its reshaping $\mathrm{res}\rho$, and the dynamics is $\mathrm{res}\rho \mapsto \mathcal{D}\mathrm{res}\rho$. For instance, $\mathrm{res} : U\rho U^\dagger \mapsto (U \otimes U^*)\mathrm{res}\rho$ for the unitary case.

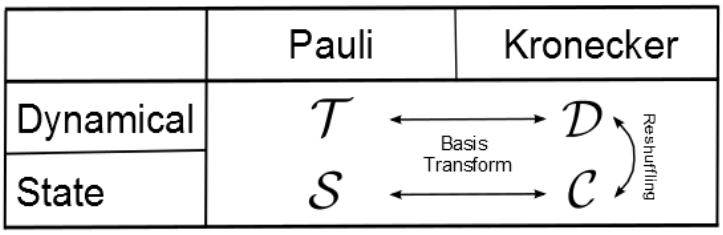

Figure 2.1: The representations of quantum channel. In the table, "Pauli" represents the Pauli basis or the generalized Pauli basis, and "Kronecker" represents the Kronecker basis, and there exists a basis transformation between the two bases. "Dynamical" means that the affine form $\mathcal{T}$ and dynamical operator $\mathcal{D}$ are operators for the dynamics of a quantum channel, and "State" means that a quantum channel is represented by a quantum state, the Choi state $\mathcal{C}$, which relates to $\mathcal{D}$ by the reshuffling operation, or the process state $\mathcal{S}$.

2.2 Distance measure

2.2.1 Norms on operator and superoperator

We consider bounded linear operators in $\mathscr{L}(\mathscr{H})$. A family of norms is known as the *Schatten p-norm* [16]

$$\|T\|_p := \left[\mathrm{tr}\left(\left(T^\dagger T\right)^{p/2}\right)\right]^{1/p}, \quad p \geq 1, \ \forall T \in \mathscr{L}(\mathscr{H}). \tag{2.33}$$

This norm includes some commonly used norms as special cases. i) Trace norm ($p = 1$): $\|T\|_{\mathrm{tr}} := \|T\|_1 = \mathrm{tr}\sqrt{T^\dagger T}$. ii) Operator (or spectral) norm ($p = \infty$): $\|T\| = \sigma_{\max}(T)$, $\sigma_{\max}$ denotes the largest singular value. It can also be defined as $\|T\| := \sup_{|\psi\rangle} \|T|\psi\rangle\|, \forall |\psi\rangle \in \mathscr{H}$, and $\||\psi\rangle\| = 1$. iii) Hilbert-Schmidt (or Frobenius) norm ($p = 2$): $\|T\|_F := \|T\|_2 = \sqrt{\mathrm{tr}(T^\dagger T)}$.

The Schatten p-norm has many useful properties. i) Positive semidefiniteness: $\|T\|_p \geq 0$ with $\|T\|_p = 0$ if $T = 0$. ii) Positive scalability: $\|\alpha T\|_p = |\alpha| \cdot \|T\|_p$ for $\alpha \in \mathbb{C}$. iii) The triangle inequality: $\|T_1 + T_2\|_p \leq \|T_1\|_p + \|T_2\|_p$. iv) Unitary invariance: $\|T\|_p = \|UTV\|_p$ for unitary operator $U, V \in \mathscr{L}(\mathscr{H})$. v) Decreasing in p: $\|T\|_p \geq \|T\|_q$ for $1 \leq p \leq q \leq \infty$.

vi) Sub-multiplicative under composition: $\|T_1T_2\|_p \leq \|T_1\|_p\|T_2\|_p$. vii) Hölder's inequality: For $p, q, r \geq 1$, $1/p + 1/q \leq 1/r$, then $\|T_1T_2\|_r \leq \|T_1\|_p\|T_2\|_q$.

For operator norms, there exists one crucial property that any two norms $\|\cdot\|_p$ and $\|\cdot\|_q$ are equivalent

$$r\|\cdot\|_p \leq \|\cdot\|_q \leq s\|\cdot\|_p, \ \exists r, s \in \mathbb{R}^+. \tag{2.34}$$

The following inequalities are important for quantum computation tasks

$$\|T\|_F \leq \|T\|_1 \leq \sqrt{r}\|T\|_F, \ \|T\| \leq \|T\|_F \leq \sqrt{r}\|T\|, \quad r := \text{rank}T. \tag{2.35}$$

In quantum computation, we often study linear mappings on $\mathscr{L}(\mathscr{H})$. A linear mapping is often called "superoperator" since it acts on operators. As the case of operator norm, superoperator norm can also be well defined. Based on the Schatten p-norm, the *induced Schatten $(q \to p)$-norm* [127] is defined as

$$\|\Pi\|_{q\to p} := \max_T \frac{\|\Pi T\|_p}{\|T\|_q}, \quad p, q \geq 1, \ \forall T \in \mathscr{L}(\mathscr{H}), \ \forall \Pi \in \mathscr{L}(\mathscr{L}(\mathscr{H})). \tag{2.36}$$

However, one unpleasant property of this norm is that for $1 \leq p < 2$, $\|\Pi\|_{1\to p}$ is not stable, i.e., $\|\Pi\|_{1\to p} \neq \|\Pi \otimes \mathbb{1}\|_{1\to p}$ with $\mathbb{1}$ acting on another space. For the case $p = q = 1$, a stabilized norm, known as diamond norm [92], is defined as

$$\|\Pi\|_\diamond := \|\Pi \otimes \mathbb{1}\|_{1\to 1} = \max_T \|(\Pi \otimes \mathbb{1})T\|_{\text{tr}}, \tag{2.37}$$

for $\mathbb{1} \in \mathscr{L}(\mathscr{L}(\mathcal{K}))$, $T \in \mathscr{L}(\mathscr{H} \otimes \mathcal{K})$, and $\dim(\mathcal{K}) \geq \dim(\mathscr{H})$. The main properties of the diamond norm include: i) Sub-multiplicative under composition: $\|\Pi_1\Pi_2\|_\diamond \leq \|\Pi_1\|_\diamond\|\Pi_2\|_\diamond$. ii) Multiplicative under tensor product: $\|\Pi_1 \otimes \Pi_2\|_\diamond = \|\Pi_1\|_\diamond\|\Pi_2\|_\diamond$. iii) Chain property: $\|\Pi_1\Pi_2 - \Pi_1'\Pi_2'\|_\diamond \leq \|\Pi_1 - \Pi_1'\|_\diamond + \|\Pi_2 - \Pi_2'\|_\diamond$. iv) Unitary invariance: $\|\Pi\|_\diamond = \|\mathcal{U}\Pi\mathcal{V}\|_\diamond$ for unitary operators $\mathcal{U}, \mathcal{V} \in \mathscr{L}(\mathscr{L}(\mathscr{H}))$.

One important application of diamond norm is to quantify the distance between quantum channels. In this case, the domain over which the optimization is taken is $\mathscr{D}(\mathscr{H})$. Furthermore, the maximum is achieved for a pure state following from the convexity of $\mathscr{D}(\mathscr{H})$.

2.2.2 Inequalities

Inequalities play important roles in operator algebra and quantum computing, here we present some inequalities relating to the channel simulation problem.

2.2.2.1 Trace distance and fidelity on quantum state

The trace distance between two quantum states ρ and σ is defined as

$$D_t(\rho,\sigma) := \frac{1}{2}\|\rho-\sigma\|_{\mathrm{tr}} = \frac{1}{2}\mathrm{tr}|\rho-\sigma|, \tag{2.38}$$

with $|\rho-\sigma| := \sqrt{(\rho-\sigma)^2}$. The fidelity between two quantum states ρ and σ is defined as

$$F(\rho,\sigma) := \mathrm{tr}\sqrt{\sqrt{\rho}\sigma\sqrt{\rho}}, \tag{2.39}$$

which is equivalent to the Bures distance $D_B(\rho,\sigma) := \sqrt{2(1-F(\rho,\sigma))}$, the infinitesimal version of which is a metric on $\mathscr{D}(\mathscr{H})$.

The well known relation between trace distance and fidelity is [123]

$$1-F(\rho,\sigma) \le D_t(\rho,\sigma) \le \sqrt{1-F(\rho,\sigma)^2}. \tag{2.40}$$

To quantify the operational distance between two quantum states in practice, using one of them, trace distance or fidelity, usually cannot guarantee good results. An application of both of them in our experiment is discussed in Chapter 6.

2.2.2.2 Trace distance of state and spectral norm of unitary operator

Proposition 3. *For unitary operators $U,\tilde{U}\in\mathscr{L}(\mathscr{H})$ it holds*

$$\left\|U-\tilde{U}\right\| \ge \sup_{|\psi\rangle} D_t\left(U|\psi\rangle\langle\psi|U^\dagger, \tilde{U}|\psi\rangle\langle\psi|\tilde{U}^\dagger\right). \tag{2.41}$$

Proof. For normalized quantum states $|\tilde{\varphi}\rangle$ and $|\varphi\rangle$, the vector 2-norm satisfies

$$\||\tilde{\varphi}\rangle-|\varphi\rangle\|_2^2 = 2-2\mathrm{Re}\langle\tilde{\varphi}|\varphi\rangle \ge 1-|\langle\tilde{\varphi}|\varphi\rangle|^2, \tag{2.42}$$

since $(1 - \mathrm{Re}\langle\tilde{\varphi}|\varphi\rangle)^2 + (\mathrm{Im}\langle\tilde{\varphi}|\varphi\rangle)^2 \geq 0$. The value $1 - |\langle\tilde{\varphi}|\varphi\rangle|^2$ is the square of the trace distance between $\tilde{\varphi} := |\tilde{\varphi}\rangle\langle\tilde{\varphi}|$ and $\varphi := |\varphi\rangle\langle\varphi|$, proved as follows. Suppose the eigenvector of $\tilde{\varphi} - \varphi$ takes the form $a|\tilde{\varphi}\rangle + b|\varphi\rangle$, that is

$$(\tilde{\varphi} - \varphi)(a|\tilde{\varphi}\rangle + b|\varphi\rangle) = \lambda(a|\tilde{\varphi}\rangle + b|\varphi\rangle). \tag{2.43}$$

Then $a\lambda = a + b\langle\tilde{\varphi}|\varphi\rangle, b\lambda = -b - a\langle\varphi|\tilde{\varphi}\rangle$, from which we find $\lambda_\pm = \pm\sqrt{1 - |\langle\tilde{\varphi}|\varphi\rangle|^2}$. The trace distance $D_t(\tilde{\varphi}, \varphi) = (|\lambda_+| + |\lambda_-|)/2 = \sqrt{1 - |\langle\tilde{\varphi}|\varphi\rangle|^2}$. As the result,

$$\||\tilde{\varphi}\rangle - |\varphi\rangle\|_2 \geq D_t(\tilde{\varphi}, \varphi). \tag{2.44}$$

For unitary operators U and $\tilde{U}$, we have

$$\left\|U - \tilde{U}\right\| = \sup_{|\psi\rangle} \left\|(U - \tilde{U})|\psi\rangle\right\|_2 \geq \sup_{|\psi\rangle} D_t\left(U|\psi\rangle\langle\psi|U^\dagger, \tilde{U}|\psi\rangle\langle\psi|\tilde{U}^\dagger\right). \tag{2.45}$$

□

An operational interpretation of this inequality is that, if the distance between two evolution U and $\tilde{U}$ is within some tolerance ϵ, then the trace distance between the final states resulting from the two unitary evolutions is also within ϵ.

Corollary 4. *For any unitary operators $U, \tilde{U} \in \mathscr{L}(\mathscr{H} \otimes \mathscr{H}')$ and any states $\rho \in \mathscr{D}(\mathscr{H})$ and $\rho' \in \mathscr{D}(\mathscr{H}')$, then*

$$\left\|U - \tilde{U}\right\| \geq \sup_{\rho} D_t\left(U(\rho \otimes \rho')U^\dagger, \tilde{U}(\rho \otimes \rho')\tilde{U}^\dagger\right). \tag{2.46}$$

Proof. For any $\sigma \in \mathscr{D}(\mathscr{H} \otimes \mathscr{H}')$ and convex-sum decomposition such that $\sigma = \sum_i p_i|\psi_i\rangle\langle\psi_i|$ for $\sum_i p_i = 1$, Prop. 3 generalizes to the mixed state case

$$\begin{aligned}
\left\|U - \tilde{U}\right\| &= \sup_{\sigma} \sqrt{\mathrm{tr}(\sigma(U - \tilde{U})^\dagger(U - \tilde{U}))} \\
&\geq \sup_{\sigma} \sum_i p_i \left\|(U - \tilde{U})|\psi_i\rangle\right\| \\
&\geq \sup_{\sigma} \sum_i p_i D_t\left(U|\psi_i\rangle\langle\psi_i|U^\dagger, \tilde{U}|\psi_i\rangle\langle\psi_i|\tilde{U}^\dagger\right) \\
&\geq \sup_{\sigma} D_t\left(U\sigma U^\dagger, \tilde{U}\sigma\tilde{U}^\dagger\right).
\end{aligned} \tag{2.47}$$

The last step employs the strong convexity of trace distance. Particularly, suppose $\sigma = \rho \otimes \rho'$ for $\rho \in \mathscr{D}(\mathscr{H})$ and $\rho' \in \mathscr{D}(\mathscr{H}')$. As $\sup_\sigma \implies \sup_\rho$, Eq. (2.46) follows. □

This result is a bipartite generalization of Prop. 3, and is used to prove Theorem 5 below.

2.2.2.3 Channel and dilated unitary operator

Theorem 5. *For $\epsilon \in \mathbb{R}^+$, $\rho \in \mathscr{D}(\mathscr{H})$ and quantum channels $\mathcal{E}, \tilde{\mathcal{E}} : \mathscr{D}(\mathscr{H}) \to \mathscr{D}(\mathscr{H})$ with respective minimal dilations $U, \tilde{U}$, then*

$$\left\| U - \tilde{U} \right\| \leq \epsilon/2 \implies \left\| \mathcal{E} - \tilde{\mathcal{E}} \right\|_\diamond \leq \epsilon. \tag{2.48}$$

Proof. The trace-distance contraction property [123]

$$D_t \left(\mathcal{E}(\rho), \tilde{\mathcal{E}}(\rho) \right) \leq D_t \left(U(\rho \otimes \rho')U^\dagger, \tilde{U}(\rho \otimes \rho')\tilde{U}^\dagger \right), \tag{2.49}$$

combined with Corollary 4 yields $\|U - \tilde{U}\| \geq \sup_\rho D_t(\mathcal{E}(\rho), \tilde{\mathcal{E}}(\rho)) = \frac{1}{2}\|\mathcal{E} - \tilde{\mathcal{E}}\|_{1\to 1}$. As $\|U - \tilde{U}\| = \|U \otimes \mathbb{1} - \tilde{U} \otimes \mathbb{1}\|$, the proof is complete. □

This theorem shows that, in order to bound the distance on two channels, one can instead bound the distance on the corresponding dilated unitary operators.

Corollary 6. *For unitary operators $U, \tilde{U}$ and the channel forms $\mathcal{U}, \tilde{\mathcal{U}}$*

$$2 \left\| U - \tilde{U} \right\| \geq \left\| \mathcal{U} - \tilde{\mathcal{U}} \right\|_\diamond. \tag{2.50}$$

Proof. This is a special case of Theorem 5. □

2.2.2.4 Channel and Choi state

The diamond-norm distance between two channels is closely related to the distance between their Choi-Jamiołkowski states [171, 137].

Proposition 7. *For CP mappings $\mathcal{N}, \tilde{\mathcal{N}} : \mathscr{D}_d \to \mathscr{D}_d$ and their Choi state $\mathcal{C}, \tilde{\mathcal{C}}$ it holds*

$$\frac{1}{d} \left\| \mathcal{N} - \tilde{\mathcal{N}} \right\|_\diamond \leq \left\| \mathcal{C} - \tilde{\mathcal{C}} \right\|_1 \leq \left\| \mathcal{N} - \tilde{\mathcal{N}} \right\|_\diamond. \tag{2.51}$$

Proof. The second inequality is proved by observing that

$$\left\|\mathcal{C}-\tilde{\mathcal{C}}\right\|_1=\left\|\mathcal{N}\otimes\mathbb{1}-\tilde{\mathcal{N}}\otimes\mathbb{1}(\eta)\right\|_1, \tag{2.52}$$

for state $\eta=\frac{1}{d}\sum_{i,j}|i,i\rangle\langle j,j|$. The first inequality is proved by using the method of gate teleportation. Suppose the state of a system A is $\rho_{\rm A}$, and the composite state of system B and system C is a Choi state $\mathcal{C}$ for a CP mapping $\mathcal{N}$. Then by the projection η on system A and system B the state of system C becomes

$$\begin{aligned}\langle\eta|\rho_{\rm A}\otimes\mathcal{C}_{\rm BC}|\eta\rangle&=\frac{1}{d}\langle\eta|\sum_{ij}\rho\otimes|i\rangle\langle j|\otimes\mathcal{N}(|i\rangle\langle j|)|\eta\rangle\\&=\frac{1}{d}\sum_{ij}\rho_{ij}\mathcal{N}(|i\rangle\langle j|)\\&=\frac{1}{d}\mathcal{N}(\rho),\end{aligned} \tag{2.53}$$

where $\frac{1}{d}$ is the success probability. Also if the system A is initially correlated to another system E, and then we find that the projection η on system A and system B leads to the state $\mathcal{N}\otimes\mathbb{1}(\rho_{\rm AE})$, with $\mathbb{1}$ acting on the system E. Then we find

$$\begin{aligned}\left\|\mathcal{N}-\tilde{\mathcal{N}}\right\|_\diamond&=\sup_{\rho_{\rm AE}}\left\|\mathcal{N}\otimes\mathbb{1}-\tilde{\mathcal{N}}\otimes\mathbb{1}\rho_{\rm AE}\right\|_1\\&=d\sup_{\rho_{\rm AE}}\left\|\langle\eta_{\rm AB}|\rho_{\rm AE}\otimes(\mathcal{C}_{\rm BC}-\tilde{\mathcal{C}}_{\rm BC})|\eta_{\rm AB}\rangle\right\|_1\\&\leq d\sup_{\rho_{\rm AE}}\left\|\rho_{\rm AE}\otimes(\mathcal{C}_{\rm BC}-\tilde{\mathcal{C}}_{\rm BC})\right\|_1\\&=d\left\|\mathcal{C}_{\rm BC}-\tilde{\mathcal{C}}_{\rm BC}\right\|_1,\end{aligned} \tag{2.54}$$

which proves the first inequality. □

2.3 Convex set

In this section we study the properties of the convex set of quantum channels. We start from primary properties of affine space and convex set in §2.3.1, wherein the materials can be found in any textbook on convex sets [69, 70]. Then we review some well known convex

sets in §2.3.2 for a better understanding of the convex set of quantum channels studied in §2.3.3.

2.3.1 Affine space and convex set

A vector space V over a field $\mathbb{F}$ (e.g. $\mathbb{R}$ or $\mathbb{C}$) is the linear span of its basis $\{e_i\}$

$$V \equiv \text{span}(\{e_i\}) = \left\{ \sum_i \lambda_i e_i | \lambda_i \in \mathbb{F} \right\}. \tag{2.55}$$

An element $v \in V$ can be written as a linear combination of its basis $v = \sum_i \lambda_i e_i,\ \lambda_i \in \mathbb{F}$. The dimension of V is $\dim V = |e|$, with $|e|$ denoting the cardinality of the set $\{e_i\}$. Note a basis of a vector space can be defined as a linearly independent set of vectors which spans the vector space. The basis of a vector space is not unique, yet there exists an *orthonormal* basis such that $e_i^* e_j = \delta_{ij}$. A set of vectors $\{\boldsymbol{x}_i\}$ is linearly independent iff the determinant of the matrix $(\boldsymbol{x}_i)$ is nonzero.

Affine space A over a field $\mathbb{F}$ is the affine span of its affine basis $\{f_i\}$

$$A \equiv \text{aff}(\{f_i\}) = \left\{ \sum_i \alpha_i f_i | \alpha_i \in \mathbb{F}, \sum_i \alpha_i = 1 \right\}. \tag{2.56}$$

An element $a \in A$ can be written as an affine combination of its affine basis $a = \sum_i \alpha_i f_i$ with $\sum_i \alpha_i = 1,\ \alpha_i \in \mathbb{F}$. The dimension of an affine space is $\dim A = |f| - 1$, with $|f|$ being the size of $\{f_i\}$. Also a set of vectors $\{\boldsymbol{x}_i\}$ is affinely independent iff the determinant of the matrix $(\boldsymbol{x}_i')$ is nonzero, for $\boldsymbol{x}_i' := (1, \boldsymbol{x}_i)$. An affine basis of an affine space is an affinely independent set of vectors which spans the affine space.

The dimension of a set $\mathscr{S} \subset V$ in a vector space V is the dimension of the smallest affine subspace $A \subset V$ containing the set, $\mathscr{S} \subset A \subset V$. A set $\mathscr{S}$ is convex if

$$(1-\lambda)x + \lambda y \in \mathscr{S},\ \forall x, y \in \mathscr{S}, \lambda \in (0,1). \tag{2.57}$$

The convex hull of a set $\mathscr{S}$ is the smallest convex set that contains $\mathscr{S}$, denoted by $\text{conv}\mathscr{S}$. There are alternative ways to define convex hull; e.g., it may be defined as the intersection

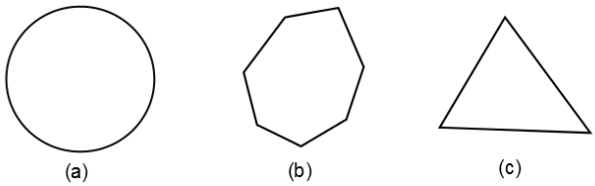

Figure 2.2: Example of two-dimensional closed (a) convex set, (b) polygon, and (c) simplex.

of all convex sets containing it, or as the set of all convex combinations of points in it. The convex hull of a convex set is the same with the convex set itself. A compact convex set is called a convex body. For instance, the set of density matrices is a convex body.

A point in a convex set is extreme if it is not a relative interior point of a line segment in the set. Alternatively, an extreme point (vertex) is a point which can not be written as convex combination of other points of the set. A polytope is a convex set such that it is the convex hull of its finite number of extreme points. Note we focus on convex polytope, although there are also concave ones [69, 70]. Generically, a polytope can be understood as a convex set with sharp boundaries (hyperplanes). The dimension of a polytope is the dimension of the smallest affine subspace containing the polytope. A k-simplex is a k-dimensional polytope that is the convex hull of its $k+1$ vertices, and element of a simplex is the convex sum of $k+1$ vertices. Examples of two-dimensional closed convex set, polytope, and simplex are shown in Fig. 2.2.

2.3.2 Examples of convex sets

2.3.2.1 The set of doubly stochastic matrices

A real $d \times d$ matrix is doubly stochastic if all its entries are nonnegative and the sum of the entries in each row and column equals 1. A $d \times d$ matrix is a permutation if, in each row and column, there exists one 1 with all other entries 0. It is easy to see that the set of doubly stochastic matrices is convex.

Theorem 8 (Birkhoff [69])**.** *The set of $d \times d$ doubly stochastic matrices is the convex hull of*

the $d \times d$ permutation matrices and each permutation matrix is an extreme point of this set.

The permutation matrices form the permutation group S_d, which has order $d!$. The convex set of doubly stochastic matrices is a polytope, known as a *Birkhoff polytope*. The Birkhoff polytope of doubly stochastic matrices has $d!$ vertices, d^2 facets, and dimension $(d-1)^2$. The dimension is computed as follows: there are d^2 elements in a matrix, and there are $2d-1$ constraints from the doubly stochastic condition, so there are $d^2-2d+1 = (d-1)^2$ independent variables, which equals the dimension. It is obvious that the Birkhoff polytope is not a simplex. One crucial fact is that this theorem does not directly generalize to the quantum case [114].

2.3.2.2 The set of contractions

A $d \times d$ matrix A is a contraction if its largest singular value is no larger than 1, i.e., $\|A\| \leq 1$. We use $A \leq 1$ to indicate that A is a contraction for simplicity. One important relation between contractions and unitary matrices is revealed by the following theorem.

Theorem 9 ([183])**.** *A matrix is a contraction if and only if it is a finite convex combination of unitary matrices.*

As there are infinite number of unitary matrices, the set of contractions form a d^2-dimensional convex set, not a polytope. A constructive proof of this theorem [183] is reviewed below.

Proof. Suppose the singluar-value decomposition (SVD) of a contraction A is $A = USV$, for unitary matrices U and V, and the diagonal matrix S of its singular values $1 \geq s_1 \geq s_2 \geq \cdots \geq s_r \geq 0$, $r \leq d$ is the rank of A. Define diagonal matrices $D_i := \mathrm{diag}(1, 1, \ldots, 1, 0, \ldots, 0)$ with the number of 1 as $i = 0, 1, \ldots, r$. Then $S = (1 - s_1)D_0 + (s_1 - s_2)D_1 + \cdots (s_{r-1} - s_r)D_{r-1} + s_r D_r$. Define $F_i := \mathrm{diag}(0, 0, \ldots, 0, -1, \ldots, -1)$ with the number of 0 as $i = 0, 1, \ldots, r$. Then $E_i := D_i + F_i$ is unitary. We find $D_i = (\mathbb{1} + E_i)/2$. Then

$$S = \frac{s_1}{2}\mathbb{1} + \frac{s_r}{2}E_r + \frac{1}{2}\sum_{i=1}^{r-1}(s_i - s_{i+1})E_i. \tag{2.58}$$

With U and V, the matrix A is decomposed into a sum of $r+1$ unitary matrices. If $r=d$, then $E_r = \mathbb{1}$, $S = \frac{1}{2}(s_1+s_d)\mathbb{1} + \frac{1}{2}\sum_{i=1}^{d-1}(s_i - s_{i+1})E_i$, the matrix A is decomposed into a sum of d unitary matrices. □

2.3.2.3 The set of positive semidefinite matrices

The set of $d \times d$ positive semi-definite matrices is also convex, yet it is neither a polytope nor simplex. The dimension of the set is d^2. The vertices (extreme points) are rank-one matrices. We are interested in the set of density operators, which are required to be trace one. The dimension of the set of $d \times d$ density operators $\mathscr{D}(\mathscr{H})$ is d^2-1. It is straightforward to see that a $d \times d$ density operator is a convex sum of at most d pure states from eigenvalue decomposition.

The geometry of $\mathscr{D}(\mathscr{H})$ is nontrivial. For qubit state, see example 1, the set of density operators forms the Bloch ball, with pure states on the sphere ($S^2 \cong P\mathbb{C}^2$) while the interior for all mixed states, and the center is the maximally mixed state. Any transformation $U \in SU(2)$ corresponds to a rotation of the Bloch ball. Using the affine map representation in Pauli basis $\{\sigma_i\}$, see §2.1.2, a qubit state is represented by a polarization vector $\boldsymbol{p}$ and a unitary operator U maps to an orthogonal matrix $R \in SO(3)$ such that

$$U \mapsto \begin{pmatrix} 1 & \mathbf{0} \\ \mathbf{0} & R \end{pmatrix}. \tag{2.59}$$

The action of U on ρ can be interpreted as a rotation of $\boldsymbol{p}$ by R, i.e. $\boldsymbol{p} \mapsto R\boldsymbol{p}$. Since $SU(2)/\mathbb{Z}_2 \cong SO(3)$, any orthogonal matrix R corresponds to a unitary evolution U. More generally, a qubit quantum channel induces a shift and distortion of the qubit Bloch ball instead of a simple rotation.

The picture for qubit states does not hold for higher-dimensional cases. For qutrit case, a unitary operator $U \in SU(3)$ does not always exist given an orthogonal rotation $R \in SO(8)$ since $SO(8) \supset SU(3)$. This is consistent with the fact that the set of qutrit states does not form a higher-dimensional ball; instead, it is only a subset of the ball, see e.g. Ref. [90].

2.3.3 The set of quantum channels

Quantum channels acting on a qudit system form a convex set, denoted as $\mathscr{S}$. The convexity means, namely, for $\mathcal{E}_1, \mathcal{E}_2 \in \mathscr{S}$, the convex combination $p\mathcal{E}_1 + (1-p)\mathcal{E}_2$ also lives in the set. For a system state ρ, the state $p\mathcal{E}_1(\rho) + (1-p)\mathcal{E}_2(\rho)$ is still a valid state. More generally, the set of completely positive, trace-decreasing mappings with fixed $\sum_{i=0}^{r-1} K_i^\dagger K_i := K \leq \mathbb{1}$ also forms a convex set, denoted as $\mathscr{S}(K)$. Clearly, $\bigcup_K \mathscr{S}(K) \supset \mathscr{S}$. The dimension of the set $\mathscr{S}(K)$ and also $\mathscr{S}$ is both $d^2(d^2-1)$, since there are d^4 entries in the Choi state $\mathcal{C}$ (2.26), and d^2 constraints, which is from the partial trace of the Choi state. In this thesis, we focus on trace-preserving case, i.e. quantum channels.

Next we focus on the set of qudit channels $\mathscr{S}$ and we will study several subsets of $\mathscr{S}$. One important subclass of channels is the unital channel. A channel is unital if it preserves identity $\mathcal{E}_{\mathrm{u}}(\mathbb{1}) = \mathbb{1}$, and $\mathcal{E}_{\mathrm{u}} \in \mathscr{S}_{\mathrm{u}}$, the set of unital channels. The set $\mathscr{S}$ contains both unital and nonunital channels. The following theorem is important for relating unital channels to unitary channels.

Theorem 10 ([114])**.** *The following statements are equivalent:*

1. *A channel $\mathcal{E}$ is unital.*
2. *A channel $\mathcal{E}$ is an affine combination of unitary channels $\mathcal{E} = \sum_i a_i \mathcal{U}_i$, with $\sum_i a_i = 1$, and $a_i \in \mathbb{R}$.*
3. *The affine representation $\mathcal{T}$ of $\mathcal{E}$ can be written as a convex sum $\mathcal{T} = \sum_\alpha p_\alpha W_\alpha$ for unitary matrices W_α.*

The proof details can be found in Ref. [114], which employs the norm properties of unital channels and the convex set property of contractions. Note that this theorem does not imply $\mathcal{E}_{\mathrm{u}} = \sum_\alpha p_\alpha \mathcal{W}_\alpha$, since W_α does not correspond to unitary operator, in which case there exists unitary operator U_α such that $W_\alpha = U_\alpha \otimes U_\alpha^*$.

This theorem manifests that the coefficients a_i could be negative. As a result, a subset of unital channels is called mixing unitary channels, for which a mixing unitary channel takes

the form $\mathcal{E} = \sum_i p_i U_i \cdot U_i^\dagger$ for unitary operators U_i and probability p_i. The set of mixing unitary channels is also convex, denoted as $\mathscr{S}_{\text{mu}}$.

There also exists a subset $\mathscr{S}_{\text{gd}}$, which is the set of generalized depolarizing channels with respect to a basis. A generalized depolarizing channel with respect to a basis $\{M_\alpha\}$, denoted as $\mathcal{E}_{\text{gd}} \in \mathscr{S}_{\text{gd}}$, has a diagonal distortion matrix Λ in the affine map representation

$$\mathcal{E}_{\text{gd}} \mapsto \mathcal{T}_{\text{gd}} = \begin{pmatrix} 1 & \mathbf{0} \\ \mathbf{0} & \Lambda \end{pmatrix} \tag{2.60}$$

with $\Lambda = \text{diag}(\lambda_1, \ldots, \lambda_{d^2-1})$. If each M_α is hermitian, then $\lambda_i \in \mathbb{R}$.

Not all mixing unitary channels has a diagonal distortion matrix, that is, $\mathscr{S}_{\text{gd}} \subset \mathscr{S}_{\text{mu}}$. The reason is as follows. For a non-diagonal distortion matrix T, it can be diagonalized from SVD (or eigenvalue decomposition) as $T = O_1 D O_2$ for orthogonal matrices O_1 and O_2. However, an orthogonal matrix may not correspond to a unitary operator since $SU(d) \subset SO(d^2 - 1)$. As a result, we have the following subset structure

$$\mathscr{S} \supset \mathscr{S}_{\text{u}} \supset \mathscr{S}_{\text{mu}} \supset \mathscr{S}_{\text{gd}}. \tag{2.61}$$

The set $\mathscr{S}_{\text{gd}}$ has a nice geometry. For the ease of terminology here, in the affine representation of a channel the vector formed by the diagonal elements in the distortion matrix T is called *distortion vector* living in *distortion space*.

Theorem 11 (Burrell [34])**.** *With respect to Heisenberg-Weyl basis (2), $\mathscr{S}_{\text{gd}}$ is a simplex $\mathbf{\Delta}$ in the distortion space.*

Proof. The boundary of $\mathscr{S}_{\text{gd}}$ is formed by $\{\lambda_i = 0\}$ for $\{\lambda_i\}$ the set of eigenvalues of the Choi state of generalized depolarizing channels. In terms of distortion coefficients, each λ_i is a linear function thus forming a hyperplane. That is, the set $\mathscr{S}_{\text{gd}}$ is a polytope with d^2 extreme points. As there are $d^2 - 1$ distortion coefficients, the distortion space is of dimension $d^2 - 1$, and then the polytope reduces to a simplex, denoted by $\mathbf{\Delta}$. □

The set $\mathscr{S}_{\rm gd}$ is a (d^2-1)-simplex. A vertex (0-facet) corresponds to a rank-one channel, an edge (1-facet) corresponds to a rank-two channel, and a face (2-facet) corresponds to a rank-three channel, etc. It follows that a generalized depolarizing channel $\mathcal{E}_{\rm gd}$ can be written as a convex combination of its extreme channels

$$\mathcal{E}_{\rm gd}(\rho) = \sum_{jk} p_{jk} M_{jk} \rho M_{jk}^\dagger, \tag{2.62}$$

for Heisenberg-Weyl operators M_{jk}. For the n-qubit case, the Heisenberg-Weyl basis is equivalent to the Pauli basis (in tensor product form). The set $\mathscr{S}_{\rm gd}$ in the Pauli basis also forms a simplex.

For the single qubit case, it turns out the geometry is simplified. An extreme unital qubit channel is just a unitary operator. As the result, any qubit unital channel can be written as a convex sum of four unitary operators, and the set of unital channels forms a tetrahedron. Further, every mixing unitary channel is unitarily equivalent to a Pauli depolarizing channel. Then $\mathscr{S}_{\rm u} = \mathscr{S}_{\rm mu} = \mathscr{S}_{\rm gd}$ for qubit case. This can be shown in the affine form. For a mixing unitary channel, the distortion matrix R can be diagonalized using SVD as $R = V\Lambda W$ for positive diagonal matrix Λ. The orthogonal matrices V and W can be each mapped to a unitary operator U_V and U_W, and the distortion matrix Λ specifies a Pauli channel. Then, a mixing unitary channel can be realized by the composition of a prior unitary operator U_W, a posterior unitary operator U_V, and a Pauli channel.

Example 4 (The tetrahedron of qubit unital channels)**.** *For a qubit ($d = 2$), $M_{00} = \mathbb{1} \equiv \sigma_0$, $M_{10} = X \equiv \sigma_1$, $iM_{11} = Y \equiv \sigma_2$, and $M_{01} = Z \equiv \sigma_3$ are the set of Pauli matrices $\{\sigma_i\}$, $(i = 0, 1, 2, 3)$. The set of unital channels form a tetrahedron, which has four 0-facets (vertices), six 1-facets (edges), and four 2-facets (faces). The four vertices correspond to rank-one unitary channels which are the Pauli operators σ_i.*

Example 5 (The simplex of qutrit genearalized depolarizing channels)**.** *For a qutrit ($d = 3$), $\omega := e^{i2\pi/3}$, and the Heisenberg-Weyl basis is provided in Eq. (2.9). The set of qutrit*

genearalized depolarizing channels form an eight-simplex, which has nine 0*-facets (vertices), 36* 1*-facets (edges), and 84* 2*-facets (faces). The nine vertices correspond to rank-one unitary channels which are the Heisenberg-Weyl basis operators* M_{jk}.

2.4 Conclusion

In this chapter we have analyzed primary results relating to quantum channels. In particular, norms on superoperators and some inequalities on superoperators are important for a proper definition of simulation accuracy. Also we have seen that the set of quantum channels is a peculiar convex set, which has extreme points corresponding to channels with ranks bigger than one. The convex-set properties of quantum channels is the starting point for the design of quantum channel simulation algorithm.

Chapter 3

Single-qubit unitary quantum gate compiling

In this chapter, we study the unitary qubit gate compiling problem and develop an algorithm for it that relies on and improves the Solovay-Kitaev algorithm, which has been published in our paper [168]. In general, quantum gate compiling refers to the problem of approximating a finite-dimensional arbitrary unitary operator U by a sequence of gates from a discrete universal gate library within a given error tolerance ϵ. We first review the definitions of universality and exact universality, and examples of universal gate libraries in §3.1, and then we review the Solovay-Kitaev theorem and Solovay-Kitaev algorithm for qubit unitary gate compiling in §3.2. We then in §3.3 develop a lookup table that initiates the first step in the Solovay-Kitaev algorithm hence completes it. We conclude in §3.4.

3.1 Universality

We first review the definition of *universality* and *exact universality*, which is originally defined in Ref. [31] for general multi-qudit cases.

Definition 6 (Universality [31]). *A set of qudit gates and two-qudit gates, denoted as S, is called universal if, for each $n \geq 2$, every n-qudit gate can be approximated with arbitrary accuracy by a unitary quantum circuit made up of gates from S.*

Definition 7 (Exact universality [31]). *A set of qudit gates and two-qudit gates, denoted as S, is called exact universal if, for each $n \geq 2$, every n-qudit gate can be obtained exactly by a unitary quantum circuit made up of gates from S.*

The reason for the distinction between universality and exact universality is that a universal gate set generates a dense subgroup of $SU(d^n)$, while an exact universal gate set should generate the group $SU(d^n)$ itself.

Many gate sets have proven to be exact universal, such as the one formed by Givens rotations and the one by Householder reflections [64]. A Givens rotation, called two-level unitary gate sometimes [123], is a unitary operator acting on a two-dimensional subspace of $\mathscr{H}$ spanned by basis states $|i\rangle$ and $|j\rangle$ and takes the form

$$G_{ij} := R_n(2\theta)_{ij} \oplus \mathbb{1}_{\bar{ij}}, \tag{3.1}$$

with $\mathbb{1}_{\bar{ij}}$ denoting the identity operator acting on the rest of $\mathscr{H}$, and $R_n(2\theta)_{ij}$ is a qubit rotation on the space span$(|i\rangle, |j\rangle)$ with

$$R_n(2\theta) := e^{-i\theta \boldsymbol{n}\cdot\boldsymbol{\sigma}} = \cos\theta \mathbb{1} - i\sin\theta(n_x X + n_y Y + n_z Z). \tag{3.2}$$

Another commonly used representation of qubit rotation is

$$U := \begin{pmatrix} e^{i\xi}\cos\theta & -e^{-i\eta}\sin\theta \\ e^{i\eta}\sin\theta & e^{-i\xi}\cos\theta \end{pmatrix} = R_z(\xi-\eta)R_y(2\theta)R_z(\xi+\eta), \tag{3.3}$$

with

$$R_z(2\alpha) = \begin{pmatrix} e^{i\alpha} & 0 \\ 0 & e^{-i\alpha} \end{pmatrix}, R_y(2\theta) = \begin{pmatrix} \cos\theta & -\sin\theta \\ \sin\theta & \cos\theta \end{pmatrix}. \tag{3.4}$$

A general unitary matrix $U \in SU(N)$ can be factorized as $N(N-1)/2 \in O(N^2)$ Givens rotations [123, 64]. If the Hilbert space $\mathscr{H}$ has a tensor-product structure, such as n-qubit system, then a Givens rotation can be further decomposed exactly as products of CNOT gates and qubit gates [123]. Then the set formed by all qubit gates and CNOT, denoted by $\{\{R\}, \text{CNOT}\}$ with R denoting a qubit gate (3.2) , is an exact universal gate library for unitary operator $U \in SU(2^n)$ [9, 117, 118, 162].

Examples for gate decomposition in terms of Givens rotations would help. A qutrit unitary operator $U \in SU(3)$ takes the form [119, 166]

$$U = \begin{pmatrix} e^{i\phi_1}c_1c_2 & e^{i\phi_3}s_1 & e^{i\phi_4}c_1s_2 \\ e^{-i\phi_4-i\phi_5}s_2s_3 - e^{i\phi_1+i\phi_2-i\phi_3}s_1c_2c_3 & e^{i\phi_2}c_1c_3 & -e^{-i\phi_1-i\phi_5}c_2s_3 - e^{i\phi_2-i\phi_3+i\phi_4}s_1s_2c_3 \\ -e^{-i\phi_2-i\phi_4}s_2c_3 - e^{i\phi_1-i\phi_3+i\phi_5}s_1c_2s_3 & e^{i\phi_5}c_1s_3 & e^{-i\phi_1-i\phi_2}c_2c_3 - e^{-i\phi_3+i\phi_4+i\phi_5}s_1s_2s_3 \end{pmatrix}, \tag{3.5}$$

with three Euler angles θ_j ($0 \leq \theta_j \leq \pi/2$; $j = 1, 2, 3$) and five phases ϕ_k ($0 \leq \phi_k \leq 2\pi$; $k = 1, 2, 3, 4, 5$), where $c_k := \cos\theta_k$ and $s_k := \sin\theta_k$, which can be further written as a product of three Givens rotations

$$U = G_{23}(\theta_3, \phi_2 - \phi_5, 0) G_{12}(\theta_1, -\phi_5, \phi_3 + \pi) G_{31}(\theta_2, \phi_1 + \phi_5, \phi_4 + \phi_5), \tag{3.6}$$

with

$$G_{23}(\theta, \xi, \eta) = \begin{pmatrix} 1 & 0 & 0 \\ 0 & e^{i\xi}\cos\theta & -e^{i\eta}\sin\theta \\ 0 & e^{-i\eta}\sin\theta & e^{-i\xi}\cos\theta \end{pmatrix}, \tag{3.7}$$

$$G_{31}(\theta, \xi, \eta) = \begin{pmatrix} e^{i\xi}\cos\theta & 0 & e^{i\eta}\sin\theta \\ 0 & 1 & 0 \\ -e^{-i\eta}\sin\theta & 0 & e^{-i\xi}\cos\theta \end{pmatrix}, \tag{3.8}$$

$$G_{12}(\theta, \xi, \eta) = \begin{pmatrix} e^{i\xi}\cos\theta & -e^{i\eta}\sin\theta & 0 \\ e^{-i\eta}\sin\theta & e^{-i\xi}\cos\theta & 0 \\ 0 & 0 & 1 \end{pmatrix}. \tag{3.9}$$

For unitary operator $U \in SU(4)$ a Givens rotation decomposition can be found in Ref. [119].

Furthermore, for the multi-qudit computation [120, 32, 25, 31], it is proved that the set containing all two-qudit gates is exact universal [31]. More importantly, the following results are known.

Definition 8 ([31]). *A two-qudit gate V is* primitive *if and only if it is decomposable $V = S \otimes T$ for some qudit gates S and T.*

Theorem 12 ([31]). *The collection of all qudit gates and a two-qudit imprimitive gate is exact universal.*

It is further shown that almost all two-qudit gate is imprimitive. A notable example of two-qudit imprimitive gate is the so-called SUM gate [48, 66]

$$\text{SUM} : |s_1\rangle|s_2\rangle \mapsto |s_1\rangle|s_1 \oplus s_2 (\text{mod } d)\rangle. \tag{3.10}$$

As a general qudit gate can be exactly decomposed into a product of Givens rotations, the set formed by all Givens rotations together with the SUM gate, $\{\{G\}, \text{SUM}\}$ with G denoting a general Givens rotation (3.1), is exact universal for $U \in SU(d^n)$.

3.2 Solovay-Kitaev theorem

For fault-tolerant computation, single-qubit gate that contains continuous parameters (e.g. Euler angles) needs to be substituted by special gates which are "discrete". It is proved that the T gate and Hadamard gate H together generate a dense subset of $SU(2)$ [125] with

$$\text{H} = \frac{1}{\sqrt{2}} \begin{pmatrix} 1 & 1 \\ 1 & -1 \end{pmatrix}, \quad \text{T} \equiv Z^{1/4} = \begin{pmatrix} 1 & 0 \\ 0 & e^{i\pi/4} \end{pmatrix}. \tag{3.11}$$

A *word* from $\{\text{H}, \text{T}\}$ is a finite-length product of H and T. The set $\{\text{H}, \text{T}, \text{CNOT}\}$ is universal for compiling any n-qubit unitary gate. Generally, given an arbitrary discrete universal gate library S for $SU(N)$, the Solovay-Kitaev theorem states that an arbitrary unitary gate $U \in SU(N)$ can be approximated within distance $\epsilon > 0$ by a sequence of gates from S with length $O(\log^c \frac{1}{\epsilon})$, for $1 \leq c \leq 4$ [92]. The Solovay-Kitaev theorem does not rely on the types of universal gate library being used. Here we recast this theorem for qubit case, and we also only present the algorithm for qubit case.

Theorem 13 (Solovay-Kitaev theorem for qubit gate [92, 123])**.** *Let S be a discrete universal gate library for $SU(2)$, then any gate $U \in SU(2)$ can be approximated within distance $\epsilon \geq 0$ by a sequence of gates from S with length $O(\log^c \frac{1}{\epsilon})$, for $1 \leq c \leq 4$, and there is a polynomial algorithm that constructs such a decomposition.*

The proof can be found in the original text [92], and two approaches are provided. One is based on the group commutator method, and the other involves ancilla and phase estimation method. Below we review the constructive approach given by Dawson and Nielsen [49] using group commutator.

Algorithm 1 The SKDN algorithm for single-qubit unitary gate compiling

Input:

U: a single-qubit unitary gate

n: the depth

Output:

U_n: the approximate unitary gate

function SKDN(U, n)

if $n = 0$ **then**

return U_0. ▷ Initial approximation from lookup table

else

$U_{n-1} \leftarrow \text{SKDN}(U, n-1)$.

$V, W \leftarrow \text{BGC}(UU_{n-1}^{\dagger})$. ▷ Balanced group commutator decomposition

$V_{n-1} \leftarrow \text{SKDN}(V, n-1)$.

$W_{n-1} \leftarrow \text{SKDN}(W, n-1)$.

return $U_n = V_{n-1}W_{n-1}V_{n-1}^{\dagger}W_{n-1}^{\dagger}U_{n-1}$.

end if

end function

3.2.1 Solovay-Kitaev algorithm for qubit gates

As the algorithm given by Dawson and Nielsen [49] is not exactly the same with the ones in the original text [92], we term the algorithm as Solovay-Kitaev-Dawson-Nielsen (SKDN) algorithm, shown in Algorithm 1. The SKDN algorithm takes an arbitrary single-qubit unitary operator U and an error tolerance ϵ, which is equivalent to the iteration depth n, as input, and delivers the approximation U_n at the n-th depth as output. The algorithm finds a polynomial-length gate sequence to approximate U by starting with an initial approximation U_0 with initial error bound ϵ_0, followed by iteratively constructing operators using balanced group commutator (BGC) to produce decreasing errors. Note the SKDN algorithm does not decompose the gate U directly in terms of products of H and T; instead the algorithm decomposes the gate U in terms of other gates, which are products of H and T.

A schematic illustration of the SKDN algorithm is shown in Fig. 3.1. Let us also take one example to see how the SKDN algorithm works. Suppose the depth $n = 2$ is good enough for our purpose, now we describe the steps. 1) Find an initial approximation U_0 from the lookup table for U, and the distance between them is below $\epsilon_0 \leq 1/32 \approx 0.03125$. 2) Find V and W such that $UU_0^\dagger = VWV^\dagger W^\dagger$ based on balanced group commutator [49]; note V and W are close to identity. 3) Find an initial approximation V_0 for V, and W_0 for W from the lookup table. 3) Output $U_1 = V_0 W_0 V_0^\dagger W_0^\dagger U_0$. 4) Find N and M such that $UU_1^\dagger = NMN^\dagger M^\dagger$; note N and M are close to identity. 5) Find an initial approximation N_0 for N. 6) Find A and B such that $NN_0^\dagger = ABA^\dagger B^\dagger$; note A and B are close to identity. 7) Find an initial approximation A_0 for A, and B_0 for B. 8) Output $N_1 = A_0 B_0 A_0^\dagger B_0^\dagger N_0$. 9) Find an initial approximation M_0 for M. 10) Find C and D such that $MM_0^\dagger = CDC^\dagger D^\dagger$; note C and D are close to identity. 11) Find an initial approximation C_0 for C, and D_0 for D. 12) Output $M_1 = C_0 D_0 C_0^\dagger D_0^\dagger M_0$. 13) Output $U_2 = N_1 M_1 N_1^\dagger M_1^\dagger U_1$.

Next we provide the proof for Theorem 13 briefly following Ref. [49], the details can be found in their original paper.

Proof. Let the error at the n-th depth be ϵ_n, and let l_n be the length of sequences of gates returned by the SKDN algorithm, and let t_n be the corresponding classical runtime. Then it is found that $\epsilon_n = c_{\text{approx}} \epsilon_{n-1}^{3/2}$, $l_n = 5 l_{n-1}$, and $t_n \leq 3 t_{n-1} + \text{const}$, where the constant overhead in t_n mainly comes from the task for balanced group commutator. In order to ensure $\epsilon_n < \epsilon_{n-1}$, it requires $\epsilon_{n-1} < 1/c_{\text{approx}}^2$. Also the initial error ϵ_0 needs to satisfy $\epsilon_0 < 1/c_{\text{approx}}^2$. From some heuristic argument [49], it is found that $c_{\text{approx}} \approx 4\sqrt{2}$, so $\epsilon_0 < 1/32$. A lookup table with the distance between any two nearby data points smaller than $1/32$ can provide the initial approximation. For the classical runtime t_n and number of quantum gates l_n, one finds that $l_n = O(5^n)$, $t_n = O(3^n)$. From the iterative relation on ϵ_n, one can express n in terms of ϵ_n. Finally, the scaling of runtime t and number of gates l becomes $l = O(\log^{3.97} \frac{1}{\epsilon})$, and $t = O(\log^{2.71} \frac{1}{\epsilon})$. □

3.3 Lookup table

One of the merits of the SKDN algorithm is that it has explicit classical complexity for the decomposition algorithm and the quantum complexity for the gate sequence. However, there are also some drawbacks. The SKDN algorithm assumes the existence of a lookup table which can be used for the initial approximation and also for later iterations, depicted schematically in Fig. 3.1, without a detailed analysis of how to build such a lookup table and how to use it. This lookup table is important for the SKDN algorithm, particularly for practical applications. Here we build such a lookup table with a 3D lattice structure, which enables a geometric search strategy for the initial approximation, depicted in Fig. 3.2. Once the lookup table is built and stored, it saves time for obtaining the initial approximation.

Any single-qubit unitary operator, denoted as $U(\boldsymbol{\theta}) = \exp(-i\boldsymbol{\theta}\cdot\boldsymbol{\sigma}), \quad \boldsymbol{\sigma} := (X, Y, Z)$, can be identified with coordinate $\boldsymbol{\theta} \in \mathbb{R}^3$. As $U(\boldsymbol{\theta}) = U(\boldsymbol{\theta}(1 - \pi/\theta))$, for $\theta := |\boldsymbol{\theta}|$, the space $\mathbb{R}^3$

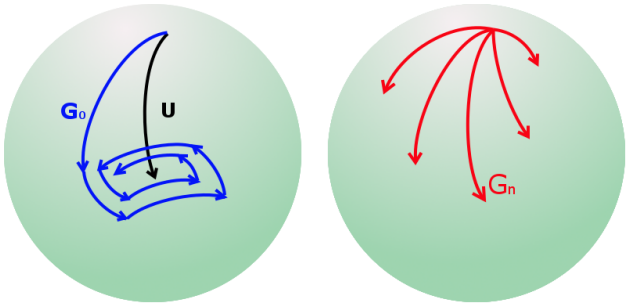

Figure 3.1: Schematic diagram for the SKDN algorithm. (Left) Representation of the algorithm on the Bloch sphere. The action of the given qubit gate U on an arbitrary state is represented by the black curved arrow. The initial approximation from the lookup table is represented by G_0, and the iterative process is represented by the collection of spiral arrows. (Right) Action of gates in the lookup table, denoted as G_n, is represented as rotations of the sphere. This table gives each G_n as a sequence of gates from the universal gate library S. [Figure from Ref. [168], Fig. 2.]

can be reduced to a radius $\pi/2$ ball, as depicted in Fig. 3.2. We therefore embed a cubic lattice into $\mathbb{R}^3$ to use as a lookup table. That is, we construct a database such that, for each cube, there is a sequence of gates from the gate library S that produces a data point gate within that cube. Each cube has side length $\frac{1}{32\sqrt{3}}$, thereby ensuring a maximum separation of $1/32$ between a unitary operator and its approximating sequence, which is sufficient for the initial step of the SKDN algorithm.

Along the radial direction, there are about 175 cubes, being each cube labeled via the coordinate of its center as $\boldsymbol{\vartheta} := (i, j, k)$. Each gate can be mapped into a point with a position $\boldsymbol{\theta} := (a, b, c)$. The points may fall into three different regions: I) inside of the ball; II) near the boundary inside of the ball; III) outside of the ball. Each point within the ball takes a positive value for $\cos\theta$. The point in region III takes a negative value for $\cos\theta$, yet it can be converted into the point within the sphere via $\theta' = \pi - \theta$, and $a' = a(1 - \pi/\theta)$,

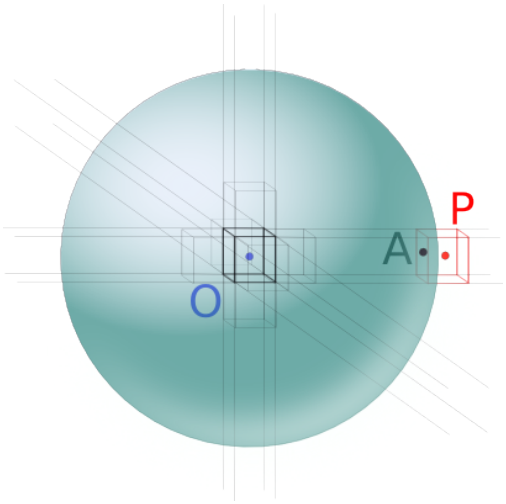

Figure 3.2: Schematic diagram for the lookup table for SKDN algorithm. The radius-$\pi/2$ ball represents the set of single-qubit gates (note that this is different from the Bloch ball). The period-$\frac{1}{32\sqrt{3}}$ lattice takes origin at O. Each cube on the lattice is labeled by the coordinate at its center, and contains one data point. At the boundary, the center of a cube can lie outside the ball but still must be a legitimate region for the search algorithm. [Figure from Ref. [168], Fig. 2.]

$b' = b(1-\pi/\theta)$, $c' = c(1-\pi/\theta)$, since the difference between the two points is a trivial global phase. Consequently all possible qubit gates can be embedded into the ball of radius $\pi/2$. There are totally about $2878147 \approx \frac{4}{3}\pi(\frac{175}{2})^3$ cells.

Then, in the SKDN algorithm, given a qubit gate U to be approximated, we identify which cube $\boldsymbol{\vartheta}$ in the lattice the gate U occupies, and then select the corresponding data point gate from the database. For instance, if the universal gate library is $\{\text{H}, \text{T}\}$, our numerical simulation shows that no more than 36 gates of them are enough to build the lookup table.

3.4 Discussion and conclusion

In the above, we have built up the lookup table for the initial stage of the SKDN algorithm. The higher-levels of recursion of this algorithm also call this lookup table; however, some improvement for our lookup table is needed. The reason is as follows. The output of the SKDN algorithm U_n is a sequence of data point gates, which are all close to the identity gate except the initial approximation U_0, which is the gate at the rightmost of the output sequence. Our lookup table is enough to deliver U_0, yet for all other gates in U_n it provides the same data point gate, which is the gate in the cube at the origin of the lookup table. That is to say, one may need to store more than one data points for the central cell, which requires further efforts.

The SKDN algorithm has some drawbacks even with a well-developed lookup table. One drawback is that SKDN algorithm yields an extremely long sequence of gates. As a result, other algorithms have been developed following different methods [96, 95, 130, 52, 146], and those algorithms can lead to shorter sequences. Also without executing higher-level recursion, Ref. [130] developed a geometric method to obtain the initial approximation, which improves the initial accuracy beyond 1/32 at the cost of a longer sequence compared with our approach.

The constant c in the scaling of Solovay-Kitaev theorem has the lower bound $c_{\min} = 1$, which is yet not reached by the SKDN algorithm. The proof for the lower bound follows from a volume argument [72, 123]. An algorithm achieving the lower bound for qubit gate compiling has been constructed [94], with constant number of ancillary qubits. The key steps of this algorithm are as follows. 1) Given U, construct $U' = |0\rangle\langle 1| \otimes U + |1\rangle\langle 0| \otimes U^\dagger$ such that $U'|1\rangle|\psi\rangle = |0\rangle U|\psi\rangle$. 2) From Householder reflection decomposition, $U' = R_1 R_2$ for $R_1 = \mathbb{1} - 2P_1$ and similar for R_2, and projector $P_1 = |\omega_1\rangle\langle\omega_1|$, and $|\omega_1\rangle$ is eigenvector of U' such that $U'|\omega_1\rangle = -|\omega_1\rangle$. One then needs to implement reflections R_1 and R_2. 3) According to number theory and ring theory, it is shown that the gate set $\{\mathrm{T}, \mathrm{H}\}$ is equivalent to the ring $\mathbb{Z}[i, 1/\sqrt{2}]$ [96, 95, 62], and the entries of a state takes the form $((a+\sqrt{2}b)+i(c+\sqrt{2}d))/\sqrt{2}^k$ for numbers a, b, c, d, and then a reflection operator can be implemented with $O(k)$ Clifford gate plus T gates. 4) For error tolerance ϵ, one needs to set $k = O(\frac{1}{\epsilon})$ [94]. Although this algorithm achieves the lower bound $c_{\min}$, an optimal algorithm without ancilla is still missing.

For conclusion, we have studied the unitary qubit gate compiling problem, and we have built up the lookup table for the initial stage of the SKDN algorithm for unitary qubit gate compiling. Our construction of the lookup table explores the geometry of the set of qubit gates. We also compared with other algorithms for qubit gate compiling to emphasize the features of the SKDN algorithm.

Chapter 4

Quantum channel decomposition and simulation

In this chapter we present the quantum channel decomposition theory and algorithm in terms of convex sum of generalized extreme channels, which have been published in our paper [169]. Quantum channel decomposition based on extreme channels has been an open problem since 2007 from Ruskai's conjecture [139], while such decomposition is appealing and beneficial for quantum simulation for the sake of resource consumption. We have developed an approximate decomposition algorithm that has been demonstrated for low-dimensional cases, including the qubit, qutrit, and two-qubit channels.

In §4.1 we provide a detailed characterization of extreme and generalized extreme channels, including the Kraus operator-sum, Choi state, and quantum circuit representations relying on Choi's theorem on extreme channels [42] and Ruskai's description of generalized extreme channels [139]. Next we present our quantum channel simulation algorithm based on the convex sum decomposition, and we construct an optimization algorithm for the design of quantum channel simulator circuit in §4.2. In §4.3 we also compare different strategies for channel decomposition and simulation, and then conclude in §4.4.

4.1 Extreme quantum channels

Before our study of quantum channel decomposition problem, we first focus on extreme and generalized extreme quantum channels. We start from the review of their mathematical characterizations, and then we present our constructions of extreme and generalized extreme channels, including the Kraus operator-sum, Choi state, and quantum circuit representations.

4.1.1 Mathematical characterization

First we review and analyze the mathematical characterization of extreme quantum channels, which is the foundation for channel simulation. From convex set theory, a channel is extreme if it cannot be written as a convex combination of other channels. For instance, unitary channels specified by unitary operators are extreme. The first mathematical characterization of extreme channels is provided by Choi [42] in his seminal work on CP mappings.

Choi's theorem is for CP mappings with a condition on the unitality, i.e., the action on the identity operator $\mathbb{1}$. We first review this theorem, and then we apply it for the case with a condition on the trace, which is more suitable for the study of quantum channels in Schrödinger picture. Denote the set of CP mappings $\mathcal{N} : \mathscr{D}_n \to \mathscr{D}_m$ with Kraus operators $\{K_i\}$ and $\sum_i K_i^\dagger K_i = L$, $\sum_i K_i K_i^\dagger = K$ by $\mathscr{S}_{n,m}(K, L)$. When there is no condition on the trace, we denote the set as $\mathscr{S}_{n,m}(K, \varnothing)$, and when there is no condition on the unitality, we denote the set as $\mathscr{S}_{n,m}(\varnothing, L)$.

Theorem 14 (Choi's theorem [42])**.** *Let a CP mapping $\mathcal{N} : \mathscr{D}_n \to \mathscr{D}_m$. Then $\mathcal{N}$ is extreme in $\mathscr{S}_{n,m}(K, \varnothing)$ iff $\mathcal{N}(\rho) = \sum_i K_i \rho K_i^\dagger$ with $\sum_i K_i K_i^\dagger = \mathcal{N}(\mathbb{1}) = K$ and $\{K_j K_i^\dagger\}$ is linearly independent.*

Proof. The "only if" part. We need to prove that if a map is extreme, then the set $\{K_j K_i^\dagger\}$ is linearly independent; that is $\sum_{ij} \lambda_{ij} K_j K_i^\dagger = 0$ for unique solution $\lambda_{ij} = 0$. Let $\mathcal{N}(\rho) = \sum_i K_i \rho K_i^\dagger$, define $\Psi_\pm(\rho) = \sum_i K_i \rho K_i^\dagger \pm \sum_{ij} \lambda_{ij} K_j \rho K_i^\dagger$. The parameters λ_{ij} form a matrix Λ, without loss of generality, suppose Λ is hermitian and $-\mathbb{1} \le \Lambda \le \mathbb{1}$. Define $P := \Gamma^\dagger \Gamma = \Lambda + \mathbb{1}$ for $\Gamma = [\gamma_{ij}]$, then $P_{j\ell} = \sum_i \gamma_{ij}^* \gamma_{i\ell} = \delta_{j\ell} + \lambda_{j\ell}$. Let $W_i = \sum_j \gamma_{ij} K_j$, then

$$\begin{aligned} \Psi_+(\rho) &= \sum_i W_i \rho W_i^\dagger \\ &= \sum_i \left(\sum_\ell \gamma_{i\ell} K_\ell \right) \rho \left(\sum_j \gamma_{ij}^* K_j^\dagger \right) \\ &= \sum_{j\ell} (\delta_{j\ell} + \lambda_{j\ell}) K_\ell \rho K_j^\dagger, \end{aligned} \tag{4.1}$$

and $\sum_i W_i W_i^\dagger = K$. This means Ψ_+ is a CP map. Also Ψ_- is a CP map. From $\mathcal{N} = (\Psi_+ + \Psi_-)/2$ and that $\mathcal{N}$ is extreme, we find $\mathcal{N} = \Psi_+ = \Psi_-$. Then Γ is an isometry which implies $\Lambda = 0$.

The "if" part. We need to prove linearly independence implies $\mathcal{N}$ is extreme. Suppose $\mathcal{N} = (\Psi_1 + \Psi_2)/2$ with $\Psi_1(\rho) = \sum_p W_p \rho W_p^\dagger$ and $\Psi_2(\rho) = \sum_q Z_q \rho Z_q^\dagger$, and $\sum_p W_p W_p^\dagger = \sum_q Z_q Z_q^\dagger = \sum_i K_i K_i^\dagger$. We can let $W_p = \sum_i u_{pi} K_i$, then $\sum_p W_p W_p^\dagger = \sum_{pij} u_{pi}^* u_{pj} K_j K_i^\dagger$, which means $[u_{pi}]$ is an isometry. Then $\mathcal{N} = \Psi_1$, and $\mathcal{N}$ is extreme. □

A recast of Choi's theorem for the case with the trace condition is as follows. The proof method is essentially the same, yet for completeness, we still include the proof below.

Theorem 15 (Choi's theorem for $\mathscr{S}_{n,m}(\varnothing, L)$)**.** *Let a CP mapping $\mathcal{N} : \mathscr{D}_n \to \mathscr{D}_m$. Then $\mathcal{N}$ is extreme in $\mathscr{S}_{n,m}(\varnothing, L)$ iff $\mathcal{N}(\rho) = \sum_i K_i \rho K_i^\dagger$ with $\sum_i K_i^\dagger K_i := \mathcal{N}^t(\mathbb{1}) = L$ and $\{K_i^\dagger K_j\}$ is linearly independent.*

Proof. The "only if" part. We need to prove that if a channel is extreme, then the set $\{K_i^\dagger K_j\}$ is linearly independent; that is $\sum_{ij} \lambda_{ij} K_i^\dagger K_j = 0$ for unique solution $\lambda_{ij} = 0$. Let $\mathcal{N}(\rho) = \sum_i K_i \rho K_i^\dagger$, define $\Psi_\pm(\rho) = \sum_i K_i \rho K_i^\dagger \pm \sum_{ij} \lambda_{ij} K_j \rho K_i^\dagger$. The parameters λ_{ij} form a matrix Λ, without loss of generality, suppose Λ is hermitian and $-\mathbb{1} \le \Lambda \le \mathbb{1}$. Define $P := \Gamma^\dagger \Gamma = \Lambda + \mathbb{1}$ for $\Gamma = [\gamma_{ij}]$, then $P_{j\ell} = \sum_i \gamma_{ij}^* \gamma_{i\ell}$. Let $W_i = \sum_j \gamma_{ij} K_j$,

$$\begin{aligned}
\Psi_+(\rho) &= \sum_i W_i \rho W_i^\dagger \\
&= \sum_i \left(\sum_\ell \gamma_{i\ell} K_\ell \right) \rho \left(\sum_j \gamma_{ij}^* K_j^\dagger \right) \\
&= \sum_{j\ell} (\delta_{j\ell} + \lambda_{j\ell}) K_\ell \rho K_j^\dagger, \qquad (4.2)
\end{aligned}$$

and $\sum_i W_i^\dagger W_i = L$. This means Ψ_+ is a CP map. Also Ψ_- is a CP map. From $\mathcal{N} = (\Psi_+ + \Psi_-)/2$ and that $\mathcal{N}$ is extreme, we find $\mathcal{N} = \Psi_+ = \Psi_-$. Then Γ is an isometry which implies $\Lambda = 0$.

The "if" part. We need to prove linearly independence implies extreme. Suppose $\mathcal{N} = (\Psi_1 + \Psi_2)/2$ with $\Psi_1(\rho) = \sum_p W_p \rho W_p^\dagger$ and $\Psi_2(\rho) = \sum_q Z_q \rho Z_q^\dagger$, and $\sum_p W_p^\dagger W_p = \sum_q Z_q^\dagger Z_q = \sum_i K_i^\dagger K_i$. We can let $W_p = \sum_i u_{pi} K_i$, then $\sum_p W_p^\dagger W_p = \sum_{pij} u_{pi}^* u_{pj} K_i^\dagger K_j$, which means $[u_{pi}]$ is an isometry. Then $\mathcal{N} = \Psi_1$, and $\mathcal{N}$ is extreme. □

Furthermore, we introduce the following corollaries for CPTP, unital CP, and unital CPTP extreme mappings, and the proofs of them are straightforward.

Corollary 16 (Extreme CPTP mappings, i.e. quantum channels)**.** *A channel $\mathcal{E} \in \mathscr{S}_{n,m}(\varnothing, \mathbb{1})$ is extreme iff $\mathcal{E}(\rho) = \sum_i K_i \rho K_i^\dagger$ with $\sum_i K_i^\dagger K_i = \mathcal{E}^t(\mathbb{1}) = \mathbb{1}$ and $\{K_i^\dagger K_j\}$ is linearly independent.*

We find that $\{K_i^\dagger K_j\}$ forms a basis for the space $\mathscr{D}_n$, so the rank of an extreme CPTP channel is upper bounded by n.

Corollary 17 (Extreme unital CP mappings)**.** *A mapping $\mathcal{N} \in \mathscr{S}_{n,m}(\mathbb{1}, \varnothing)$ is extreme iff $\mathcal{N}(\rho) = \sum_i K_i \rho K_i^\dagger$ with $\sum_i K_i K_i^\dagger = \mathcal{N}(\mathbb{1}) = \mathbb{1}$ and $\{K_j K_i^\dagger\}$ is linearly independent.*

We find that $\{K_j K_i^\dagger\}$ forms a basis for space $\mathscr{D}_m$, so the rank of an extreme unital CP mapping is upper bounded by m.

The set of unital CP mappings is also convex, so a unital CP mapping is in the convex hull of its extreme points. According to Birkhoff's theorem 8, which states that doubly stochastic matrices are in the convex hull of permutations, one might expect that the quantum version is that unital CP mappings, which are doubly stochastic CP mappings, are in the convex hull of unitary operators. This turns out not to be true according to Theorem 10, since there are unital CP mappings which are not a convex combination of unitary operators. The reason is that there are extreme points with rank bigger than one for the set of unital CP mappings, demonstrated by Landau and Streater's theorem.

Theorem 18 (Landau and Streater [100]). *A mapping $\mathcal{N} \in \mathscr{S}_{n,m}(K, L)$ is extreme iff $\mathcal{N}(\rho) = \sum_i K_i \rho K_i^\dagger$ with $\sum_i K_i^\dagger K_i = \mathcal{N}^t(\mathbb{1}) = L$, $\sum_i K_i K_i^\dagger = \mathcal{E}(\mathbb{1}) = K$ and $\{K_i^\dagger K_j\}$ and $\{K_j K_i^\dagger\}$ are both linearly independent.*

This theorem directly applies to the case of unital channels. Also it is clear that the condition for unital extreme channels is weaker than that for extreme channels. It follows that the rank of an extreme unital channel is bounded above by $\sqrt{2}d$, which is bigger than that for a general extreme channel. This implies, for the implementation of extreme channel, the extreme unital channel requires larger ancillary dimension than a general extreme channel. Also since one unital channel is also in the convex hull of general extreme channels, we can use the same method for the simulation of unital and nonunital channels, and we do not need to employ convex combination of extreme unital channels.

Furthermore, one important property of extreme channel is the unitary invariance stated as follows. For simplicity, we term the linear-independence condition on Kraus operators as the extremality of a CP mapping.

Proposition 19. *The extremality of an extreme CP mapping $\mathcal{N}^{\mathrm{e}}$ remains under the composition with initial and final unitary channels, denoted as $\mathcal{V}$ and $\mathcal{W}$, respectively. That is, $\mathcal{W}\mathcal{N}^{\mathrm{e}}\mathcal{V}$ is also extreme.*

Proof. The proof is straightforward by observing that the linear-independence condition of Kraus operators is irrelevant with initial and final unitary channels. □

The extreme channels also form a set, yet not closed. Generally for the set $\mathscr{S}_{n,m}$ define the set of rank up to n channels as $\mathscr{S}_{n,m}^{\leq n}$. A channel $\mathcal{E} \in \mathscr{S}_{n,m}^{\leq n}$ is called a generalized extreme channel [139], which may be extreme if the linearly independence condition is satisfied, quasi-extreme if not. The following theorem is originally due to Ruskai [139], while here we include it in a more compact way for the understanding of generalized extreme channels.

Theorem 20 (Ruskai's theorem [139]). *The set $\mathscr{S}_{n,m}^{\leq n}$ is the closure of the set of extreme channels in $\mathscr{S}_{n,m}$.*

Proof. The method is to prove that a not-extreme channel in $\mathscr{S}_{n,m}^{\leq n}$ is arbitrarily close to an extreme channel. Suppose a channel $\Phi \in \mathscr{S}_{n,m}^{\leq n}$ is not extreme and its Kraus operators are $\{A_k\}$ for $0 \leq k \leq r-1$. If $r < n$, we can add new Kraus operators $A_m = 0$ to form a rank-n channel. That is, without loss of generality, we can let the rank of Φ be n. Let $\mathcal{E}$ be a rank-n extreme channel with Kraus operators B_k. Define $C_k := A_k + \epsilon B_k$. Then the set $\{C_j^\dagger C_k\}$ can be linearly independent. Define $M := [\text{res}C_j^\dagger C_k]$ as the matrix with each column as the reshaping vector for each $C_j^\dagger C_k$. Then the linear-independence of $\{C_j^\dagger C_k\}$ is equivalent to $\det M \neq 0$. Suppose the smallest positive root of $\det M$ is ϵ_*, then for $\epsilon \in (0, \epsilon_*)$ the set $\{C_j^\dagger C_k\}$ is linearly independent. Then, Kraus operators $\{C_k S^{-1/2}\}$ defines an extreme channel $\Phi(\epsilon)$, with $S = \sum_k C_k^\dagger C_k$ a positive operator for some ϵ. Then $\lim_{\epsilon \to 0} \Phi(\epsilon) = \Phi$, which means Φ belongs to the closure of the set of extreme channels. □

A recent result [57] shows that the set of extreme channels dominates the set of generalized extreme channels from a semi-algebraic geometry approach. For clarity, we denote a generalized extreme channel as $\mathcal{E}^{\text{g}}$, and a quasi-extreme channel as $\mathcal{E}^{\text{q}}$. It is clear that a channel $\mathcal{E}^{\text{q}}$ can be written as a convex sum of at least two extreme channels for its decomposition. Those theorems above are the mathematical starting points of our study.

4.1.2 Kraus operator-sum representation of extreme channels

In the following we focus on the representation of extreme qudit channels. For Ruskai's theorem 20, let $n = m := d$, we find the rank of an extreme qudit channel $\mathcal{E}^{\text{e}}$ is upper bounded by d. We denote the set of qudit channels as $\mathscr{S}_d$ by indicating the dimension explicitly.

Proposition 21. *A rank-d extreme qudit channel $\mathcal{E}^{\text{e}} \in \mathscr{S}_d$ can be represented by*

$$\mathcal{E}^{\text{e}}(\rho) = \sum_{i=0}^{d-1} K_i \rho K_i^\dagger \tag{4.3}$$

for any Kraus operators satisfying

$$K_i := WF_iV,\ F_i := X_iE_i,\ E_i := \sum_{j=0}^{d-1} a_{ij}Z_j,\ i \in \mathbb{Z}_d, \tag{4.4}$$

for any unitary operators $V, W \in SU(d)$, provided that $\{a_{ij} \in \mathbb{C}\}$ is chosen such that the set $\{F_i^\dagger F_j\}$ is linearly independent and $\sum_{i=0}^{d-1} F_i^\dagger F_i = \mathbb{1}$ is satisfied.

Proof. Per definition, Eq. (4.3) holds for any rank-d extreme qudit channel with $\{K_i^\dagger K_j\}$ being linearly independent. Thus, the proof focuses on showing that the construction (4.4) yields arbitrary linearly independent operators $\{K_i^\dagger K_j\}$.

Linear independence of $\{K_i^\dagger K_j\}$ requires that

$$\Xi := \sum_{i,j=0}^{d-1} \gamma_{ij}K_i^\dagger K_j = 0 \iff \gamma_{ij} \equiv 0\ \forall i, j. \tag{4.5}$$

From Eq. (4.4), $\Xi = V^\dagger \left(\sum_{ij} \gamma_{ij}F_i^\dagger F_j\right) V$. This is a unitary conjugation of the sum in parentheses so we ignore V in the proof. Therefore, we need to require linear independence of $\{F_i^\dagger F_j\}$. For

$$b_{i\mu\nu} := \sum_{k,l=0}^{d-1} a_{ik}^* a_{i+\mu,l} \mathrm{e}^{\mathrm{i}2\pi[\mu l+\nu(l-k)]/d},\ \mu \in \mathbb{Z}_d, \tag{4.6}$$

we observe that $F_i^\dagger F_{i+\mu} = \sum_{\nu=0}^{d-1} b_{i\mu\nu}|\nu\rangle\langle\nu+\mu|$, which yields $\mathrm{tr}[(F_i^\dagger F_{i+\mu})^\dagger F_j^\dagger F_{j+\mu'}] = 0$ for $\mu \neq \mu'$. Now we partition

$$\left\{F_i^\dagger F_{i+\mu}; i, \mu \in \mathbb{Z}_d\right\} \to \left\{\{F_i^\dagger F_{i+\mu}; i \in \mathbb{Z}_d\}; \mu \in \mathbb{Z}_d\right\}. \tag{4.7}$$

For $\{F_i^\dagger F_{i+\mu}\}$ to be a linearly independent set, each subset must be linearly independent. For each subset, $\Xi_\mu := \sum_{i=0}^{d-1} \gamma_{i,i+\mu}F_i^\dagger F_{i+\mu}$ so $\Xi = \sum_{\mu=0}^{d-1} \Xi_\mu$. Then $\Xi \equiv 0$ implies $\Xi_\mu \equiv 0\ \forall\mu$.

Now we establish linear independence of $\{F_i^\dagger F_j\}$ by constraining each subset (4.7). First we map each matrix $F_i^\dagger F_{i+\mu}$ to a vector $\boldsymbol{b}_{i\mu} := (b_{i\mu\nu})$. Then linear independence of $\{F_i^\dagger F_{i+\mu}\}$ can be ensured by the condition that the determinant of each matrix $B_\mu := (\boldsymbol{b}_{i\mu})$ is nonzero; i.e. $\det B_\mu \neq 0\ \forall\mu$ (except for a subset of values of a_{ij} of measure zero). Then $\Xi_\mu \equiv 0$ implies $\gamma_{i,i+\mu} \equiv 0\ \forall i, \mu$, which establishes linear independence of $\{F_i^\dagger F_j\}$ hence also $\{K_i^\dagger K_j\}$.

As $\{F_i^\dagger F_j\}$ spans $\mathscr{L}(\mathscr{H})$, hence a basis, the composition with V and also W ensures that an arbitrary basis $\{K_i^\dagger K_j\}$ can be realized. Subsequent to this, the proof showing extremality of the channel (4.3) is complete. □

Corollary 22. *The set of Kraus operators F_i ($\{a_{ij} \in \mathbb{C}\}$) has at most $d^2 - d$ independent real parameters.*

Proof. With Prop. 21 and defining $\tilde{a}_{i,l+i} := \sum_{j=0}^{d-1} a_{ij}\, \mathrm{e}^{\mathrm{i}\, 2\pi(l+i)j/d}$, we find that the unnormalized Choi state $\mathcal{C}^{\mathrm{e}}$ corresponding to $\{F_i\}$ is

$$\mathcal{C}^{\mathrm{e}} = \sum_{i=0}^{d-1} \sum_{k,l=0}^{d-1} \tilde{a}^*_{i,k+i} \tilde{a}_{i,l+i} |l, l+i\rangle\langle k, k+i|, \tag{4.8}$$

which is a d-sparse, rank-d positive semidefinite matrix with at most d^2 real parameters. Constrained by normalization, $\{F_i\}$ has at most $d^2 - d$ independent parameters. □

When the set $\{K_i^\dagger K_j\}$ is not linearly independent our construction (4.4) yields quasi-extreme channels, which are in the closure of the set of extreme channels based on Theorem 20. As mentioned in the proof of Prop. 21 and also from Ref. [57], the set of extreme channels dominates the set of all generalized extreme channels. Also both extreme and quasi-extreme channels with rank smaller than d can be realized if some of the Kraus operators are zero matrices.

Corollary 23. *A rank-d generalized extreme qudit channel $\mathcal{E}^{\mathrm{g}} \in \mathscr{S}_d$ can be represented by*

$$\mathcal{E}^{\mathrm{g}}(\rho) = \sum_{i=0}^{d-1} K_i \rho K_i^\dagger \tag{4.9}$$

for any Kraus operators satisfying

$$K_i := W F_i V,\ F_i := X_i E_i,\ E_i := \sum_{j=0}^{d-1} a_{ij} Z_j,\ i \in \mathbb{Z}_d, \tag{4.10}$$

for any unitary operators $V, W \in SU(d)$ and $\sum_{i=0}^{d-1} F_i^\dagger F_i = \mathbb{1}$.

Proof. From the construction, it holds $\mathrm{tr}F_i^\dagger F_j = 0$ for $i \neq j$, which means the set $\{F_i\}$ (also $\{K_i\}$) is linearly independent. The unitary operators V and W can take this set to an arbitrary linearly independent set with the same cardinality. This proves that the proposed form (4.9) can represent arbitrary rank $\leq d$ channels. □

There are extreme channels with different ranks. A rank-d extreme channel can simulate a rank$\leq d$ extreme channel, since a rank$\leq d$ extreme channel can be viewed as a special case of rank-d extreme channel by setting some of its Kraus operators as zero matrix. However, A rank-d extreme channel can not be simulated by sum of rank$\leq d$ extreme channels, since the rank-d extreme channel is extreme.

The prior and posterior unitary operators V and W have different usages. The operator V transfers the basis $\{F_i^\dagger F_j\}$ to other basis. The action of the operator W is much more transparent in the affine representation, as discussed in §2.1.2. The operator W will change the shift vector due to the affine mapping. That is, operator V does not affect the shift vector, while operator W does not contribute to basis transformation.

Next we extend our construction of extreme channel to multi-partite case, which would be useful for the study in Chapter 7, the two-qubit quantum channel simulation.

Lemma 24. *An extreme n-qudit channel $\mathcal{E}^{\mathrm{e}} \in \mathscr{S}_{d^n}$ is represented by d^n Kraus operators $\{K_i\}$ with $d^{2n}-d^n$ independent parameters. The Kraus operators are formed in the following manner: the Heisenberg-Weyl basis for each qudit is partitioned in d parts as an ordered set $\{\{M_{00},\ldots,M_{0d-1}\},\ldots,\{M_{d-10},\ldots,M_{d-1d-1}\}\}$, and each Kraus operator takes the form $K_i := WF_iV$ for any $W,V \in SU(d^n)$ with*

$$F_i \equiv F_{(i_1,\cdots,i_n)} = \sum_{j_1,\cdots,j_n=0}^{d-1} \alpha(j_1,\cdots,j_n) M_{i_1j_1} \otimes M_{i_2j_2} \otimes \cdots \otimes M_{i_nj_n}, \tag{4.11}$$

where $i \equiv (i_1,\cdots,i_n)$ is a tuple of the indices $i_\ell \in \{1,\ldots,d\}$, $\forall \ell \in \{1,\ldots,n\}$ of the i_ℓ-th set of the ℓth qudit, and $M_{i_\ell j_\ell}$ is one of the basis operator of the i_ℓ-th set of the ℓ-th qudit. The coefficients $\{\alpha(j_1,\cdots,j_n) \in \mathbb{C}\}$ are chosen such that the set $\{F_i^\dagger F_j\}$ is linearly independent

and $\sum_{i=0}^{d-1} F_i^\dagger F_i = \mathbb{1}$ *is satisfied.*

Proof. The proof is similar with that for single qudit extreme channel in Prop. 21. We only need to show that the parameters $\alpha(j_1, \cdots, j_n)$ can be chosen arbitrarily to satisfy the linear-independence condition except for a measure-zero special subset. From the proof of single qudit case, we know that $\mathrm{tr}[(F_i^\dagger F_{i+\mu})^\dagger F_j^\dagger F_{j+\mu'}] = 0$ for $\mu \neq \mu'$. Here we also have such property, except that the index now is $i \equiv (i_1, \cdots, i_n)$ and $\mu \equiv (\mu_1, \cdots, \mu_n)$. We can then also partition the set $\{F_i^\dagger F_{i+\mu}\}$ into orthogonal subsets for different μ. When the set $\{F_i^\dagger F_j\}$ is linearly dependent, the channel is quasi-extreme. □

For multi-qubit channels, we can use Pauli basis $\{\sigma_i\}$ instead, and the next corollary follows straightforwardly.

Corollary 25. *An extreme n-qubit channel* $\mathcal{E}^{\mathrm{e}} \in \mathscr{S}_{2^n}$ *is represented by* 2^n *Kraus operators* $\{K_i\}$ *with* $4^n - 2^n$ *independent parameters. The Kraus operators are formed in the following manner: the Pauli basis for each qubit is partitioned in two parts as an ordered set* $\{\{\mathbb{1}, Z\}, \{X, Y\}\}$*, and each Kraus operator takes the form* $K_i := WF_iV$ *for any* $W, V \in SU(2^n)$ *with*

$$F_i \equiv F_{(i_1,\cdots,i_n)} = \sum_{j_1,\cdots,j_n=0}^{d-1} \alpha(j_1, \cdots, j_n)\sigma_{i_1 j_1} \otimes \sigma_{i_2 j_2} \otimes \cdots \otimes \sigma_{i_n j_n}, \tag{4.12}$$

where $i \equiv (i_1, \cdots, i_n)$ *is a tuple of the indices* $i_\ell \in \{1, \ldots, d\}$*,* $\forall \ell \in \{1, \ldots, n\}$ *of the* i_ℓ*-th set of the* ℓ*-th qubit, and* $\sigma_{i_\ell j_\ell}$ *is one of the basis operator of the* i_ℓ*-th set of the* ℓ*-th qubit. The coefficients* $\{\alpha(j_1, \cdots, j_n) \in \mathbb{C}\}$ *are chosen such that the set* $\{F_i^\dagger F_j\}$ *is linearly independent and* $\sum_{i=0}^{d-1} F_i^\dagger F_i = \mathbb{1}$ *is satisfied.*

Example 9 (Two-qubit extreme channel)**.** *The four Kraus operators are*

$$K_0 = \alpha_{00}\mathbb{1}\otimes\mathbb{1} + \alpha_{01}\mathbb{1}\otimes Z + \alpha_{10}Z\otimes\mathbb{1} + \alpha_{11}Z\otimes Z,$$

$$K_1 = \alpha_{02}\mathbb{1}\otimes X + \alpha_{03}\mathbb{1}\otimes Y + \alpha_{12}Z\otimes X + \alpha_{13}Z\otimes Y,$$

$$K_2 = \alpha_{20}X\otimes\mathbb{1} + \alpha_{21}X\otimes Z + \alpha_{30}Y\otimes\mathbb{1} + \alpha_{31}Y\otimes Z,$$

$$K_3 = \alpha_{22}X\otimes X + \alpha_{23}X\otimes Y + \alpha_{32}Y\otimes X + \alpha_{33}Y\otimes Y,$$

for coefficients $\{\alpha_{ij}\}$ *chosen such that* $\{K_i^\dagger K_j\}$ *is linearly independent.*

Example 10 (The qubit-qutrit extreme channel)**.** *For a qubit-qutrit system,* $\mathbb{C}^6 \cong \mathbb{C}^2\otimes\mathbb{C}^3$*, we can use Pauli basis and Heisenberg-Weyl basis together. The six Kraus operators are*

$$K_0 = \alpha_{00}\mathbb{1}\otimes\mathbb{1} + \alpha_{01}\mathbb{1}\otimes M_{01} + \alpha_{02}\mathbb{1}\otimes M_{02} + \alpha_{10}Z\otimes\mathbb{1} + \alpha_{11}Z\otimes M_{01} + \alpha_{12}Z\otimes M_{02},$$

$$K_1 = \alpha_{03}\mathbb{1}\otimes M_{10} + \alpha_{04}\mathbb{1}\otimes M_{11} + \alpha_{05}\mathbb{1}\otimes M_{12} + \alpha_{13}Z\otimes M_{10} + \alpha_{14}Z\otimes M_{11} + \alpha_{15}Z\otimes M_{12},$$

$$K_2 = \alpha_{06}\mathbb{1}\otimes M_{20} + \alpha_{07}\mathbb{1}\otimes M_{21} + \alpha_{08}\mathbb{1}\otimes M_{22} + \alpha_{16}Z\otimes M_{20} + \alpha_{17}Z\otimes M_{21} + \alpha_{18}Z\otimes M_{22},$$

$$K_3 = \alpha_{20}X\otimes\mathbb{1} + \alpha_{21}X\otimes M_{01} + \alpha_{22}X\otimes M_{02} + \alpha_{30}Y\otimes\mathbb{1} + \alpha_{31}Y\otimes M_{01} + \alpha_{32}Y\otimes M_{02},$$

$$K_4 = \alpha_{23}X\otimes M_{10} + \alpha_{24}X\otimes M_{11} + \alpha_{25}X\otimes M_{12} + \alpha_{33}Y\otimes M_{10} + \alpha_{34}Y\otimes M_{11} + \alpha_{35}Y\otimes M_{12},$$

$$K_5 = \alpha_{26}X\otimes M_{20} + \alpha_{27}X\otimes M_{21} + \alpha_{28}X\otimes M_{22} + \alpha_{36}Y\otimes M_{20} + \alpha_{37}Y\otimes M_{21} + \alpha_{38}Y\otimes M_{22},$$

for coefficients $\{\alpha_{ij}\}$ *chosen such that* $\{K_i^\dagger K_j\}$ *is linearly independent.*

4.1.3 Choi state representation of extreme channels

Choi state (2.26) is a bipartite positive matrix, which allows a natural block-matrix form representation. We first review the block-matrix form of positive semidefinite matrices, and then focus on Choi state and extreme Choi state.

Theorem 26 ([76, 183])**.** *For* $A, B \geq 0$*, then*

$$\begin{pmatrix} A & X \\ X^\dagger & B \end{pmatrix} \geq 0 \Leftrightarrow X = \sqrt{A}R\sqrt{B} \quad for \quad R \leq 1. \tag{4.13}$$

Note that R is a contraction (see Theorem 9), and also A and B can have different sizes, i.e., the blocks can have different sizes. This two-by-two block-matrix form can be directly applied to represent any quantum state. Also this block-matrix form can be generalized to $r \times r$ block-matrix form. Next we consider n-qudit quantum states.

Corollary 27. *An n-qudit state ρ can be written in the block-matrix form*

$$\rho = \begin{pmatrix} \rho_1 & \rho_{12} & \cdots & \rho_{1d^n-1} \\ \cdot & \rho_2 & \cdots & \cdot \\ \vdots & \vdots & \ddots & \vdots \\ \cdot & \cdot & \cdots & \rho_{d^n-1} \end{pmatrix}, \tag{4.14}$$

and $\mathrm{tr}\rho = 1$, $\rho_{kl} = \sqrt{\rho_k} R_{kl} \sqrt{\rho_l}$, *with contraction* $R_{kl} \leq 1$, $\rho_k \geq 0$, *and* $\rho_k \in \mathcal{M}_d$.

Proof. The block form follows from the following two facts: i) The positive semidefiniteness of a matrix is equivalent to the condition that all the principle minors are nonnegative. Note that the principle minor is the determinant of the submatrices formed by columns and rows in the same set. ii) The 2×2 case is proved in Theorem 26, and the form (4.14) is a generalization of it. □

The block-matrix form of Choi state for an n-qudit channel follows.

Corollary 28. *The Choi state $\mathcal{C}$ for an n-qudit channel $\mathcal{E}$ can be written in the block-matrix form*

$$\mathcal{C} = \begin{pmatrix} C_1 & C_{12} & \cdots & C_{1d^n} \\ \cdot & C_2 & \cdots & \cdot \\ \vdots & \vdots & \ddots & \vdots \\ \cdot & \cdot & \cdots & C_{d^n} \end{pmatrix}, \tag{4.15}$$

and $\mathrm{tr}_1\mathcal{C} = \mathcal{E}(\mathbb{1})$ *and* $\mathrm{tr}_2\mathcal{C} = \mathbb{1}$, $C_{kl} = C_{lk}^\dagger = \sqrt{C_k} R_{kl} \sqrt{C_l}$, *with* $R_{kl} \leq 1$, $C_k \geq 0$ *and* $C_k \in \mathcal{M}_{d^n}$. *Here* $\mathrm{tr}_{1(2)}$ *means the partial trace over the first (second) part of Choi state.*

The single qudit case follows directly. Furthermore, we also find the block-matrix form of generalized extreme Choi states, in which the contraction matrices are substituted by unitary matrices.

Corollary 29. *The Choi state $\mathcal{C}^{\mathrm{g}}$ for any generalized extreme qudit channel $\mathcal{E}^{\mathrm{g}}$ can be written in the block-matrix form*

$$\mathcal{C}^{\mathrm{g}} = \begin{pmatrix} C_1^{\mathrm{g}} & C_{12}^{\mathrm{g}} & \dots & C_{1d}^{\mathrm{g}} \\ \cdot & C_2^{\mathrm{g}} & \dots & \cdot \\ \vdots & \vdots & \ddots & \vdots \\ \cdot & \cdot & \dots & C_d^{\mathrm{g}} \end{pmatrix}, \tag{4.16}$$

for $tr_1\mathcal{C}^{\mathrm{g}} = \mathcal{E}^{\mathrm{g}}(\mathbb{1})$ and $tr_2\mathcal{C}^{\mathrm{g}} = \mathbb{1}$, with $d \times d$ positive matrices $C_k^{\mathrm{g}} \geq 0$ $(k = 1, 2, \dots, d)$, and

$$C_{kl}^{\mathrm{g}} = \sqrt{C_k^{\mathrm{g}}} U_{kl} \sqrt{C_l^{\mathrm{g}}}, \tag{4.17}$$

and unitary operators

$$U_{kl} := \prod_{s=k}^{l-1} U_{s,s+1} \tag{4.18}$$

with unitary operators $U_{s,s+1} \in SU(d)$.

Proof. The matrix $\mathcal{C}^{\mathrm{g}}$ can be decomposed as $\mathcal{C}^{\mathrm{g}} = AUA$, with

$$A = \begin{pmatrix} \sqrt{C_1^{\mathrm{g}}} & & & 0 \\ & \sqrt{C_2^{\mathrm{g}}} & & \\ & & \ddots & \\ 0 & & & \sqrt{C_d^{\mathrm{g}}} \end{pmatrix}, U = \begin{pmatrix} \mathbb{1} & U_{12} & \dots & U_{1d} \\ \cdot & \mathbb{1} & \dots & \cdot \\ \vdots & \vdots & \ddots & \vdots \\ \cdot & \cdot & \dots & \mathbb{1} \end{pmatrix}, \tag{4.19}$$

where A is a diagonal block matrix, and U can be further written as $U = \tilde{U}^{\dagger}\tilde{\mathbb{1}}\tilde{U}$, with

$$\tilde{U} = \begin{pmatrix} \mathbb{1} & U_{12} & \dots & U_{1d} \\ & \mathbb{1} & \dots & \cdot \\ & & \ddots & \vdots \\ 0 & & & \mathbb{1} \end{pmatrix}, \tilde{\mathbb{1}} = \begin{pmatrix} \mathbb{1} & & & 0 \\ & \mathbf{0} & & \\ & & \ddots & \\ 0 & & & \mathbf{0} \end{pmatrix}, \tag{4.20}$$

where $\tilde{U}$ is an upper triangular matrix, $\mathbf{0}$ represents zero block matrix, and the large zeros represents zero entries. As a result,

$$\mathcal{C}^{\mathrm{g}} = A\tilde{U}^{\dagger}\tilde{\mathbb{1}}\tilde{U}A. \tag{4.21}$$

This factorization implies that $\mathcal{C}^{\mathrm{g}}$ is positive semidifinite, and its rank is bounded above by d, which is the same as the number of Kraus operators for the generalized extreme channel. □

From our construction of (generalized) extreme channel based on Kraus operator-sum representation, we find there exists some special forms of its Choi state representation. Next, we prove the Choi state form for generalized extreme channel without prior and posterior unitary operators. For convenience, we define *generalized permutation* as a generalization of permutation (see Theorem 8) such that the nontrivial entries can be 1 and -1.

Proposition 30. *A generalized extreme Choi state $\mathcal{C}^{\mathrm{g}}$ for an n-qudit channel $\mathcal{E}$ without initial and final unitary operators takes the form*

$$\mathcal{C}^{\mathrm{g}} = \begin{pmatrix} C_1^{\mathrm{g}} & C_{12}^{\mathrm{g}} & \dots & C_{1d^n}^{\mathrm{g}} \\ \cdot & C_2^{\mathrm{g}} & \dots & \cdot \\ \vdots & \vdots & \ddots & \vdots \\ \cdot & \cdot & \dots & C_{d^n}^{\mathrm{g}} \end{pmatrix}, \tag{4.22}$$

with $C_{kl}^{\mathrm{g}} = \sqrt{C_k^{\mathrm{g}}}U_{kl}\sqrt{C_l^{\mathrm{g}}}$, $C_k^{\mathrm{g}} \geq 0$, and unitary operators $U_{kl} := \prod_{s=k}^{l-1} U_{s,s+1}$ with generalized permutations $U_{s,s+1} \in SU(d^n)$.

Proof. The Choi state takes the form $\mathcal{C}^{\mathrm{g}} = \sum_i \mathrm{res}K_i[\mathrm{res}K_i]^{\dagger} \equiv \sum_i \mathcal{C}_i^{\mathrm{g}}$. From Eq. (4.8) $\mathcal{C}_i^{\mathrm{g}}$ is d-sparse with d elements in each row and each column. For $\mathcal{C}_i^{\mathrm{g}}$, suppose its nonzero diagonal entries are $c_{aa}[i]$ for a set of index $\{a\}$. We ignore $[i]$ for simplicity. Let $c_{aa} = \gamma_a^2$ for γ_a being determined by the parameters in K_i. Then, there are entries $c_{aa'} = \gamma_a\gamma_{a'}$ on off-diagonal places of $\mathcal{C}_i^{\mathrm{g}}$. For $\mathcal{C}_j^{\mathrm{g}}$, its nonzero entries will be in different places compared with $\mathcal{C}_i^{\mathrm{g}}$. Denote the diagonal entries as γ_b^2, then the off-diagonal entries are $\gamma_b\gamma_{b'}$, for a set of index $\{b\}$.

For Eq. (4.8), we can see that a block matrix C_l^{g} on the diagonal place is diagonal, and C_{kl}^{g} on the off-diagonal place is one-sparse. For C_l^{g}, there is one entry from each of the extreme state $\mathcal{C}_i^{\mathrm{g}}$. Define an "order matrix" of C_l^{g} as O_l, which is a diagonal matrix such that its entry labels the correspondence between the entries of C_l^{g} and $\mathcal{C}_i^{\mathrm{g}}$. For instance, if the first diagonal entry of C_l^{g} is from $\mathcal{C}_2^{\mathrm{g}}$, then the first diagonal entry of O_l is 2. We can also introduce an order matrix O_k for C_k^{g}. Then, there exists a permutation P_{kl} such that $O_l = P_{kl} O_k P_{kl}^\dagger$. Also $C_{kl}^{\mathrm{g}} = D_{kl} P_{kl}^\dagger$ with D_{kl} a diagonal matrix whose order matrix is O_k.

We need to prove that each U_{kl} is a generalized permutation, which follows from

$$\begin{aligned} U_{kl} =& \frac{1}{\sqrt{C_k^{\mathrm{g}}}} C_{kl}^{\mathrm{g}} \frac{1}{\sqrt{C_l^{\mathrm{g}}}} \\ =& \frac{1}{\sqrt{C_k^{\mathrm{g}}}} D_{kl} P_{kl}^\dagger \frac{1}{\sqrt{C_l^{\mathrm{g}}}} \\ =& P_{kl}^\dagger P_{kl} \frac{1}{\sqrt{C_k^{\mathrm{g}}}} P_{kl}^\dagger P_{kl} D_{kl} P_{kl}^\dagger \frac{1}{\sqrt{C_l^{\mathrm{g}}}} \\ =& P_{kl}^\dagger \tilde{\mathbb{1}}, \end{aligned} \tag{4.23}$$

with $\tilde{\mathbb{1}}$ as a diagonal matrix with entries 1 and -1. We have used the fact $P_{kl} \frac{1}{\sqrt{C_k^{\mathrm{g}}}} P_{kl}^\dagger$ and $P_{kl} D_{kl} P_{kl}^\dagger$ both have order matrix O_l. In addition, if all γ_a, γ_b, etc are positive, then $\tilde{\mathbb{1}}$ reduces to identity operator $\mathbb{1}$, and U_{kl} becomes the permutation $P_{kl}^\dagger$. □

4.1.4 Quantum circuit of extreme qudit channels

From Stinespring dilation theorem 1, a quantum channel can also be represented by a quantum circuit that implements a unitary operator U such that $F_i = \langle i|U|0\rangle$ realizes the set of Kraus operators $\{F_i\}$, which satisfy the linear independence and $\sum_i F_i^\dagger F_i = \mathbb{1}$. In this section, we present a quantum circuit representation of any extreme and generalized extreme qudit channels. The unitary operator U for a generalized extreme qudit channel acts on a qudit system S and a qudit ancilla A, thus $U \in SU(d^2)$.

First we present the single- and two-qudit gate set for this circuit construction. Three

types of single-qudit gates are specified by the bit-flip gate

$$X_{jk} := |j\rangle\langle k| + |k\rangle\langle j|, \tag{4.24}$$

by the one-parameter Givens rotation [123]

$$G_{jk}(\theta) := \cos\theta(|j\rangle\langle j| + |k\rangle\langle k|) + \sin\theta(|k\rangle\langle j| - |j\rangle\langle k|), \tag{4.25}$$

and by the gate X_i from the Heisenberg-Weyl basis ($i, j, k \in \mathbb{Z}_d$). Note the gate X_i corresponds to a permutation π_i on the set $\mathbb{Z}_d$ such that $\langle a|X_i|b\rangle = 1$ if $\pi_i(b) = a$ for $a, b \in \mathbb{Z}_d$. There exists a cycle notation for permutation such that, starting from some element $i \in \mathbb{Z}_d$, a permutation π can be represented by

$$\pi := (i, \pi(i), \pi(\pi(i)), \dots) \tag{4.26}$$

as the sequence of images of i under π until the image returns to i. Our gate notation implies an identity operator acting on the rest of the space.

We augment these gates by their two-qudit controlled counterparts

$$CX_{jk} := |j\rangle_{\mathrm{s}}\langle j| \otimes X_{jk} \tag{4.27}$$

and

$$CG_{jk}(\theta) := |j\rangle_{\mathrm{s}}\langle j| \otimes G_{jk}(\theta) \tag{4.28}$$

with the system as control, and

$$CX_i := X_i \otimes |i\rangle_{\mathrm{a}}\langle i| \tag{4.29}$$

with the ancilla as control. We introduce a qudit multiplexer, which generalizes the qubit case [148], as a sequence of two controlled-Givens rotations

$$M_{jk}(\alpha, \beta) := CG_{jk}(\alpha)CG_{kj}(-\beta) \tag{4.30}$$

depicted in Fig. 4.1.

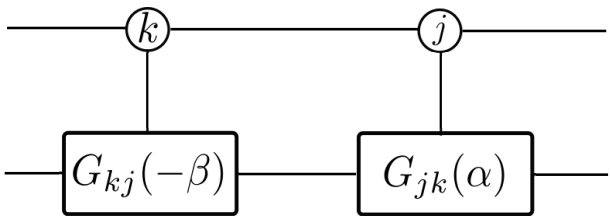

Figure 4.1: Circuit diagram for a quantum multiplexer $M_{jk}(\alpha, \beta)$. Each wire represents an evolving qudit in the d-ary representation with ⓙ and ⓚ d-ary control operation.

Qubit quantum multiplexer is defined such that a target qubit is acted on by gate U_0 (U_1) when the control qubit is in computational state $|0\rangle$ ($|1\rangle$) [148]. That is, it realizes the logic "if-then-else" and executes operator $|0\rangle\langle 0| \otimes U_0 + |1\rangle\langle 1| \otimes U_1$. A multiplexer is also called a uniformly controlled gate [118, 117].

The parameters in Kraus operators can be expressed using trigonometric function since absolute value of the entries of Kraus operators are smaller than one. The entries would relate to the rotation angles in the quantum circuit to implement an extreme channel.

For the Kraus operators in Eq. (4.9), observe that F_0 is diagonal and all others can also become diagonal followed by a certain permutation X_i. A channel with diagonal Kraus operators can be realized by a sequence of controlled-operations, with the system as control and ancilla as target. A sequence of permutations can turn this into an extreme channel with all Kraus operators taking the correct forms. As a result, we have the following proposition.

Proposition 31. *Given any* $\mathcal{V}(\bullet) := V \bullet V^\dagger$ *and* $\mathcal{W}(\bullet) := W \bullet W^\dagger$ *with* $V, W \in SU(d)$*, any channel* $\mathcal{W}\,(tr_a \mathcal{U})\,\mathcal{V}$ *is extreme provided that*

$$U := \prod_{i=d-1}^{1} CX_i \prod_{j=d-1}^{1} \prod_{k=j-1}^{0} M_{jk}(\alpha_{jk}, \beta_{jk}), \tag{4.31}$$

for all but a zero-measure subset of the rotation-angle sets $\{\alpha_{jk}\}$ *and* $\{\beta_{jk}\}$ *with at most* $(d^2 - d)/2$ *elements per set.*

Proof. We prove the theorem by showing that the partial trace of U (4.31) yields Kraus operators $F_i = \langle i|U|0\rangle$ that satisfy the normalization and linear independence conditions of

Prop. 21. To this end we define U' as a product of controlled-Givens rotations such that

$$U = \left(\prod_{i=d-1}^{1} CX_i \right) U'. \tag{4.32}$$

We define $\{u_{i\ell} \in \mathbb{R}; i, \ell \in \mathbb{Z}_d\}$ such that

$$U'|0\rangle_{\rm a}|\ell\rangle_{\rm s} = \sum_{i=0}^{d-1} u_{i\ell}|i\rangle_{\rm a}|\ell\rangle_{\rm s}. \tag{4.33}$$

The unitary operator U' corresponds to a channel with diagonal Kraus operators $\{E_i\}$ such that

$$E_i|\ell\rangle_{\rm s} = u_{i\ell}|\ell\rangle_{\rm s} \tag{4.34}$$

as

$$U'|0\rangle_{\rm a}|\ell\rangle_{\rm s} = \sum_{i=0}^{d-1} |i\rangle_{\rm a}\langle i|U'|0\rangle_{\rm a}|\ell\rangle_{\rm s} = \sum_{i=0}^{d-1} |i\rangle_{\rm a} E_i|\ell\rangle_{\rm s}. \tag{4.35}$$

We can identify E_i in Eq. (4.35) with E_i in Eq. (4.4) by setting

$$u_{i\ell} \equiv \tilde{a}_{i\ell} := \sum_{j=0}^{d-1} a_{ij}\, {\rm e}^{{\rm i}\, 2\pi\ell j/d}\,. \tag{4.36}$$

Reincorporating the gates CX_i yields

$$U|0\rangle_{\rm a}|\ell\rangle_{\rm s} = \sum_{i=0}^{d-1} |i\rangle_{\rm a} X_i E_i|\ell\rangle_{\rm s} = \sum_{i=0}^{d-1} |i\rangle_{\rm a} F_i|\ell\rangle_{\rm s}. \tag{4.37}$$

A projection $|i\rangle_{\rm a}\langle i|$ on the ancilla corresponds to the action of F_i on the system. The angles α_{jk} and β_{jk} can be chosen (e.g., randomly) to satisfy the linear independence of $\{F_i^\dagger F_j\}$. This means the circuit U realizes the Kraus operators $\{F_i\}$ for an extreme channel. As there are $\binom{d}{2}$ multiplexers, the total number of independent parameters is consistent with Corollary 22. □

As for constructing Kraus operators, when the set $\{F_i^\dagger F_j\}$ is not linearly independent, the circuit (4.31) realizes quasi-extreme channels. As a result, the circuit in Prop. 31 successfully yields simulations of arbitrary generalized extreme channels. A schematic diagram for the quantum circuit of generalized extreme channel is shown in Fig. 4.2.

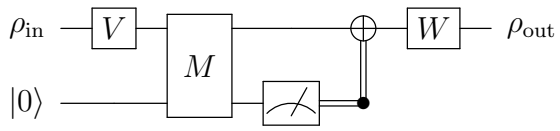

Figure 4.2: The schematic diagram for the quantum circuit of generalized extreme channel. Single qudit ancilla is initially prepared in state $|0\rangle$. V is a prior rotation and W is a posterior rotation. The sequence of multiplexers is represented by M. The sequence of CX_i can be realized by classically i-controlled X_i gates, represented by the meter and the classically controlled-NOT symbol.

A permutation gate X_i can be decomposed as a sequence of bit-flip gates. A permutation π_i can be realized as a sequences of flips, which only permute two elements. For instance, for a qutrit gate $X_1 = |0\rangle\langle 2| + |1\rangle\langle 0| + |2\rangle\langle 1|$, the permutation is $\pi_1 = (120)$, which means the change $0 \mapsto 1$, $1 \mapsto 2$, and $2 \mapsto 0$. This permutation can be realized as a product of two flips: $f_{01} = (01)$, $f_{02} = (02)$, and $\pi_1 = f_{01}f_{02}$. Note f_{01} applies first. The decomposition is not unique, though; e.g., π_1 can also be realized as $\pi_1 = f_{02}f_{12}$ for $f_{12} = (12)$. Correspondingly, the qutrit gate X_1 can be decomposed as $X_1 = X_{02}X_{01}$ or $X_1 = X_{12}X_{02}$. Generally, since X_i is a shift operation, it is easy to see that about d bit-flip operations can realize a permutation operation. This is indeed the case. Furthermore, if classical feedback is allowed, the sequence of CX_i can merely be realized by classically i-controlled X_i gates, since the ancilla is traced out at the end of the circuit.

4.2 Quantum channel decomposition

Now we continue to study the problem of quantum channel decomposition. We first review Ruskai's conjecture to highlight the difficulty, and then we develop the optimization approach for quantum channel simulation. Afterwards we analyze the space and time cost of quantum simulation circuit.

4.2.1 Ruskai's conjecture

Now we consider the channel decomposition in terms of convex sum of generalized extreme channels. This is a nontrivial problem, and actually this has been conjectured as follows.

Conjecture 1 (Ruskai's conjecture [139])**.** *Any channel $\mathcal{E} \in \mathscr{S}_{n,m}$ can be decomposed as*

$$\mathcal{E} = \frac{1}{m} \sum_{i=1}^{m} \mathcal{E}_i^{\mathrm{g}}, \quad \mathcal{E}_i^{\mathrm{g}} \in \mathscr{S}_{n,m}^{\leq n}. \tag{4.38}$$

The equal probability $\frac{1}{m}$ in the sum (4.38) can be relaxed to general case and then the conjecture becomes $\mathcal{E} = \sum_{i=1}^{m} p_i \mathcal{E}_i^{\mathrm{g}}$ for probability $p_i \in [0,1]$ such that $\sum_{i=1}^{m} p_i = 1$. As we only consider qudit channel simulation, we recast the conjecture for qudit case.

Conjecture 2 (Ruskai's conjecture for qudit case)**.** *Any qudit channel $\mathcal{E} \in \mathscr{S}_d$ can be decomposed as*

$$\mathcal{E} = \sum_{i=1}^{d} p_i \mathcal{E}_i^{\mathrm{g}}, \tag{4.39}$$

for $\mathcal{E}_i^{\mathrm{g}} \in \mathscr{S}_d$, and probability $p_i \in [0,1]$ such that $\sum_{i=1}^{d} p_i = 1$.

This conjecture is based on some partial results for special cases. The case for $n = m = 2$ have been proved [140], the method of which can be extended to the case for $m = 2$ [139], while in general this decomposition is still an open problem in quantum information and computation. The method in Refs. [139, 140] relies on the convex set property of contraction matrices that a contraction can be written as a convex sum of unitary matrices, discussed in Theorem 9. However, we show here that this contraction-decomposition method in general does not work. We show this by analyzing it for the qutrit case.

For a qutrit channel, the Choi state is a nine-by-nine matrix

$$\mathcal{C} = \begin{pmatrix} A_1 & \sqrt{A_1} R_{12} \sqrt{A_2} & \sqrt{A_1} R_{13} \sqrt{A_3} \\ \sqrt{A_2} R_{21} \sqrt{A_1} & A_2 & \sqrt{A_2} R_{23} \sqrt{A_3} \\ \sqrt{A_3} R_{31} \sqrt{A_1} & \sqrt{A_3} R_{32} \sqrt{A_2} & A_3 \end{pmatrix}, \tag{4.40}$$

with three-by-three matrices A_k and $R_{kl} = R_{lk}^\dagger$ for $k, l = 1, 2, 3$, $k \neq l$. The three contractions are not independent, and particularly, the contraction R_{23} is a function of R_{12} and R_{13} [47] for the sake of the positivity of $\mathcal{C}$. The Choi state for a generalized extreme qutrit channel is

$$\mathcal{C}^{\mathrm{g}} = \begin{pmatrix} C_1^{\mathrm{g}} & \sqrt{C_1^{\mathrm{g}}} U_{12} \sqrt{C_2^{\mathrm{g}}} & \sqrt{C_1^{\mathrm{g}}} U_{13} \sqrt{C_3^{\mathrm{g}}} \\ \sqrt{C_2^{\mathrm{g}}} U_{12}^\dagger \sqrt{C_1^{\mathrm{g}}} & C_2^{\mathrm{g}} & \sqrt{A_2} U_{23} \sqrt{C_3^{\mathrm{g}}} \\ \sqrt{C_3^{\mathrm{g}}} U_{13}^\dagger \sqrt{C_1^{\mathrm{g}}} & \sqrt{C_3^{\mathrm{g}}} U_{23}^\dagger \sqrt{C_2^{\mathrm{g}}} & C_3^{\mathrm{g}} \end{pmatrix}, \tag{4.41}$$

for unitary operators U_{12}, U_{23}, and $U_{13} = U_{12} U_{23}$.

From Theorem 9, a contraction can be decomposed as a convex sum of unitary matrices. If we decomposition $R_{12} = p_1 U_{12;1} + p_2 U_{12;2} + p_3 U_{12;3}$, $R_{23} = p_1 U_{23;1} + p_2 U_{13;2} + p_3 U_{13;3}$ then $R_{13} = p_1 U_{12;1} U_{23;1} + p_2 U_{12;2} U_{23;2} + p_3 U_{12;2} U_{23;2}$, which will conflict the function relation between R_{13} and R_{12} with R_{23}. This generalizes to higher-dimensional cases, and we conclude that the contraction-decomposition method in general does not work for quantum channel decomposition.

4.2.2 Optimization for quantum channel simulation

As an analytical formula for quantum channel decomposition (4.39) remains unknown, we turn to an algorithmic approach for such a decomposition, that is, we will seek an approximate decomposition. Next we describe the algorithm for the simulation of a general qudit channel. The algorithm accepts the dimension d of the Hilbert space, the description of a channel $\mathcal{E}$ and an error tolerance ϵ as input. The output is the description of a quantum circuit C and a bound $\tilde{\epsilon}$ on the resultant circuit with respect to the actual channel $\mathcal{E}$ being simulated. A schematic illustration has been presented in the introduction, Fig. 1.3. The description of $\mathcal{E}$ and C, denoted by $[\mathcal{E}]$ and $[C]$, refer to the finite-precision bit-string representation of them, while such a finite precision is treated to be irrelevant to the simulation accuracy in our algorithm.

Our algorithmic procedure is as follows. Ruskai's conjecture 2 shows that any channel can be decomposed into a d-fold sum of generalized extreme channels, and we know from Prop. 31

a description of the circuit for arbitrary generalized extreme channel. Thus, a quantum circuit for the qudit channel can be realized by choosing generalized extreme channel circuits randomly with each $\imath^{\text{th}}$ circuit chosen with probability $p_\imath$.

Our algorithm initially chooses a set of d generalized extreme channels randomly and tests whether the resultant guessed channel $\tilde{\mathcal{E}}$ is within distance ϵ of the correct channel $\mathcal{E}$. Typically the guessed channel fails to be within the error tolerance so we employ an optimization algorithm to pick a new set of parameters for $\mathcal{E}$ and try again. This procedure is repeated until a satisfactory circuit is found. The procedure is aborted if the optimization routine fails to find a good circuit within a pre-specified number of trials. The code for the simulation algorithm is presented in Appendix C.

We now determine the number of parameters in $\mathcal{E}$ for optimization. The unitary matrices V and W in Prop. 21 could be constructed as products

$$V = \prod_i V_i,\ W = \prod_j W_j \tag{4.42}$$

with as many unitary operators $\varkappa$ in the two products as needed to provide enough parameters for the optimization. As there are d generalized extreme channels and $d^2 - 1$ free parameters in $SU(d)$, we have $\varkappa d(d^2-1)$ free parameters associated with V and W. We add this number of parameters to the number of parameters for d generalized extreme channels, namely $d(d^2 - d)$ with $d^2 - d$ the number of free angles $\{\alpha_{jk}, \beta_{jk}\}$, and then add these to the number of probabilities $\{p_\imath\}$. The total number of parameters for the approximate channel should satisfy the inequality

$$\varkappa d(d^2-1) + d(d^2-d) + (d-1) \geq d^4 - d^2 \tag{4.43}$$

with the right-hand side corresponding to the number of parameters that specify the qudit channel. For the most efficient simulation, we minimize $\varkappa$ so

$$\varkappa = \left\lceil \frac{(d-1)(d^2+d+1)}{d(d+1)} \right\rceil, \tag{4.44}$$

which can be simplified to d since d is the minimal integer that is no smaller than the expression in the ceiling function, and $d-1$ is smaller than the expression in the ceiling function. As an example, a qutrit channel has 72 parameters, but our optimization is over 92 parameters. Our analysis reduces to the qubit case [168]. In that case $d=2$ so the channel $\mathcal{E}$ has 12 parameters whereas the optimization of $\mathcal{E}$ is over 17 parameters.

The final step for the algorithm is to construct the objective function for the optimization problem. Mathematically we represent the correct $\mathcal{E}$ channel by the Choi state $\mathcal{C}$, and the approximate circuit is represented by the state $\mathcal{C}' = \sum_\imath p_\imath \mathcal{C}_\imath^{\mathrm{g}}$.

The objective function for optimization is given by the trace distance $D_t(\mathcal{C},\mathcal{C}')$, which bounds the $\diamond$-norm distance between two channels $\mathcal{E}$ and $\mathcal{E}'$ according to Prop. 7

$$D_t(\mathcal{C},\mathcal{C}') \leq \frac{\epsilon}{2d} \implies \|\mathcal{E}-\mathcal{E}'\|_\diamond \leq \epsilon. \tag{4.45}$$

Note here we employ the normalized version of Choi state, while in our paper [169] the unnormalized version has been used. Each $\mathcal{C}_i^{\mathrm{g}}$ can be parameterized by a set of rotation angles $\{\theta_{\imath\jmath} : \jmath = 1,\ldots,\varkappa(d^2-1)\}$ for the prior and posterior unitary operators, and a set of rotation angles $\{\varphi_{\imath\jmath} : \jmath = 1,\ldots,d^2-d\}$, which denote the sets $\{\alpha_{jk}\}$ and $\{\beta_{jk}\}$ altogether from Eq. (4.31). The range of the objective function is

$$0 \leq D_t(\mathcal{C},\mathcal{C}') \leq 1. \tag{4.46}$$

Our goal is to find the best possible $\mathcal{C}'$ by optimization

$$\begin{aligned} &\min_{\{\{p_\imath\},\{\theta_{\imath\jmath}\},\{\varphi_{\imath\jmath}\}\}} D_t(\mathcal{C},\mathcal{C}') \\ &\text{subject to } \sum_\imath p_\imath - 1 = 0. \end{aligned} \tag{4.47}$$

We have tested our optimization algorithm numerically for systems up to four dimensions successfully using the simple nonlinear programming method [180] on channels generated by partial trace of Haar-random-generated unitary operators on the dilated space [157]. The simulation is performed on MATLAB® using optimization algorithms, namely, MultiStart

and GlobalSearch, and we also employed simulated annealing, which was less effective. Our simulations yields errors in the range $10^{-2} \sim 10^{-4}$ for qubit channels (see Chapter 5), and in the order 10^{-2} for qutrit channels, and 10^{-1} for two-qubit channels (see Chapter 7).

The errors for the case $d = 4$ from the numerical simulation is rather large yet acceptable for demonstrating the efficacy of our algorithm. For high-accuracy simulation, significantly greater computational resources are required. As the system dimension d increases, we expect at least a quadratic increase in run-time of the simulation with respect to d due to the built-in method employed by GlobalSearch or MultiStart program. Moreover, given that resources are finite, e.g. run-time, numerical optimization is not even guaranteed to succeed due to becoming stuck at certain points in the parameter space. Such problems are quite generic for optimization problems. The simulations for qutrit and two-qubit channels are discussed in Chapter 7.

4.2.3 Space and time cost of quantum simulation circuit

Next we consider the time and space cost for the quantum circuit to simulate a generalized extreme qudit channel $\mathcal{E}^{\mathrm{g}}$ on a quantum computer based on qudits and single- and two-qudit unitary gates. The generalized extreme qudit channel is dilated to a unitary operator U on two qudits, which contains a sequence of multiplexers and a sequence of CX_i gates acting between the system and the ancillary qudits, and also a prior qudit rotation and a posterior qudit rotation acting on the system.

An arbitrary single qudit rotation can be decomposed into a product of at most $d(d-1)/2 \in O(d^2)$ two-level unitary gates (§4.5.1, [123]). A controlled-Givens rotation $CG_{jk}(\theta)$ can be realized by two Givens rotations and a CX_{jk} gate, similar to the qubit case [9]. The sequence of CX_i gates can be realized by classically controlled X_i gates since the ancillary system is traced out, with an X_i gate acting on the system conditioned on a projector $|i\rangle\langle i|$ on the ancilla. As a result, the generalized extreme channel circuit can be realized by a product of $O(d^2)$ CX_{jk} gates and continuously-parameterized Givens rotations.

To assess the cost of the quantum circuit, we employ the SKDN algorithm for qudits [49]. From the error tolerance ϵ, which is an algorithmic input for circuit design, any Givens rotation can be approximated by an $O\left(\log \frac{d^2}{\epsilon}\right)$ sequence of universal qudit gates [49]. As a result, the number of elementary gates, hence computational time cost, of the generalized extreme channel circuit is

$$O\left(d^2 \log \frac{d^2}{\epsilon}\right), \tag{4.48}$$

and the quantum space cost is two qudits.

The circuit corresponding to $\tilde{U}$ yields an approximation $\tilde{\mathcal{E}}^{\mathrm{g}}$ to the desired generalized extreme channel $\mathcal{E}^{\mathrm{g}}$. From Theorem 5, we obtain

$$\|U - \tilde{U}\| \leq \frac{\epsilon}{2} \implies \|\mathcal{E}^{\mathrm{g}} - \tilde{\mathcal{E}}^{\mathrm{g}}\|_{\diamond} \leq \epsilon. \tag{4.49}$$

From strong convexity and the chain property of trace distance, relations (4.45) and (4.49) above together ensure the desired simulation accuracy.

Finally simulating an arbitrary channel is implemented by probabilistically implementing different generalized extreme channels according to the distribution $\{p_\iota\}$. The space and time costs of a single-shot implementation of the channel are one dit and two qudits for space and the classical time cost for generating the random dits plus $O\left(d^2 \log \frac{d^2}{\epsilon}\right)$ quantum gates. In other words, the quantum computational cost for simulating a random qudit channel is the same as for simulating the generalized extreme channel, and the additional cost is only classical: dits plus running a random-number generator. This cost can be explained by recognizing that the qudit channel simulator is simply a randomized generalized extreme channel simulator. On the other hand, estimating qudit observables accurately could require many shots, with the number of shots depending on the particular observable.

4.3 Alternative strategies

There could be many different strategies for algorithmic quantum channel simulation besides the convex-sum decomposition approach we employed. Here we discuss several strategies

Table 4.1: Comparison of alternative quantum simulation methods. In the table, $\times$ means the factorization decomposition is not applicable or feasible for arbitrary channel, the p represents the probabilistic success of simulation of single Kraus operator.

	Feasibility	Space	Time	Bits	Success
Factorization	$\times$	-	-	-	-
Kraus	$\surd$	two qudits	$O(d^2)$	$\surd$	p
$\mathcal{E} \mapsto U$	$\surd$	three qudits	$O(d^6)$	$\times$	1
Convex sum	$\surd$	two qudits	$O(d^2)$	$\surd$	1

that are explored before: i) Dilation method. This is the standard approach that to directly employ Stinespring dilation theorem 1 and extend a channel $\mathcal{E}$ to a unitary operator U. ii) Factorization decomposition. This approach is to decompose a channel $\mathcal{E}$ approximately as a composition of many other smaller channels $\mathcal{E}_i$ such that $\mathcal{E} \approx \prod_i \mathcal{E}_i$, analog to the decomposition of a unitary operator U. However, this approach is not feasible in general. iii) Simulate each Kraus operator separately. From Kraus operator-sum representation, a quantum channel can be viewed as a convex sum of completely positive mappings specified by each Kraus operator, then the channel simulation can be done by convex sum of the simulation of each Kraus operator. Below we discuss these three methods in details.

4.3.1 Dilation approach for simulation

Consider a qudit system and a rank $r \leq d^2$ channel $\mathcal{E}$ acting on it. Given the Kraus operator-sum representation

$$\mathcal{E}(\rho) = \sum_{i=0}^{r-1} K_i \rho K_i^\dagger, \tag{4.50}$$

each Kraus operator K_i can be viewed as a POVM operator $M_i := K_i^\dagger K_i$ on the system. The Stinespring dilation enables to implement each Kraus operator by a projection on an extended system, which is acted on by a unitary operator U such that $K_i = \langle i|U|0\rangle$, with

$\{|i\rangle\}$ as an orthonormal basis of the ancilla, the dimension of which is just r. In general, the dilated unitary operator U acts on d^3-dimensional space, and then the quantum circuit cost for simulating it is $O(d^6)$. The simulation accuracy can be ensured by restricting on the spectral norm on U and its approximate $\tilde{U}$.

Furthermore, in order to employ this approach a constructive procedure is required for the dilation $\mathcal{E} \mapsto U$, which is called "mocking up" of a unitary operator U [123]. As the set of Kraus operators only occupy part of the whole unitary operator U, this dilation problem corresponding to the problem of matrix completion [64] constrained by the unitarity of U, which is not a trivial problem.

4.3.2 Factorization decomposition

We have studied in Chapter 3 that an arbitrary unitary operator U can be exactly or approximately decomposed as the product of a sequence of other unitary operators U_i such that

$$U \approx \prod_i U_i = U_n \cdots U_2 U_1. \tag{4.51}$$

This is ensured by the fact that the set of unitary operators form a group. Similarly, the set of quantum channels $\mathcal{E}$ form a semigroup, instead of a group, since a generic channel $\mathcal{E}$ does not have an inverse. This implicitly implies that the following decomposition

$$\mathcal{E} \approx \prod_i \mathcal{E}_i = \mathcal{E}_n \circ \cdots \circ \mathcal{E}_2 \circ \mathcal{E}_1 \tag{4.52}$$

is impossible. The factorization of a channel $\mathcal{E}$ into a nontrivial product of another two channels $\mathcal{E} = \mathcal{E}_2 \circ \mathcal{E}_1$ has been studied [177], which proves that factorizing, called dividing quantum channels in Ref. [177], is possible only for full rank channel $\mathcal{E}$, while impossible in general. Particularly, rank-three unital qubit channels are not divisible.

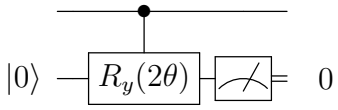

Figure 4.3: Quantum circuit for the gate $N(a) = \mathrm{diag}(1, a)$ for $a \in (0, 1)$. The top wire is for a qubit and the bottom wire is for a qubit ancilla initially in state $|0\rangle$ and finally projected in state $|0\rangle$. The rotation angle θ is defined such that $\cos\theta = a$.

4.3.3 Simulate each Kraus operator probabilistically

Given the set of Kraus operators $\{K_i\}$ for a rank-r channel, one can simulate each Kraus operator separately and probabilistically, and then combine them together using classical method. Here we study one of these approaches in detail [154], which proved that the CNOT and single-qubit non-unitary gate forms a universal set for non-unitary gates, invertible or not.

For an operator K, which is just a Kraus operator, first perform the SVD such that $K = U\Lambda V$ for unitary operators U and V, which can be implemented by unitary quantum circuits, and diagonal positive semidefinite operator $\Lambda = \mathrm{diag}(\lambda_1, \lambda_2, \ldots, \lambda_d)$ for $\lambda_i \in [0, 1]$, d is the dimension. Define $\Lambda_i = \mathrm{diag}(1, \cdots, 1, \lambda_i, 1, \cdots, 1)$ with λ_i at the ith column, then the matrix Λ can be decomposed as

$$\Lambda = \Lambda_1 \Lambda_2 \cdots \Lambda_d. \tag{4.53}$$

The matrix Λ_i is a controlled-$N_1(a)$ gate with $(n-1)$ control qubits (if $d = 2^n$) and a single-qubit gate $N(a) = \mathrm{diag}(1, a)$ for $a \in [0, 1)$. A multiple-qubit controlled gate can be realized as a product of CNOT gates and single-qubit gates.

Next we consider how to implement a gate $N(a)$. First, if $a = 0$, the operator $N(a)$ is not invertible and reduces to a projector. This requires post-selection. When $a \neq 0$, the operator $N(a)$ becomes invertible. With dilation, $N(a)$ can be realized by a single-qubit

rotation $R_y(2\theta)$ for $\cos\theta = a$, CNOT, and the projector $N(0)$ as shown in Fig. 4.3.

In addition, there are several other approaches for simulating a single Kraus operator, which have limited applications so far, while may be improved with further efforts [1, 131, 35]. First, one approach is to use a nonunitary generalization of Solovay-Kitaev algorithm to decompose invertible Kraus operators [1], while a universal gate library for invertible gates is unknown. Second, using dilation one can simulate each K by a unitary operator W with a qubit ancilla. Given K, one can find another Kraus operator K_0 such that $\{K, K_0\}$ forms a CPTP channel $\mathcal{K}$. Then the channel $\mathcal{K}$ can be simulated by a unitary operator W, and the projector $|0\rangle\langle 0|$ acts on the ancilla realizes K probabilistically. Third, using direct-sum dilation a $d \times d$ Kraus operator K can be converted to a $2d \times 2d$ unitary operator

$$U := \begin{pmatrix} K & \sqrt{\mathbb{1} - KK^\dagger} \\ \sqrt{\mathbb{1} - K^\dagger K} & -K^\dagger \end{pmatrix}. \tag{4.54}$$

However, due to the direct sum, there exists some "super-selection" rules on the initial states and final states [35].

4.4 Conclusion

In this chapter we developed the quantum channel decomposition and simulation methods based on extreme channels. Different representations including the Kraus operator-sum, Choi state, and quantum circuit are constructed to characterize extreme and generalized extreme channels. As an analytical formula for channel decomposition still remains to be discovered, we developed a classical optimization algorithm for approximate quantum channel decomposition, which is suitable for quantum channel simulation. Our approach is unique and serves as a preferable method compared with many other approaches we have analyzed.

Chapter 5

Qubit quantum channel simulation

In this chapter we present the simulation scheme of qubit quantum channels, which has been published in our paper [168]. The representations for qubit quantum channels is reviewed in §5.1. Next in §5.2 we study qubit channel decomposition by firstly reviewing the theory developed by Ruskai, Szarek, and Werner [140], and then presenting a geometrical interpretation for qubit channel decomposition, and also highlighting our approach for qubit channel simulation. Our qubit channel simulation algorithm is presented in §5.3 including the optimization results and the analysis of quantum circuit cost. Finally in §5.4 we briefly discuss some other approaches and then conclude by highlighting the key features of our qubit-channel simulator: deterministic, universal, digital, optimal, and algorithmic.

5.1 Qubit channel representations

First we study the qubit channel representations. For an arbitrary qubit quantum channel $\mathcal{E} : \mathscr{D}(\mathscr{H}_2) \to \mathscr{D}(\mathscr{H}_2) : \rho \mapsto \mathcal{E}(\rho)$, the representations are as follows. i) Kraus operator-sum representation. A qubit channel $\mathcal{E}$ can be represented as

$$\mathcal{E} : \mathscr{D}(\mathscr{H}_2) \to \mathscr{D}(\mathscr{H}_2) : \rho \mapsto \sum_{i=0}^{r-1} K_i \rho K_i^\dagger \tag{5.1}$$

for the rank $r \leq 4$ and a set of Kraus operators $\{K_i\}$, which form a linearly independent set, and the trace-preserving condition is $\sum_i K_i^\dagger K_i = \mathbb{1}$. ii) Stinespring dilation. A channel can be dilated to a unitary operator on the joint Hilbert space $\mathscr{H}^{\mathrm{SA}} = \mathscr{H}^{\mathrm{S}} \otimes \mathscr{H}^{\mathrm{A}}$ with S (A) denoting the system (ancilla). From dilation $\mathcal{E} \mapsto U$, $U : \mathscr{H}^{\mathrm{SA}} \to \mathscr{H}^{\mathrm{SA}}$, and

$$\mathcal{U} : \mathscr{D}(\mathscr{H}^{\mathrm{SA}}) \to \mathscr{D}(\mathscr{H}^{\mathrm{SA}}) : \rho^{\mathrm{SA}} \mapsto \rho'^{\mathrm{SA}} = U \rho^{\mathrm{SA}} U^\dagger \tag{5.2}$$

such that $\mathrm{tr}_{\mathrm{A}}\rho^{\mathrm{SA}} = \rho^{\mathrm{S}}$, $\mathrm{tr}_{\mathrm{A}}\rho'^{\mathrm{SA}} = \rho'^{\mathrm{S}}$ and $\mathcal{E} : \rho^{\mathrm{S}} \mapsto \rho'^{\mathrm{S}}$. Kraus operators $K_i = {}^{\mathrm{A}}\langle i|U|0\rangle^{\mathrm{A}}$ for $|i\rangle^{\mathrm{A}}$ (including $|0\rangle^{\mathrm{A}}$) an orthonormal basis state of the ancilla [98]. The unitary operator U is a minimal dilation of $\mathcal{E}$ if U is a dilation such that $\dim\mathscr{H}^{\mathrm{A}} = \left(\dim\mathscr{H}^{\mathrm{S}}\right)^2$. For the case of a single qubit, $\dim\mathscr{H}^{\mathrm{A}} = 4$ for minimal dilation of a full rank qubit channel. iii) Choi state and process state representations. The Choi state is a four-by-four matrix that can have 16 parameters. With the trace-preserving condition $\sum_i K_i^\dagger K_i = \mathbb{1}$, there are totally 12 independent real parameters. In Pauli basis $\{\sigma_i\}$, the process state $\mathcal{S}$, also called process matrix χ, is defined with entries $S_{jk} = \sum_i \mathrm{tr}(K_i^\dagger \sigma_j)\mathrm{tr}(K_i\sigma_k)^*$. It holds $\mathcal{C} = U\mathcal{S}U^\dagger$ for the basis transformation U from Pauli basis to Kronecker basis

$$U = \frac{\sqrt{2}}{2}\begin{pmatrix} 1 & 0 & 0 & 1 \\ 0 & 1 & -i & 0 \\ 0 & 1 & i & 0 \\ 1 & 0 & 0 & -1 \end{pmatrix}, \tag{5.3}$$

with $U_{\alpha\beta} = \mathrm{tr}(\tau_\alpha^\dagger \sigma_\beta)$. iv) Dynamical representations. The affine map for a qubit channel is

$$\mathcal{T} = \begin{pmatrix} 1 & \mathbf{0} \\ \boldsymbol{t} & \boldsymbol{T} \end{pmatrix}, \tag{5.4}$$

which is a four-by-four real matrix with $\mathcal{T}_{ij} = \frac{1}{2}\mathrm{tr}[\sigma_i\mathcal{E}(\sigma_j)]$. In this representation, $\rho = \frac{1}{2}(\mathbb{1} + \boldsymbol{p}\cdot\boldsymbol{\sigma})$, where $\boldsymbol{p}$ is a three-dimensional vector and $\boldsymbol{\sigma} := (X, Y, Z)$. The channel is an affine map [91]

$$\mathcal{E} : \rho \mapsto \frac{1}{2}(\mathbb{1} + \boldsymbol{p}'\cdot\boldsymbol{\sigma}), \quad \boldsymbol{p}' = \boldsymbol{T}\boldsymbol{p} + \boldsymbol{t}. \tag{5.5}$$

Geometrically, $\mathcal{E}$ maps the Bloch ball into an ellipsoid, with $\boldsymbol{t}$ the shift from the ball's origin and $\boldsymbol{T}$ a distortion matrix for the ball. The $\boldsymbol{T}$ matrix can be diagonalized from SVD

$$\mathcal{T} = \begin{pmatrix} 1 & 0 & 0 & 0 \\ s_1 & \lambda_1 & 0 & 0 \\ s_2 & 0 & \lambda_2 & 0 \\ s_3 & 0 & 0 & \lambda_3 \end{pmatrix} \equiv \begin{pmatrix} 1 & 0 \\ \boldsymbol{s} & \boldsymbol{\Lambda} \end{pmatrix}, \tag{5.6}$$

with two rotations O_1 and O_2 such that $O_2\boldsymbol{s} = \boldsymbol{t}$, $O_2\boldsymbol{\Lambda}O_1 = \boldsymbol{T}$. From $SU(2)/\mathbb{Z}_2 \cong SO(3)$, the rotations O_1 and O_2 correspond to prior and posterior $SU(2)$ rotations U_1 and U_2, respectively. There are totally 12 independent parameters in $\mathcal{T}$, with six from the prior and posterior rotations, and six from the rest. Also the dynamical operator $\mathcal{D}$ can be obtained as $\mathcal{D} = U\mathcal{T}U^\dagger$. The dynamics is $\mathrm{res}(\rho) \mapsto \mathcal{D}\mathrm{res}(\rho)$ for $\mathrm{res}(\rho) = (\rho_{00}, \rho_{01}, \rho_{10}, \rho_{11})^{\mathrm{T}}$, which is a representation of ρ in Kronecker basis, see example 1.

5.2 Qubit channel decomposition

5.2.1 Theory of Ruskai-Szarek-Werner

Ruskai, Szarek, and Werner [140] studied in details the properties for the set of qubit quantum channels, and in particular, they developed qubit channel decomposition formula in terms of convex sum of generalized extreme channels. Properties of generalized extreme channels are further analyzed by several others [138, 34, 164, 23]. Here we present the qubit channel decomposition theory based on their original result [140].

Denote the set of extreme qubit channels as $\mathscr{S}_2^{\mathrm{e}}$, the set of rank ≤ 2 qubit channels as $\mathscr{S}_{\leq 2}$, the set of rank ≤ 2 unital qubit channel as $\mathscr{S}_{\leq 2}^{\mathrm{u}}$. Then $\mathscr{S}_{\leq 2} \supset \mathscr{S}^{\mathrm{e}}$, and $\mathscr{S}_{\leq 2} \supset \mathscr{S}_{\leq 2}^{\mathrm{u}}$.

Theorem 32 (Ruskai-Szarek-Werner (RSW) [140])**.** *For a qubit channel $\mathcal{E} \in \mathscr{S}_2$, the following conditions are equivalent:*

1. $\mathcal{E}$ belongs to the closure of the set of extreme channels of $\mathscr{S}_2$, i.e., $\mathcal{E} \in \mathrm{cl}\mathscr{S}_2^{\mathrm{e}}$.

2. The Choi state takes the form

$$\mathcal{C} = \begin{pmatrix} A & \sqrt{A}U\sqrt{B} \\ \sqrt{B}U^\dagger\sqrt{A} & B \end{pmatrix} \tag{5.7}$$

for $0 \leq A, B \leq 1$ and a unitary matrix U.

3. The $\mathcal{T}$ matrix can be reduced to the form

$$\mathcal{T} = \begin{pmatrix} 1 & 0 & 0 & 0 \\ 0 & \lambda_1 & 0 & 0 \\ 0 & 0 & \lambda_2 & 0 \\ t & 0 & 0 & \lambda_3 \end{pmatrix}, \tag{5.8}$$

with $\lambda_3 = \lambda_1\lambda_2$, $t^2 = (1-\lambda_1)^2(1-\lambda_2)^2$.

- *The rank of the Choi state satisfies $r_{\mathcal{C}} \leq 2$.*

This theorem provides a characterization of qubit generalized extreme channels and also extreme channels. The $\mathcal{T}$ matrix can also be parameterized using rotation angles. Let $\lambda_1 = \cos u$, $\lambda_2 = \cos v$, then $\lambda_3 = \cos u \cos v$, $t = \sin u \sin v$, for rotation angles u and v. From Eq.(5.8), one can obtain the two Kraus operators

$$F_0 = \begin{pmatrix} \cos\beta & 0 \\ 0 & \cos\alpha \end{pmatrix}, \quad F_1 = \begin{pmatrix} 0 & \sin\alpha \\ \sin\beta & 0 \end{pmatrix}, \tag{5.9}$$

with $\alpha = (u+v)/2$ and $\beta = (u-v)/2$.

A classification of qubit generalized extreme channels has also been provided [140], and there are three classes: (I) Rank-two extreme channels that are non-unital; (II) Rank-one extreme channels, which are unitary; (III) Rank-two quasi-extreme channels, which are rank-two unital channels, i.e., can be written as a convex sum of two unitary channels. This classification can be explained based on Eq.(5.9). When $\alpha = \beta$, we find $F_0 = \cos\alpha \mathbb{1}$, $F_1 = \sin\alpha X$, which represents rank-two quasi-extreme channels. Furthermore, when $\alpha = \beta$, $\cos\alpha = 0$ or $\sin\alpha = 0$, the channel becomes unitary. From class (III) we see that quasi-extreme channels can be written as convex sum of extreme channels with smaller ranks.

Corollary 33. *A channel $\mathcal{E} \in \mathscr{S}_{\leq 2}$ is either extreme or unital, i.e., $\mathscr{S}_{\leq 2} = \mathscr{S}_2^{\mathrm{e}} \cup \mathscr{S}_{\leq 2}^{\mathrm{u}}$.*

The qubit channel decomposition formula is provided based on the Choi state form of generalized extreme channels.

Theorem 34 ([140]). *Any qubit channel $\mathcal{E}$ can be written as a convex combination of two generalized extreme channels*

$$\mathcal{E} = p\mathcal{E}_1^{\mathrm{g}} + (1-p)\mathcal{E}_2^{\mathrm{g}},\ p \in [0,1]. \tag{5.10}$$

Proof. In the Choi state form (5.7), the contraction R can be written as a convex sum of two unitary matrices $R = pU_1 + (1-p)U_2$ from Theorem 9, then $\mathcal{C} = p\mathcal{C}_1^{\mathrm{g}} + (1-p)\mathcal{C}_2^{\mathrm{g}}$, with $\mathcal{C}_1^{\mathrm{g}}$ ($\mathcal{C}_2^{\mathrm{g}}$) denoting the generalized extreme channel Choi state when R is substituted by U_1 (U_2). The decomposition of contraction can be shown by a particular example. The contraction R can be decomposed by singular value decomposition as

$$\begin{aligned} R &= V \begin{pmatrix} \cos\theta_1 & 0 \\ 0 & \cos\theta_2 \end{pmatrix} W \\ &= \frac{1}{2} V \begin{pmatrix} e^{i\theta_1} & 0 \\ 0 & e^{i\theta_2} \end{pmatrix} W + \frac{1}{2} V \begin{pmatrix} e^{-i\theta_1} & 0 \\ 0 & e^{-i\theta_2} \end{pmatrix} W. \end{aligned} \tag{5.11}$$

Then $R = \frac{1}{2}(U_1 + U_2)$, and $\mathcal{C} = \frac{1}{2}(\mathcal{C}_1^{\mathrm{g}} + \mathcal{C}_2^{\mathrm{g}})$. □

5.2.2 Geometry for qubit channel decomposition

From Theorem 34 above we know that a convex sum of no more than two generalized extreme channels is sufficient to decompose any qubit channel. Such a decomposition can be understood geometrically. Set up a coordinate system by $(\lambda_1, \lambda_2, \lambda_3)$ based on the affine representation. Note the space of $(\lambda_1, \lambda_2, \lambda_3)$ is also called distortion space from Theorem 11. The coordinate for a generalized extreme channel is $(\cos(\alpha-\beta), \cos(\alpha+\beta), \cos(\alpha-\beta)\cos(\alpha+\beta))$. The set of unital qubit channels forms a tetrahedron, as shown in the left panel of Fig. 5.1. The origin $(0,0,0)$ is at the center of the tetrahedron, which corresponds to the case $\alpha = \pi/2$, $\beta = 0$. The coordinates for Pauli operators are $X : (1,-1,-1)$, $-iY : (-1,1,-1)$, $Z : (-1,-1,1)$, and $\mathbb{1} : (1,1,1)$, which are the four vertices. Rank-two channels sit on the

six edges, rank-three channels sit on the four faces, and rank-four channels sit inside the tetrahedron.

By comparison, the set of non-unital channels have a more complicated shape for fixed values of t. To determine the shape of this set, one can use the necessary condition [140] for complete positivity

$$(\lambda_1 \pm \lambda_2)^2 \leq (1 \pm \lambda_3)^2 - t^2. \tag{5.12}$$

For a fixed t, the above two equations correspond to two curved planes, which enclose a region for the two inequalities. This region is termed as an unsymmetrically "rounded" tetrahedron [140]. Note when $t = 0$, this rounded tetrahedron just becomes a tetrahedron, and each curved plane becomes two planes intersected at a sharp edge, which corresponds to the edge of the tetrahedron, and the intersections generate the four edges and six vertices of the tetrahedron. We show one example for the case $t = 0.2$ in the right panel of Fig. 5.1. it can be seen that there is one curved plane that covers the other from the top, and the intersection of the two curved planes is highlighted by blue stars, which form a closed curve. The closed curve corresponds to generalized extreme channels.

It is known that a qubit unital channel can be written as a convex sum of four unitary channels. This can be understood from the geometry of the tetrahedron. Any point in the tetrahedron corresponds to a qubit unital channel, and it can be written as a convex sum of

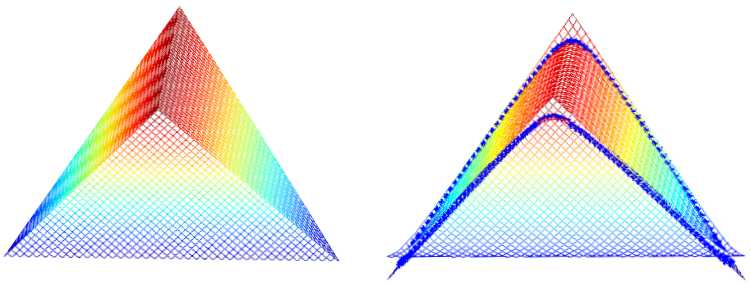

Figure 5.1: The geometry of the set of qubit channels. (Left) Unital case, the set of unital qubit channels forms a tetrahedron. (Right) Non-unital case for the particular value $t = 0.2$ in Eq. (5.8), and the blue stars highlights the intersection of the two curved planes.

the four vertices of the tetrahedron, which are unitary channels.

The four vertices are not extreme channels for the set of non-unital channels anymore. That is to say, a non-unital channel cannot be written as a convex sum of unitary channels. Instead, the extreme channels for the non-unital case are the closed intersected curve. This implies there are infinite number of extreme channels. Then, for qubit channel decomposition, given an arbitrary qubit channel, unital or not, one only needs a convex sum of two generalized extreme channels $\mathcal{E} = p\mathcal{E}_1^{\mathrm{g}} + (1-p)\mathcal{E}_2^{\mathrm{g}}$, following from the geometry: the point in the body corresponding to the given qubit channel can be expressed as the convex sum of two points from the opposite edges of the rounded tetrahedron.

5.2.3 Our approach for qubit channel simulation

We intend to develop an algorithm for qubit channel simulation. However, the RSW method is not straightforward to be employed due to the following reasons. First, the RSW channel decomposition (5.10) takes a special form, in that the two generalized extreme channels all have the same block matrices on the diagonal of the Choi states $\mathcal{C}_i^{\mathrm{g}}$ with those in the Choi state $\mathcal{C}$ of the channel to be decomposed. This requires to express a Choi state in block-matrix form and the decomposition of contraction, which is not necessary for our qubit channel simulation. Second, the Choi state for a generalized extreme channel corresponds to a $\mathcal{T}$ matrix (5.8), together with a prior and a posterior basis transformation. That is to say, the Kraus operators of an arbitrary generalized extreme channel are $K_0 = UF_0V$ and $K_1 = UF_1V$ for unitary operators U and V. The RSW paper does not analyze how to find those basis transformations U and V. Third, the RSW approach does not address the problem of circuit-design for the simulation of generalized extreme channels.

By comparison, we do not require the block matrices on the diagonal of the generalized extreme channel Choi states are the same with those for the given channel. This is much more convenient for numerical simulation. As a result, we do not use decomposition of contraction. Also we address the problem of circuit-design for the simulation of generalized

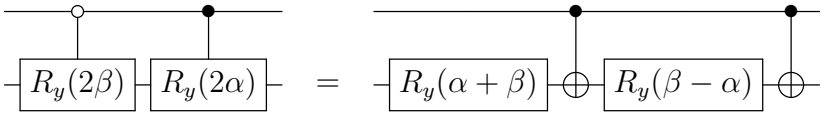

Figure 5.2: The quantum circuit for the qubit multiplexer $M_{10}(\alpha, \beta)$ with the top wire for the system and the bottom for the ancilla. The circuit equivalence can be easily verified [123, 117]. When the system is in state $|0\rangle$, the ancilla is acted on by $R_y(2\beta)$; when the system is in state $|1\rangle$, the ancilla is acted on by $XR_y(\beta-\alpha)XR_y(\alpha+\beta)$, which is just $R_y(2\alpha)$.

extreme channels, which is a central component for the design of qubit channel simulator.

5.3 Qubit channel simulation algorithm

5.3.1 Representations of generalized extreme qubit channels

In this section we present a detailed characterization of any qubit generalized extreme channel $\mathcal{E}^{\rm g}$ specified by the two Kraus operators (5.9). From dilation, the channel $\mathcal{E}^{\rm g}$ can be realized by the unitary operator

$$U_{\rm qub} := \textsc{cnot} M_{10}(\alpha, \beta), \tag{5.13}$$

where the multiplexor $M_{10}(\alpha, \beta)$, shown in Fig. 5.2, takes the form

$$M_{10}(\alpha, \beta) := R_y(2\beta) \oplus R_y(2\alpha) = \begin{pmatrix} \cos\beta & -\sin\beta & 0 & 0 \\ \sin\beta & \cos\beta & 0 & 0 \\ 0 & 0 & \cos\alpha & -\sin\alpha \\ 0 & 0 & \sin\alpha & \cos\alpha \end{pmatrix}, \tag{5.14}$$

and the CNOT gate allows the ancilla as control.

Further, when the ancilla qubit is prepared in state $|0\rangle$, we can save one CNOT gate and the multiplexer can be realized as $\tilde{M} := (\mathbb{1}\otimes R_y(2\gamma_1))\textsc{cnot}(\mathbb{1}\otimes R_y(2\gamma_2))$ for $2\gamma_1 = \beta - \alpha + \pi/2$

and $2\gamma_2 = \beta + \alpha - \pi/2$. Now we check the actions of $M \equiv M_{10}(\alpha, \beta)$ and $\tilde{M}$.

$$M|0\rangle|0\rangle = |0\rangle R_y(2\beta)|0\rangle; M|1\rangle|0\rangle = |1\rangle R_y(2\alpha)|0\rangle; \tag{5.15}$$

$$\tilde{M}|0\rangle|0\rangle = |0\rangle R_y(2\beta)|0\rangle; \tilde{M}|1\rangle|0\rangle = |1\rangle X R_y(\pi - 2\alpha)|0\rangle = |1\rangle R_y(2\alpha) Z|0\rangle. \tag{5.16}$$

We see that $\tilde{M}$ introduces one additional Z operation when the system is $|1\rangle$, while the Z operation acts trivially on ancilla state $|0\rangle$. In general, when the ancilla can be prepared in arbitrary state, the additional Z operation will cause a phase error.

In matrix form, the unitary operator U_{qub} is

$$U_{\text{qub}} = \begin{pmatrix} \cos\beta & -\sin\beta & 0 & 0 \\ 0 & 0 & \sin\alpha & \cos\alpha \\ 0 & 0 & \cos\alpha & -\sin\alpha \\ \sin\beta & \cos\beta & 0 & 0 \end{pmatrix}. \tag{5.17}$$

The circuit diagram of U_{qub} is shown in Fig 5.3, with two additional rotations for basis transformation. Next we explain the action of the operator U_{qub}. If the system qubit were in the state $|0\rangle$, then the CNOT would have no action on the ancilla, and the two rotations combine to give $R_y(2\beta)$, which yields the state $\cos\beta|0\rangle + \sin\beta|1\rangle$. If the system is in the state $|1\rangle$, then an X operation flips the ancilla, and then the two rotations give $\cos\alpha|0\rangle + \sin\alpha|1\rangle$. Measuring the ancilla in the state $|0\rangle$ then multiplies state $|0\rangle$ for the system by $\cos\beta$ and state $|1\rangle$ by $\cos\alpha$; this is the action of F_0. Similarly, measuring the ancilla in the state $|1\rangle$ multiplies state $|0\rangle$ for the system by $\sin\beta$, and state $|1\rangle$ by $\sin\alpha$; this is the action of the operator

$$F_1' = \begin{pmatrix} \sin\beta & 0 \\ 0 & \sin\alpha \end{pmatrix}. \tag{5.18}$$

In that case we can simply apply X, which gives the required Kraus operator F_1.

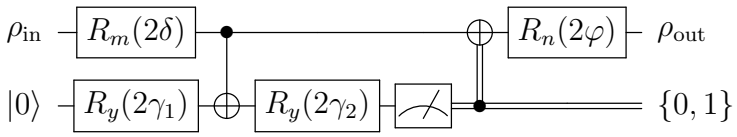

Figure 5.3: The quantum circuit to implement a generalized extreme qubit channel $\mathcal{E}^{\text{g}}$, together with additional prior rotation $R_m(2\delta)$ and posterior rotation $R_n(2\varphi)$. $R_y(2\gamma) = \exp(-iY\gamma) = \mathbb{1}\cos\gamma - iY\sin\gamma$; the two angles are $2\gamma_1 = \beta - \alpha + \pi/2$ and $2\gamma_2 = \beta + \alpha - \pi/2$. Ignoring the prior and posterior rotations, the measurement in the computational basis with the outcome $|0\rangle$ ($|1\rangle$) corresponds to the realization of the Kraus operator F_0 (F_1) in Eq. (5.9). The final operation is a classically controlled X operation. [Figure from Ref. [168], Fig. 1.]

The Choi state corresponding to $\mathcal{E}^{\text{g}}$ takes the form

$$\mathcal{C}_{\text{qub}} = \frac{1}{2}\begin{pmatrix} \cos^2\beta & 0 & 0 & \cos\alpha\cos\beta \\ 0 & \sin^2\alpha & \sin\alpha\sin\beta & 0 \\ 0 & \sin\alpha\sin\beta & \sin^2\beta & 0 \\ \cos\alpha\cos\beta & 0 & 0 & \cos^2\alpha \end{pmatrix} \equiv \begin{pmatrix} A_1 & C_{12} \\ C_{21} & A_2 \end{pmatrix}, \tag{5.19}$$

with $C_{12} = \sqrt{A_1}U\sqrt{A_2}$. The unitary U is a modified permutation operator which depends on the parameters α and β as follows. i) If $\sin\alpha\sin\beta > 0$, $\cos\alpha\cos\beta > 0$, $U = X$; ii) If $\sin\alpha\sin\beta < 0$, $\cos\alpha\cos\beta < 0$, $U = -X$; iii) If $\sin\alpha\sin\beta < 0$, $\cos\alpha\cos\beta > 0$, $U = iY$; iv) if $\sin\alpha\sin\beta > 0$, $\cos\alpha\cos\beta < 0$, $U = -iY$. The eigenvalues of $\mathcal{C}_{\text{qub}}$ are $\lambda_1 = (\sin^2\alpha + \sin^2\beta)/2$, $\lambda_2 = (\cos^2\alpha + \cos^2\beta)/2$, $\lambda_3, \lambda_4 = 0$. The rank of Choi state equals the number of Kraus operators which is two.

For completeness, the process matrix $\mathcal{S}_{\text{qub}}$ takes the form

$$\mathcal{S}_{\text{qub}} = \frac{1}{4}\begin{pmatrix} (\cos\alpha + \cos\beta)^2 & 0 & 0 & \cos^2\beta - \cos^2\alpha \\ 0 & (\sin\alpha + \sin\beta)^2 & i(\sin\beta^2 - \sin\alpha^2) & 0 \\ 0 & -i(\sin^2\beta - \sin^2\alpha) & (\sin\alpha - \sin\beta)^2 & 0 \\ \cos^2\beta - \cos^2\alpha & 0 & 0 & (\cos\alpha - \cos\beta)^2 \end{pmatrix} \tag{5.20}$$

Algorithm 2 Algorithm for qubit quantum channel $\mathcal{E}$ simulation

Input:
  $[\mathcal{E}]$: bit-string description of the qubit channel
  ϵ: the error tolerance
Output:
  ϵ': actual simulation error
  $[C]$: bit-string description of the circuit
  function ChaSim($[\mathcal{E}]$, ϵ)
    $[C] \leftarrow \varnothing$. ▷ Initializes as the empty-string
    $U \leftarrow$ Haar-rand-$SU(8)$. ▷ Generate random unitary operator
    for $i = 0$ to 3 **do**
      $K_i \leftarrow \langle i|U|0\rangle$. ▷ Generate Kraus operators
    end for
    $\mathcal{C} \leftarrow \{K_i\}$. ▷ Generate input Choi state $\mathcal{C}$
    for $\imath = 1$ to 2 **do**
      $p \leftarrow \text{rand}[0,1]$. ▷ Generate probability
      $W^{(\imath)}, V^{(\imath)} \leftarrow$ Haar-rand-$SU(2)$. ▷ Generate random unitary operators
      $\vec{\theta}^{(\imath)} \leftarrow 2\pi\text{rand}[0,1]^{\otimes 2}$. ▷ Generate rotation angles
      $M_{10}(\theta_1^{(\imath)}, \theta_2^{(\imath)}) \leftarrow R_y(2\theta_2^{(\imath)}) \oplus R_y(2\theta_1^{(\imath)})$.
      $U^{(\imath)} \leftarrow \text{CNOT} M_{10}^{(\imath)}(\theta_1^{(\imath)}, \theta_2^{(\imath)})$.
      for $i = 0$ to 1 **do**
        $F_i^{(\imath)} \leftarrow W^{(\imath)}\langle i|U^{(\imath)}|0\rangle V^{(\imath)}$. ▷ Kraus operators for each generalized extreme channel
      end for
      $\mathcal{C}^{(\imath)} \leftarrow \{K_i^{(\imath)}\}$.
    end for
    $\{\epsilon', \vec{p}', \vec{\theta}'^{(\imath)}, W^{(\imath)}, V^{(\imath)}\} \leftarrow \text{CJ}(\mathcal{C}, \epsilon, \vec{p}, \{\mathcal{C}^{(\imath)}\})$. ▷ Choi-Jamiołkowski state decomposition
    if $\epsilon' \leq \epsilon$ **then**
      return $U^{(\imath)} \leftarrow \vec{\theta}^{(\imath)}, W^{(\imath)}, V^{(\imath)}$.
      for $\imath = 1$ to 2 **do**
        $\tilde{W}^{(\imath)}, \tilde{V}^{(\imath)}, \tilde{R}_y \leftarrow \text{SK}(W^{(\imath)}, V^{(\imath)}, R_y, \epsilon)$. ▷ Solovay-Kitaev algorithm
        $[C^{(\imath)}] \leftarrow \tilde{W}^{(\imath)}, \tilde{V}^{(\imath)}, \tilde{R}_y$. ▷ Construct the generalized extreme channel circuit
      end for
      return ϵ'.
      return $[C] \leftarrow [C^{(1)}][C^{(2)}][p]$.
    else
      return false.
    end if
  end function

following from the relation $\mathcal{S} = U^\dagger \mathcal{C} U$ with Choi state for basis transformation U (5.3). It can be easily checked that $\mathcal{S}_{\text{qub}}$ is rank two and has the same eigenvalues with $\mathcal{C}_{\text{qub}}$.

5.3.2 Optimization algorithm for qubit channel simulation

Now we describe the algorithm for the simulation of a general qubit channel, shown in Algorithm 2. The algorithm accepts the description of a qubit channel $\mathcal{E}$ and an error tolerance ϵ as input. The output is a quantum circuit, and also a bound ϵ' on the resultant circuit with respect to the actual channel $\mathcal{E}$ being simulated.

An arbitrary qubit channel $\mathcal{E}$ has 12 parameters whereas the optimization of $\mathcal{E}$ is over 17 parameters. We note that the optimization precludes an efficient circuit-design algorithm, while the optimization does not require much computational resource. An input qubit channel is obtained from a unitary operator $U \in SU(8)$ according to dilation, and the randomness of the input qubit channel is ensured by randomly choosing the dilated unitary operator. Our algorithm employs an iterative optimization procedure, which is repeated until a satisfactory circuit is found or aborted if the optimization routine fails to find a good circuit within a pre-specified number of trials. The objective function for optimization is given by the trace distance $D_t(\mathcal{C}, \mathcal{C}')$, as established in Eq. (4.45) in Chapter 4.

Our algorithm employs a simple nonlinear programming method [180] on channels generated by partial trace of Haar-random-generated unitary operators on the dilated space [157]. We simulate on MATLAB® using GlobalSearch algorithm. Fig. 5.4 shows the simulation results for 20 randomly chosen qubit channels. We can see that our simulations yield errors of order $10^{-2} \sim 10^{-4}$ for qubit channels, and the convergence on average only takes several minutes. The "jumps" is due to the intrinsic procedure of the GlobalSearch program, and does not require an apparent explanation. Instead, only the long-time convergence matters for the optimization. We can see that the simulation accuracy for qubit channel decomposition is high enough, especially compared with the qutrit and two-qubit cases in Chapter 7.

5.3.3 Quantum circuit cost

We summarize our result for single-qubit channel simulation as follows.

Proposition 35. *Any single-qubit channel $\mathcal{E}$ can be implemented by a convex sum of two generalized extreme qubit channels, each of which can be simulated by a quantum circuit with one ancillary qubit, one* CNOT*, one classically controlled* NOT *gate, and four qubit rotations, and the convex sum requires a random classical bit.*

Given the simulation error tolerance ϵ, each of the generalized extreme qubit channels in

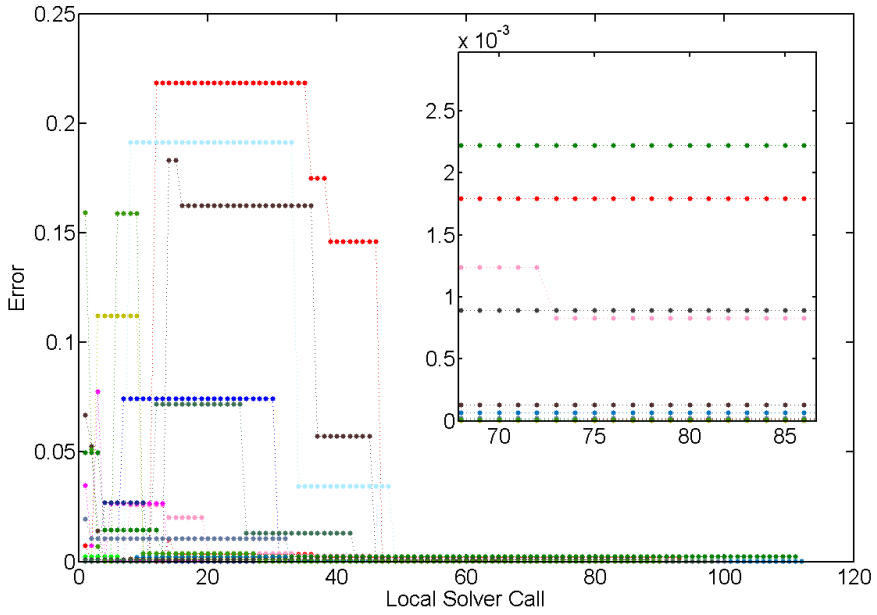

Figure 5.4: Simulation results for 20 randomly chosen qubit channels. The number of calls to local solvers in GlobalSearch algorithm corresponds to the simulation runtime, and the simulation error is the trace distance between the input qubit Choi state and the approximate Choi state. The inset magnifies part of the figure to show the convergence more clearly.

the convex combination is to be simulated within distance ϵ by the convexity of the one-norm distance. The error bound for a generalized extreme qubit channel is satisfied if its dilated two-qubit unitary operators is approximated within distance $\epsilon/2$, according to Theorem 5. There are four single-qubit unitary operators used within the circuit. The error bound will be satisfied, provided each of these unitary operators is approximated within distance $\epsilon/8$. These unitary operators can be approximated via the SKDN algorithm with $O(\log^{3.97}(1/\epsilon))$ gates from a universal library S. Using our lookup database in Chapter 3, the SKDN algorithm may be implemented efficiently, in that the classical complexity to determine the gate sequence does not exceed $O(\log^{2.71}(1/\epsilon))$. However, due to the optimization procedure, the classical circuit-design algorithm would not have a clear scaling. While the quantum circuit has a clear scaling, which comprises $O(\log^{3.97}(1/\epsilon))$ quantum gates. Better scaling

can also be achieved if algorithms other than SKDN algorithm are employed, such as those discussed in the last section of Chapter 3.

5.4 Discussion and conclusion

Here we discuss some other approaches for single-qubit channel and open-system dynamics simulation, from which the merits of our simulator are emphasized. First, the simulation of single-qubit channels using a mixed-state environment has been studied [122, 156]. It is proved that this approach cannot simulate all qubit channels. In the affine representation, it is shown that 3/8 of generalized depolarizing qubit channels can be simulated by the one-qubit mixed-state environment. Further, counterexamples are shown that cannot be simulated by a circuit with one-qubit mixed-state environment [122, 182]. Our approach, instead, successfully achieved the universality for simulating arbitrary qubit channels by convex sum of smaller qubit channels, which are the generalized extreme qubit channels.

The simulation of Markovian dynamics has also been studied [7]. This employs a Trotter-Suzuki formula [158, 153] for nonunitary operators to decompose a Markovian dynamics $\mathcal{E} = e^{\mathcal{L}t}$ into a product of other Markovian dynamics $\prod_i e^{\mathcal{L}_i t_i}$. Each term $e^{\mathcal{L}_i t_i}$ needs to be realized by a dilated unitary operator, hence a large number of CNOT gates are required generally. Instead, using the framework of quantum channel simulation the Markovian dynamics can be converted into a quantum channel form first [26], and then simulated using our scheme.

Also simulation based on bang-bang control and feedback has been developed [109]. Using polar decomposition, a quantum channel can be expressed as $\mathcal{E} : \rho \mapsto \sum_i U_i B_i \rho B_i U_i^\dagger$, which is interpreted as a separation of a channel in terms of a measurement step B_i, followed by a feedback step for the unitary operators U_i. The measurement $\{B_i\}$ can be performed using bang-bang control technique, and a resettable qubit ancilla is employed to feedback the measurement results and selectively implement each unitary operator U_i. This approach also applies to qudit channel simulation, thus it is claimed that an arbitrary open-system

dynamics can be simulated using just one qubit ancilla more than required to simulate closed-system dynamics. However, compared to our approach, this simulation would require a large amount of CNOT gates for the bang-bang control, also this simulation requires the engineering of Hamiltonian-driven evolution.

For conclusion, we have demonstrated that our scheme for single-qubit quantum channel simulation is 1) deterministic, which means no post-selection is required, 2) universal, which means it applies for arbitrary single-qubit channel, 3) digital, which means it comprises quantum gates that can be implemented at discrete time instead of gates based on Hamiltonian-driven evolution, 4) optimal, which means it only requires a single CNOT gate and a single-qubit ancilla, and also 5) algorithmic, which means the simulation accuracy is promised.

Chapter 6

Photonic qubit-channel simulator

In this chapter, we report the realization of a photonic qubit-channel simulator [111]. The simulation algorithm is based on Chapter 5. The simulator is universal instead of dedicated, and digital instead of analog. The accuracy of the simulator is well characterized from quantum process tomography. In §6.1 the experimental setup for the simulator is reviewed, and in §6.2 we show how to simulate an arbitrary qubit channel. Furthermore, in §6.3 a weak measurement process is simulated, and in §6.4 the transpose operation is simulated. We conclude in §6.5.

6.1 Setup

To simulate a generalized extreme channel $\mathcal{E}^{\mathrm{g}}$, we design the setup shown in Fig. 6.1b. The system and ancilla photonic qubits are generated by shining the ultraviolet pluses on two collinear β-barium borate (BBO) crystals emitting photon pairs $|HV\rangle_{ij}$ along the pumping direction, with $|H\rangle$ and $|V\rangle$ the horizontal and vertical polarization states, and i, j denote the path mode. The generated photons in the pair $|HV\rangle_{ij}$ are separated by a polarizing beam splitter (PBS), which transmits the $|H\rangle$ component and reflects the $|V\rangle$ component for each photon. Reflected photons 2 and 4 are collected by single-mode fibers (SMFs) and detected by single-photon counting modules (SPCMs) to herald that photons 1 (system) and 3 (ancilla) are underway, respectively.

Rotation around the y axis by angle 2γ, represented by $R_y(2\gamma)$, is realized by a half-wave plate (HWP) setting at angle $\tau = \gamma/2$ together with a HWP set at 0°. An arbitrary rotation gate $R_{\boldsymbol{r}}(2\theta)$ is realized by a HWP sandwiched between two quarter-wave plates (QWP). The CNOT gate is realized by applying a controlled-phase (C-phase) gate with two Hadamard

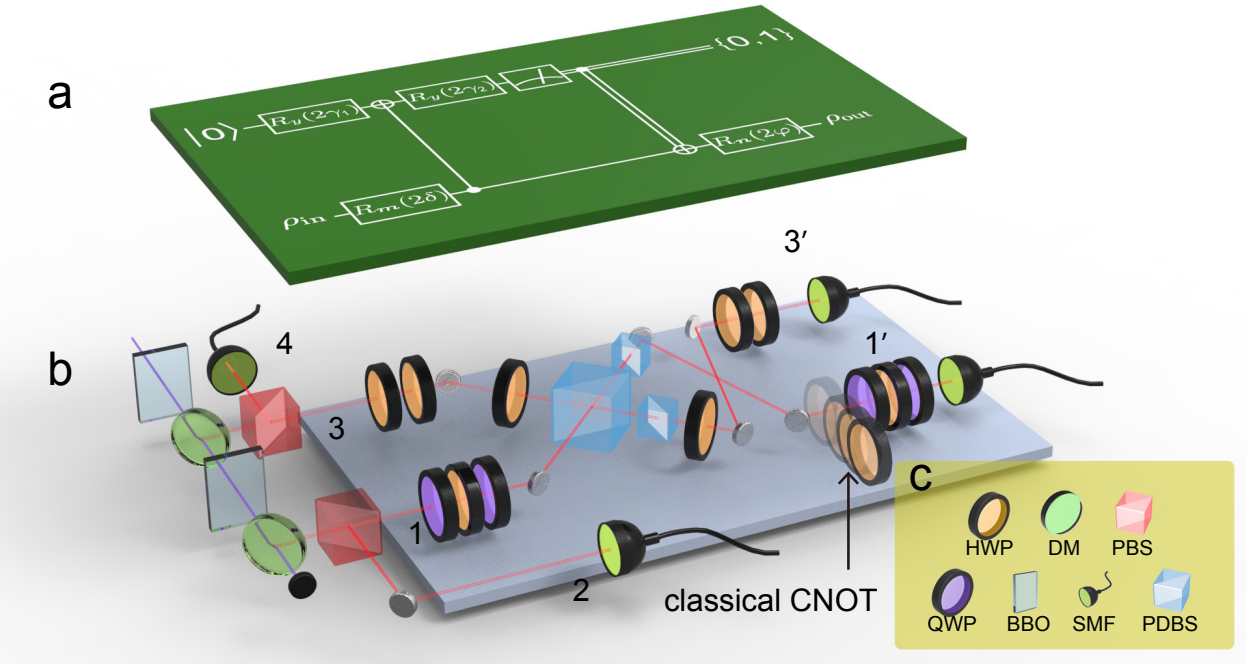

Figure 6.1: Experimental scheme for qubit quantum channel simulation. **a,** The quantum circuit of a generalized extreme channel, comprising single-qubit rotations, one quantum CNOT gate, and one classical CNOT gate. When the measurement result on ancilla is $|0\rangle$ ($|1\rangle$), the circuit acts as K_0 (K_1). **b,** Schematic drawing of the experimental setup. An ultraviolet pulse (150 fs, 80MHz, 390 nm) passes through two 2-mm-thick collinear BBO crystals, creating two pairs of photons $|HV\rangle_{ij}$ with central wavelength of 780nm. The ultraviolet pulse (390nm) and the generated photons (780nm) are along the same direction and separated by a dichroic mirror (DM). The generated photons $|HV\rangle_{ij}$ are separated by a PBS and the reflected photons are detected to guarantee that the transmitted photons are underway. All four photons are collected by the SMF and detected by the SPCM. We use a homemade Field Programmable Gate Array (FPGA) to record the fourfold coincidence (not shown here). **c,** Symbols used in **b**.

gates (HWPs set at 67.5°) on target photon 1 before and after the C-phase gate. The C-phase gate is implemented by overlapping photons 1 and 3 on a polarization-dependent beamsplitter (PDBS) ($T_H = 1$ and $T_V = 1/3$) with two supplemental PDBSs ($T_V = 1$ and $T_H = 1/3$) at each exit port of the overlapping PDBS [75, 101, 88, 124]. The probabilistic CNOT gate has a success probability of 1/9. We experimentally characterize the quantum CNOT gate via quantum process tomography (QPT) technology [43, 133]. The gate fidelity $F = 0.83 \pm 0.02$ is observed.

The classical CNOT flips the system-qubit state $1'$ conditioned on the measurement on the ancillary qubit $3'$. Experimentally, the classical CNOT is statistically simulated: we set the measurement basis of ancillary photon $3'$ on $|H\rangle$ or $|V\rangle$ with equal probability. No further operation on the system qubit $1'$ occurs when the measurement basis choice of ancillary photon $3'$ is $|H\rangle$, whereas an X operation (an HWP set at 45°) is applied on the system qubit $1'$ when the measurement basis choice of ancillary photon $3'$ is $|V\rangle$. If the ancilla-qubit measurement result is $|H\rangle$ ($|V\rangle$), the simulator is described by K_0 (K_1).

The probability p (5.10) is also statistically simulated. We first run the generalized extreme channel $\mathcal{E}_1^{\mathrm{g}}$ with our simulator and collect data under $\mathcal{E}_1^{\mathrm{g}}$ for time t_1. Then we run the generalized extreme channel $\mathcal{E}_2^{\mathrm{g}}$, and collect data under $\mathcal{E}_2^{\mathrm{g}}$ for time t_2. The combinational results correspond to the combination of $\mathcal{E}_1^{\mathrm{g}}$ and $\mathcal{E}_2^{\mathrm{g}}$, $\mathcal{E} = (t_1\mathcal{E}_1^{\mathrm{g}} + t_2\mathcal{E}_2^{\mathrm{g}})/(t_1+t_2)$. By choosing t_1 and t_2 appropriately, any $p \in [0, 1]$ can be simulated.

6.2 Simulation of arbitrary qubit channel

We now show how to program an arbitrary single-qubit channel with our setup with an example of a simulation for a randomly chosen channel. In the process-matrix representation, we choose a random input channel as

$$\mathcal{S} = \begin{pmatrix} 0.3938 & 0.0075 + 0.0739i & 0.0172 + 0.0155i & 0.0801 - 0.0614i \\ 0.0075 - 0.0739i & 0.1594 & -0.0733 - 0.0801i & -0.066 + 0.0172i \\ 0.0172 - 0.0155i & -0.0733 + 0.0801i & 0.2241 & -0.014 - 0.075i \\ 0.0801 + 0.0614i & -0.066 - 0.0172i & -0.014 + 0.075i & 0.2228 \end{pmatrix}. \tag{6.1}$$

The channel $\mathcal{S}$ can be realized by the circuit (Fig. 6.1b) with appropriate non-unique parameters. For $\mathcal{E}_1^{\rm g}$, $\delta = -0.42\pi$, $m_1 = 0.1876$, $m_2 = 0.7948$, $m_3 = 0.5771$ for $R_{\boldsymbol{m}}(2\delta)$, and $\varphi = 0.36\pi$, $n_1 = -0.7813$, $n_2 = -0.5804$, $n_3 = 0.2295$ for $R_{\boldsymbol{n}}(2\varphi)$. The two Kraus operators of $\mathcal{E}_1^{\rm g}$ are $K_0 = [0.6845, 0; 0, 0.8443]$, $K_1 = [0, 0.5358; 0.7290, 0]$ with corresponding $\alpha = 0.18\pi$, $\beta = 0.26\pi$, and $\gamma_1 = (\beta - \alpha + \pi/2)/2 = 0.29\pi$, $\gamma_2 = (\beta + \alpha - \pi/2)/2 = -0.03\pi$. For $\mathcal{E}_2^{\rm g}$, $\delta = -0.7486\pi$, $m_1 = 0.3919$, $m_2 = 0.5051$, $m_3 = 0.7690$ for $R_{\boldsymbol{m}}(2\delta)$, and $\varphi = 0.5589\pi$, $n_1 = -0.0919$, $n_2 = -0.9817$, $n_3 = 0.1668$ for $R_{\boldsymbol{n}}(2\varphi)$. The two Kraus operators of $\mathcal{E}_2^{\rm g}$ are $K_0 = [0.309, 0; 0, -0.8763]$, $K_1 = [0, 0.4818; 0.9511, 0]$ with corresponding $\alpha = 0.84\pi$, $\beta = 0.4\pi$, and $\gamma_1 = 0.03\pi$, $\gamma_2 = 0.36\pi$. For $p = 0.6$, we set $t_1 = 60$s and $t_2 = 40$s.

To verify that the channel $\mathcal{S}$ is accurately simulated, we use QPT technology to reconstruct the matrix representation of $\mathcal{S}$. Fig. 6.2 shows the experimentally reconstructed matrix of $\mathcal{S}_{\rm exp}$. We calculate the process fidelity $F_{\rm P} = (\mathrm{Tr}\sqrt{\sqrt{\mathcal{S}}\mathcal{S}_{\rm exp}\sqrt{\mathcal{S}}})^2$, and discover that $F_{\rm P} = 0.94 \pm 0.02$. Average fidelity $\bar{F}$ is related to $F_{\rm P}$ by $\bar{F} = (dF_{\rm P} + 1)/(d + 1)$ [20]. We apply our data ($d = 2$), and find that $\bar{F} = 0.96 \pm 0.01$. As further analysis, we calculate the trace distance $D(\mathcal{S}, \mathcal{S}_{\rm exp}) = \mathrm{Tr}\,|\mathcal{S} - \mathcal{S}_{\rm exp}|/2 = 0.22 \pm 0.02$. Fidelity $F_{\rm P}$ is related to D by the inequality $1 - \sqrt{F_{\rm P}} \leq D \leq \sqrt{1 - F_{\rm P}}$, according to relation (2.40). Note the square of the fidelity used in the relation (2.40) is employed in the experiment. In our case ($F_{\rm P} = 0.94$), the upper and lower bounds of D are 0.06 and 0.24.

In addition, we also have simulated a few interesting quantum noise channels, namely the amplitude-damping, the bit-flip, the phase-flip, and the depolarizing channels [123]. We find that the average process fidelity is over 0.90 and the average trace distance is below 0.22.

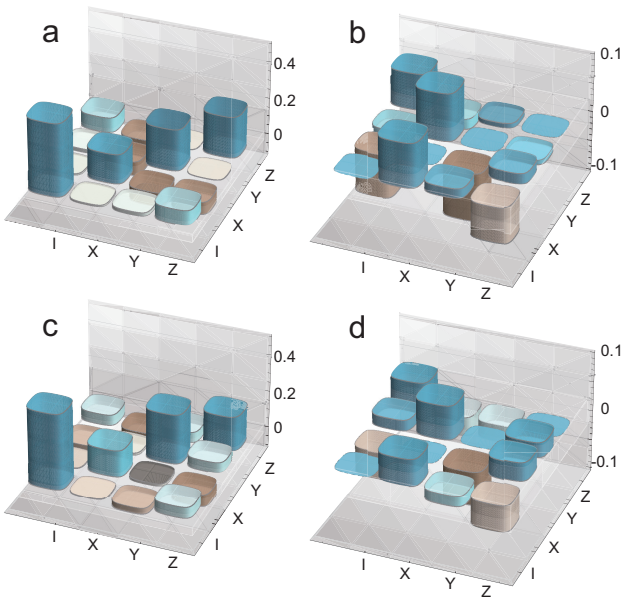

Figure 6.2: The reconstructed process matrix $\mathcal{S}$ for a randomly chosen qubit channel in Eq. (6.1), with the real part of $\mathcal{S}^{\text{exp}}$ (a) and $\mathcal{S}$ (c), and imaginary part of $\mathcal{S}^{\text{exp}}$ (b) and $\mathcal{S}$ (d).

6.3 Protecting superposition via weak measurement

Here we make a further step to show that our simulator can also simulate CP channels that are not trace-preserving. The basic starting point for simulating not-TP channels is to convert a not-TP channel into a CPTP channel and then perform postselection.

Recently, weak measurement and measurement reversals have been suggested to protect quantum superposition and quantum entanglement against decohering noise [97]. This approach has been demonstrated experimentally [89] and may have applications in quantum information processing. Decoherent noise on a single-qubit quantum state, which may contain some encoded information, is modeled as an amplitude-damping (AD) channel, which destroys the quantum superposition of the initial state ρ_{in}. By performing two weak measurements M and N before and after the AD channel respectively, the fidelity of the quantum state is significantly improved. Such a quantum process is CP but not TP. Mathematically,

this process can be described as:

$$\rho_{\mathrm{f}} = \mathcal{E}_{\mathrm{w}}(\rho_{\mathrm{in}}) = N\mathcal{E}_{\mathrm{AD}}(M\rho_{\mathrm{in}}M^{\dagger})N^{\dagger} \tag{6.2}$$

for any qubit state ρ_{in}, and M and N are in the form $M = [1, 0; 0, m]$, $N = [n, 0; 0, 1]$ with $m = \sqrt{1 - p_{\mathrm{pre}}}$ and $n = \sqrt{1 - p_{\mathrm{post}}}$. The parameters $p_{\mathrm{pre}}, p_{\mathrm{post}} \in [0, 1]$ are the measurement strength of pre-measurement M and post-measurement N, respectively. Notice that when $p_{\mathrm{pre}} = p_{\mathrm{post}} = 1$, M and N become projection measurements, which means M and N are strong measurements. Using the AD-channel formula, this process can be rewritten as $\mathcal{E}_{\mathrm{w}}(\rho_{\mathrm{in}}) = \sum_{i=0}^{1} K_i \rho_{\mathrm{in}} K_i^{\dagger}$, where $K_0 = \left[n, 0; 0, m\sqrt{1-\lambda}\right]$ and $K_1 = \left[0, mn\sqrt{\lambda}; 0, 0\right]$.

To simulate $\mathcal{E}_{\mathrm{w}}$ we employ convex combinations of two generalized extreme channels. As $\mathcal{E}_{\mathrm{w}}$ is not TP, we post-select such that each generalized extreme channel provides one Kraus operator. For $\mathcal{E}_1^{\mathrm{g}}$, we fix $\cos\beta = n$ and $\cos\alpha = m\sqrt{1-\lambda}$; then we choose the measurement basis of the ancilla photon as state $|H\rangle$. For $\mathcal{E}_2^{\mathrm{g}}$, we set $\sin\beta = mn\sqrt{\lambda}$ and $\sin\alpha = 0$; then we choose the measurement basis of the ancilla photon as state $|V\rangle$. The two generalized extreme channel $\mathcal{E}_1^{\mathrm{g}}$ and $\mathcal{E}_2^{\mathrm{g}}$ are combined with equal probability ($p = 0.5$). With this program, the channel $\mathcal{E}_{\mathrm{w}}$ can be simulated.

Superior protection against decoherence is achieved for stronger measurement strength p_{pre} and p_{post} [170]. In our simulation, we choose a sufficiently strong measurement strength $p_{\mathrm{pre}} = 0.8$ without causing much cost for the post-selection. As shown in Fig. 6.3, the dashed line represents the theoretical calculation of state-fidelity dynamics under AD channel with magnitude of decoherence λ, and the dots represent the experimentally collected data. We choose $|H\rangle$, $|V\rangle$, $|D\rangle = 1/\sqrt{2}(|H\rangle + |V\rangle)$ and $|L\rangle = 1/\sqrt{2}(|H\rangle + i|V\rangle)$ for the input states. The red dashed line depicts dynamics without weak measurement. Note that $|H\rangle$ input is immune to the AD channel.

If the parameter λ is unknown, the general (nonoptimal) strategy of choosing measurement strength p_{post} is to fix $p_{\mathrm{pre}} = p_{\mathrm{post}}$. But if we know the magnitude of the decoherence λ, we can perform the optimal weak measurement strategy $p_{\mathrm{post}} = p_{\mathrm{pre}} + \lambda(1 - p_{\mathrm{pre}})$ [170]. The

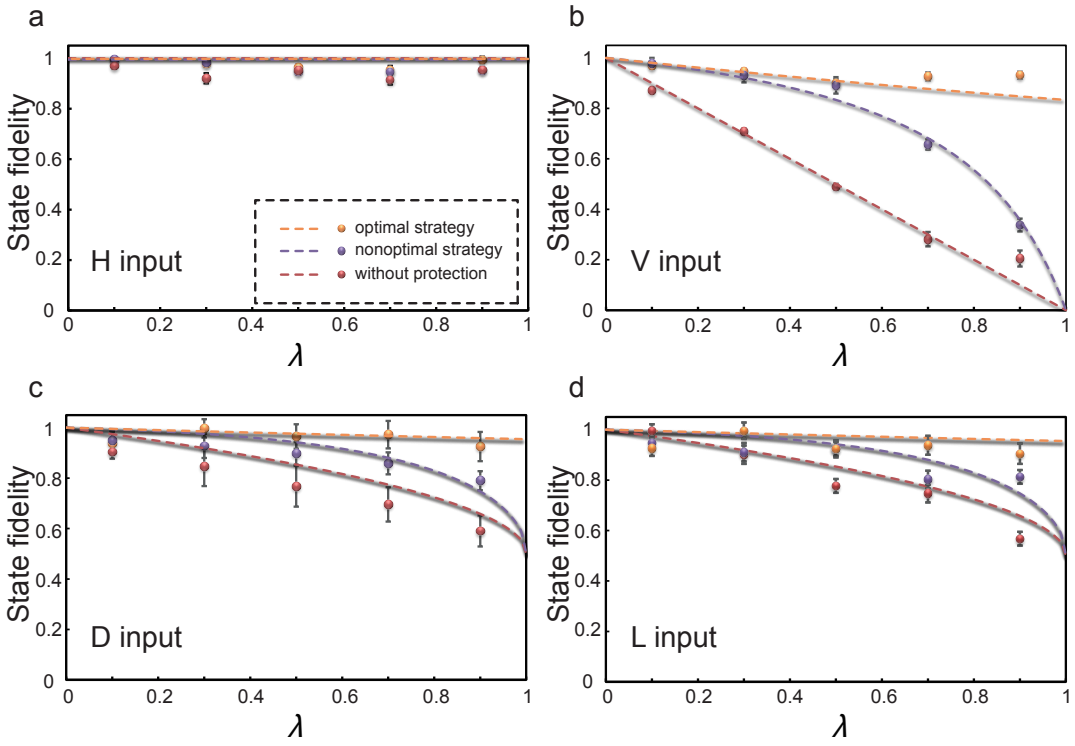

Figure 6.3: State fidelity under AD channel with weak measurement protection. The dashed line represents the theoretical calculation and the dot represent the experimental results. The red, blue and yellow represent no weak measurement, non-optimal measurement strategy and optimal measurement strategy, respectively. **a,** $|H\rangle$ state input. **b,** $|V\rangle$ state input. **c,** $|D\rangle$ state input. **d,** $|L\rangle$ state input.

blue dashed line is the nonoptimal cases whereas the yellow dashed line represent optimal cases. The experimental results agree well with the theoretical calculation for all three cases.

In fact, the strategy of this decoherence suppression scheme is to convert the AD channel to an identity operation $\mathbb{1}$. This can be illustrated from its process matrix

$$\mathcal{S}_{\mathrm{w}} = \begin{pmatrix} \alpha_+^2 & 0 & 0 & \alpha_+\alpha_- \\ 0 & \beta^2 & -i\beta^2 & 0 \\ 0 & i\beta^2 & \beta^2 & 0 \\ \alpha_+\alpha_- & 0 & 0 & \alpha_-^2 \end{pmatrix}, \tag{6.3}$$

for $\alpha_\pm = n \pm m\sqrt{1-\lambda}$, and $\beta = mn\sqrt{\lambda}$. The optimal strategy leads to $\alpha_- = 0$, and the

process fidelity between $\mathcal{E}_{\rm w}$ and $\mathbb{1}$ is $F_{\rm P} = 1/(1+\frac{\lambda}{2}m^2)$, which achieves the maximal value 1 when $m \to 0$ and then $\mathcal{E}_{\rm w} \to \mathbb{1}$. In our experiment, we achieve an average process fidelity 0.88 ± 0.02 for our choice of parameters.

6.4 Simulation of transpose and positive mappings

Here we demonstrate that our method can be employed for simulating not-CP, but positive mappings, which are valuable for many applications including entanglement witness [77]. Unfortunately, positive not-CP mappings cannot be directly implemented as they are unphysical, e.g., leading to a state operator with negative eigenvalues. A general method called structural physical approximation (SPA) of positive mappings can approximate a positive mapping by a CP mapping while retaining its ability to witness entanglement [79]. As a result, our simulation can open the door to study experimental realizations of desired positive mappings as an entanglement witness.

The SPA of transpose leads to an entanglement-breaking channel T

$$T_0 \mapsto T = (1-s)T_0 + sD, \tag{6.4}$$

for T_0 as the transpose operation, and a map $D(\rho) = \mathbb{1}/d \ \forall \rho$, and $s \geq d/d+1$. Here we implement the channel T for the qubit case ($d = 2$) using our simulator instead of using the measurement-plus-preparation method, which is the standard way to realize entanglement-breaking channels [78, 87, 106].

For the qubit case, the channel T is rank three and the corresponding Choi state is

$$\mathcal{C}_T = \frac{1}{6}\begin{pmatrix} 2 & 0 & 0 & 0 \\ 0 & 1 & 1 & 0 \\ 0 & 1 & 1 & 0 \\ 0 & 0 & 0 & 2 \end{pmatrix}. \tag{6.5}$$

The process matrix of transpose $\mathcal{S}_T$ is diagonal and can be rewritten in the Pauli basis as $\mathcal{S}_T = (\mathbb{1}\otimes\mathbb{1} + X\otimes X + Z\otimes Z)/3$. Due to the succinct formula of $\mathcal{S}_T$, we can easily find

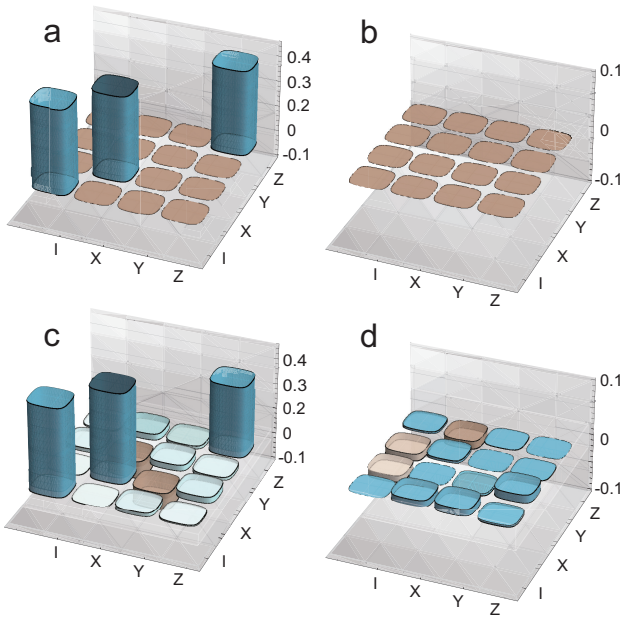

Figure 6.4: The reconstructed matrix of $\mathcal{S}_T$, with the real part of $\mathcal{S}_T$ (a) and $\mathcal{S}_T^{\rm exp}$ (c), and the imaginary part of $\mathcal{S}_T$ (b) and $\mathcal{S}_T^{\rm exp}$ (d).

the parameters for our simulator without performing a numerical simulation. For $\mathcal{E}_1^{\rm g}$, we set $\alpha = \beta = \pi/4$. For $\mathcal{E}_2^{\rm g}$, we set $\alpha = \pi$ and $\beta = 0$. The combination coefficient p is set by $2/3$ (e.g., $t_1 = 10$s and $t_2 = 20$s). With this parameter setting, we can construct the $\mathcal{S}_T$ channel. We first analyze $\mathcal{S}_T$ by QPT. As shown in Fig. 6.4, the process fidelity between the ideal $\mathcal{S}_T$ and simulated $\mathcal{S}_T^{\rm exp}$ is $F_{\rm P} = {\rm Tr}(\sqrt{\sqrt{\mathcal{S}_T}\mathcal{S}_T^{\rm exp}\sqrt{\mathcal{S}_T}})^2 = 0.95 \pm 0.02$.

To test how $\mathcal{S}_T$ works, we inject a state $|L\rangle$ as input and use quantum state tomography (QST) to reconstruct the output state. We find that the fidelity between the out put state and the ideal output state under operation $\mathcal{S}_T$ is 0.99 ± 0.01.

Furthermore, a general single-qubit positive mapping $\mathcal{P}$ can be approximately realized by combining the SPA of transpose and qubit channels, since single-qubit positive map is decomposable [178]

$$\mathcal{P} = r\mathcal{E}_1 + (1-r)\mathcal{E}_2 \circ T_0, \tag{6.6}$$

for $r \in [0, 1]$. It is straightforward to generalize our scheme to simulate positive mappings: a positive mapping $\mathcal{P}$ can be specified by r and two channels $\mathcal{E}_1$ and $\mathcal{E}_2$ in the formula (6.6),

and the transpose T_0 is substituted by its SPA approximation T. Then our method can be further employed for detection of entanglement.

6.5 Conclusion

We have shown that our single-qubit quantum channel simulation has been experimentally implemented to build a universal digital photonic single-qubit quantum channel simulator. Single-qubit nonunitary processes, including CPTP, CP but not-TP, and TP but not-CP mappings can be simulated by our simulator. The cost of our simulator, which is decided to be the number of single-qubit, two-qubit entangling and classical CNOT gates, is appreciably lower compared to the standard scheme based on dilation. This photonic qubit-channel simulator can be employed to serve as a nonunitary gate to simulate quantum noises, and to simulate dissipative quantum dynamics combined with two-qubit entangling gates.

Chapter 7

Qutrit and two-qubit quantum channel simulations

In this chapter we study the simulation of qutrit and two-qubit quantum channels, which is an expansion of the general result in Chapter 4 and the result in our paper [169]. We provide detailed studies for the quantum circuit representations and optimization simulation for both the qutrit (in §7.1) and two-qubit (in §7.2) quantum channels. In particular, a classification of generalized extreme qutrit channels is presented, and the classification of generalized extreme two-qubit channels is also addressed. We conclude in §7.3.

7.1 Qutrit quantum channel simulation

7.1.1 Extreme qutrit channels

From the general construction of generalized extreme qudit channel (4.31), we obtain the unitary operator for the quantum circuit of a qutrit generalized extreme channel $\mathcal{E}_{\rm qut}^{\rm g}$

$$U_{\rm qut} := CX_2CX_1M_{21}(f,e)M_{20}(d,c)M_{10}(b,a), \tag{7.1}$$

acting on two qutrits, one for the qutrit system and the other for a qutrit ancilla for rotation angles $a,b,c,d,e,f \in [0,2\pi]$. The circuit diagram is shown in Fig. 7.1. The permutation gates are

$$X_1 = (021) = \begin{pmatrix} 0 & 1 & 0 \\ 0 & 0 & 1 \\ 1 & 0 & 0 \end{pmatrix}, X_2 = (012) = \begin{pmatrix} 0 & 0 & 1 \\ 1 & 0 & 0 \\ 0 & 1 & 0 \end{pmatrix}, \tag{7.2}$$

where we also included their permutation representation. The gates X_1 in CX_1 can be decomposed as $X_{21}X_{10}$, and X_2 can be decomposed as $X_{21}X_{20}$, and then

$$CX_2CX_1 = CX_{21}CX_{20}CX_{21}CX_{10} \tag{7.3}$$

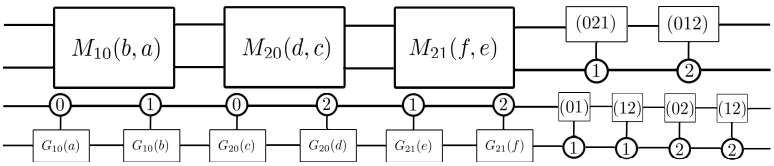

Figure 7.1: The generalized extreme qutrit channel circuit. (Up) Representation using multiplexers and controlled-permutation gates. (Bottom) Representation with controlled-Givens rotations and controlled-bit flip gates.

with the ancilla as control for all of the four CX_{jk} gates. Also there will be prior and posterior qutrit rotations acting on the system for a more general qutrit generalized extreme channel. In the following we will present the corresponding Kraus operators, Choi state, and the analysis of circuit component of U_{qut}.

The three multiplexers can be decomposed into six controlled-Givens rotations, which can be implemented by six CX_{jk} gates and nine Givens rotations obtained from basic technique of circuit design [9]. The prior and posterior qutrit rotations acting on the system can be realized by six Givens rotations since a qutrit rotation can be decomposed as a product of three Givens rotations each acting on a qubit subspace of the qutrit [166]. In all, there are ten CX_{jk} gates and 15 Givens rotations in the circuit for a qutrit generalized extreme channel. Furthermore, if classical feedback is available, the last four CX_{jk} gates can be replaced by classically controlled X_{jk} gates, as the case of qubit channel simulation [168].

If we are limited to quantum computers based on qubits, we have to simulate qudit channels by multi-qubit channels. Generally, one qudit extreme channel can be simulated by an $m = \lceil \log_2 d \rceil$-qubit extreme channel. For the qutrit extreme channel, we can use two qubits and employ the subspace $|00\rangle, |01\rangle, |10\rangle$ as the qutrit system. We also need two qubits for the ancilla. The Kraus operators and the circuit unitary operator can be extended from the qutrit case to the two-qubit case easily. It is clear to see that the probability for the ancilla to be at state $|11\rangle$ at the end of the circuit is zero, which means we do not need to consider post-selection effect.

From $F_i = \langle i|U_{\rm qut}|0\rangle$ $(i = 0, 1, 2)$ we obtain the three Kraus operators for the extreme channel $\mathcal{E}^{\rm g}_{\rm qut}$

$$F_0 = \begin{pmatrix} \cos a \cos c & 0 & 0 \\ 0 & \cos b & 0 \\ 0 & 0 & \cos d \end{pmatrix}, F_1 = \begin{pmatrix} 0 & \sin b \cos e & 0 \\ 0 & 0 & -\sin d \sin f \\ \sin a & 0 & 0 \end{pmatrix}, \tag{7.4a}$$

$$F_2 = \begin{pmatrix} 0 & 0 & \sin d \cos f \\ \cos a \sin c & 0 & 0 \\ 0 & \sin b \sin e & 0 \end{pmatrix}. \tag{7.4b}$$

The Choi state can also be obtained, which is shown in equation (A.1) in the Appendix A. In the following we prove that the circuit indeed realizes the three Kraus operators. The unitary operator for the extreme channel before tracing out the ancilla is shown in Eq. (A.7). The colors green, red, and yellow indicate the corresponding elements come from Kraus operators F_0, F_1, and F_2. Next we show the evolution of an arbitrary input state ρ. We need to show that $\langle i|U_{\rm qut}(\rho \otimes |0\rangle\langle 0|)U^\dagger_{\rm qut}|i\rangle = F_i \rho F_i^\dagger$, which means the projection $|i\rangle\langle i|$ on the ancilla is equivalent to the action of F_i on the system.

First we consider a pure state $|\psi\rangle = x|0\rangle + y|1\rangle + w|2\rangle$ with $|x|^2 + |y|^2 + |w|^2 = 1$. The final state of the whole system, i.e. system plus ancilla, takes the form in Eq. (A.8). In the computational basis of system and ancilla, the final state can be expressed as $\rho_{\rm SA} = \sum_{i_{\rm S}, i_{\rm A}} \sum_{j_{\rm S}, j_{\rm A}} \rho_{i_{\rm S}, i_{\rm A}, j_{\rm S}, j_{\rm A}} |i_{\rm S}, i_{\rm A}\rangle\langle j_{\rm S}, j_{\rm A}|$. The action of the projection $|i\rangle\langle i|$ on the state $\rho_{\rm SA}$ can be obtained.

The Kraus operator F_0 acts on system state resulting in

$$F_0 \rho F_0^\dagger = \begin{pmatrix} x^2 \cos^2 a \cos^2 c & xy \cos a \cos b \cos c & wx \cos a \cos c \cos d \\ xy \cos a \cos b \cos c & y^2 \cos^2 b & wy \cos b \cos d \\ wx \cos a \cos c \cos d & wy \cos b \cos d & w^2 \cos^2 d \end{pmatrix}, \tag{7.5}$$

which is the same with the projection $|0\rangle\langle 0|$ on the state $\rho_{\rm SA}$.

The Kraus operator F_1 acts on system state resulting in

$$F_1\rho F_1^\dagger = \begin{pmatrix} y^2\cos^2 e\sin^2 b & -wy\cos e\sin b\sin d\sin f & xy\cos e\sin a\sin b \\ -wy\cos e\sin b\sin d\sin f & w^2\sin^2 d\sin^2 f & -wx\sin a\sin d\sin f \\ xy\cos e\sin a\sin b & -wx\sin a\sin d\sin f & x^2\sin^2 a \end{pmatrix}, \tag{7.6}$$

which is the same with the projection $|1\rangle\langle 1|$ on the state $\rho_{\rm SA}$.

The Kraus operator F_2 acts on system state resulting in

$$F_2\rho F_2^\dagger = \begin{pmatrix} w^2\cos^2 f\sin^2 d & wx\cos a\cos f\sin c\sin d & wy\cos f\sin b\sin d\sin e \\ wx\cos a\cos f\sin c\sin d & x^2\cos^2 a\sin^2 c & xy\cos a\sin b\sin c\sin e \\ wy\cos f\sin b\sin d\sin e & xy\cos a\sin b\sin c\sin e & y^2\sin^2 b\sin^2 e \end{pmatrix}, \tag{7.7}$$

which is the same with the projection $|2\rangle\langle 2|$ on the state $\rho_{\rm SA}$. That is, we have proved the projection $|i\rangle\langle i|$ on the ancilla is equivalent to the action of F_i on the system.

7.1.2 Classification of extreme and quasi-extreme qutrit channels

Here we present a brief study for the classification of extreme and quasi-extreme channels.

(I) Rank-one extreme channels. This can only be the unitary operators, similar with the qubit case. It is straightforward to see that this occurs when any two of the three Kraus operators (7.4) are zero matrices.

(II) Rank-two extreme and quasi-extreme channels. This occurs when one Kraus operator is zero. There are three cases.

1. $F_1 = \mathbf{0}$ for $a, b, e, f = 0$;

$$F_0 = \begin{pmatrix} \cos c & 0 & 0 \\ 0 & 1 & 0 \\ 0 & 0 & \cos d \end{pmatrix}, F_2 = \begin{pmatrix} 0 & 0 & \sin d \\ \sin c & 0 & 0 \\ 0 & 0 & 0 \end{pmatrix}. \tag{7.8}$$

The set $\{F_1^\dagger F_1, F_1^\dagger F_2, F_2^\dagger F_1, F_2^\dagger F_2\}$ is linearly dependent when $\cos^2 c + \sin^2 d = 1$. For instance, this occurs when $c = d$, while this does not lead to unital channel by checking

$\mathcal{E}(\mathbb{1}) \neq \mathbb{1}$. This is different from the qubit case, for which all rank-two quasi-extreme qubit channels are unital channels, see Chapter 5.

2. $F_2 = \mathbf{0}$ for $c, d, e, f = 0$;

$$F_0 = \begin{pmatrix} \cos a & 0 & 0 \\ 0 & \cos b & 0 \\ 0 & 0 & 1 \end{pmatrix}, F_1 = \begin{pmatrix} 0 & \sin b & 0 \\ 0 & 0 & 0 \\ \sin a & 0 & 0 \end{pmatrix}, \tag{7.9}$$

The set $\{F_0^\dagger F_0, F_0^\dagger F_1, F_1^\dagger F_0, F_1^\dagger F_1\}$ is linearly dependent when $\cos^2 a + \sin^2 b = 1$. For instance, this occurs when $a = b$, while, similar to the former case, this does not lead to unital channel by checking $\mathcal{E}(\mathbb{1}) \neq \mathbb{1}$.

3. $F_0 = \mathbf{0}$, which occurs for two cases.

3(a) If $b, c, d = \pi/2$,

$$F_1 = \begin{pmatrix} 0 & \cos e & 0 \\ 0 & 0 & -\sin f \\ \sin a & 0 & 0 \end{pmatrix}, F_2 = \begin{pmatrix} 0 & 0 & \cos f \\ \cos a & 0 & 0 \\ 0 & \sin e & 0 \end{pmatrix}, \tag{7.10}$$

The set $\{F_1^\dagger F_1, F_2^\dagger F_2, F_1^\dagger F_2, F_2^\dagger F_1\}$ is linearly independent when $\tan^2 a \neq \tan^2 f \neq \tan^{-2} e$. Particularly, this case leads to rank-two unital qutrit channels, which occurs when $\cos^2 e + \cos^2 f = 1$, $\sin^2 f + \cos^2 a = 1$, and $\sin^2 a + \sin^2 e = 1$ hold at the same time. For instance, if $a = f = \pi/2 - e$, this leads to unital channel $\mathcal{E}(\mathbb{1}) = \mathbb{1}$.

3(b) If $a, b, d = \pi/2$,

$$F_1 = \begin{pmatrix} 0 & \cos e & 0 \\ 0 & 0 & -\sin f \\ 1 & 0 & 0 \end{pmatrix}, F_2 = \begin{pmatrix} 0 & 0 & \cos f \\ 0 & 0 & 0 \\ 0 & \sin e & 0 \end{pmatrix}, \tag{7.11}$$

The set $\{F_1^\dagger F_1, F_2^\dagger F_2, F_1^\dagger F_2, F_2^\dagger F_1\}$ is linearly dependent when $\cos^2 e + \sin^2 f = 1$. For instance, this occurs when $e = f$, while, similar to the former cases, this does not lead to unital channel by checking $\mathcal{E}(\mathbb{1}) \neq \mathbb{1}$.

Furthermore, one might expect that rank-two qutrit generalized extreme channels reproduce a qubit extreme channel on a two-dimensional subspace. However, this is not the case. The reason is that, from the quantum circuit, there is a sequence of controlled-bit flip gates that enables a rank-two qutrit generalized extreme channels act on the whole space of a qutrit, instead of a two-dimensional subspace.

(III) Rank-three quasi-extreme channels. This occurs for many cases. For instance, when all three elements for each Kraus operator are the same, each Kraus operator reduces to a unitary operator, and the channel is a rank-three mixed unitary channel. This corresponds to the edge of a polytope of the set of mixed unitary channels, which has been studied in Example 5. There are also rank-three nonunital quasi-extreme channels.

7.1.3 Simulation results

Next we discuss the simulation of arbitrary qutrit channel. The input qutrit channel $\mathcal{E}$ needs to be chosen randomly, and this is realized by randomly generating unitary operator in $SU(27)$ according to Haar measure, since a channel can be realized by unitary operator followed by a partial trace on the environment [123]. We employ the MATLAB® package developed in Ref. [157]. For instance, a unitary operator $U \in SU(27)$ is generated with command "runitary(3,3)". The set of Kraus operators for the input channel is obtained from the relation $K_i = \langle i|U|0\rangle$. For example, we generate a unitary operator (not shown here since it is 27×27), and obtain the Choi state for an input channel as shown in Eq. (A.14), which has eigenvalues 0.0018, 0.0244, 0.0662, 0.1366, 0.2499, 0.4415, 0.5808, 0.6519, 0.8469.

According to our decomposition method, we need to decompose the Choi state as

$$\mathcal{C} = \sum_{i=1}^{3} p_i \mathcal{C}_i^{\mathrm{g}}, \quad \sum_{i=1}^{3} p_i = 1, \quad 0 \le p_i \le 1, \tag{7.12}$$

and each $\mathcal{C}_i^{\mathrm{g}}$ corresponds to one generalized extreme channel. Each generalized extreme channel is specified by three Kraus operators, shown in Eq. (7.4), and three initial and final unitary operators, denoted as R_1, R_2, and $R_3 \in SU(3)$ acting on the system. We let there

Table 7.1: The simulation result for the decomposition of a randomly generated qutrit channel in Eq. (A.14). The table on the left contains the parameters for prior and posterior unitary operators, and the table on the right contains the parameters (a, b, c, d, e, f) for Kraus operators and the probability p, and also the three eigenvalues λ for each generalized extreme channels. [Table from Ref. [169], Table B1.]

	$\mathcal{C}_1^{\mathrm{g}}$			$\mathcal{C}_2^{\mathrm{g}}$			$\mathcal{C}_3^{\mathrm{g}}$		
	R_1	R_2	R_3	R_1	R_2	R_3	R_1	R_2	R_3
θ_1	1.2344	0.2292	0.9562	0.6197	0.3668	1.1377	0.3082	1.1345	0.3574
θ_2	1.2781	0.6352	0.1978	1.1258	0.4069	1.1456	0.6092	0.5117	1.1794
θ_3	0.6618	0.4768	0.5194	0.9545	0.0651	1.4608	1.4406	0.6749	0.3582
ϕ_1	1.1865	4.0185	2.6995	4.0777	1.8266	3.9186	4.9068	4.7498	2.1275
ϕ_2	4.1535	3.3050	5.1831	1.8561	4.9335	2.3296	5.4269	3.1036	2.5366
ϕ_3	1.6894	5.0089	2.1618	3.6516	2.8210	4.3385	2.6902	5.3635	5.1105
ϕ_4	0.8490	2.1711	3.9187	4.9058	2.1526	5.4539	2.8977	4.5586	3.3091
ϕ_5	4.7523	3.6288	1.2381	2.2728	3.1790	3.1468	0.6585	3.6124	2.2142

	$\mathcal{C}_1^{\mathrm{g}}$	$\mathcal{C}_2^{\mathrm{g}}$	$\mathcal{C}_3^{\mathrm{g}}$
a	2.1417	2.3442	2.0610
b	4.8284	1.8620	3.9621
c	2.3434	4.7272	1.6220
d	4.0164	2.2822	1.0321
e	2.7418	4.0726	2.5719
f	3.1900	4.8792	5.2118
λ_1	0.5667	0.5088	0.5457
λ_2	0.8868	1.0942	0.7287
λ_3	1.5465	1.3970	1.7256
p	0.2974	0.3676	0.3350

be two initial unitary operators R_3 followed by R_2, and one final unitary operator R_1. The unitary operator in $SU(3)$ which has eight real parameters [166] is parameterized as shown in Eq. (3.5).

The optimization is implemented such that the trace distance $D_t(\mathcal{C}, \mathcal{C}') \leq \epsilon/2$. Algorithms such as MultiStart, GlobalSearch or Simulated Annealing in MATLAB® are employed, and we choose a relatively good simulation result that has the smallest simulation error among many different runs of the simulation for the given input channel.

Next we present one simulation result, which contains 92 parameters with two for the probability p_1 and p_2, and 30 for each generalized extreme channel: six in the Kraus operators and 24 in the initial and final unitary operators. The result is summarized in Table 7.1. The approximate Choi state $\mathcal{C}'$ is shown in Eq. (A.15), with eigenvalues 0.0039, 0.0280, 0.0797, 0.1264, 0.2473, 0.4395, 0.5825, 0.6515, and 0.8413. The actual error from the simulation is 0.046. This means the probability to distinguish the true channel from the approximate

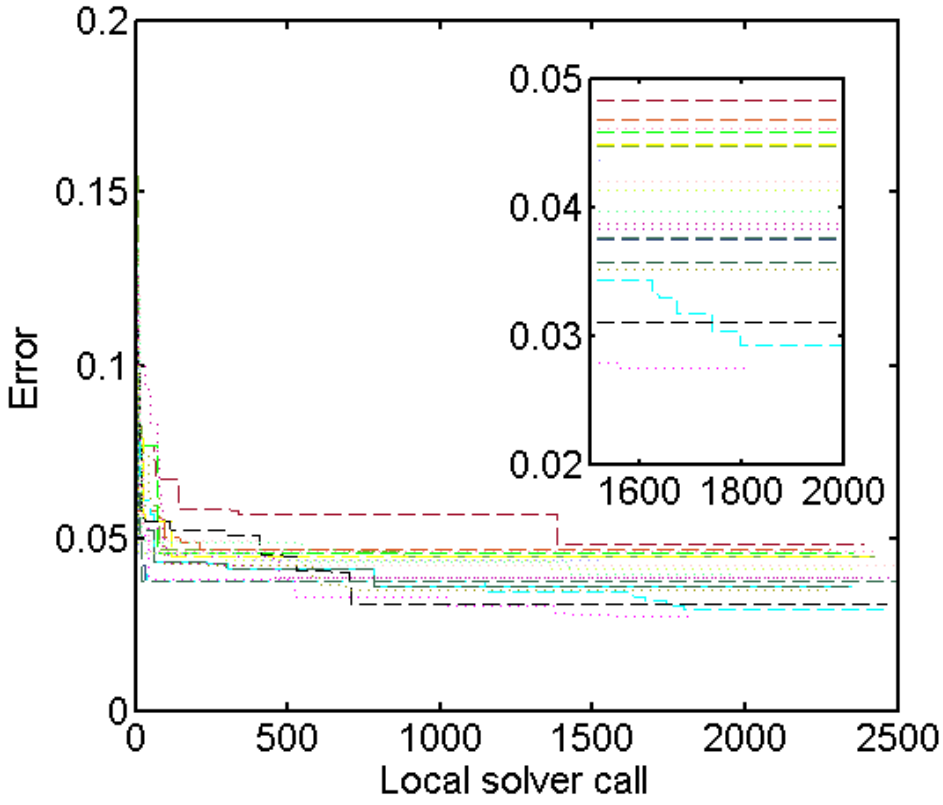

Figure 7.2: Simulation results for 20 randomly chosen qutrit channels. The number of calls to local solvers in GlobalSearch algorithm corresponds to the simulation runtime, and the simulation error is the trace distance between the input qutrit Choi state and the approximate Choi state. The inset magnifies part of the figure to show the convergence more clearly.

one is $\frac{1}{2}(1 + 0.046)$. As $0.046 \ll 1$, this indicates that the channel decomposition is good enough for accurate simulation. We have performed simulations for about 50 randomly chosen channels, and the errors are all in the order 0.01. In addition, we have checked the block-matrix structure in Eq. (4.41) to verify our simulations. More details are shown in Appendix A.

Furthermore, the simulation results of 20 randomly chosen qutrit channels are shown in Fig. 7.2. The convergence takes much longer time (several hours) than the qubit case. Our simulations yield on average the simulation error on the order 10^{-2}, which is good enough

for accurate quantum simulation. If $\epsilon \approx 0.01$, it means there is a probability $\frac{1}{2}(1+0.01)$ to distinguish the true channel from the simulator by distinguishing their output states.

7.2 Two-qubit quantum channel simulation

7.2.1 Extreme two-qubit channels

For a two-qubit extreme channel, the system and ancilla both contain two qubits, and we denote the basis as $|00\rangle \sim |0\rangle$, $|01\rangle \sim |1\rangle$, $|10\rangle \sim |2\rangle$, and $|11\rangle \sim |3\rangle$. The operator executed by the circuit takes the form

$$\begin{aligned} U_{\text{twoqub}} :=& CX_3CX_2CX_1M_{32}(n,m)M_{31}(q,p)M_{30}(h,g) \\ & M_{21}(f,e)M_{20}(d,c)M_{10}(b,a), \end{aligned} \tag{7.13}$$

for rotation angles $a, b, c, d, e, f, g, h, p, q, m, n \in [0, 2\pi]$. The permutation gates X_1, X_2 and X_3 are

$$X_1 = \begin{pmatrix} 0 & 1 & 0 & 0 \\ 0 & 0 & 1 & 0 \\ 0 & 0 & 0 & 1 \\ 1 & 0 & 0 & 0 \end{pmatrix}, X_2 = \begin{pmatrix} 0 & 0 & 1 & 0 \\ 0 & 0 & 0 & 1 \\ 1 & 0 & 0 & 0 \\ 0 & 1 & 0 & 0 \end{pmatrix}, X_3 = \begin{pmatrix} 0 & 0 & 0 & 1 \\ 1 & 0 & 0 & 0 \\ 0 & 1 & 0 & 0 \\ 0 & 0 & 1 & 0 \end{pmatrix}. \tag{7.14}$$

Using notation for permutation (4.26), $X_1 = (3210)$, $X_2 = (0231)$, and $X_3 = (0123)$. The permutation gates can be realized by six controlled-bit flip gates. The six multiplexers can be implemented with 12 controlled-bit flip gates CX_{jk} and 18 Givens rotations. The unitary operator is shown in Eq. (B.1) in Appendix B. The colors green, red, yellow, and blue indicate the corresponding elements come from Kraus operators F_0,F_1,F_2, and F_3, respectively. A schematic diagram for the quantum circuit is shown in Fig. 7.3.

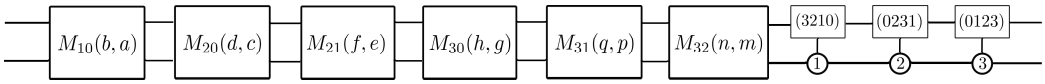

Figure 7.3: The generalized extreme two-qubit channel circuit, which contains six multiplexers and three controlled-permutation gates.

The four Kraus operators are

$$F_0 = \begin{pmatrix} \cos a \cos c \cos g & 0 & 0 & 0 \\ 0 & \cos b & 0 & 0 \\ 0 & 0 & \cos d & 0 \\ 0 & 0 & 0 & \cos h \end{pmatrix}, \tag{7.15a}$$

$$F_1 = \begin{pmatrix} 0 & \sin b \cos e \cos p & 0 & 0 \\ 0 & 0 & -\sin d \sin f & 0 \\ 0 & 0 & 0 & -\sin h \sin q \\ \sin a & 0 & 0 & 0 \end{pmatrix}, \tag{7.15b}$$

$$F_2 = \begin{pmatrix} 0 & 0 & \sin d \cos f \cos m & 0 \\ 0 & 0 & 0 & -\sin h \cos q \sin n \\ \cos a \sin c & 0 & 0 & 0 \\ 0 & \sin b \sin e & 0 & 0 \end{pmatrix}, \tag{7.15c}$$

$$F_3 = \begin{pmatrix} 0 & 0 & 0 & \sin h \cos q \cos n \\ \cos a \cos c \sin g & 0 & 0 & 0 \\ 0 & \sin b \cos e \sin p & 0 & 0 \\ 0 & 0 & \sin d \cos f \sin m & 0 \end{pmatrix}. \tag{7.15d}$$

7.2.2 Classification of extreme and quasi-extreme two-qubit channels

The classification of extreme and quasi-extreme two-qubit channels can in principle be done according to different ranks. For instance, rank-one extreme channels can only be unitary

operators, similar with the qubit and qutrit cases. However, for higher-rank extreme channels, compared with the qutrit case, the analysis for two-qubit case is extremely tedious. As a result, we would not perform this detailed classification here.

However, we observe that, when expressed in Pauli basis, as shown in Eq. (B.2), a rank-two generalized extreme two-qubit channel can be used to simulate a generalized extreme qubit channel. For instance, when F_1 and F_2 are zero matrices, which can occur for $a = c = e = d = h = 0$, $p = \pi/2$, the rest of the four Kraus operators are

$$F_0 = \begin{pmatrix} \cos g & 0 & 0 & 0 \\ 0 & \cos b & 0 & 0 \\ 0 & 0 & 1 & 0 \\ 0 & 0 & 0 & 1 \end{pmatrix}, F_3 = \begin{pmatrix} 0 & \sin b & 0 & 0 \\ \sin g & 0 & 0 & 0 \\ 0 & 0 & 0 & 0 \\ 0 & 0 & 0 & 0 \end{pmatrix}. \tag{7.16}$$

The two Kraus operators F_0 and F_3 act as a generalized extreme qubit channel on the subspace spanned by $|0\rangle$ and $|1\rangle$. Furthermore, one might expect that rank-three generalized extreme two-qubit channel can be used to simulate generalized extreme qutrit channel. However, this is not the case. The reason is due to the sequence of controlled-permutation gates in the circuit. This is similar with the fact that, rank-two generalized extreme qutrit channel cannot be used to simulate generalized extreme qubit channel, as shown in §7.1.

7.2.3 Simulation results

Next we discuss the simulation of arbitrary two-qubit channel. The input two-qubit channel $\mathcal{E}$ is obtained from random unitary operator in $SU(64)$ according to Haar measure, and the set of Kraus operators for the input channel is obtained from the relation $K_i = \langle i|U|0\rangle$.

According to our decomposition method, we need to decompose the Choi state as

$$\mathcal{C} = \sum_{i=1}^{4} p_i \mathcal{C}_i^{\mathrm{g}}, \quad \sum_{i=1}^{4} p_i = 1, \quad 0 \leq p_i \leq 1, \tag{7.17}$$

and each $\mathcal{C}_i^{\mathrm{g}}$ corresponds to one generalized extreme two-qubit channel. Each generalized extreme channel is specified by four Kraus operators, shown in Eq. (7.15), and four initial and

final unitary operators acting on the system. We let there be two initial unitary operators and two final unitary operator. A unitary operator in $SU(4)$ has 15 real parameters. The optimization is implemented such that the trace distance $D_t(\mathcal{C}, \mathcal{C}') \leq \epsilon/2$. From our simulations for the qubit and qutrit cases, we find the GlobalSearch algorithm performs better than others such as MultiStart or Simulated Annealing, so we rely on the GlobalSearch algorithm in MATLAB®. The optimization is over 291 parameters, and it takes much longer time to converge. The computation time is on the order of days, and we find that it takes about one week to obtain simulation errors around 0.1, which are on the order 10^{-1}. In addition, we also expect at least a quadratic increase of the optimization convergence time due to the inner procedure of GlobalSearch. That is to say, the optimization would not be practical for even larger dimensional channels.

7.3 Conclusion

In this chapter we have presented our simulation algorithm for the qutrit and two-qubit channels. We have provided a detailed classification of qutrit extreme and quasi-extreme channels, while the classification for two-qubit case can also be carried out, in principle.

Our simulation for the qutrit case can be performed numerically with reasonable computational resources, since the optimization is still tractable on a standard classical computer. While we face a problem for the simulation of the two-qubit case, which takes about ten times computational time of the qutrit case. It soon becomes intractable for higher-dimensional cases, which is expected to be the case since optimization problem can be as hard as the hardest problem in the computational complexity class NP [73]. However, more advanced algorithms other than those we employed in MATLAB® are expected to benefit for a better convergence.

Chapter 8

Concepts of quantum simulation

In this chapter, more general quantum simulation problems are analyzed based on my publication [167]. Different types of quantum simulations and quantum simulation problems are defined according to different operator topologies on a Hilbert space; namely, uniform, strong, and weak quantum simulations. Our study of quantum channel simulation in former chapters is a strong simulation, so here the focus is on uniform and weak quantum simulations, which have not been widely explored in the literature. Exploring different quantum simulation problems is important for the understanding of quantum simulation and the design of various simulation algorithms.

The chapter is presented as follows. Firstly, the definitions of these three quantum simulations are provided in §8.1, and examples of simulation problems are also discussed. Afterwards in §8.2 a weak quantum simulation problem is proposed and a quantum algorithm that solves this problem follows. In the end the simulation of a general quantum channel is studied in the query model using uniform quantum simulation method in §8.3. The conclusion is presented in §8.4.

8.1 Quantum simulation frameworks

Quantum physical quantities are represented by operators, e.g., quantum states are positive semidefinite trace-class operators, quantum evolution are unitary operators or nonunitary CP mappings, and observable effects are represented by hermitian operators or POVM. Given a quantum operator, the task of simulation is to find one mathematical or physical approximation of it or its properties within some distance quantified by a properly chosen metric. Also it is required that the distance could be reduced if the approximate operator

could converge to the given operator. That is, in principle the simulator can approach to the target arbitrarily close provided infinite amount of resources, such as time and space. Mathematically, the problem of simulation can be characterized with notions from topology of bounded linear operators on a Hilbert space [18]. There exist different kinds of convergence in different topologies of the set of bounded linear operators on Hilbert space. Most commonly, there are uniform (or called norm), strong operator, and weak operator topologies, defined as follows.

Definition 11 (Uniform topology)**.** *For a finite-dimensional Hilbert space $\mathscr{H}$, the uniform topology on $\mathscr{L}(\mathscr{H})$ is the norm convergence, i.e. $\tilde{T}_i \to T$ in norm if $\lim_{i\to\infty} \|\tilde{T}_i - T\| = 0$, for $T, \tilde{T}_i \in \mathscr{L}(\mathscr{H})$.*

Definition 12 (Strong operator topology)**.** *For a finite-dimensional Hilbert space $\mathscr{H}$, the strong operator topology on $\mathscr{L}(\mathscr{H})$ is the pointwise norm convergence, i.e. $\tilde{T}_i \to T$ strongly if $\lim_{i\to\infty} \|(\tilde{T}_i - T)|\psi\rangle\| = 0$, for $T, \tilde{T}_i \in \mathscr{L}(\mathscr{H})$, and $\forall\ |\psi\rangle \in \mathscr{H}$.*

Definition 13 (Weak operator topology)**.** *For a finite-dimensional Hilbert space $\mathscr{H}$, the weak operator topology on $\mathscr{L}(\mathscr{H})$ is the pointwise weak convergence, i.e. $\tilde{T}_i \to T$ weakly if $\lim_{i\to\infty} |\langle\psi|\tilde{T}_i - T|\phi\rangle| = 0$, for $T, \tilde{T}_i \in \mathscr{L}(\mathscr{H})$, and $\forall\ |\psi\rangle, |\phi\rangle \in \mathscr{H}$.*

With these notions of topologies, we can now define three kinds of quantum simulations. Then we are able to formalize quantum simulation or computation problems in this framework, and we also discuss examples for these three kinds quantum simulations.

Definition 14 (Weak quantum simulation)**.** *Given any quantum operator $T \in \mathscr{L}(\mathscr{H})$ for a finite-dimensional Hilbert space $\mathscr{H}$, the weak quantum simulation is to approximate T by $\tilde{T}$ within distance $\epsilon > 0$ such that $|\langle\psi|\tilde{T} - T|\psi\rangle| \leq \epsilon$, $\forall\ |\psi\rangle \in \mathscr{H}$.*

Note that this definition slightly deviates from the weak operator topology in that expectation value of operator is involved, which is related to measurement of observable, instead of the value evaluated with two different states $|\psi\rangle$ and $|\phi\rangle$. Although "weak value" (the notion

"weak" is in a different sense) could exist when post-selection is considered [4], here we limit ourself to the standard context of quantum computing and standard quantum mechanics.

Definition 15 (Strong quantum simulation)**.** *Given any quantum operator $T \in \mathscr{L}(\mathscr{H})$ for a finite-dimensional Hilbert space $\mathscr{H}$, the strong quantum simulation is to approximate the action of T on state $|\psi\rangle \in \mathscr{H}$ by $\tilde{T}$ within vector 2-norm distance $\epsilon > 0$ for the worst case such that $\|T - \tilde{T}\| := \sup_{|\psi\rangle} \|(T - \tilde{T})|\psi\rangle\| \leq \epsilon$.*

Note that although the same symbol T is used in the definitions for both weak and strong quantum simulations, these two simulations naturally apply for different operators. The weak quantum simulation is more suitable for the simulation of observable effects for a particular measurement, while the strong quantum simulation is more suitable for the simulation of dynamics.

Example 16 (Strong quantum simulation of unitary operator)**.** *The problem of strong quantum simulation of one unitary operator U, e.g. $U = e^{-i\hat{H}t}$ if it is generated by a time-independent Hamiltonian $\hat{H}$, is to approximate it by another unitary $\tilde{U}$ satisfying the spectral norm distance condition $\|U - \tilde{U}\| \leq \epsilon$. The approximation can be achieved by, e.g., either constructing an approximate Hamiltonian $\tilde{\hat{H}}$ using easy-to-implement interactions or a direct approximation $\tilde{U}$ using elementary quantum gates.*

Example 17 (Quantum state generation)**.** *The problem of quantum state generation is to generate a state $|\psi\rangle$ within distance ϵ so that $\||\psi\rangle - |\tilde{\psi}\rangle\| \leq \epsilon$. Now suppose $|\psi\rangle = U|0\rangle$, and $|\tilde{\psi}\rangle = \tilde{U}|0\rangle$ for some unitary operators U and $\tilde{U}$, and then the accuracy condition becomes $\|U|0\rangle - \tilde{U}|0\rangle\| \leq \epsilon$, which can be ensured if we can simulate U by $\tilde{U}$ strongly; i.e. $\|U - \tilde{U}\| \leq \epsilon$.*

Definition 18 (Uniform quantum simulation)**.** *Given any quantum operator $T \in \mathscr{L}(\mathscr{H})$ for a finite-dimensional Hilbert space $\mathscr{H}$, the uniform quantum simulation is to approximate T by $\tilde{T}$ within distance $\epsilon > 0$ quantified by a certain operator norm.*

Example 19 (Uniform quantum simulation of unitary operator)**.** *For unitary operator U, the uniform quantum simulation is to approximate it without referring to its effects on states or observable. As $\| \bullet \| \leq \| \bullet \|_F \leq \| \bullet \|_1$ (see Chapter 2), the norm to be employed can be trace norm $\| \bullet \|_1$ or Frobenius norm $\| \bullet \|_F$. The uniform quantum simulation of U is to approximate it by $\tilde{U}$ such that $\|U - \tilde{U}\|_{F(1)} \leq \epsilon$. It is obvious to see that the uniform simulation is stronger than strong simulation of one unitary operator.*

The different quantum simulations have natural physical interpretations. The scenario for uniform quantum simulation is that, given an unknown process, one would like to simulate or approximate the process itself after knowing enough information of the process. One closely-related, yet not the same, task is the quantum process tomography [123], for which one needs to construct the process matrix of the process itself. For strong quantum simulation, one has to make sure that the output state from a simulator should be close enough to the ideal output state for any input state. This only requires the simulator has the similar effects on all input states. The requirement of weak quantum simulation is merely to ensure that the simulation provides similar observable effects for a given quantum state and observable, without referring to quantum process tomography or state tomography.

The definitions above can be generalized to the case of simulation of linear mappings. We focus on quantum channels $\mathcal{E} \in \mathscr{L}(\mathscr{D})$. For weak quantum simulation with respect to channels, since there is no so-called "super-observable" living in $\mathscr{L}(\mathscr{D})$, we need to consider observable living in $\mathscr{L}(\mathscr{H})$ instead.

Definition 20 (Weak quantum simulation II)**.** *Given any quantum operator $T \in \mathscr{L}(\mathscr{H})$, the weak quantum simulation is to approximate T by $\tilde{T}$ within distance $\epsilon > 0$ such that $\mathrm{tr}((T - \tilde{T})\rho) \leq \epsilon$, $\forall\ \rho \in \mathscr{D}$.*

Example 21 (Weak quantum simulation of observable)**.** *Let the operator be one quantum observable A. The simulation accuracy condition is $\sup_\rho |\mathrm{tr}(A\rho) - \mathrm{tr}(\tilde{A}\rho)| \leq \epsilon$. In detail, $\mathrm{tr}(A\rho) - \mathrm{tr}(\tilde{A}\rho) = \mathrm{tr}(A_t\rho_0) - \mathrm{tr}(\tilde{A}_t\rho_0)$ in Heisenberg picture, A_t is the evolved observable $\mathcal{E}(A)$*

for a certain channel $\mathcal{E}$, and ρ_0 is the initial state; while in Schrödinger picture, $\mathrm{tr}(A\rho) - \mathrm{tr}(\tilde{A}\rho) = \mathrm{tr}(A\rho_t) - \mathrm{tr}(A\tilde{\rho}_t)$*, the final state is $\rho_t = \mathcal{E}(\rho)$. The weak quantum simulation can be guaranteed by strong quantum simulation or quantum mixed-state generation, since $\|\rho - \tilde{\rho}\|_1 \leq \epsilon$ implies $|\mathrm{tr}(A\rho) - \mathrm{tr}(A\tilde{\rho})| \leq \epsilon\|A\|$, following from properties of trace norm.*

Definition 22 (Strong quantum simulation II)**.** *Given any quantum operator $\mathcal{E} \in \mathscr{L}(\mathscr{D})$, the strong quantum simulation is to approximate the action of $\mathcal{E}$ on $\rho \in \mathscr{D}$ by $\tilde{\mathcal{E}}$ within trace distance $\epsilon > 0$, such that the diamond norm distance [92] satisfies $\|\mathcal{E} - \tilde{\mathcal{E}}\|_\diamond \leq \epsilon$.*

Example 23 (Strong quantum simulation of channels)**.** *For quantum channel simulation, the strong simulation is to simulate the evolution $\mathcal{E}$, e.g. $\mathcal{E} = e^{\mathcal{L}t}$ if it is generated by a time-independent Liouvillian $\mathcal{L}$, by another operator $\tilde{\mathcal{E}}$ satisfying $\|\mathcal{E} - \tilde{\mathcal{E}}\|_\diamond \leq \epsilon$, or the induced Schatten 1-norm distance (when no correlation of the system to others is allowed) $\|\mathcal{E} - \tilde{\mathcal{E}}\|_{1\to 1} := \sup_\rho \|(\mathcal{E} - \tilde{\mathcal{E}})\rho\|_1 \leq \epsilon$.*

Example 24 (Quantum mixed-state generation)**.** *The problem is to generate a state ρ within distance ϵ, so that $\|\rho - \tilde{\rho}\|_1 \leq \epsilon$. Now suppose $\rho = \mathcal{E}(\rho_0)$, and $\tilde{\rho} = \tilde{\mathcal{E}}(\rho_0)$. The simulation can be ensured if we can simulate $\mathcal{E}$ by $\tilde{\mathcal{E}}$ strongly; i.e. $\|\mathcal{E} - \tilde{\mathcal{E}}\|_\diamond \leq \epsilon$.*

Definition 25 (Uniform quantum simulation II)**.** *Given any quantum operator $\mathcal{E} \in \mathscr{L}(\mathscr{D})$, the uniform quantum simulation is to approximate $\mathcal{E}$ by $\tilde{\mathcal{E}}$ within distance $\epsilon > 0$ quantified by a certain operator norm.*

Example 26 (Uniform quantum simulation of channels)**.** *As we have seen from the channel-state duality, a channel can be represented by a single matrix. As the result, we need to consider uniform simulation in Choi state representation. The norm we employ is the trace norm on Choi state. Then, the norm simulation of a quantum channel represented by Choi state $\mathcal{C}$ is to approximate $\mathcal{C}$ by $\tilde{\mathcal{C}}$ such that $\|\mathcal{C} - \tilde{\mathcal{C}}\|_1 \leq \epsilon$. Since $N\|\mathcal{C} - \tilde{\mathcal{C}}\|_1 \geq \|\mathcal{E} - \tilde{\mathcal{E}}\|_\diamond \geq \|\mathcal{E} - \tilde{\mathcal{E}}\|_{1\to 1}$, for N the system dimension, the uniform simulation is stronger than strong simulation of channels.*

In the above we have defined three types of quantum simulations, and it is evident that there exists an "order" in their simulation abilities. Although there could be different quantum simulations and simulation algorithms, their simulation abilities are constrained by the computational ability of quantum computing. This can be understood from the viewpoint of quantum state generation as follows. For uniform quantum simulation, based on channel-state duality, the efficient state generation of a Choi state ensures the efficiency of uniform quantum simulation. Weak quantum simulation also requires quantum state generation for a certain state, which serves to yield measurement results. Also strong quantum simulation requires quantum state generation. As quantum state generation is constrained by the computational ability of quantum computers, the three quantum simulations we propose are also constrained by the computational ability of quantum computing.

8.2 Weak quantum simulation

In this section, we define weak quantum simulation problem and provide a concise algorithm for solving it, which contains a classical preprocessing part and a quantum circuit to realize the algorithm. It turns out the circuit complexity is in general the same with that for a strong simulation algorithm. We focus on the general case instead of efficient simulation for special cases.

Definition 27 (Weak quantum simulation problem)**.** *For one N-dimensional quantum system prepared in state ρ, and measured by POVM $\mathcal{M} = \{M_i; i = 1, 2, \ldots, m \leq N^2\}$ for an observable $\hat{O}$ after an evolution $\mathcal{E}$, which is a quantum channel, construct an efficient quantum circuit, implemented using universal set of gates, which can approximate the expectation value $\langle \hat{O} \rangle$ on final state within the error tolerance ϵ for all instances ρ.*

Before our analysis, it is better to note the differences from strong simulation. If strong quantum simulation were considered, one needs to simulate the evolution $\mathcal{E}$ itself, whereas for weak quantum simulation one does not necessarily have to do this. Also the POVM $\mathcal{M}$ is

not required to be simulated; instead, one only needs to approximate the expectation value $\langle\hat{O}\rangle$ for all instances.

Furthermore, for weak quantum simulation there could also be different algorithms. The problem merely requires the approximation of $\langle\hat{O}\rangle$ without specifying how to approximate it. A notable example is the simulation method based on matrix product state [163, 10], which employs an open-system dynamics to approximate the dynamical observable of a many-body system based on a duality mapping. One can use a quantum circuit to realize the open-system dynamics, and then the simulation of the many-body system is in fact a weak quantum simulation, and the analysis of duality relation is the classical part of this simulation method. In the following we present an algorithm which contains a classical analysis of the output probability distribution and a quantum circuit for the weak simulation.

With the POVM $\{M_i\}$, an observable $\hat{O}$ can be expressed as $\hat{O} = \sum_{i=1}^{m} o_i M_i$ for $p_i = \mathrm{tr}(\rho_f M_i)$ and $\langle\hat{O}\rangle = \mathrm{tr}(\rho_f \hat{O}) = \sum_{i=1}^{m} o_i p_i$, with final state $\rho_f = \mathcal{E}(\rho)$. Given the set $\{M_i\}$ and $\hat{O}$, we can obtain o_i explicitly. Then the problem to approximate $\langle\hat{O}\rangle$ can be reduced to the approximation of the probability distribution $\{p_i\}$.

The next step in our method is to construct a quantum circuit, which can map any state ρ onto a well-defined state σ, projective measurement on which yields the (approximate) probability distribution $\{p_i\}$. Without loss of generality, we assume $m = N^2$ and denote $N \equiv d$; i.e., the system is a qudit. One easily finds that the state σ can be chosen as

$$\sigma = \mathrm{diag}(p_0, p_1, \cdots, p_{d^2-1}). \tag{8.1}$$

We employ the *replacement channel* $\mathcal{R}$ to map any state ρ onto σ

$$\mathcal{R}(\rho) = \sigma = \sum_{i,j} K_{ij} \rho K_{ij}^{\dagger}, \tag{8.2}$$

with Kraus operators

$$K_{ij} = \sqrt{p_i}|i\rangle\langle j|, \tag{8.3}$$

for $0 \le i \le d^2 - 1$, $0 \le j \le d - 1$.

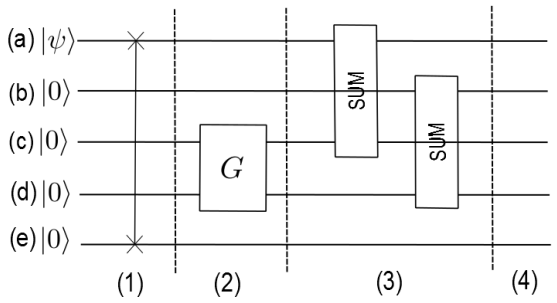

Figure 8.1: The circuit for the replacement channel $\mathcal{R}$. The gate on the most left with two crosses represents qudit swap gate SWAP. The two SUM gates, as defined in Eq. (3.10), contain (c) and (d) as the controller, (a) and (b) as the target, respectively. The bottom three ancillas are traced out finally. The labels $(1-4)$ are for the steps in the circuit.

Note that state σ has higher dimension than the input state ρ, which implies that a qudit ancilla is required. Also there are d^3 Kraus operators, so another three qudit ancillas are required for the implementation of this channel. The index i in K_{ij} can be split into two indices, i_1 and i_2 with $0 \leq i_1, i_2 \leq d-1$, and $p_i \equiv p_{i_1 i_2}$.

The quantum circuit to implement the channel $\mathcal{R}$ is shown in Fig. 8.1. We use the d-ary representation in the circuit diagram, so each wire represents a qudit. There are five registers (from top to bottom): (a) the system, (b) the ancilla which is a part of the output system, and (c,d,e) the bottom three ancillas to implement the projections.

The qudit swap gate SWAP [48] is defined as

$$\text{SWAP} : |i\rangle|j\rangle \mapsto |j\rangle|i\rangle, \ i, j \in \mathbb{Z}_d. \tag{8.4}$$

The gate G is defined as

$$G|0\rangle|0\rangle = \sum_i \sqrt{p_i}|i\rangle = \sum_{i_1,i_2} \sqrt{p_{i_1 i_2}}|i_1\rangle|i_2\rangle, \tag{8.5}$$

and can be realized by an $O(d^2)$ sequence of rotations $\{G_{i,i+1}\}$ which only act on two basis states

$$G = \prod_{i=d^2-1}^{0} G_{i,i+1}, \quad G_{i,i+1}|i\rangle = \cos\theta_i|i\rangle + \sin\theta_i|i+1\rangle, \tag{8.6}$$

containing d^2 parameters $0 \leq \theta_i \leq 2\pi$, which can be obtained from p_i based on the following concise relations

$$p_i = \sum_{S_i \subseteq S} \prod_{n \in S_i} \sin\theta_n \prod_{m \notin S_i} \cos\theta_m \tag{8.7}$$

with S denote the set $\{0, 1, \ldots, d^2 - 1\}$, S_i denote the set $\{\alpha_1, \ldots, \alpha_i\}$ and $\alpha_1 \neq \alpha_2 \neq \cdots \neq \alpha_i \in S$.

Next we show the action of the quantum circuit. For input state $|\psi\rangle|0\rangle|0\rangle|0\rangle|0\rangle$ with system state $|\psi\rangle = \sum_{j=0}^{d-1} c_j|j\rangle$, the quantum circuit proceeds as:

(1) The gate SWAP leads to $|0\rangle|0\rangle|0\rangle|0\rangle|\psi\rangle$;

(2) The gate G leads to $|0\rangle|0\rangle(\sum_{i_1,i_2} \sqrt{p_{i_1 i_2}}|i_1\rangle|i_2\rangle)|\psi\rangle$;

(3) The two SUM gates yields state $(\sum_{i_1,i_2} \sqrt{p_{i_1 i_2}}|i_1\rangle|i_2\rangle|i_1\rangle|i_2\rangle)|\psi\rangle$;

(4) The projector $P_{ij} = |i_1, i_2, j\rangle\langle i_1, i_2, j|$ on the bottom three ancillas leads to state $\sqrt{p_{i_1 i_2}} c_j|i_1\rangle|i_2\rangle$ which is equivalent to the action $K_{ij}|\psi\rangle$.

We see that the projective measurement

$$\mathcal{P} = \{P_{ij}; P_{ij} = |i, j\rangle\langle i, j|, 0 \leq i \leq d^2 - 1, 0 \leq j \leq d - 1\} \tag{8.8}$$

realizes the Kraus operators $\{K_{ij}\}$ and leads to the probability distribution $\{p_i c_j^2\}$. The distribution $\{p_i\}$ is obtained by combining $p_i c_j^2$ for all js since $\sum_j p_i c_j^2 = p_i$.

In order to ensure the simulation accuracy, a weak quantum simulation accuracy condition is defined as

$$\sup_{\rho} |\langle \hat{O} \rangle - \langle \tilde{\hat{O}} \rangle| \leq \epsilon. \tag{8.9}$$

In order to satisfy this, we require

$$\|\mathcal{R} - \tilde{\mathcal{R}}\|_{\diamond} \leq \epsilon \|\hat{O}\|/2, \tag{8.10}$$

which implies

$$\sup_{\rho} D_t(\sigma, \tilde{\sigma}) \leq \epsilon \|\hat{O}\|/2, \tag{8.11}$$

and then the weak simulation accuracy condition in Eq. (8.9) is satisfied. The condition (8.10) can be ensured if the whole circuit unitary operator U can be approximated by $\tilde{U}$ such that $\|U-\tilde{U}\| \leq \epsilon\|\hat{O}\|/4$, since $\|\mathcal{R}-\tilde{\mathcal{R}}\|_\diamond \leq 2\|U-\tilde{U}\|$ according to Theorem 5.

Next we analyze the complexity of the circuit. The $O(d^2)$ sequence of gates $G_{i,i+1}$ can be realized by sequence of Givens rotations and bit-flip gates in the same order. There are two SUM gates, and the SWAP gate can be realized by $O(d)$ bit-flip gates. Employing Solovay-Kitaev type algorithms [49, 95, 94], the complexity of the circuit becomes $O(d^2 \log \frac{d^2}{\epsilon})$.

For strong quantum simulation of one unitary evolution $U \in SU(d)$ or quantum channel $\mathcal{E}$, the circuit complexity is $O(d^2 \log \frac{d^2}{\epsilon})$ [169]. By comparison, one finds the complexity is the same for weak and strong quantum simulations. This is reasonable since a POVM with d^2 elements is informationally complete so that the final state can be fully reproduced [123]. If there are fewer number of POVM elements, the weak simulation cost could be smaller than that for strong simulation. For instance, for a POVM with d elements, the circuit complexity reduces to $O(d \log \frac{d}{\epsilon})$.

8.3 Query model for quantum channel simulation

In this section, we turn to the quantum channel simulation problem in the quantum query model. This is motivated by the problem that the query lower bound for simulating a general quantum channel is unknown, even for the unitary case [86, 14, 45]. Here our method is to consider the uniform quantum simulation. We start by a short introduction of query model.

Instead of designing quantum circuit based on channel parameters, in query model the parameters are provided in a black box, i.e. *oracle*, which can only be queried by an oracle call to extract limited information of the channel each time. The total number of queries to this oracle and others to be used are counted as the query complexity. Query model has quite a broad application, for instance, the well known Grover searching algorithm was originally presented involving queries [67]. We construct a quantum algorithm with query

complexity $O(\sqrt{N})$ using uniform quantum simulation method, by establishing a connection between quantum simulation problem and quantum state generation problem. The uniform quantum simulation problem in query model is stated as follows.

Definition 28 (Uniform quantum simulation problem in query model)**.** *For a quantum channel $\mathcal{E} \in \mathscr{L}(\mathscr{D})$ acting on an N-dimensional system, represented by the set of Kraus operators $\{K_\alpha\}$, $\alpha = 0, \ldots, N^2-1$, $K_\alpha = \sum_{i,j=0}^{N-1} k_{ij}^{(\alpha)} |i\rangle\langle j|$, there exists oracle call O_α such that $O_\alpha |i\rangle|j\rangle|\alpha\rangle|0\rangle = |i\rangle|j\rangle|\alpha\rangle|k_{ij}^{(\alpha)}\rangle$. The problem is to simulate $\mathcal{E}$ by generating its Choi state $\mathcal{C}$, and provide the query complexity.*

We use the Choi state $\mathcal{C}$ representation of a channel $\mathcal{E}$, which takes the form

$$\mathcal{C} = \frac{1}{N} \sum_{\alpha=0}^{N^2-1} \sum_{ijkl}^{N-1} k_{ij}^{(\alpha)} k_{kl}^{(\alpha)*} \left(|i\rangle\langle k|\right) \otimes \left(|j\rangle\langle l|\right). \tag{8.12}$$

We introduce the uniform simulation accuracy condition, which takes the form

$$\|\mathcal{C} - \tilde{\mathcal{C}}\|_1 \leq \frac{\epsilon}{N}, \tag{8.13}$$

which ensures the strong and weak simulations of the channel. This is also the condition we employed for the classical optimization algorithm in Chapter 4 for the convex-sum decomposition.

In this part we only consider the query complexity scaling with respect to N, instead of a full assessment of cost, which would also include the circuit cost. The analysis for the scaling with respect to ϵ would be in principle similar with those in Chapter 4 by involving Solovay-Kitaev algorithm [49] for the approximate implementation of each quantum gates in the circuit. Further, in the problem statement the parameters $\{k_{ij}^{(\alpha)}\}$ are assumed to be provided in bit-string representations. That is to say, we do not consider the error resulting from the approximation of each $k_{ij}^{(\alpha)}$ by a bit-string, neither.

The norm $\| \bullet \|_1$ is twice trace distance, which has the operational meaning of distinguishing two quantum states. That is to say, the successful generation of the Choi state

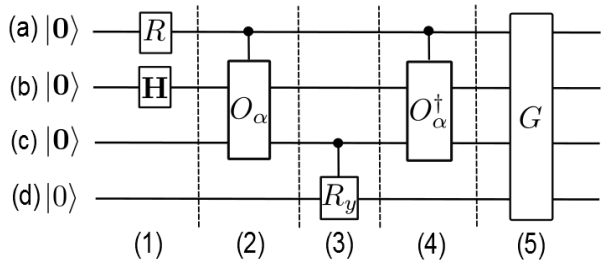

Figure 8.2: The circuit for the generation of a mixed state ρ. State $|\mathbf{0}\rangle$ in bold form represents a qubit-string of $|0\rangle$. R is a multi-qubit gate to generate superposition depending on the form of the mixed state. $\mathbf{H}$ is the Walsh-Hadamard gate. R_y is single-qubit rotation about y axis. O_α and its hermitian conjugate are queries. G represents the generalized Grover searching algorithm [22, 80, 110]. The controller (a) is traced out at the end. The generation of pure state is achieved when the controller is omitted, so the query complexities for generation of pure and mixed states are the same. The labels $(1-5)$ are for the steps in the circuit. [Figure from Ref. [167], Fig. 2.]

implies the channel can be simulated in the uniform simulation. Given the Choi state $\mathcal{C}$, the channel $\mathcal{E}$ can be effected by the method of gate teleportation, which was involved for the proof of Prop. 7. Following from this, we convert quantum simulation problem to quantum state generation problem; i.e. we consider how to generate Choi state by a quantum circuit.

A circuit for generating Choi state is shown in Fig. 8.2. There are four registers: the controller (a), the system (b), and two ancillas (c) and (d). Firstly, we consider pure quantum state generation, which is implemented when the controller (a) is omitted.

We consider how to generate the dual state of a unitary operator. A unitary operator can be viewed as a channel with only one Kraus operator which is unitary. For unitary operator $U \in SU(N)$, and $U = \sum_{i,j=0}^{N-1} u_{ij}|i\rangle\langle j|$, its dual Choi state is $|\psi_U\rangle = \frac{1}{\sqrt{N}} \sum_{i,j=0}^{N-1} u_{ij}|i,j\rangle$. The oracle in the circuit does not depend on α in this case. The oracle O works as $O|i\rangle|j\rangle|0\rangle = |i\rangle|j\rangle|u_{ij}\rangle$. Note that the ancilla is not a single qubit. The algorithm follows from Grover's method [68]. The algorithm proceeds as:

(1) The Walsh-Hadamard gate $\mathbf{H}$ leads to the state $\frac{1}{\sqrt{N}}\sum_{i,j=0}^{N-1}|i,j\rangle|\mathbf{0}\rangle|0\rangle$;

(2) From oracle call we get the state $\frac{1}{\sqrt{N}}\sum_{i,j=0}^{N-1}|i,j\rangle|u_{ij}\rangle|0\rangle$;

(3) The controlled-rotation of R_y gate yields the state

$$\frac{1}{\sqrt{N}}\sum_{i,j=0}^{N-1}|i,j\rangle|u_{ij}\rangle\left(u_{ij}|0\rangle+\sqrt{1-u_{ij}^2}|1\rangle\right); \tag{8.14}$$

(4) From the inverse oracle call we get the state

$$\frac{1}{\sqrt{N}}\sum_{i,j=0}^{N-1}|i,j\rangle|0\rangle\left(u_{ij}|0\rangle+\sqrt{1-u_{ij}^2}|1\rangle\right); \tag{8.15}$$

(5) To use Grover's searching algorithm, or generally, amplitude amplification G to convert the second ancilla to $|0\rangle$, which needs Grover oracle call $O(\sqrt{N})$;

(6) Tracing out the two ancillas (c) and (d) we get state $|\psi_U\rangle$.

It is known that pure quantum state generation can be realized by search algorithm with $O(\sqrt{N})$ queries along with failure probability $O(1/N)$, which could be further reduced to zero with generalized search algorithms [22, 80, 110].

For the generation of a mixed Choi state, first observe that the Choi state takes the form $\mathcal{C}\equiv\sum_{\alpha=0}^{N^2-1}p_\alpha|\psi_\alpha\rangle\langle\psi_\alpha|$, with $|\psi_\alpha\rangle=K_\alpha\otimes\mathbb{1}(\eta)=\frac{1}{\sqrt{N}}\sum_{i,j=0}^{N-1}k_{ij}^{(\alpha)}|i,j\rangle$, for $\eta=\frac{1}{N}\sum_{ij}|i,i\rangle\langle j,j|$, and $p_\alpha=\mathrm{tr}[K_\alpha^\dagger K_\alpha\otimes\mathbb{1}(\eta)]$, with $\sum_{\alpha=0}^{N^2-1}p_\alpha=1$. Although state $|\psi_\alpha\rangle$ is not normalized, the algorithm above for generation of pure state still applies. The algorithm for generating Choi state proceeds as follows.

(1) On input state $|\mathbf{0},\mathbf{0},\mathbf{0},0\rangle$, the gate R generates state $\sum_{\alpha=0}^{N^2-1}\sqrt{p_\alpha}|\alpha\rangle|\mathbf{0},\mathbf{0},0\rangle$. Note the state $|\alpha\rangle$ is a computational basis state. After the Walsh-Hadamard gate $\mathbf{H}$, the state becomes $\frac{1}{\sqrt{N}}\sum_{\alpha=0}^{N^2-1}\sum_{i,j=0}^{N-1}\sqrt{p_\alpha}|\alpha\rangle|i,j\rangle|\mathbf{0},0\rangle$;

(2) From controlled-oracle call we get the state $\frac{1}{\sqrt{N}}\sum_{\alpha=0}^{N^2-1}\sum_{i,j=0}^{N-1}\sqrt{p_\alpha}|\alpha\rangle|i,j\rangle|k_{ij}^{(\alpha)}\rangle|0\rangle$;

(3) The controlled-rotation of R_y gate yields

$$\frac{1}{\sqrt{N}}\sum_{\alpha=0}^{N^2-1}\sum_{i,j=0}^{N-1}\sqrt{p_\alpha}|\alpha\rangle|i,j\rangle|k_{ij}^{(\alpha)}\rangle\left(k_{ij}^{(\alpha)}|0\rangle+\sqrt{1-|k_{ij}^{(\alpha)}|^2}|1\rangle\right); \tag{8.16}$$

(4) From the inverse oracle call we get the state

$$\frac{1}{\sqrt{N}}\sum_{\alpha=0}^{N^2-1}\sum_{i,j=0}^{N-1}\sqrt{p_\alpha}|\alpha\rangle|i,j\rangle|\mathbf{0}\rangle\left(k_{ij}^{(\alpha)}|0\rangle+\sqrt{1-|k_{ij}^{(\alpha)}|^2}|1\rangle\right); \tag{8.17}$$

(5) To use amplitude amplification G to convert the second ancilla to $|0\rangle$, which needs Grover oracle call $O(\sqrt{N})$;

(6) Tracing out the controller (a) and the two ancillas (c) and (d), we obtain the Choi state.

The result shows that the query costs for generating pure state and mixed state with the same dimension are the same, and the query costs for simulation of unitary operator and quantum channel acting on the same dimensional system are also the same.

Next we study quantum algorithm achieving the query cost for strong quantum simulation. The algorithm is a "one-shot" algorithm, that is, it generates the corresponding final state given one initial state within error tolerance for each instance. If we could prepare the initial state and final state successfully, then we say the simulation is successful.

First we consider the strong simulation of a unitary operator. Given U acting on N-dimensional $\mathscr{H}$, suppose $U|\lambda_i\rangle = e^{-i\theta_i}|\lambda_i\rangle$, with eigenstate $|\lambda_i\rangle$ and eigenvalue $e^{-i\theta_i}$. Any pure state can be expressed in the form $|\psi\rangle = \sum_{i=0}^{N-1}\psi_i|\lambda_i\rangle$, and the evolution generates the final state $|\psi_f\rangle = \sum_{i=0}^{N-1}\psi_i e^{-i\theta_i}|\lambda_i\rangle$, with each coefficient ψ_i accumulating a phase $e^{-i\theta_i}$. Introduce a unitary operator oracle $O_U|i\rangle|0\rangle = |i\rangle|e^{-i\theta_i}\rangle$, which actually performs phase estimation [179]. Combined with the state oracle $O_\psi|i\rangle|0\rangle = |i\rangle|\psi_i\rangle$, we introduce the oracle $O|i\rangle|0\rangle|0\rangle = |i\rangle|\psi_i\rangle|e^{-i\theta_i}\rangle$. With the circuit for quantum state generation in Fig. 8.2, it is easy to see that the initial state $|\psi\rangle$ is generated with two calls to O_ψ and $O(\sqrt{N})$ calls to oracle in Grover algorithm, and the final state $|\psi_f\rangle$ is generated with two calls to O and $O(\sqrt{N})$ calls to oracle in Grover algorithm. The mixed state case can be reduced to the pure state case by expanding a density operator as a mixture of pure states.

Next we consider the strong simulation of a quantum channel. Using results on strong simulation of a quantum channel based on convex combination of generalized extreme chan-

nels in Chapter 4, it is known that a quantum channel acting on N-dimensional system can be simulated by convex combination of N generalized extreme quantum circuits, each of which has a well-defined structure with one initial and one final unitary operators acting on the system. For the query model, we use oracle calls for the initial and final unitary operators, while the rest of the circuit keeps the same gate operations. The algorithm is the combination of the one for unitary operator above and the generalized extreme channel circuit. In this way, we can simulate a quantum channel in the query model with the same query complexity as a unitary operator.

8.4 Conclusion

In this chapter three types of quantum simulations are introduced according to operator topologies on a Hilbert space. Particularly, a weak quantum simulation algorithm and a uniform quantum simulation algorithm in the query model are constructed. Also it is shown that the simulation efficiencies for uniform, strong, and weak quantum simulations are all limited by the ability of quantum computing. The query complexity for quantum channel simulation is also obtained.

Chapter 9

Conclusions

Now comes the conclusion of this thesis. We have presented the results for algorithmic quantum channel simulation, including our work on Solovay-Kitaev algorithm, quantum channel simulation based on convex sum of generalized extreme channels, particularly the cases for qubit, qutrit, and two-qubit channels, also the work on photonic qubit channel simulator, and finally the construction of alternative quantum simulation problems. A summary of the main results and significance is provided in §9.1, and also for a further understanding of the achievements in this thesis, several potential improvements and extensions of those results is discussed in §9.2.

9.1 Summary

We first summarize the main achievement in this thesis as the following four aspects. This summary can be viewed as a complement of the summary provided in Chapter 1.

9.1.1 Qubit-channel simulation

We have developed a quantum qubit-channel simulation algorithm that accepts arbitrary single qubit channel and a promised error tolerance as input, and yields the description of the qubit-channel simulator circuit, which can generate approximate qubit state within the promised error tolerance for the worst case. The qubit-channel simulation algorithm explores solid results on qubit extreme channel decomposition theory [140], which leads to a natural consumption of classical resources, namely bits, and hence a reduction of cost of quantum resources. The qubit-channel simulator circuit only requires a single CNOT gate, which is the minimal number of CNOT gates needed for any generic two-qubit process. The

unitary qubit gates in the qubit-channel simulator can be further replaced by sequence of gates from a universal gate library, such as $\{\mathrm{H}, \mathrm{T}\}$, using the unitary qubit gate compiling algorithms, such as the Solovay-Kitaev-Dawson-Nielsen (SKDN) algorithm [49]. Our qubit-channel simulation algorithm can be viewed as an extension of SKDN algorithm to general nonunitary qubit gates, and the qubit-channel simulator serves as a nonunitary qubit gate that uses classical resources and minimal quantum resources.

9.1.2 Photonic qubit-channel simulator

Our qubit-channel simulation scheme has been implemented by a linear optics setup. Qubit is encoded in the polarization of photons and two additional photons are employed to ensure the presence of the system and ancilla photons. A scheme for using classical bits for the convex combination of qubit generalized extreme channels is developed, namely, by varying the data collection time for different channels. To demonstrate the photonic qubit-channel simulator, along with the simulation of randomly-chosen arbitrary qubit channel and some well-known qubit noises, we also deploy our simulator to simulate qubit processes that are not trace preserving or not completely positive. In particular, a protocol for the protection of quantum superposition via weak measurement and measurement reversals [97, 89], which is not trace preserving, is realized by our simulator, and also the structural physical approximation of the well-known transpose operation [79], which is not completely positive. The photonic qubit-channel simulator is ready for the use as nonunitary qubit gate, qubit noise generator, and also for large-scale simulations when combined with other gates for the simulation and study of nontrivial dissipative quantum dynamics.

9.1.3 Qudit-channel simulation

We have developed a nontrivial generalization of our single qubit-channel simulation algorithm to the case of qudit-channel simulation. The generalization to the qutrit case is even not straightforward due to the complicated structure of the set of qutrit channels compared

with the qubit case, and the quantum channel decomposition in terms of convex combination of (generalized) extreme channels is known as an open problem [139]. In the spirit of algorithmic quantum simulation, we have constructed a classical optimization procedure for an approximate quantum channel decomposition, and the benefit is significant: the quantum circuit cost is greatly reduced, without causing a large simulation error for the low-dimensional cases, namely qutrit and two-qubit channels. Our quantum channel simulation algorithm serves as a distinct simulation task besides the well-known simulation of local Hamiltonian evolution [108], and it generalizes quantum simulation from unitary evolution to more general nonunitary dynamics, and also it employs the new method based on extreme channel decomposition that can reduce the simulation cost significantly compared with other methods as those discussed in Chapter 4.

9.1.4 Alternative quantum simulation problems

Besides our work on quantum channel simulation, other quantum simulation problems are also explored, namely, the weak quantum simulation and uniform quantum simulation problems. Based on operator topology [18], the weak quantum simulation is introduced for the simulation of measurement of a certain observable, and the strong quantum simulation for the simulation of effects of a certain evolution operator on states, while the uniform quantum simulation for the simulation of a process itself. As an initial application of these alternative quantum simulation methods, a weak quantum simulation algorithm is constructed to solve a weak quantum simulation of measurement effects, and the query complexity [86, 14, 45] for the simulation of a general quantum channel is obtained using the uniform quantum simulation method.

9.2 Outlook

Along with the summary of our work in this thesis, an outlook for further exploration is necessary and beneficial for a better understanding of our work. The following five aspects are closely related to our main results.

9.2.1 Improvement of the lookup table

The Solovay-Kitaev-Dawson-Nielsen algorithm [49] we studied is a standard algorithm for a constructive proof of the notable Solovay-Kitaev theorem [92, 123], which essentially proves the ability of approximating arbitrary unitary quantum processes using just a small discrete universal gate library. However, the SKDN algorithm requires a lookup table to start, which was not well developed originally. This motivates our construction of the lookup table and a geometric method for searching it. However, as already mentioned in Chapter 3, the SKDN requires the approximation of gates close to identity for further steps, which then requires more than one data points in our lookup table. Besides, the construction of such a lookup table would not be efficient or feasible for qudit case [121]. Although a qudit gate can be decomposed firstly into a product of Givens rotations, and a Givens rotation can be decomposed into a product of controlled-bit flip gates (CNOT) and qubit gates effectively, and then only requires SKDN for qubit case, an improvement of SKDN algorithm for the qudit case is still important for the completion of the Solovay-Kitaev theorem and demonstration of the capability of the group commutator method.

9.2.2 Alternative algorithms for channel decomposition

For the problem of decomposing a channel into a convex sum of generalized extreme channels, we have developed an optimization algorithm for it. However, as is well known [73], optimization problem could be hard, and also not easy to analyze the complexity scaling. As a result, it is an open problem whether there exists a step-by-step procedure for decomposing

a given channel into a convex sum of generalized extreme channels, which would effectively provide an analytical formula for Ruskai's conjecture [139]. If this is not the case, there are still rooms to explore for an approximate decomposition other than our method. As mentioned in Chapter 4, the construction for generalized extreme channels is not unique in principle. As a result, it is highly interesting to explore better constructions, if they exist, to characterize generalized extreme channels, and also better optimization algorithms in order to benefit the channel decomposition.

9.2.3 Efficient channel simulation

For quantum channel decomposition problem we have focused on the simulation of arbitrary quantum channels. As one can see our simulation algorithm is generically not efficient, namely, the classical optimization is probably not efficient with respect to $\log d$, although there is no close form for such a scaling, and the quantum circuit can only be quadratic with respect to d, which is exponential with respect to $\log d$. This inefficiency, however, is reasonable since the scaling is primarily determined by the number of parameters to specify a quantum channel. If, instead, we consider the simulation of special types of channels, such as those in practice that generally do not have exponential number of parameters, e.g. local Markovian dynamics [93], the efficiency of our simulation algorithm is possible. However, our current algorithm is anonymous to the description of the input channel, also it is even a problem that what special types of quantum channels are of interest for quantum physics and quantum computing.

9.2.4 Efficiency gap for different simulation methods

It is an open question that whether there exists some efficiency gap among the uniform, strong, and weak quantum simulations for the simulation of specific quantum processes. That is, whether there exist quantum processes such that the simulation with one simulation method is efficient while inefficient with other methods.

The possibility for the existence of efficiency gap has been demonstrated for the classical simulation of quantum processes [28, 24, 161, 160]. It has been found that for the simulation of some quantum algorithms there exists such an efficiency gap between strong and weak classical simulations [161, 24]. Here the 'weak classical simulation' is to sample the quantum computational result, and the 'strong classical simulation' is to evaluate the quantum computational result. By a direct comparison, the 'strong classical simulation' corresponds to our weak simulation method, since both of which evaluate observable quantities. Such studies can benefit our understanding of quantum simulation and the design of different quantum simulation algorithms.

9.2.5 Relating to other channel problems

Quantum channels play a vital role in quantum computing and quantum information processing, and quantum channel simulation is basically one of many ways to explore the properties of quantum channels. Other important tasks involving channels include quantum process tomography [123], which is in fact to detect the Choi state, quantum parameter estimation [58, 83], which is to determine the parameters in a channel, quantum channel discrimination [141, 51], which is to determine an unknown process that is promised to be one of several formulas, and quantum error correction [123], which is essentially to find the inverse of a noisy channel, and also to construct arbitrary channels using primary physical elements, e.g., two-body interactions, depolarizing processes, and decay processes. Quantum channel simulators could play roles for other tasks, such as serving as quantum noise generator to test the robustness of a quantum error correction code. It is also important to explore the relationship between quantum channel simulation problem with other problems, such as quantum channel discrimination [141, 51].

Appendix A

Qutrit quantum channel simulation

The Choi state for a generalized extreme qutrit channel is

$$
\mathcal{C}_{\mathrm{qut}} = \begin{pmatrix}
(\cos a)^2(\cos c)^2 & 0 & 0 & 0 & \cos a\cos b\cos c & 0 & 0 & 0 & \cos a\cos c\cos d \\
0 & 0 & 0 & 0 & 0 & 0 & 0 & 0 & 0 \\
0 & 0 & 0 & 0 & 0 & 0 & 0 & 0 & 0 \\
0 & 0 & 0 & 0 & 0 & 0 & 0 & 0 & 0 \\
\cos a\cos b\cos c & 0 & 0 & 0 & (\cos b)^2 & 0 & 0 & 0 & \cos b\cos d \\
0 & 0 & 0 & 0 & 0 & 0 & 0 & 0 & 0 \\
0 & 0 & 0 & 0 & 0 & 0 & 0 & 0 & 0 \\
0 & 0 & 0 & 0 & 0 & 0 & 0 & 0 & 0 \\
\cos a\cos c\cos d & 0 & 0 & 0 & \cos b\cos d & 0 & 0 & 0 & (\cos d)^2
\end{pmatrix}
$$

$$
+ \begin{pmatrix}
0 & 0 & 0 & 0 & 0 & 0 & 0 & 0 & 0 \\
0 & (\sin b)^2(\cos e)^2 & 0 & 0 & 0 & -\sin b\cos e\sin d\sin f & \sin b\cos e\sin a & 0 & 0 \\
0 & 0 & 0 & 0 & 0 & 0 & 0 & 0 & 0 \\
0 & 0 & 0 & 0 & 0 & 0 & 0 & 0 & 0 \\
0 & 0 & 0 & 0 & 0 & 0 & 0 & 0 & 0 \\
0 & -\sin b\cos e\sin d\sin f & 0 & 0 & 0 & (\sin d)^2(\sin f)^2 & \sin a\sin d\sin f & 0 & 0 \\
0 & \sin b\cos e\sin a & 0 & 0 & 0 & \sin a\sin d\sin f & (\sin a)^2 & 0 & 0 \\
0 & 0 & 0 & 0 & 0 & 0 & 0 & 0 & 0 \\
0 & 0 & 0 & 0 & 0 & 0 & 0 & 0 & 0
\end{pmatrix} \tag{A.1}
$$

$$
+ \begin{pmatrix}
0 & 0 & 0 & 0 & 0 & 0 & 0 & 0 & 0 \\
0 & 0 & 0 & 0 & 0 & 0 & 0 & 0 & 0 \\
0 & 0 & (\sin d)^2(\cos f)^2 & \cos a\sin c\sin d\cos f & 0 & 0 & 0 & \sin b\sin e\sin d\cos f & 0 \\
0 & 0 & \cos a\sin c\sin d\cos f & (\cos a)^2(\sin c)^2 & 0 & 0 & 0 & \sin b\sin e\cos a\sin c & 0 \\
0 & 0 & 0 & 0 & 0 & 0 & 0 & 0 & 0 \\
0 & 0 & 0 & 0 & 0 & 0 & 0 & 0 & 0 \\
0 & 0 & 0 & 0 & 0 & 0 & 0 & 0 & 0 \\
0 & 0 & \sin b\sin e\sin d\cos f & \sin b\sin e\cos a\sin c & 0 & 0 & 0 & (\sin b)^2(\sin e)^2 & 0 \\
0 & 0 & 0 & 0 & 0 & 0 & 0 & 0 & 0
\end{pmatrix} \tag{A.2}
$$

$$
\equiv \begin{pmatrix}
A_1 & C_{12} & C_{13} \\
C_{21} & A_2 & C_{23} \\
C_{31} & C_{32} & A_3
\end{pmatrix}, \tag{A.3}
$$

with $C_{12} = \sqrt{A_1}U\sqrt{A_2}$, $C_{23} = \sqrt{A_2}V\sqrt{A_3}$, $C_{13} = \sqrt{A_1}UV\sqrt{A_3}$, and

$$U = \begin{pmatrix} 0 & \frac{\cos a \cos b \cos c}{|\cos a \cos b||\cos c|} & 0 \\ 0 & 0 & -\frac{\sin b \cos e \sin d \sin f}{|\sin b \cos e||\sin d \sin f|} \\ \frac{\cos a \sin c \sin d \cos f}{|\cos a \sin c||\sin d \cos f|} & 0 & 0 \end{pmatrix}, \tag{A.4}$$

$$V = \begin{pmatrix} 0 & \frac{\cos a \sin c \sin b \sin e}{|\cos a \sin c||\sin b \sin e|} & 0 \\ 0 & 0 & \frac{\cos b \cos d}{|\cos b||\cos d|} \\ \frac{\sin a \sin d \sin f}{|\sin a||\sin d \sin f|} & 0 & 0 \end{pmatrix}. \tag{A.5}$$

For instance, when the parameters in the absolute values are positive,

$$U = \begin{pmatrix} 0 & 1 & 0 \\ 0 & 0 & -1 \\ 1 & 0 & 0 \end{pmatrix}, V = \begin{pmatrix} 0 & 1 & 0 \\ 0 & 0 & 1 \\ 1 & 0 & 0 \end{pmatrix}. \tag{A.6}$$

The quantum circuit U_{qut} takes the form in Eq. (A.7).

The state ρ_{SA} takes the form in Eq. (A.8).

We also checked the case for a mixed initial system state

$$\rho = \begin{pmatrix} p_0 & p_{01} & p_{02} \\ p_{10} & p_1 & p_{12} \\ p_{20} & p_{21} & p_2 \end{pmatrix}. \tag{A.9}$$

The Kraus operator F_0 acts on system state resulting in

$$F_0 \rho F_0^\dagger = \begin{pmatrix} p_0 \cos a^2 \cos c^2 & p_{01} \cos a \cos b \cos c & p_{02} \cos a \cos c \cos d \\ p_{10} \cos a \cos b \cos c & p_1 \cos b^2 & p_{12} \cos b \cos d \\ p_{20} \cos a \cos c \cos d & p_{21} \cos b \cos d & p_2 \cos d^2 \end{pmatrix}, \tag{A.10}$$

which is the same with the projection $|0\rangle\langle 0|$ on the state ρ_{SA}.

The Kraus operator F_1 acts on system state resulting in

$$F_1 \rho F_1^\dagger = \begin{pmatrix} p_1 \cos e^2 \sin b^2 & -p_{12} \cos e \sin b \sin d \sin f & p_{10} \cos e \sin a \sin b \\ -p_{21} \cos e \sin b \sin d \sin f & p_2 \sin d^2 \sin f^2 & -p_{20} \sin a \sin d \sin f \\ p_{01} \cos e \sin a \sin b & -p_{02} \sin a \sin d \sin f & p_0 \sin a^2 \end{pmatrix}, \tag{A.11}$$

$$U_{\text{qut}} = \begin{pmatrix} \cos a \cos c & -\cos c \sin a & -\sin c & 0 & 0 & 0 & 0 & 0 & 0 \\ 0 & 0 & 0 & \cos e \sin b & \cos b \cos e & -\sin e & 0 & 0 & 0 \\ 0 & 0 & 0 & 0 & 0 & 0 & \cos f \sin d & \sin f & \cos d \cos f \\ 0 & 0 & 0 & \cos b & -\sin b & 0 & 0 & 0 & 0 \\ 0 & 0 & 0 & 0 & 0 & 0 & -\sin d \sin f & \cos f & -\cos d \sin f \\ \cos a \sin c & -\sin a \sin c & \cos c & 0 & 0 & 0 & 0 & 0 & 0 \\ 0 & 0 & 0 & 0 & 0 & 0 & \cos d & 0 & -\sin d \\ \sin a & \cos a & 0 & 0 & 0 & 0 & 0 & 0 & 0 \\ 0 & 0 & 0 & \sin b \sin e & \cos b \sin e & \cos e & 0 & 0 & 0 \end{pmatrix}. \tag{A.7}$$

$$\rho_{\mathrm{SA}} = U_{\mathrm{qut}}(\rho \otimes |0\rangle\langle 0|)U_{\mathrm{qut}}^{\dagger} \tag{A.8}$$

$$= \begin{pmatrix}
x^2\cos a^2\cos c^2 & xy\cos a\cos c\cos e\sin b & wx\cos a\cos c\cos f\sin d & xy\cos a\cos b\cos c \\
xy\cos a\cos c\cos e\sin b & y^2\cos e^2\sin b^2 & wy\cos e\cos f\sin b\sin d & y^2\cos b\cos e\sin b \\
wx\cos a\cos c\cos f\sin d & wy\cos e\cos f\sin b\sin d & w^2\cos f^2\sin d^2 & wy\cos b\cos f\sin d \\
xy\cos a\cos b\cos c & y^2\cos b\cos e\sin b & wy\cos b\cos f\sin d & y^2\cos b^2 \\
-wx\cos a\cos c\sin d\sin f & -wy\cos e\sin b\sin d\sin f & -w^2\cos f\sin d^2\sin f & -wy\cos b\sin d\sin f \\
x^2\cos a^2\cos c\sin c & xy\cos a\cos e\sin b\sin c & wx\cos a\cos f\sin c\sin d & xy\cos a\cos b\sin c \\
wx\cos a\cos c\cos d & wy\cos d\cos e\sin b & w^2\cos d\cos f\sin d & wy\cos b\cos d \\
x^2\cos a\cos c\sin a & xy\cos e\sin a\sin b & wx\cos f\sin a\sin d & xy\cos b\sin a \\
xy\cos a\cos c\sin b\sin e & y^2\cos e\sin b^2\sin e & wy\cos f\sin b\sin d\sin e & y^2\cos b\sin b\sin e
\end{pmatrix}$$

$$\begin{pmatrix}
-wx\cos a\cos c\sin d\sin f & x^2\cos a^2\cos c\sin c & wx\cos a\cos c\cos d & x^2\cos a\cos c\sin a & xy\cos a\cos c\sin b\sin e \\
-wy\cos e\sin b\sin d\sin f & xy\cos a\cos e\sin b\sin c & wy\cos d\cos e\sin b & xy\cos e\sin a\sin b & y^2\cos e\sin b^2\sin e \\
-w^2\cos f\sin d^2\sin f & wx\cos a\cos f\sin c\sin d & w^2\cos d\cos f\sin d & wx\cos f\sin a\sin d & wy\cos f\sin b\sin d\sin e \\
-wy\cos b\sin d\sin f & xy\cos a\cos b\sin c & wy\cos b\cos d & xy\cos b\sin a & y^2\cos b\sin b\sin e \\
w^2\sin d^2\sin f^2 & -wx\cos a\sin c\sin d\sin f & -w^2\cos d\sin d\sin f & -wx\sin a\sin d\sin f & -wy\sin b\sin d\sin e\sin f \\
-wx\cos a\sin c\sin d\sin f & x^2\cos a^2\sin c^2 & wx\cos a\cos d\sin c & x^2\cos a\sin a\sin c & xy\cos a\sin b\sin c\sin e \\
-w^2\cos d\sin d\sin f & wx\cos a\cos d\sin c & w^2\cos d^2 & wx\cos d\sin a & wy\cos d\sin b\sin e \\
-wx\sin a\sin d\sin f & x^2\cos a\sin a\sin c & wx\cos d\sin a & x^2\sin a^2 & xy\sin a\sin b\sin e \\
-wy\sin b\sin d\sin e\sin f & xy\cos a\sin b\sin c\sin e & wy\cos d\sin b\sin e & xy\sin a\sin b\sin e & y^2\sin b^2\sin e^2
\end{pmatrix}.$$

which is the same with the projection $|1\rangle\langle 1|$ on the state $\rho_{\rm SA}$.

The Kraus operator F_2 acts on system state resulting in

$$F_2\rho F_2^\dagger = \begin{pmatrix} p_2\cos f^2\sin d^2 & p_{20}\cos a\cos f\sin c\sin d & p_{21}\cos f\sin b\sin d\sin e \\ p_{02}\cos a\cos f\sin c\sin d & p_0\cos a^2\sin c^2 & p_{01}\cos a\sin b\sin c\sin e \\ p_{12}\cos f\sin b\sin d\sin e & p_{10}\cos a\sin b\sin c\sin e & p_1\sin b^2\sin e^2 \end{pmatrix}, \tag{A.12}$$

which is the same with the projection $|2\rangle\langle 2|$ on the state $\rho_{\rm SA}$.

The system state can be initially correlated with another adversary (denoted as D), namely, a qutrit. The initial "system+adversary" state is a two-qutrit state $\rho_{\rm DS}$ which takes the form

$$\rho_{\rm DS} = \begin{pmatrix} p_0 & p_{01} & p_{02} & p_{03} & p_{04} & p_{05} & p_{06} & p_{07} & p_{08} \\ p_{10} & p_1 & p_{12} & p_{13} & p_{14} & p_{15} & p_{16} & p_{17} & p_{18} \\ p_{20} & p_{21} & p_2 & p_{23} & p_{24} & p_{25} & p_{26} & p_{27} & p_{28} \\ p_{30} & p_{31} & p_{32} & p_3 & p_{34} & p_{35} & p_{36} & p_{37} & p_{38} \\ p_{40} & p_{41} & p_{42} & p_{43} & p_4 & p_{45} & p_{46} & p_{47} & p_{48} \\ p_{50} & p_{51} & p_{52} & p_{53} & p_{54} & p_{55} & p_{56} & p_{57} & p_{58} \\ p_{60} & p_{61} & p_{62} & p_{63} & p_{64} & p_{65} & p_6 & p_{67} & p_{68} \\ p_{70} & p_{71} & p_{72} & p_{73} & p_{74} & p_{75} & p_{76} & p_7 & p_{78} \\ p_{80} & p_{81} & p_{82} & p_{83} & p_{84} & p_{85} & p_{86} & p_{87} & p_8 \end{pmatrix}. \tag{A.13}$$

The whole final state is

$$\rho_{\rm DSA} = (\mathbb{1}_{\rm D}\otimes U_{\rm SA})\,(\rho_{\rm DS}\otimes|0\rangle\langle 0|)\,(\mathbb{1}_{\rm D}\otimes U_{\rm SA}^\dagger).$$

Note we have omitted the subscript "qut" on the unitary operator $U_{\rm SA}$ for simplicity. We also checked that $\langle i|\rho_{\rm DSA}|i\rangle = (\mathbb{1}_{\rm D}\otimes F_i)\rho_{\rm DS}(\mathbb{1}_{\rm D}\otimes F_i^\dagger)$, which means the projection $|i\rangle\langle i|$ on the ancilla is equivalent to the action of $\mathbb{1}_{\rm D}\otimes F_i$ on the system+adversary.

The Choi state for the qutrit channel simulation example is

$$\mathcal{C} = \begin{pmatrix} 0.3105 + 0.0000i & 0.1052 + 0.0154i & 0.0394 - 0.0099i & 0.0554 + 0.0013i & -0.0892 - 0.0667i \\ 0.1052 - 0.0154i & 0.2526 + 0.0000i & -0.0174 + 0.0148i & 0.0715 - 0.0388i & -0.0307 - 0.0814i \\ 0.0394 + 0.0099i & -0.0174 - 0.0148i & 0.2473 + 0.0000i & 0.0302 + 0.0637i & 0.0600 + 0.0425i \\ 0.0554 - 0.0013i & 0.0715 + 0.0388i & 0.0302 - 0.0637i & 0.2891 + 0.0000i & -0.0066 - 0.0301i \\ -0.0892 + 0.0667i & -0.0307 + 0.0814i & 0.0600 - 0.0425i & -0.0066 + 0.0301i & 0.2667 + 0.0000i \\ 0.0185 - 0.0149i & -0.1021 - 0.0296i & 0.0800 - 0.1476i & -0.0147 - 0.0141i & 0.0816 - 0.0849i \\ -0.0070 - 0.0066i & -0.0250 - 0.0841i & -0.0986 - 0.0101i & -0.0501 + 0.0559i & -0.0968 - 0.1558i \\ -0.1068 - 0.1226i & 0.0778 + 0.0614i & 0.0475 + 0.0007i & 0.1728 + 0.0571i & 0.0234 + 0.0100i \\ 0.1131 - 0.0192i & -0.0717 - 0.0218i & -0.0440 - 0.0073i & 0.1132 - 0.0481i & -0.0568 + 0.0703i \end{pmatrix}$$

$$\begin{pmatrix} 0.0185 + 0.0149i & -0.0070 + 0.0066i & -0.1068 + 0.1226i & 0.1131 + 0.0192i \\ -0.1021 + 0.0296i & -0.0250 + 0.0841i & 0.0778 - 0.0614i & -0.0717 + 0.0218i \\ 0.0800 + 0.1476i & -0.0986 + 0.0101i & 0.0475 - 0.0007i & -0.0440 + 0.0073i \\ -0.0147 + 0.0141i & -0.0501 - 0.0559i & 0.1728 - 0.0571i & 0.1132 + 0.0481i \\ 0.0816 + 0.0849i & -0.0968 + 0.1558i & 0.0234 - 0.0100i & -0.0568 - 0.0703i \\ 0.3716 + 0.0000i & 0.0306 + 0.1539i & -0.1073 - 0.0026i & 0.0882 + 0.0653i \\ 0.0306 - 0.1539i & 0.4004 + 0.0000i & -0.0986 + 0.0147i & -0.0247 - 0.0042i \\ -0.1073 + 0.0026i & -0.0986 - 0.0147i & 0.4807 + 0.0000i & -0.0641 - 0.0998i \\ 0.0882 - 0.0653i & -0.0247 + 0.0042i & -0.0641 + 0.0998i & 0.3811 + 0.0000i \end{pmatrix}. \tag{A.14}$$

The approximate Choi state $\mathcal{C}'$ from the simulation is

$$\mathcal{C}' = \begin{pmatrix} 0.3103 + 0.0000i & 0.1082 + 0.0119i & 0.0386 - 0.0089i & 0.0559 + 0.0007i & -0.0859 - 0.0676i \\ 0.1082 - 0.0119i & 0.2522 + 0.0000i & -0.0243 + 0.0256i & 0.0726 - 0.0333i & -0.0393 - 0.0777i \\ 0.0386 + 0.0089i & -0.0243 - 0.0256i & 0.2520 + 0.0000i & 0.0309 + 0.0603i & 0.0645 + 0.0313i \\ 0.0559 - 0.0007i & 0.0726 + 0.0333i & 0.0309 - 0.0603i & 0.2951 + 0.0000i & -0.0095 - 0.0290i \\ -0.0859 + 0.0676i & -0.0393 + 0.0777i & 0.0645 - 0.0313i & -0.0095 + 0.0290i & 0.2677 + 0.0000i \\ 0.0207 - 0.0164i & -0.0922 - 0.0272i & 0.0765 - 0.1407i & -0.0133 - 0.0100i & 0.0871 - 0.0753i \\ -0.0090 - 0.0044i & -0.0260 - 0.0903i & -0.1034 - 0.0120i & -0.0521 + 0.0552i & -0.0975 - 0.1628i \\ -0.1058 - 0.1225i & 0.0797 + 0.0632i & 0.0461 - 0.0006i & 0.1708 + 0.0550i & 0.0246 + 0.0135i \\ 0.1126 - 0.0218i & -0.0676 - 0.0221i & -0.0414 - 0.0107i & 0.1136 - 0.0481i & -0.0505 + 0.0714i \end{pmatrix}$$

$$\begin{pmatrix} 0.0207 + 0.0164i & -0.0090 + 0.0044i & -0.1058 + 0.1225i & 0.1126 + 0.0218i \\ -0.0922 + 0.0272i & -0.0260 + 0.0903i & 0.0797 - 0.0632i & -0.0676 + 0.0221i \\ 0.0765 + 0.1407i & -0.1034 + 0.0120i & 0.0461 + 0.0006i & -0.0414 + 0.0107i \\ -0.0133 + 0.0100i & -0.0521 - 0.0552i & 0.1708 - 0.0550i & 0.1136 + 0.0481i \\ 0.0871 + 0.0753i & -0.0975 + 0.1628i & 0.0246 - 0.0135i & -0.0505 - 0.0714i \\ 0.3731 + 0.0000i & 0.0329 + 0.1523i & -0.1037 - 0.0034i & 0.0828 + 0.0638i \\ 0.0329 - 0.1523i & 0.3946 + 0.0000i & -0.0987 + 0.0171i & -0.0253 - 0.0012i \\ -0.1037 + 0.0034i & -0.0987 - 0.0171i & 0.4802 + 0.0000i & -0.0628 - 0.1009i \\ 0.0828 - 0.0638i & -0.0253 + 0.0012i & -0.0628 + 0.1009i & 0.3749 + 0.0000i \end{pmatrix}. \tag{A.15}$$

For the block-matrix form (4.41), the followings matrices are obtained from the simulation. For $\mathcal{C}_1^{\mathrm{g}}$,

$$U_{12} = \begin{pmatrix} 0.6447 + 0.4127i & 0.0355 - 0.6373i & -0.0145 + 0.0800i \\ -0.5466 - 0.1318i & -0.2428 - 0.6346i & -0.4684 + 0.0530i \\ -0.1571 - 0.2705i & 0.2678 - 0.2434i & 0.5297 + 0.7005i \end{pmatrix}, \tag{A.16a}$$

$$U_{13} = \begin{pmatrix} 0.0547 - 0.0727i & 0.7935 + 0.3901i & 0.0457 + 0.4559i \\ 0.1883 + 0.2699i & 0.4069 - 0.2137i & -0.7012 - 0.4346i \\ -0.1225 + 0.9319i & -0.0702 - 0.0457i & 0.1043 + 0.3141i \end{pmatrix}, \tag{A.16b}$$

$$U_{23} = \begin{pmatrix} -0.3661 - 0.3717i & 0.5018 + 0.0826i & 0.5568 + 0.3990i \\ -0.4284 + 0.3060i & -0.1913 + 0.8002i & 0.1086 - 0.1846i \\ 0.5074 + 0.4397i & -0.2514 + 0.0344i & 0.6164 + 0.3239i \end{pmatrix}, \tag{A.16c}$$

and $U_{13} = U_{12}U_{23}$ holds.

For $\mathcal{C}_2^{\mathrm{g}}$,

$$U_{12} = \begin{pmatrix} 0.0809 + 0.3094i & -0.8235 + 0.2156i & 0.3801 + 0.1690i \\ 0.3137 - 0.2927i & -0.1586 + 0.2900i & -0.5990 + 0.5898i \\ 0.4114 + 0.7378i & 0.4051 - 0.0435i & 0.0625 + 0.3413i \end{pmatrix}, \tag{A.17a}$$

$$U_{13} = \begin{pmatrix} -0.4679 - 0.2075i & -0.7440 + 0.3210i & 0.2854 + 0.0073i \\ -0.8432 - 0.0240i & 0.3609 - 0.2833i & -0.1467 + 0.2375i \\ -0.1406 + 0.0813i & -0.2610 - 0.2547i & -0.5468 - 0.7359i \end{pmatrix}, \tag{A.17b}$$

$$U_{23} = \begin{pmatrix} -0.3574 + 0.0108i & -0.0601 + 0.3608i & -0.8581 + 0.0446i \\ 0.4069 + 0.5470i & 0.4478 - 0.2782i & -0.3309 - 0.3846i \\ 0.2969 + 0.5650i & -0.7150 + 0.2777i & 0.0523 + 0.0394i \end{pmatrix}, \tag{A.17c}$$

and $U_{13} = U_{12}U_{23}$ holds.

For $\mathcal{C}_3^{\mathrm{g}}$,

$$U_{12} = \begin{pmatrix} -0.2497 - 0.3598i & -0.2683 + 0.1669i & -0.0001 - 0.8416i \\ -0.2315 - 0.0241i & 0.2404 - 0.9128i & -0.1515 - 0.1787i \\ -0.6432 + 0.5834i & 0.0382 + 0.0880i & 0.4837 - 0.0533i \end{pmatrix}, \tag{A.18a}$$

$$U_{13} = \begin{pmatrix} 0.0381 + 0.0587i & -0.6987 + 0.6269i & 0.3135 - 0.1249i \\ 0.3836 + 0.6633i & -0.1680 + 0.0308i & -0.6187 - 0.0296i \\ -0.6370 - 0.0467i & -0.0744 + 0.2900i & -0.4371 + 0.5580i \end{pmatrix}, \tag{A.18b}$$

$$U_{23} = \begin{pmatrix} 0.2470 + 0.2564i & 0.2041 - 0.5622i & 0.7172 + 0.0320i \\ -0.5421 + 0.5418i & 0.2462 - 0.1799i & -0.1943 - 0.5309i \\ -0.5317 - 0.0564i & -0.5591 - 0.4865i & -0.0370 + 0.4044i \end{pmatrix}, \tag{A.18c}$$

and $U_{13} = U_{12}U_{23}$ holds.

Appendix B

Extreme two-qubit quantum channel in Pauli basis

The unitary operator U_{twoqub} in Heisenberg-Weyl basis is shown in Eq. (B.1).

Switching from Heisenberg-Weyl basis to Pauli basis, we only need to change the permutation gates. In tensor-product of Pauli basis $\{\sigma_i \otimes \sigma_j\}$ $(i, j = 0, 1, 2, 3)$, the four Kraus operators for the generalized extreme two-qubit channel are

$$F_0 = \begin{pmatrix} \cos a \cos c \cos g & 0 & 0 & 0 \\ 0 & \cos b & 0 & 0 \\ 0 & 0 & \cos d & 0 \\ 0 & 0 & 0 & \cos h \end{pmatrix}, \tag{B.2a}$$

$$F_1 = \begin{pmatrix} 0 & 0 & 0 & -\sin h \sin q \\ 0 & 0 & -\sin d \sin f & 0 \\ 0 & \sin b \cos e \cos p & 0 & 0 \\ \sin a & 0 & 0 & 0 \end{pmatrix}, \tag{B.2b}$$

$$F_2 = \begin{pmatrix} 0 & 0 & \sin d \cos f \cos s & 0 \\ 0 & 0 & 0 & -\sin h \cos q \sin t \\ \cos a \sin c & 0 & 0 & 0 \\ 0 & \sin b \sin e & 0 & 0 \end{pmatrix}, \tag{B.2c}$$

$$F_3 = \begin{pmatrix} 0 & \sin b \cos e \sin p & 0 & 0 \\ \cos a \cos c \sin g & 0 & 0 & 0 \\ 0 & 0 & 0 & \sin h \cos q \cos t \\ 0 & 0 & \sin d \cos f \sin s & 0 \end{pmatrix}. \tag{B.2d}$$

$$
U_{\text{twoqub}} = \begin{pmatrix}
\cos a \cos c \cos g & -\cos c \cos g \sin a & -\cos g \sin c & -\sin g & 0 & 0 & 0 & 0 \\
0 & 0 & 0 & 0 & \cos e \cos p \sin b & \cos b \cos e \cos p & -\cos p \sin e & -\sin p \\
0 & 0 & 0 & 0 & 0 & 0 & 0 & 0 \\
0 & 0 & 0 & 0 & 0 & 0 & 0 & 0 \\
0 & 0 & 0 & 0 & \cos b & -\sin b & 0 & 0 \\
0 & 0 & 0 & 0 & 0 & 0 & 0 & 0 \\
0 & 0 & 0 & 0 & 0 & 0 & 0 & 0 \\
\cos a \cos c \sin g & -\cos c \sin a \sin g & -\sin c \sin g & \cos g & 0 & 0 & 0 & 0 \\
0 & 0 & 0 & 0 & 0 & 0 & 0 & 0 \\
0 & 0 & 0 & 0 & 0 & 0 & 0 & 0 \\
\cos a \sin c & -\sin a \sin c & \cos c & 0 & 0 & 0 & 0 & 0 \\
0 & 0 & 0 & 0 & \cos e \sin b \sin p & \cos b \cos e \sin p & -\sin e \sin p & \cos p \\
0 & 0 & 0 & 0 & 0 & 0 & 0 & 0 \\
\sin a & \cos a & 0 & 0 & 0 & 0 & 0 & 0 \\
0 & 0 & 0 & 0 & \sin b \sin e & \cos b \sin e & \cos e & 0 \\
0 & 0 & 0 & 0 & 0 & 0 & 0 & 0
\end{pmatrix}
$$

$$
\begin{pmatrix}
0 & 0 & 0 & 0 & 0 & 0 & 0 & 0 \\
0 & 0 & 0 & 0 & 0 & 0 & 0 & 0 \\
\cos f \cos m \sin d & \cos m \sin f & \cos d \cos f \cos m & -\sin m & 0 & 0 & 0 & 0 \\
0 & 0 & 0 & 0 & \cos n \cos q \sin h & \cos n \sin q & \sin n & \cos h \cos n \cos q \\
0 & 0 & 0 & 0 & 0 & 0 & 0 & 0 \\
-\sin d \sin f & \cos f & -\cos d \sin f & 0 & 0 & 0 & 0 & 0 \\
0 & 0 & 0 & 0 & -\cos q \sin h \sin n & -\sin n \sin q & \cos n & -\cos h \cos q \sin n \\
0 & 0 & 0 & 0 & 0 & 0 & 0 & 0 \\
\cos d & 0 & -\sin d & 0 & 0 & 0 & 0 & 0 \\
0 & 0 & 0 & 0 & -\sin h \sin q & \cos q & 0 & -\cos h \sin q \\
0 & 0 & 0 & 0 & 0 & 0 & 0 & 0 \\
0 & 0 & 0 & 0 & 0 & 0 & 0 & 0 \\
0 & 0 & 0 & 0 & \cos h & 0 & 0 & -\sin h \\
0 & 0 & 0 & 0 & 0 & 0 & 0 & 0 \\
0 & 0 & 0 & 0 & 0 & 0 & 0 & 0 \\
\cos f \sin d \sin m & \sin f \sin m & \cos d \cos f \sin m & \cos m & 0 & 0 & 0 & 0
\end{pmatrix}. \tag{B.1}
$$

The generalized extreme Choi state takes the form

$$\mathcal{C}_{\text{twoqub}} = \begin{pmatrix} A_1 & C_{12} & C_{13} & C_{14} \\ C_{21} & A_2 & C_{23} & C_{24} \\ C_{31} & C_{32} & A_3 & C_{34} \\ C_{41} & C_{42} & C_{43} & A_4 \end{pmatrix},$$

with

$$C_{12} = \sqrt{A_1}U\sqrt{A_2}, C_{13} = \sqrt{A_1}UV\sqrt{A_3}, C_{14} = \sqrt{A_1}UVW\sqrt{A_4} \tag{B.3}$$

$$C_{23} = \sqrt{A_2}V\sqrt{A_3}, C_{24} = \sqrt{A_2}VW\sqrt{A_4}, C_{34} = \sqrt{A_3}W\sqrt{A_4}. \tag{B.4}$$

The permutation (ignoring the sign) operators are

$$U = \begin{pmatrix} 0 & 1 & 0 & 0 \\ 1 & 0 & 0 & 0 \\ 0 & 0 & 0 & 1 \\ 0 & 0 & 1 & 0 \end{pmatrix}, V = \begin{pmatrix} 0 & 0 & 0 & 1 \\ 0 & 0 & 1 & 0 \\ 0 & 1 & 0 & 0 \\ 1 & 0 & 0 & 0 \end{pmatrix}, W = \begin{pmatrix} 0 & 1 & 0 & 0 \\ 1 & 0 & 0 & 0 \\ 0 & 0 & 0 & 1 \\ 0 & 0 & 1 & 0 \end{pmatrix}. \tag{B.5}$$

The unitary circuit for a generalized extreme channel takes the form

$$\begin{aligned} U'_{\text{twoqub}} :=& CX_3CX_2CX_1M_{32}(n,m)M_{31}(q,p)M_{30}(h,g) \\ & M_{21}(f,e)M_{20}(d,c)M_{10}(b,a), \end{aligned} \tag{B.6}$$

The permutation gates in the controlled-permutation gates are

$$X_1 = \begin{pmatrix} 0 & 0 & 0 & 1 \\ 0 & 0 & 1 & 0 \\ 0 & 1 & 0 & 0 \\ 1 & 0 & 0 & 0 \end{pmatrix}, X_2 = \begin{pmatrix} 0 & 0 & 1 & 0 \\ 0 & 0 & 0 & 1 \\ 1 & 0 & 0 & 0 \\ 0 & 1 & 0 & 0 \end{pmatrix}, X_3 = \begin{pmatrix} 0 & 1 & 0 & 0 \\ 1 & 0 & 0 & 0 \\ 0 & 0 & 0 & 1 \\ 0 & 0 & 1 & 0 \end{pmatrix}. \tag{B.7}$$

Using notation for permutation, $X_1 = (03)(12)$, $X_2 = (02)(13)$, and $X_3 = (01)(23)$. The unitary operator U'_{twoqub} is shown in Eq. (B.8). The colors (green, red, yellow, blue) indicate the corresponding elements come from Kraus operators (F_0,F_1,F_2,F_3).

$$
U'_{\text{twoqub}} = \begin{pmatrix}
\cos a \cos c \cos g & -\cos c \cos g \sin a & -\cos g \sin c & -\sin g & 0 & 0 & 0 & 0 \\
0 & 0 & 0 & 0 & 0 & 0 & 0 & 0 \\
0 & 0 & 0 & 0 & 0 & 0 & 0 & 0 \\
0 & 0 & 0 & 0 & \cos e \sin b \sin p & \cos b \cos e \sin p & -\sin e \sin p & \cos p \\
0 & 0 & 0 & 0 & \cos b & -\sin b & 0 & 0 \\
0 & 0 & 0 & 0 & 0 & 0 & 0 & 0 \\
0 & 0 & 0 & 0 & 0 & 0 & 0 & 0 \\
\cos a \cos c \sin g & -\cos c \sin a \sin g & -\sin c \sin g & \cos g & 0 & 0 & 0 & 0 \\
0 & 0 & 0 & 0 & 0 & 0 & 0 & 0 \\
0 & 0 & 0 & 0 & \cos e \cos p \sin b & \cos b \cos e \cos p & -\cos p \sin e & -\sin p \\
\cos a \sin c & -\sin a \sin c & \cos c & 0 & 0 & 0 & 0 & 0 \\
0 & 0 & 0 & 0 & 0 & 0 & 0 & 0 \\
0 & 0 & 0 & 0 & 0 & 0 & 0 & 0 \\
\sin a & \cos a & 0 & 0 & 0 & 0 & 0 & 0 \\
0 & 0 & 0 & 0 & \sin b \sin e & \cos b \sin e & \cos e & 0 \\
0 & 0 & 0 & 0 & 0 & 0 & 0 & 0
\end{pmatrix}
$$

$$
\begin{pmatrix}
0 & 0 & 0 & 0 & 0 & 0 & 0 & 0 \\
0 & 0 & 0 & 0 & -\sin h \sin q & \cos q & 0 & -\cos h \sin q \\
\cos f \cos s \sin d & \cos s \sin f & \cos d \cos f \cos s & -\sin s & 0 & 0 & 0 & 0 \\
0 & 0 & 0 & 0 & 0 & 0 & 0 & 0 \\
0 & 0 & 0 & 0 & 0 & 0 & 0 & 0 \\
-\sin d \sin f & \cos f & -\cos d \sin f & 0 & 0 & 0 & 0 & 0 \\
0 & 0 & 0 & 0 & -\cos q \sin h \sin t & -\sin t \sin q & \cos t & -\cos h \cos q \sin t \\
0 & 0 & 0 & 0 & 0 & 0 & 0 & 0 \\
\cos d & 0 & -\sin d & 0 & 0 & 0 & 0 & 0 \\
0 & 0 & 0 & 0 & 0 & 0 & 0 & 0 \\
0 & 0 & 0 & 0 & 0 & 0 & 0 & 0 \\
0 & 0 & 0 & 0 & \cos t \cos q \sin h & \cos t \sin q & \sin t & \cos h \cos t \cos q \\
0 & 0 & 0 & 0 & \cos h & 0 & 0 & -\sin h \\
0 & 0 & 0 & 0 & 0 & 0 & 0 & 0 \\
0 & 0 & 0 & 0 & 0 & 0 & 0 & 0 \\
\cos f \sin d \sin s & \sin f \sin s & \cos d \cos f \sin s & \cos s & 0 & 0 & 0 & 0
\end{pmatrix}. \tag{B.8}
$$

Appendix C

Algorithm for quantum channel simulation

Algorithm 3 Algorithm for qudit quantum channel $\mathcal{E}$ simulation

Input:
$[\mathcal{E}]$: bit-string description of the channel
d: the qudit dimension
ϵ: the error tolerance
Output:
$[C]$: bit-string description of the circuit
function ChaSim($[\mathcal{E}]$, d, ϵ)
  $[C] \leftarrow \varnothing$. ▷ Initializes as the empty-string
  $U \leftarrow$ Haar-rand-$SU(d^3)$. ▷ Generate random unitary operator
  for $i = 0$ to $d^2 - 1$ **do**
    $K_i \leftarrow \langle i|U|0\rangle$. ▷ Generate Kraus operators
  end for
  $[\mathcal{E}] \leftarrow \{K_i\}$. ▷ Generate input channel
  $\mathcal{C} \leftarrow [\mathcal{E}]$. ▷ Convert channel to Choi-Jamiołkowski state $\mathcal{C}$
  for $\imath = 1$ to d **do**
    $\vec{p} \leftarrow \text{rand}[0,1]^{\otimes d}$. ▷ Generate probability
    $W^{(\imath)}, V^{(\imath)} \leftarrow$ Haar-rand-$SU(d)$. ▷ Generate random unitary operators
    for $i = 1$ to $d - 1$ **do**
      for $j = 0$ to $i - 1$ **do**
        $\vec{\theta}^{(\imath)} \leftarrow 2\pi\text{rand}[0,1]^{\otimes d^2-d}$. ▷ Generate rotation angles
        $G_{ij}^{(\imath)}(\theta_{ij}^{(\imath)}) \leftarrow \cos\theta_{ij}^{(\imath)}(|i\rangle\langle i| + |j\rangle\langle j|) + \sin\theta_{ij}^{(\imath)}(|j\rangle\langle i| - |i\rangle\langle j|)$.
        $CG_{ij}^{(\imath)}(\theta_{ij}^{(\imath)}) \leftarrow |i\rangle\langle i| \otimes G_{ij}^{(\imath)}(\theta_{ij}^{(\imath)})$.
      end for
    end for
    for $i = 1$ to $d - 1$ **do**
      $X_i \leftarrow \sum_{\ell=0}^{d-1} |\ell\rangle\langle\ell + i|$.
      $CX_i \leftarrow X_i \otimes |i\rangle\langle i|$. ▷ Controlled-$X_i$ gates
    end for
    $U^{(\imath)} \leftarrow \prod_{i=1}^{d-1} CX_i \prod_{i=d-1}^{1} \prod_{j=i-1}^{0} CG_{ij}^{(\imath)}(\theta_{ij}^{(\imath)}) CG_{ji}^{(\imath)}(\theta_{ji}^{(\imath)})$.
    for $i = 0$ to $d - 1$ **do**
      $F_i^{(\imath)} \leftarrow \langle i|U^{(\imath)}|0\rangle$.
      $K_i^{(\imath)} \leftarrow W^{(\imath)} F_i^{(\imath)} V^{(\imath)}$. ▷ Kraus operators for each generalized extreme channel
    end for
    $\mathcal{C}^{(\imath)} \leftarrow \{K_i^{(\imath)}\}$.
  end for
  $\{\epsilon', \vec{p}', \vec{\theta}^{(\imath)}, W^{(\imath)}, V^{(\imath)}\} \leftarrow \text{CJ}(\mathcal{C}, \epsilon, \vec{p}, \{\mathcal{C}^{(\imath)}\})$. ▷ Choi-Jamiołkowski state decomposition
  if $\epsilon' \leq \epsilon$ **then**
    return $U^{(\imath)} \leftarrow \vec{\theta}^{(\imath)}, W^{(\imath)}, V^{(\imath)}$.
    for $\imath = 1$ to d **do**
      $\tilde{W}^{(\imath)}, \tilde{V}^{(\imath)}, \tilde{G}_{ij}^{(\imath)} \leftarrow \text{SK}(W^{(\imath)}, V^{(\imath)}, G_{ij}^{(\imath)}, \epsilon)$. ▷ Solovay-Kitaev algorithm
      $[C^{(\imath)}] \leftarrow \tilde{W}^{(\imath)}, \tilde{V}^{(\imath)}, \tilde{G}_{ij}^{(\imath)}$. ▷ Construct the generalized extreme channel circuit
    end for
    return $[C] \leftarrow [C^{(1)}][C^{(2)}] \cdots [C^{(d)}][\vec{p}']$.
  else
    return false.
  end if
end function

Bibliography

[1] Dorit Aharonov, Itai Arad, Elad Eban, and Zeph Landau. Polynomial quantum algorithms for additive approximations of the Potts model and other points of the Tutte plane, 2007. arXiv:quant-ph/0702008.

[2] Dorit Aharonov, Alexei Kitaev, and Noam Nisan. Quantum circuits with mixed states. In *Proc. 13th Annual ACM Symp. on Theory of Comp.*, pages 20–30. ACM, 1997.

[3] Dorit Aharonov and Amnon Ta-Shma. Adiabiatic quantum state generation and statistical zero knowledge. In *Proc. 35th Annual ACM Symp. on Theory of Comp.*, volume 35, New York, 2003. ACM.

[4] Yakir Aharonov, David Z. Albert, and Lev Vaidman. How the result of a measurement of a component of the spin of a spin-1/2 particle can turn out to be 100. *Phys. Rev. Lett.*, 60:1351–1354, Apr 1988.

[5] Alán Aspuru-Guzik, Anthony D. Dutoi, Peter J. Love, and Martin Head-Gordon. Simulated quantum computation of molecular energies. *Science*, 309(5741):1704–1707, Sep 2005.

[6] Alán Aspuru-Guzik and Philip Walther. Photonic quantum simulators. *Nat. Phys.*, 8(4):285–291, Apr 2012.

[7] Dave Bacon, Andrew M. Childs, Isaac L. Chuang, Julia Kempe, Debbie W. Leung, and Xinlan Zhou. Universal simulation of Markovian quantum dynamics. *Phys. Rev. A*, 64:062302, Nov 2001.

[8] Jerry Banks. Principles of Simulation. In Jerry Banks, editor, *Handbook of Simulation: Principles, Methodology, Advances, Applications, and Practices*, chapter 1: Principles of Simulation. John Wiley & Sons, Inc., New York, 1998.

[9] Adriano Barenco, Charles H. Bennett, Richard Cleve, David P. DiVincenzo, Norman Margolus, Peter Shor, Tycho Sleator, John A. Smolin, and Harald Weinfurter. Elementary gates for quantum computation. *Phys. Rev. A*, 52:3457–3467, Nov 1995.

[10] Sean Barrett, Klemens Hammerer, Sarah Harrison, Tracy E. Northup, and Tobias J. Osborne. Simulating quantum fields with cavity QED. *Phys. Rev. Lett.*, 110:090501, Feb 2013.

[11] Ingemar Bengtsson and Karol Życzkowski. *Geometry of Quantum States*. Cambridge University Press, Cambridge U.K., 2006.

[12] Charles H. Bennett, Ethan Bernstein, Gilles Brassard, and Umesh Vazirani. Strengths and weaknesses of quantum computing. *SIAM J. Comput.*, 26(5):1510–1523, 1997.

[13] Dominic W. Berry, Graeme Ahokas, Richard Cleve, and Barry C. Sanders. Efficient quantum algorithms for simulating sparse Hamiltonians. *Commun. Math. Phys.*, 270(2):359–371, 2007.

[14] Dominic W. Berry and Andrew M. Childs. Black-box Hamiltonian simulation and unitary implementation. *Quantum Inf. Comput.*, 12(1-2):29–62, 2012.

[15] Dominic W. Berry, Andrew M. Childs, Richard Cleve, Robin Kothari, and Rolando D. Somma. Simulating Hamiltonian dynamics with a truncated Taylor series. *Phys. Rev. Lett.*, 114:090502, Mar 2015.

[16] Rajendra Bhatia. *Positive Definite Matrices*. Princeton University Press, Princeton, NJ, 2007.

[17] J. D. Biamonte, V. Bergholm, J. D. Whitfield, J. Fitzsimons, and A. Aspuru-Guzik. Adiabatic quantum simulators. *AIP Advances*, 1(2):022126, 2011.

[18] Bruce Blackadar. *Operator algebras*. Springer-Verlag Berlin, 2006.

[19] Immanuel Bloch, Jean Dalibard, and Sylvain Nascimbene. Quantum simulations with ultracold quantum gases. *Nat. Phys.*, 8:267, April 2012.

[20] Mark D Bowdrey, Daniel KL Oi, Anthony J Short, Konrad Banaszek, and Jonathan A Jones. Fidelity of single qubit maps. *Phys. Lett. A*, 294(5):258–260, 2002.

[21] Stephen P. Boyd and Lieven Vandenberghe. *Convex Optimization*. Cambridge University Press, Cambridge U.K., 2004.

[22] Gilles Brassard, Peter Høyer, Michele Mosca, and Alain Tapp. Quantum amplitude amplification and estimation, 2000. arXiv:quant-ph/0005055.

[23] Daniel Braun, Olivier Giraud, Ion Nechita, Clement Pellegrini, and Marko Znidaric. A universal set of qubit quantum channels. *J. Phys. A: Math. Theor.*, 47:135302, 2014.

[24] Michael J. Bremner, Richard Jozsa, and Dan J. Shepherd. Classical simulation of commuting quantum computations implies collapse of the polynomial hierarchy. In *Proceedings of the Royal Society A: Mathematical, Physical and Engineering Science*, pages 459–472, 2011.

[25] Gavin K. Brennen, Dianne P. O'Leary, and Stephen S. Bullock. Criteria for exact qudit universality. *Phys. Rev. A*, 71:052318, May 2005.

[26] Heinz-Peter Breuer and Francesco Petruccione. *The Theory of Open Quantum System*. Oxford University Press, Oxford, U.K., 2003.

[27] Joseph W. Britton, Brian C. Sawyer, Adam C. Keith, C.-C. Joseph Wang, James K. Freericks, Hermann Uys, Michael J. Biercuk, and John J. Bollinger. Engineered two-dimensional Ising interactions in a trapped-ion quantum simulator with hundreds of spins. *Nature*, 484(7395):489–492, April 2012.

[28] Daniel E. Browne. Efficient classical simulation of the quantum Fourier transform. *New J. Phys.*, 9:146, May 2007.

[29] E. Brüning, H. Mäkelä, A. Messina, and F. Petruccione. Parametrizations of density matrices. *J. Mod. Opt.*, 59(1):1–20, 2012.

[30] Wojciech Bruzda, Valerio Cappellini, Hans-Jürgen Sommers, and Karol Życzkowski. Random quantum operations. *Phys. Lett. A*, 373:320–324, 2009.

[31] J.-L. Brylinski and R. Brylinski. Universal Quantum Gates. In R. Brylinski and G. Chen, editors, *Mathematics of Quantum Computation*, chapter 4: Universal Quantum Gates. CRC Press, Boca Raton, 2002.

[32] Stephen S. Bullock, Dianne P. O'Leary, and Gavin K. Brennen. Asymptotically optimal quantum circuits for d-level systems. *Phys. Rev. Lett.*, 94:230502, Jun 2005.

[33] Iulia Buluta and Franco Nori. Quantum simulators. *Science*, 326(5949):108–111, Oct 2009.

[34] Christian K. Burrell. Geometry of generalized depolarizing channels. *Phys. Rev. A*, 80:042330, Oct 2009.

[35] Francesco Buscemi, G. Mauro D'Ariano, and Massimiliano F. Sacchi. Physical realizations of quantum operations. *Phys. Rev. A*, 68:042113, Oct 2003.

[36] Paul Busch, Marian Grabowski, and Pekka J. Lahti. *Operational Quantum Physics*. Springer, Berlin, 1995.

[37] Howard J. Carmichael. *Statistical Methods in Quantum Optics 1: Master Equations and Fokker-Planck Equations*. Theoretical and Mathematical Physics. Springer, Berlin, 2003.

[38] J. Casanova, L. Lamata, I. L. Egusquiza, R. Gerritsma, C. F. Roos, J. J. Garcí a Ripoll, and E. Solano. Quantum simulation of quantum field theories in trapped ions. *Phys. Rev. Lett.*, 107:260501, Dec 2011.

[39] J. Casanova, A. Mezzacapo, L. Lamata, and E. Solano. Quantum simulation of interacting fermion lattice models in trapped ions. *Phys. Rev. Lett.*, 108:190502, May 2012.

[40] Andrew M. Childs. On the relationship between continuous- and discrete-time quantum walk. *Commun. Math. Phys.*, 294(2):581–603, 2010.

[41] Andrea Chiuri, Chiara Greganti, Laura Mazzola, Mauro Paternostro, and Paolo Mataloni. Linear optics simulation of quantum non-Markovian dynamics. *Sci. Rep.*, 2:968, Dec 2012.

[42] Man-Duen Choi. Positive linear maps on complex matrices. *Linear Algebra Appl.*, 290(10):285–290, 1975.

[43] Isaac L. Chuang and M. A. Nielsen. Prescription for experimental determination of the dynamics of a quantum black box. *J. Mod. Opt.*, 44(11-12):2455–2467, 1997.

[44] J. Ignacio Cirac and Peter Zoller. Goals and opportunities in quantum simulation. *Nat. Phys.*, 8(2275):264, April 2012.

[45] Richard Cleve, Gottesman Daniel, Michele Mosca, Rolando D. Somma, and David Yonge-Mallo. Efficient discrete-time simulations of continuous-time quantum query algorithms. In *Proc. 41th Annual ACM Symp. on Theory of Comp.*, pages 409–416. ACM, 2009.

[46] J.R.B. Cockett and Pieter J.W. Hofstra. Categorical simulations. *J. Pure Appl. Algebr.*, 214(10):1835–1853, 2010.

[47] T. Constantinescu and V. Ramakrishna. Parametrizing quantum states and channels. *Quant. Inform. Process.*, 2(3):221, June 2003.

[48] Jamil Daboul, Xiaoguang Wang, and Barry C. Sanders. Quantum gates on hybrid qudits. *J. Phys. A: Math. Theor.*, 36:2525–2536, 2003.

[49] Chris M. Dawson and Michael A. Nielsen. The Solovay-Kitaev algorithm. *Quantum Inf. Comput.*, 6(1):81–95, 2006.

[50] David P. DiVincenzo. The Physical Implementation of Quantum Computation, 2000. arXiv:quant-ph/0002077.

[51] Runyao Duan, Yuan Feng, and Mingsheng Ying. Perfect distinguishability of quantum operations. *Phys. Rev. Lett.*, 103:210501, Nov 2009.

[52] Guillaume Duclos-Cianci and Krysta M. Svore. Distillation of nonstabilizer states for universal quantum computation. *Phys. Rev. A*, 88:042325, Oct 2013.

[53] J. Eckhoff. Helly, Radon, and Carathéodory type theorems. In P. M. Gruber and J. M. Wills, editors, *Handbook of Convex Geometry*, chapter 2.1: Helly, Radon, and Carathéodory type theorems. Elsevier, Amsterdam: North-Holland, 1993.

[54] J. Eisert. Computational difficulty of global variations in the density matrix renormalization group. *Phys. Rev. Lett.*, 97:260501, Dec 2006.

[55] J. Emerson, Y. S. Weinstein, M. Saraceno, S. Lloyd, and D. G. Cory. Pseudo-random unitary operators for quantum information processing. *Science*, 302:2098–2100, Dec 2003.

[56] Richard P. Feynman. Simulating physics with computers. *Int. J. Theor. Phys.*, 21(6/7):467–488, 1982.

[57] Shmuel Friedland and Raphael Loewy. On the extreme points of quantum channels, 2013. arXiv:quant-ph/1309.5898.

[58] Akio Fujiwara. Quantum channel identification problem. *Phys. Rev. A*, 63:042304, Mar 2001.

[59] J. Gemmer, M. Michel, and G. Mahler. *Quantum Thermodynamics: Emergence of Thermodynamic Behavior within Composite Quantum Systems*. Springer, Berlin, 2005.

[60] I. M. Georgescu, S. Ashhab, and Franco Nori. Quantum simulation. *Rev. Mod. Phys.*, 86:153–185, Mar 2014.

[61] Michael A Gibson and Jehoshua Bruck. Efficient exact stochastic simulation of chemical systems with many species and many channels. *J. Phys. Chem. A*, 104(9):1876–1889, 2000.

[62] Brett Giles and Peter Selinger. Exact synthesis of multiqubit Clifford+T circuits. *Phys. Rev. A*, 87:032332, 2013.

[63] Gian Luca Giorgi, Simone Paganelli, and Fernando Galve. Ion-trap simulation of the quantum phase transition in an exactly solvable model of spins coupled to bosons. *Phys. Rev. A*, 81:052118, May 2010.

[64] Gene H. Golub. *Matrix Computations*. Johns Hopkins University Press, Baltimore, 2013.

[65] Vittorio Gorini, Andrzej Kossakowski, and E. C. G. Sudarshan. Completely positive dynamical semigroups of N-level systems. *J. Math. Phys.*, 17:821, 1976.

[66] Daniel Gottesman, Alexei Kitaev, and John Preskill. Encoding a qubit in an oscillator. *Phys. Rev. A*, 64:012310, Jun 2001.

[67] Lov K. Grover. Quantum mechanics helps in searching for a needle in a haystack. *Phys. Rev. Lett.*, 79:325–328, Jul 1997.

[68] Lov K. Grover. Synthesis of quantum superpositions by quantum computation. *Phys. Rev. Lett.*, 85:1334–1337, Aug 2000.

[69] Peter M. Gruber. *Convex and Discrete Geometry*. Springer-Verlag, Berlin, 2007.

[70] Branko Grünbaum. *Convex Polytopes*. Springer-Verlag, New York, 2003.

[71] Aram W. Harrow, Avinatan Hassidim, and Seth Lloyd. Quantum algorithm for linear systems of equations. *Phys. Rev. Lett.*, 103:150502, Oct 2009.

[72] Aram W. Harrow, Benjamin Recht, and Isaac L. Chuang. Efficient discrete approximations of quantum gates. *J. Math. Phys.*, 43(9):4445, 2002.

[73] Alexander K. Hartmann and Heiko Rieger. *Optimization Algorithms in Physics*. Wiley-VCH Verlag Berlin GmbH, Berlin, 2002.

[74] Philipp Hauke, Fernando M. Cucchietti, Luca Tagliacozzo, Ivan Deutsch, and Maciej Lewenstein. Can one trust quantum simulators? *Rep. Prog. Phys.*, 75(8):082401, 2012.

[75] Holger F. Hofmann and Shigeki Takeuchi. Quantum phase gate for photonic qubits using only beam splitters and postselection. *Phys. Rev. A*, 66:024308, Aug 2002.

[76] R. A. Horn and C. R. Johnson. *Topics in Matrix Analysis*. Cambridge University Press, Cambridge, U.K., 1991.

[77] M. Horodecki, P. Horodecki, and R. Horodecki. Separability of mixed states: necessary and sufficient conditions. *Phys. Lett. A*, 223:1, Nov 1996.

[78] Michael Horodecki, Peter W. Shor, and Mary Beth Ruskai. Entanglement breaking channels. *Rev. Math. Phys.*, 15:629, Aug 2003.

[79] Paweł Horodecki and Artur Ekert. Method for direct detection of quantum entanglement. *Phys. Rev. Lett.*, 89:127902, Aug 2002.

[80] Peter Høyer. Arbitrary phases in quantum amplitude amplification. *Phys. Rev. A*, 62:052304, Oct 2000.

[81] Albert S. Jackson. *Analog Computation*. McGraw-Hill, London & New York, 1960.

[82] A Jamiołkowski. Linear transformations which preserve trace and positive semidefiniteness of operators. *Rep. Math. Phys.*, 3:275, 1972.

[83] Z. Ji, Guoming Wang, R. Duan, Yuan Feng, and M. Ying. Parameter estimation of quantum channels. *IEEE Trans. Inf. Theory*, 54(11):5172–5185, Nov 2008.

[84] P. Jordan and E. Wigner. Über das paulische Äquivalenzverbot. *Zeitschrift für Physik*, 631:47, 1928.

[85] Stephen P. Jordan, Keith S. M. Lee, and John Preskill. Quantum algorithms for quantum field theories. *Science*, 336(6085):1130–3, June 2012.

[86] Stephen P. Jordan and Pawel Wocjan. Efficient quantum circuits for arbitrary sparse unitaries. *Phys. Rev. A*, 80:062301, Dec 2009.

[87] Amir Kalev and Joonwoo Bae. Optimal approximate transpose map via quantum designs and its applications to entanglement detection. *Phys. Rev. A*, 87:062314, Jun 2013.

[88] Nikolai Kiesel, Christian Schmid, Ulrich Weber, Rupert Ursin, and Harald Weinfurter. Linear optics controlled-phase gate made simple. *Phys. Rev. Lett.*, 95:210505, 2005.

[89] Yong-Su Kim, Jong-Chan Lee, Osung Kwon, and Yoon-Ho Kim. Protecting entanglement from decoherence using weak measurement and quantum measurement reversal. *Nat. Phys.*, 8(2):117–120, 02 2012.

[90] Gen Kimura. The Bloch vector for N-level systems. *Phys. Lett. A*, 314(56):339 – 349, 2003.

[91] C. King and M.B. Ruskai. Minimal entropy of states emerging from noisy quantum channels. *IEEE Trans. Inf. Theory*, 47(1):192–209, 2001.

[92] A. Kitaev, A. H. Shen, and M. N. Vyalyi. *Classical and Quantum Computation*, volume 47 of *Graduate Studies in Mathematics*. American Mathematical Society, Providence, 2002.

[93] M. Kliesch, T. Barthel, C. Gogolin, M. Kastoryano, and J. Eisert. Dissipative Quantum Church-Turing Theorem. *Phys. Rev. Lett.*, 107(12):120501, Sep 2011.

[94] Vadym Kliuchnikov. Synthesis of unitaries with Clifford+T circuits, 2013. arXiv:quant-ph/1306.3200.

[95] Vadym Kliuchnikov, Dmitri Maslov, and Michele Mosca. Asymptotically optimal approximation of single qubit unitaries by Clifford and T circuits using a constant number of ancillary qubits. *Phys. Rev. Lett.*, 110:190502, 2013.

[96] Vadym Kliuchnikov, Dmitri Maslov, and Michele Mosca. Fast and efficient exact synthesis of single qubit unitaries generated by Clifford and T gates. *Quantum Inf. Comput.*, 13:0607—0630, 2013.

[97] Alexander N. Korotkov and Kyle Keane. Decoherence suppression by quantum measurement reversal. *Phys. Rev. A*, 81:040103, Apr 2010.

[98] Karl Kraus. *States, Effects, and Operations: Fundamental Notions of Quantum Theory*, volume 190 of *Lecture Notes in Physics*. Springer-Verlag, Berlin, 1983.

[99] L. Lamata, J. León, T. Schätz, and E. Solano. Dirac equation and quantum relativistic effects in a single trapped ion. *Phys. Rev. Lett.*, 98:253005, Jun 2007.

[100] L. J. Landau and R. F. Streater. On Birkhoff's Theorem for Doubly Stochastic Completely Positive Maps of Matrix Algebras. *Linear Algebra Appl.*, 193:107–127, 1993.

[101] N. K. Langford, T. J. Weinhold, R. Prevedel, K. J. Resch, A. Gilchrist, J. L. O'Brien, G. J. Pryde, and A. G. White. Demonstration of a simple entangling optical gate and its use in Bell-state analysis. *Phys. Rev. Lett.*, 95:210504, 2005.

[102] Ben P. Lanyon, C. Hempel, D. Nigg, Markus Müller, R. Gerritsma, F. Zähringer, P. Schindler, Julio T. T. Barreiro, M. Rambach, G. Kirchmair, M. Hennrich, Peter Zoller, Rainer Blatt, and Christian-F. Roos. Universal digital quantum simulation with trapped ions. *Science*, 334(6052):57–61, 10 2011.

[103] Franois Le Gall. Powers of tensors and fast matrix multiplication, 2014. arXiv:1401.7714v1.

[104] Maciej Lewenstein, Anna Sanpera, and Veronica Ahufinger. *Ultracold Atoms in Optical Lattices: Simulating quantum many-body systems*. Oxford University Press, Oxford, 2012.

[105] Maciej Lewenstein, Anna Sanpera, Veronica Ahufinger, Bogdan Damski, Aditi Sen De, and Ujjwal Sen. Ultracold atomic gases in optical lattices: mimicking condensed matter physics and beyond. *Adv. Phys.*, 56(1-2):243–379, Jan-Apr 2007.

[106] Hyang-Tag Lim, Young-Sik Ra, Yong-Su Kim, Joonwoo Bae, and Yoon-Ho Kim. Experimental implementation of the universal transpose operation using the structural physical approximation. *Phys. Rev. A*, 83:020301, Feb 2011.

[107] G. Lindblad. On the generators of quantum dynamical semigroups. *Commun. Math. Phys.*, 48:119–130, 1976.

[108] Seth Lloyd. Universal quantum simulators. *Science*, 273(5278):1073–1078, Aug 1996.

[109] Seth Lloyd and Lorenza Viola. Engineering quantum dynamics. *Phys. Rev. A*, 65:010101(R), Dec 2001.

[110] G. L. Long. Grover algorithm with zero theoretical failure rate. *Phys. Rev. A*, 64:022307, Jul 2001.

[111] He Lu, Chang Liu, Dong-Sheng Wang, Luo-Kan Chen, Zheng-Da Li, Xing-Can Yao, Li Li, Nai-Le Liu, Cheng-Zhi Peng, Barry C. Sanders, Yu-Ao Chen, and Jian-Wei Pan. Universal digital photonic single-qubit quantum channel simulator, 2015. arXiv:quant-ph/1505.02879.

[112] Easwar Magesan, Daniel Puzzuoli, Christopher E. Granade, and David G. Cory. Modeling quantum noise for efficient testing of fault-tolerant circuits. *Phys. Rev. A*, 87:012324, Jan 2013.

[113] Roger McHaney. *Understanding Computer Simulation*. Ventus Publishing ApS, 2009.

[114] Christian B. Mendl and Michael M. Wolf. Unital Quantum Channels-Convex Structure and Revivals of Birkhoff's Theorem. *Commun. Math. Phys.*, 289:1057–1096, 2009.

[115] Jarosław Adam Miszczak. Singular value decomposition and matrix reorderings in quantum information theory. *Int. J. Mod. Phys. C*, 22(09):897–918, 2011.

[116] Sarah Mostame, Patrick Rebentrost, Alexander Eisfeld, Andrew J Kerman, Dimitris I Tsomokos, and Alán Aspuru-Guzik. Quantum simulator of an open quantum system using superconducting qubits: exciton transport in photosynthetic complexes. *New J. Phys.*, 14(10):105013, 2012.

[117] Mikka Möttönen and Juha J. Vartiainen. Decompositions of General Quantum Gates. In Susan Shannon, editor, *Trends in Quantum Computing Research*, chapter 7: Decompositions of General Quantum Gates. Nova, New York, 2006.

[118] Mikko Möttönen, Juha J. Vartiainen, Ville Bergholm, and Martti M. Salomaa. Quantum circuits for general multiqubit gates. *Phys. Rev. Lett.*, 93:130502, Sep 2004.

[119] Francis D. Murnaghan. *The Unitary and Rotation Groups*. Spartan books, Washington, D. C., 1962.

[120] Ashok Muthukrishnan and C. R. Stroud. Multivalued logic gates for quantum computation. *Phys. Rev. A*, 62:052309, Oct 2000.

[121] Attila B. Nagy. On an implementation of the Solovay-Kitaev algorithm, 2006. arXiv:quant-ph/0606077.

[122] Geetu Narang and Arvind. Simulating a single-qubit channel using a mixed-state environment. *Phys. Rev. A*, 75:032305, Mar 2007.

[123] Michael A. Nielsen and Isaac L. Chuang. *Quantum Computation and Quantum Information*. Cambridge University Press, Cambridge U.K., 2000.

[124] Ryo Okamoto, Holger F. Hofmann, Shigeki Takeuchi, and Keiji Sasaki. Demonstration of an optical quantum controlled-NOT gate without path interference. *Phys. Rev. Lett.*, 95:210506, 2005.

[125] P. Oscar Boykin, Tal Mor, Matthew Pulver, Vwani Roychowdhury, and Farrokh Vatan. A new universal and fault-tolerant quantum basis. *Inform. Process. Lett.*, 75:101–107, 2000.

[126] G. S. Paraoanu. Recent progress in quantum simulation using superconducting circuits. *J. Low. Temp. Phys.*, 175:633–654, 2014.

[127] Vern Paulsen. *Completely bounded maps and oeprator algebras*. Cambridge University Press, Cambridge U.K., 2002.

[128] Carlos A. Pérez-Delgado and Pieter Kok. Quantum computers: Definition and implementations. *Phys. Rev. A*, 83:012303, Jan 2011.

[129] D. Perez-Garcia, F. Verstraete, M. M. Wolf, and J. I. Cirac. Matrix product state representations. *Quantum Inf. Comput.*, 7:401, 2007.

[130] Tien Trung Pham, Rodney Van Meter, and Clare Horsman. Optimising the Solovay-Kitaev algorithm. *Phys. Rev. A*, 87:052332, 2013.

[131] Marco Piani, David Pitkanen, Rainer Kaltenbaek, and Norbert Lütkenhaus. Linear-optics realization of channels for single-photon multimode qudits. *Phys. Rev. A*, 84:032304, Sep 2011.

[132] David Poole and Adrian E. Raftery. Inference for deterministic simulation models: The bayesian melding approach. *JASA*, 95(452):1244–1255, 2000.

[133] J. F. Poyatos, J. I. Cirac, and P. Zoller. Complete characterization of a quantum process: The two-bit quantum gate. *Phys. Rev. Lett.*, 78:390–393, Jan 1997.

[134] Tomaž Prosen and Iztok Pižorn. Quantum phase transition in a far-from-equilibrium steady state of an xy spin chain. *Phys. Rev. Lett.*, 101:105701, Sep 2008.

[135] Sadegh Raeisi, Nathan Wiebe, and Barry C. Sanders. Designing quantum circuits for efficient many-body quantum simulation. *New J. Phys.*, 14:103017, 2012.

[136] Clyde L Rhodes. The process simulation revolution: Thermophysical property needs and concerns. *J. Chem. Eng. Data*, 41(5):947–950, 1996.

[137] B. Rosgen and J. Watrous. On the hardness of distinguishing mixed-state quantum computations. In *Proc. 20th Annual Conference on Computational Complexity*, pages 344–354. IEEE, 2005.

[138] Mary Beth Ruskai. Qubit entanglement breaking channels. *Rev. Math. Phys.*, 15:643–662, 2003.

[139] Mary Beth Ruskai. Open problems in quantum information theory, Aug 2007. arXiv:quant-ph/0708.1902.

[140] Mary Beth Ruskai, Stanislaw Szarek, and Elisabeth Werner. An analysis of completely-positive trace-preserving maps on M2. *Linear Algebra Appl.*, 347(1–3):159–187, May 2002.

[141] Massimiliano F. Sacchi. Optimal discrimination of quantum operations. *Phys. Rev. A*, 71:062340, Jun 2005.

[142] S G Schirmer, T Zhang, and J V Leahy. Orbits of quantum states and geometry of Bloch vectors for N-level systems. *J. Phys. A*, 37(4):1389, 2004.

[143] C. Schön, E. Solano, F. Verstraete, J. I. Cirac, and M. M. Wolf. Sequential generation of entangled multiqubit states. *Phys. Rev. Lett.*, 95:110503, Sep 2005.

[144] Norbert Schuch, Ignacio Cirac, and F. Verstraete. Computational Difficulty of Finding Matrix Product Ground States. *Phys. Rev. Lett.*, 100:250501, Jun 2008.

[145] Norbert Schuch, Michael M. Wolf, Frank Verstraete, and J. Ignacio Cirac. Computational complexity of projected entangled pair states. *Phys. Rev. Lett.*, 98:140506, Apr 2007.

[146] Peter Selinger. Efficient Clifford + T Approximation of Single-qubit Operators. *Quantum Inf. Comput.*, 15(1-2):159–180, January 2015.

[147] G. Sentís, B. Gendra, S. D. Bartlett, and A. C. Doherty. Decomposition of any quantum measurement into extremals. *J. Phys. A: Math. Theor.*, 46(37):375302, Sep 2013.

[148] Vivek V. Shende, Stephen S. Bullock, and Igor L. Markov. Synthesis of Quantum-Logic Circuits. *IEEE Trans. Comput.-Aided Des.*, 25(6):1000–1010, 2006.

[149] Peter Shor. Polynomial-Time Algorithms for Prime Factorization and Discrete Logarithms on a Quantum Computer. In *Proc. 35th Annual Symposium on Foundations of Computer Science*, page 124. IEEE Computer Society, Los Alamitos, 1994.

[150] John A. Sokolowski and Catherine M. Banks. *Principles of Modeling and Simulation: A Multidisciplinary Approach*. John Wiley & Sons, Hoboken, NJ, 2011.

[151] Rolando D. Somma, Gerardo Ortiz, Emanuel H. Knill, and James Gubernatis. Quantum simulations of physics problems. *Proc. SPIE 5105, Quantum Information and Computation, 96*, 2003.

[152] W. Forrest Stinespring. Positive Functions on C*-algebras. *Proc. Am. Math. Soc.*, 6(2):211–216, Apr 1955.

[153] Masuo Suzuki. Fractal Decomposition of Exponential Operators with Applications to Many-Body Theories and Monte Carlo Simulations. *Phys. Lett. A*, 146(6):319–323, 1990.

[154] Hiroaki Terashima and Masahito Ueda. Nonunitary quantum circuit. *Int. J. Quantum Inform.*, 3:633–647, 2005.

[155] Barbara M. Terhal and Guido Burkard. Fault-tolerant quantum computation for local non-Markovian noise. *Phys. Rev. A*, 71:012336, Jan 2005.

[156] Barbara M. Terhal, Isaac L. Chuang, David P. DiVincenzo, Markus Grassl, and John A. Smolin. Simulating quantum operations with mixed environments. *Phys. Rev. A*, 60:881–885, Aug 1999.

[157] Géza Tóth. Qubit4matlab v3.0: A program package for quantum information science and quantum optics for matlab. *Comput. Phys. Commun.*, 179:430–437, Apr 2008.

[158] H. Trotter. On the product of semi-groups of operators. *Proc. Am. Math. Soc.*, 10:545–551, 1959.

[159] Matthias Troyer and Uwe-Jens Wiese. Computational complexity and fundamental limitations to fermionic quantum monte carlo simulations. *Phys. Rev. Lett.*, 94:170201, May 2005.

[160] Maarten Van den Nest. Classical simulation of quantum computation, the Gottesman-Knill theorem, and slightly beyond. *Quantum Inf. Comput.*, 10(3-4):0258–0271, 2010.

[161] Maarten Van den Nest. Simulating quantum computers with probabilistic methods. *Quantum Inf. Comput.*, 11(9-10):784–812, 2011.

[162] Juha J. Vartiainen, Mikko Möttönen, and Martti M. Salomaa. Efficient decomposition of quantum gates. *Phys. Rev. Lett.*, 92:177902, Apr 2004.

[163] F. Verstraete and J. I. Cirac. Continuous matrix product states for quantum fields. *Phys. Rev. Lett.*, 104:190405, May 2010.

[164] F. Verstraete and H. Verschelde. On quantum channels, 2003. arXiv:quant-ph/0202124.

[165] F. Verstraete, Michael M. Wolf, and J. Ignacio Cirac. Quantum computation and quantum-state engineering driven by dissipation. *Nat. Phys.*, 5(9):633–636, July 2009.

[166] Nikolay V. Vitanov. Synthesis of arbitrary SU(3) transformations of atomic qutrits. *Phys. Rev. A*, 85:032331, Mar 2012.

[167] Dong-Sheng Wang. Weak, strong, and uniform quantum simulations. *Phys. Rev. A*, 91:012334, Jan 2015.

[168] Dong-Sheng Wang, Dominic W. Berry, Marcos C. de Oliveira, and Barry C. Sanders. Solovay-Kitaev decomposition strategy for single-qubit channels. *Phys. Rev. Lett.*, 111:130504, Sep 2013.

[169] Dong-Sheng Wang and Barry C. Sanders. Quantum circuit design for accurate simulation of qudit channels. *New J. Phys.*, 14(3):033016, March 2015.

[170] Shu-Chao Wang, Zong-Wen Yu, Wen-Jie Zou, and Xiang-Bin Wang. Protecting quantum states from decoherence of finite temperature using weak measurement. *Phys.*

Rev. A, 89:022318, Feb 2014.

[171] J. Watrous. Theory of quantum information. Lecture Notes, 2013.

[172] Hendrik Weimer, Markus Müller, Hans-Peter Bühler, and Igor Lesanovsky. Digital quantum simulation with Rydberg atoms. *Quant. Inform. Process.*, 10(6):885–906, Sep 2011.

[173] Yaakov S. Weinstein. Pseudorandom circuits from Clifford-plus-T gates. *Phys. Rev. A*, 88:062303, Dec 2013.

[174] Steven R. White. Density matrix formulation for quantum renormalization groups. *Phys. Rev. Lett.*, 69:2863–2866, Nov 1992.

[175] Stephen Wiesner. Simulations of many-body quantum systems by a quantum computer, 1996. arXiv:quant-ph/9603028.

[176] Peter Wittek and Fernando M. Cucchietti. A second-order distributed Trotter-Suzuki solver with a hybrid CPUGPU kernel. *Comput. Phys. Commun.*, 184:1165, April 2013.

[177] Michael M. Wolf and J. Ignacio Cirac. Dividing quantum channels. *Commun. Math. Phys.*, 279(1):147–168, February 2008.

[178] S. L. Woronowicz. Positive maps of low dimensional matrix algebras. *Rep. Math. Phys.*, 10:165, Oct 1976.

[179] A. Yu. Kitaev. Quantum measurements and the abelian stabilizer problem, 1995. arXiv:quant-ph/9511026.

[180] Ya-Xiang Yuan and Wenyu Sun. *Optimization Theory and Methods: Nonlinear Programming*, volume 1 of *Springer Optimization and Its Applications*. Springer, New York, 2006.

[181] Christof Zalka. Efficient simulation of quantum systems by quantum computers, 1996. arXiv:quant-ph/9603026.

[182] Christof Zalka and Eleanor Rieffel. Quantum operations that cannot be implemented using a small mixed environment. *J. Math. Phys.*, 43(9):4376, May 2002.

[183] Fuzhen Zhang. *Matrix Theory: Basic Results and Techniques*. Universitext. Springer, New York, 2011.